UNIVERSITY OF CINCINNATI

Date: May 28, 2004

I, Sara Elizbeth Edison,

hereby submit this work as part of the requirements for the degree of:

Doctor of Philosophy (Ph.D.)

in:

Chemistry

It is entitled:

Investigation of Nickel(II)-Oximate Complexes that React with
Molecular Oxygen

This work and its defense approved by:

Chair: Dr. Michael J. Baldwin
Dr. Apryll M. Stalcup
Dr. William B. Connick

Investigation of Nickel(II)-Oximate Complexes that React with Molecular Oxygen

Dissertation for the degree of Doctor of Philosophy (Ph.D.) in Chemistry from the Department of Chemistry, McMicken College of Arts and Sciences, University of Cincinnati

June 11, 2004

by

Sara Elizabeth Edison

M.S. in Chemistry, University of Cincinnati, 2003

B.A. in Chemistry, Bellarmine University, 2000

Chair: Michael J. Baldwin, Ph.D.

Abstract

Ni(II) complexes containing amidates and thiolates have been shown to react with O_2 via irreversible ligand oxidation. We have constructed a series of Ni(II) complexes based on a tripodal amine bis(oxime) ligand framework. These complexes display oxygen reactivity upon deprotonation of the oximes without requiring irreversible ligand oxidation. This project investigated the reaction involving one of the complexes in the library, $[Ni(TRISOXH_3)(NO_3)(H_2O)](NO_3)\bullet (H_2O)$, where $TRISOXH_3$ = (tris(1-propan-2-onyl oxime)amine). It was discovered that the reaction of this complex with molecular oxygen is contingent upon the presence of a source of hydrogen atoms. This two-hydrogen atom donor acts as a substrate. Several primary alcohols, including the relatively inert methanol, and amines were catalytically oxidized by this reaction. Spectroscopic analysis using a variety of techniques has demonstrated that reversible oxidation occurs on the oximate nitrogen to form an iminoxyl radical.

Many of the other complexes in the series were also investigated to examine their electronic structure, their electrochemical properties, and their ability to oxidize methanol.

Acknowledgments

The following institutions have provided funding for this work:

The Petroleum Research Fund (PRF) administered by the American Chemical Society (ACS-PRF 33960-G3 and ACS-PRF 37653-AC3).

The Research Associates of the Department of Chemistry, University of Cincinnati.

Procter and Gamble, (Research Fellowship).

Grant In Aid of Research, National Academy of Sciences, Administered by Sigma Xi, The Scientific Research Society.

The Department of Chemistry, University of Cincinnati.

X-ray crystallographic data were obtained by Jeanette A. Krause Bauer through the Ohio Crystallographic Consortium located at the University of Toledo, Toledo, Ohio 43606 (Ohio Board of Regents 1995 Investment Fund CAP-075) and through Dr. Alan Pinkerton, Department of Chemistry, University of Toledo. Mass spectral data were collected at the University of Cincinnati Mass Spectrometry Facility, which is part of the Ohio Mass Spectrometry Consortium.

The following people worked on this project in our lab:

Dr. Michael J. Goldcamp, Dr. Dell T. Rosa, Elizabeth A. Deters, Leah N. Squires, Neil K. Vowels, Jason Juang, Nicholas A. Landers, and Dr. Rick Hotz.

These people donated their time and skills:

Jeanette A. Krause Bauer (X-ray crystallography, UC), Nathan L. Coker (Mr. Fix-It, UC), Necati Kaval and Sean D. Conklin (spectroelectrochemistry, UC), Lionel Cheruzel (EPR, University of Louisville), Derek W. Yoder and Matthew J. Kidd (XANES, University of Michigan).

The following people put up with my Chemqueen drama:
Jeremy Edison, Janet and Perry Robison, Rachel Zipperian, Michelle Bernard, Tony Carman, Melanie Moses, and the Fricke.

Table of Contents:

List of Figures, Tables, and Schemes

List of Symbols and Abbreviations.

TACO = *N*,*N*,*N*-trimethyl-*N*-(1-propan-2-onyl oxime)ammonium chloride
GLABOH_3 = *N*,*N*-bis(1-propan-2-onyl oxime)-glycine *N*’-methylamide
PRABOH_2 = N-*n*-propyl-N,N-bis(1-propan-2-onyl oxime)amine
BALBOH_2K = potassium *N*,*N*-bis(1-propan-2-onyl oxime)- β-alaninate
GLYBOH_2K = potassium *N*,*N*-bis(1-propan-2-onyl oxime)-glycinate
TRISOXH_3 = tris(1-propan-2-onyl oxime)amine
PAMBOH_3 = *N*,*N*-bis(1-propan-2-onyl oxime)-L-phenylalanine *N*’-methylamide
PEABOH_2 = N-phenethyl-N,N-bis(1-propan-2-onyl oxime)amine
ABOH_2 = N-phenyl-N,N-bis(1-propan-2-onyl oxime)amine
OBOH_2 = N-*n*-octyl-N,N-bis(1-propan-2-onyl oxime)amine
Fc^+ = ferrocenium
Fc = ferrocene
PPh_3 = triphenylphosphine
$OPPh_3$ or $O{=}PPh_3$ = triphenylphosphine oxide
FTIR = Fourier transform infrared
NMR = nuclear magnetic resonance
EPR = electron paramagnetic resonance
CV = cyclic voltammagram or cyclic voltammetry
UV/vis = ultraviolet / visible
%T = percent transmittance
ε = molar absorptivity
GC = gas chromatography
MS = mass spectrometry
FID = flame ionization detector
BE = bulk electrolysis
CHN = carbon, hydrogen, nitrogen elemental analysis

Chapter 1. Introduction to Oxygen Activation by Nickel(II) Complexes.

1.1 Introduction. The reaction of transition metals with dioxygen is of interest and importance in both biological systems and in industrial oxidation processes.[1] This is because many organic substrates display an increase in value and utility upon oxidation.[2] Dioxygen is an excellent candidate for use as an oxidant for several reasons. It is cheap (or free), abundant, and environmentally friendly, unlike many of the commonly used stoichiometric oxidants such as chromates. However, O_2 does have the formidable drawback of being unable to oxidize many substrates of interest, as well as being kinetically unfavorable in many oxidation reactions. In order to overcome this second hurdle, transition metal catalysts are often used to promote the reaction by reducing dioxygen to various intermediates, such as superoxide (O_2^-), peroxide (O_2^{2-}) and oxo (O^{2-}), which can then perform the useful oxidation chemistry. The formation of superoxide by transition metal complexes occurs upon single electron reduction of O_2. Reduction of dioxygen by two electrons results in the formation of several peroxo complexes such as *cis*-μ-1,2-peroxo or *trans*-μ-1,2-peroxo end-on bridging forms, the μ-η^2: η^2-peroxo side-on bridging form, and the monodentate peroxides and hydroperoxides. There are also examples of bis(μ-oxo) dinuclear complexes that are formed from a four electron reduction of O_2.[3-5] The reduction of O_2 occurs via an inner sphere electron transfer, and many first row transition metals (Fe(II), Mn(II), Co(II), Cu(I)) appear to react with dioxygen, forming oxo, peroxo and superoxide species.[6-9] Examples are shown in Figure 1.1.

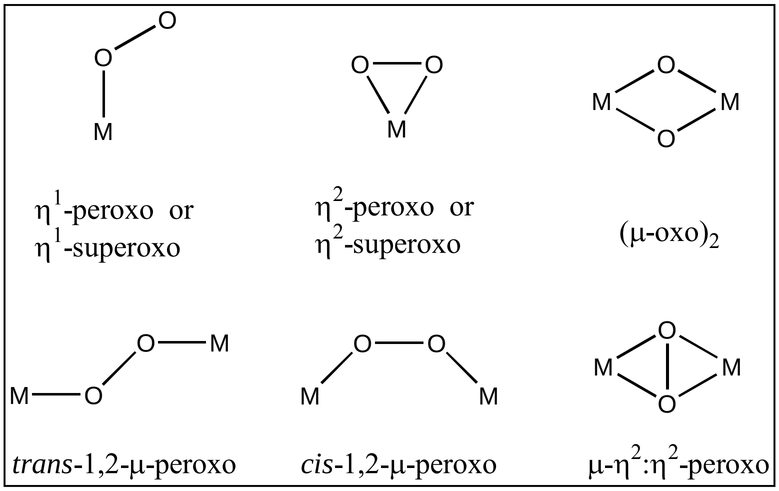

Figure 1.1. Structures and binding modes of metal-dioxygen adducts.

Nickel, in its most common oxidation state of 2+, does not typically react with dioxygen. This is due in part to the relatively high oxidation potentials for the Ni(II)/Ni(III) and Ni(III)/Ni(IV) couples. There are a few instances reported in the literature where a Ni(II) complex reacts with O_2; however, it is always due to ligand oxidation. For example, in the reaction of a Ni-peptide complex with dioxygen, hydroxylation of the peptide occurs rather than oxidation of the metal.[10-13] In these reactions, a Ni(III)-superoxide intermediate is believed to be responsible for the reactivity. Another system in which ligand hydroxylation promotes O_2 reactivity involves Ni(II)-macrocycle complexes that contain amidate donor groups.

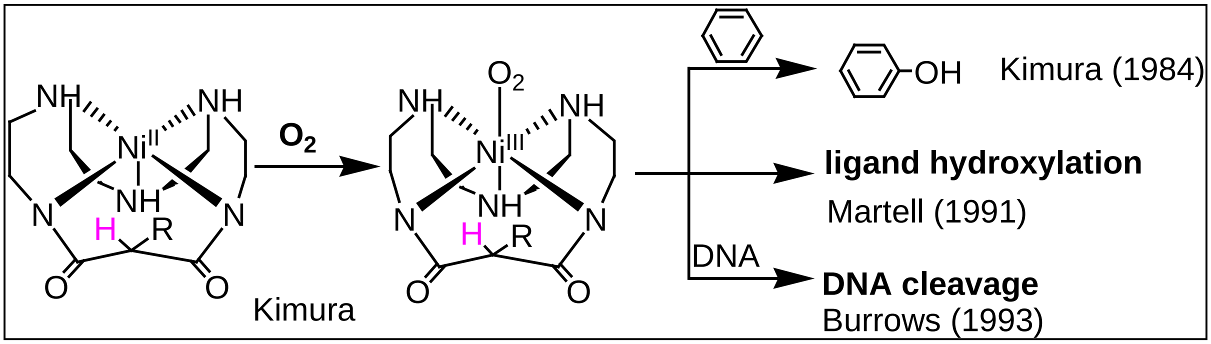

Figure 1.2. A Ni(II) macrocyclic amidate complex that reacts with dioxygen. Ligand hydroxylation occurs at the hydrogen indicated in pink.[14-17]

Here, a putative Ni(III)-superoxide is proposed as the active species. Figure 1.2 shows this reaction.

Although this reaction was initially shown to perform substrate oxidations,[14,15] later researchers determined that ligand hydroxylation was actually the main reaction pathway and the substrate oxidations were the result of a minor secondary reaction.[16,17] Ni(II) thiolates have also been shown to be oxygen active. However, oxidation occurs on the sulfur forming various sulfur oxygenates.[18] It is proposed that the thiolate sulfur must be converted to a sulfur-oxo or a thioether derivative for Ni(III) to be stable relative to sulfur oxidation. Figure 1.3 shows this reaction. The oxidation of all of these thiolate and amidate ligands makes the complexes unsuitable for catalysis.

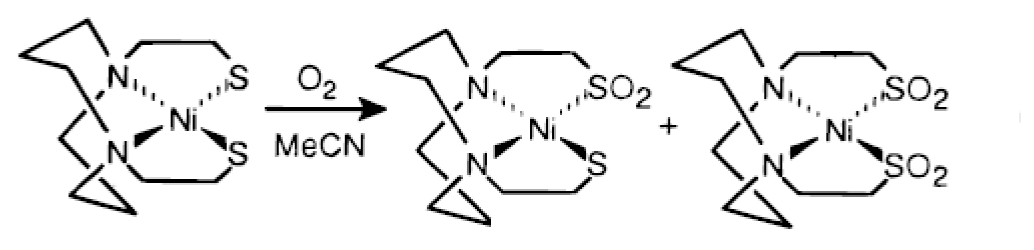

Figure 1.3. Reaction of a Ni(II) thiolate with dioxygen to form sulfur oxygenates.[18]

Another approach to achieving oxygen activation of nickel is to start with a reduced form of oxygen relative to O_2. For example, hydrogen peroxide has been used to produce $Ni(III)_2$ bis(μ-oxo) dimers from a Ni(II) complex of pyridyl containing ligands. These complexes display a characteristic UV/vis absorption band at approximately 410 nm as well as a resonance Raman band at 600-610 cm^{-1} that shifts to 570-580 cm^{-1} upon ^{18}O substitution. It is postulated, based on kinetic studies and isotope labeling experiments, that an intermediate, for example a peroxo dinickel(II) dimer, is present during the formation of the bis(μ-oxo)dinickel(III) complex. These bis(μ-oxo)dinickel(III) complexes also appear to perform hydrogen atom abstraction chemistry, not only from the substrate moiety, but also from exogenous H-atom donors such as phenols and 1,4-cyclohexadiene.[5]

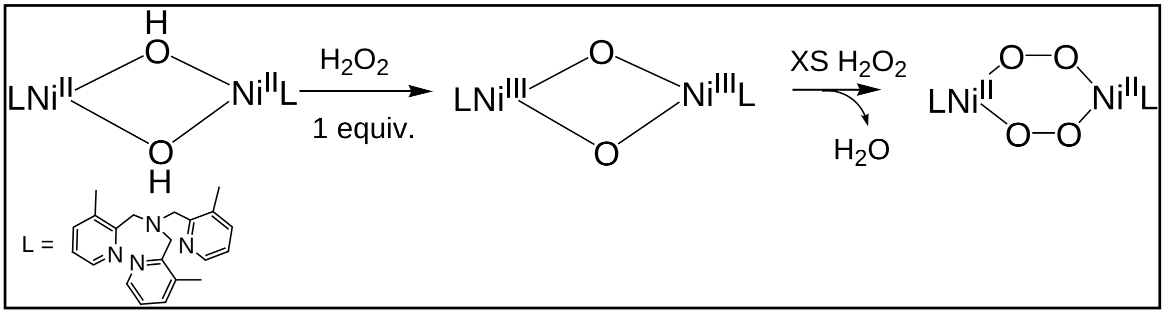

Figure 1.4. Structure of a bis(μ-oxo)Ni^{III}_2.[5]

Excess hydrogen peroxide has been shown to form a $Ni(II)_2$(μ-superoxo)$_2$ dimer from a $Ni(II)_2$(μ-$OH)_2$ complex whose ligand also consisted of pyridyl groups, as shown in Figure 1.4. In this reaction, one equivalent of H_2O_2 was added to the $Ni(II)_2$(μ-$OH)_2$ complex to form a Ni(III)(μ-$O)_2$Ni(III) complex which was then further reacted with excess (> 10 equivalents) hydrogen peroxide to yield the superoxo dimer. All three nickel complexes were characterized by X-ray crystallography. The $Ni(II)_2$(μ-superoxo)$_2$ dimer was also analyzed by resonance Raman spectroscopy. This analysis revealed an isotope-sensitive band at 1096 cm^{-1} that shifted to 1044 cm^{-1} upon labeling with $^{18}O_2$. These complexes appear to be stable at low temperatures, but at > -20 ^{o}C both the $Ni(III)_2$bis(μ-oxo) complex and the $Ni(II)_2$(μ-superoxo)$_2$ complex decompose with partial hydroxylation of one of the methyl groups on the ligand. Furthermore, in the superoxo complex, decomposition causes one of the methyl groups to become oxidized to a carboxylate group, and evolution of dioxygen is also observed during the decomposition process. This indicates that a possible decomposition pathway for the superoxo complex involves disproportionation of two coordinated superoxides to dioxygen and peroxide followed by scission of the O-O bond of peroxide to regenerate the bis(μ-oxo)Ni(III)$_2$ complex which can then perform the hydroxylation and the oxidation of the methyl group on the ligand. The Ni(II)$_2$(μ-superoxo)$_2$ species is also able to oxidize external substrates, such as 2,4-di-*tert*-butylphenol and triphenylphosphine.[1]

It has also been demonstrated that Ni(I)thioether complexes can react at low temperatures to form Ni(III)$_2$(μ-O)$_2$ complexes (Figure 1.5). This approach uses a reduced form of nickel (Ni(I)), relative to Ni(II), to induce oxygen activation. These complexes have been characterized spectroscopically, displaying two intense MLCT bands at 410 nm and 565 nm. The complexes are EPR silent (due to the antiferromagnetic coupling between the two Ni(III)s) and have a peak at 585 cm^{-1} in the resonance Raman spectrum that shifts to 555 cm^{-1} upon isotopic labeling with $^{18}O_2$. X-ray absorption spectroscopy confirms that a Ni(III) oxidation state is present and the Ni EXAFS data corroborate the Ni(III)$_2$(μ-O)$_2$ core, with an average Ni-O distance of 1.82 Å and a Ni scatterer at 2.83 Å.[4]

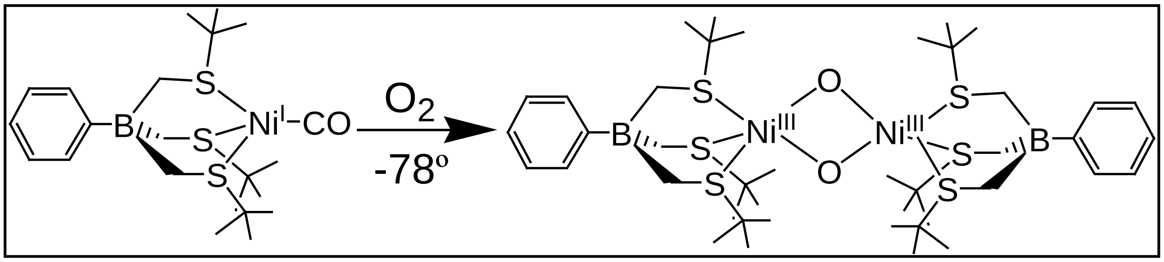

Figure 1.5. Ni(I)-thioether complex which reacts at low temperature with dioxygen to form a Ni(III)$_2$(μ-O)$_2$ dimer, a four electron transfer.

Additionally, Ni(II)/O$_2$ systems have been reported to perform epoxidation reactions when aldehydes are also present.[19-21] It is speculated that the metal initiates free radical formation in the aldehydes, which then react with O_2 to form peroxy acids, the active oxygenation species.

Recently, the reaction of a π-allylnickel(II)(N-heterocyclic carbene) chloride complex with O_2 was reported. This reaction forms a μ-hydroxo Ni(II) dimer, as confirmed by X-ray crystallography, and cinnamaldehyde and phenyl vinyl ketone in a 5:3 ratio. The carbonyl containing products are due to oxidation of the π-allyl coligand and isotopic labeling with $^{18}O_2$ showed that the oxygen on both of the carbonyls and the hydroxo linkage was from O_2. Figure 1.6 shows this reaction.[22]

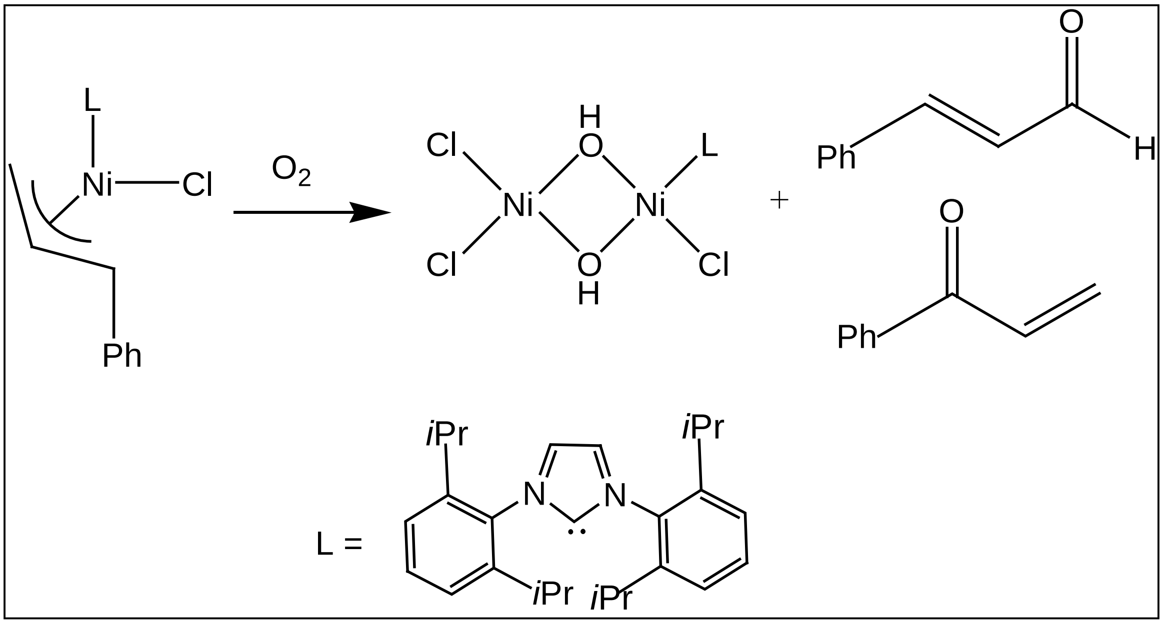

Figure 1.6. Reaction of a π–allylnickel(II)(N-heterocyclic carbene) chloride complex with dioxygen.[23]

1.2 Designing an oxygen active nickel(II) complex to accomplish substrate oxidations. None of the previously mentioned systems involved reaction of a Ni(II) complex with O_2, nature's primary oxidant, without irreversible ligand oxidation. Therefore, the Baldwin group embarked on a project to design a ligand system that would allow oxygen activation of a Ni(II) complex to do catalytic substrate oxidations. This is a significant project because nickel is cheaper than many other transition metals used in catalysis and O_2 is an inexpensive and environmentally friendly oxidant.

As mentioned previously, the oxidation potentials to access high valent nickel are usually too high (≥ +500 mV vs. the ferrocinium/ferrocene (Fc^+/Fc) couple) for dioxygen reactivity to occur. Lowering the oxidation potentials can allow oxygen activity to occur. It has been demonstrated that strongly electron-donating ligands can support high valent nickel. Ligands containing amidate (deprotonated amide) donor groups often form stable Ni(III) complexes.[23-24] Ni(IV) amidate complexes are also known, although they are not as prevalent.[25] Ligands containing oximate (deprotonated oxime) donor groups are known to stabilize Ni(IV) complexes,[26-30] as well as some Ni(III) complexes.[31] Examples of oximate and amidate functional groups are shown in Figure 1.7.

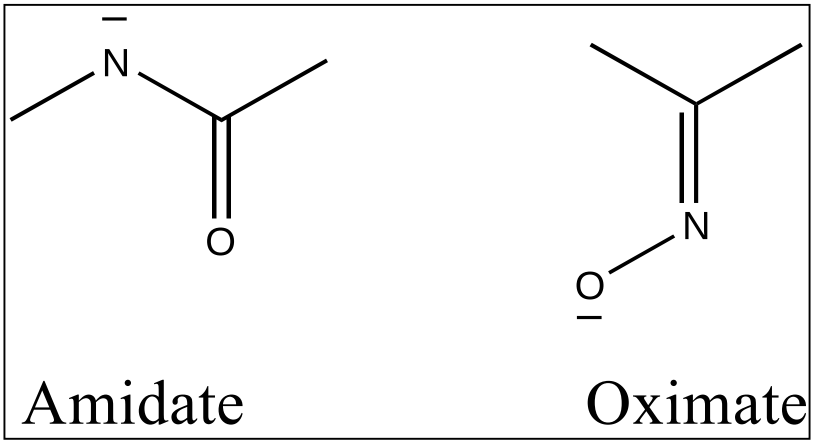

Figure 1.7. Amidate and oximate groups have been shown to stabilize high valent nickel.

In order to access higher nickel oxidation states, our group has designed a library of ligands based on a tripodal amine framework that contains at least two oxime arms that can be deprotonated to provide oximate donor groups. This tripodal amine motif allows dioxygen to coordinate to the metal, which allows inner sphere activation to occur. The ligands provide two available *cis*-coordination positions that can accommodate multiple binding modes of O_2 and its reduced intermediates. Another advantage of the ligand framework is that it avoids the common Ni(II) square planar coordination geometry. Although square planar structures have two axial coordination positions available, they resist inner sphere reactivity.[32] A fairly large ligand field energy barrier must be overcome when changing from a square planar to a square mono-pyramidal geometry upon binding of O_2. It is therefore advantageous to avoid square planar geometry in complexes designed to react with dioxygen. The X-ray crystal structures of the Ni(II) complexes of our neutral ligands reveal a six-coordinate psuedo-octahedral geometry, with the two available coordination positions being occupied by counter ions or solvent. These ligands are sufficiently labile in solution to allow dioxygen reactivity to take place.

In addition to the two oxime arms on the tripodal amine ligands in the library, a variable third arm is present that can be changed to control the electronic structure of the complex and to tune different chemical and physical properties to ultimately tune and enhance the reactivity. These complexes have non-coordinating third arms (alkyl and aryl groups), weakly coordinating third arms (amidates), or strongly coordinating third arms (alcohol, pyridyl, carboxylate, and oximate groups). This library can be viewed in Figure 1.8.[33]

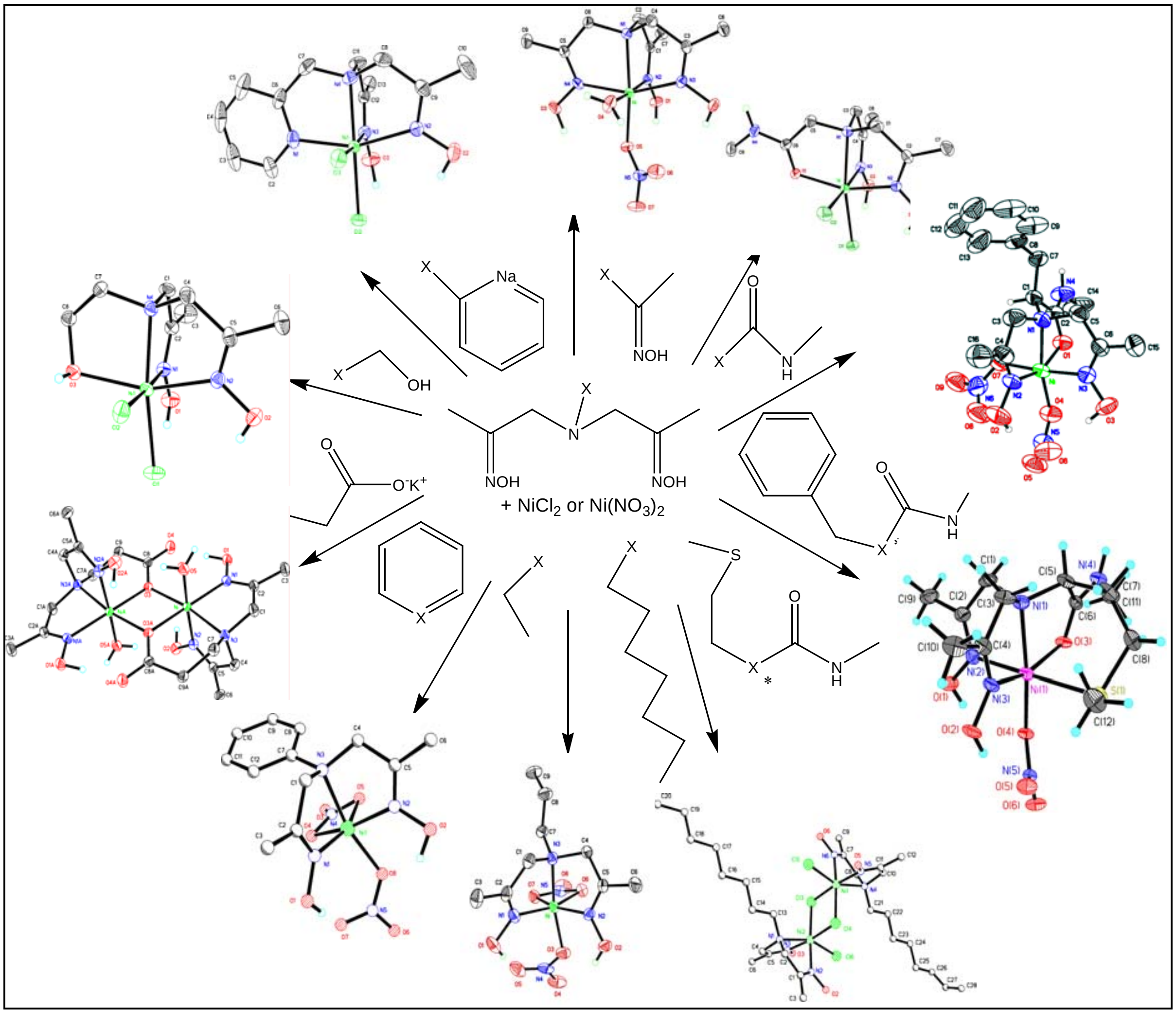

Figure 1.8. X-ray crystal structures in the Baldwin Group library.[33]

The electronic, electrochemical, and reactivity properties of many of the members of the ligand library were studied during this project and the results, along with the synthesis of the ligand and complex containing on octyl group as the third arm, can be found in Chapter 4.

Chapters 2 and 3 report the reactivity and spectroscopic studies of [Ni(TRISOXH$_3$)(NO$_3$)(H$_2$O)](NO$_3$)• (H$_2$O), **1**.

1.3. Previous work on [Ni(TRISOXH$_3$)(NO$_3$)(H$_2$O)](NO$_3$)• (H$_2$O). The original ligand and complex synthesis and characterization was performed by Dr. Michael Goldcamp, a former Baldwin group member.[34] The crystal structure is shown in Figure 1.9. Dr. Goldcamp observed that addition of base resulted in the formation of an oxygen active species, **3**. This species undergoes a color change from purple to brown that is not observed under anaerobic conditions.

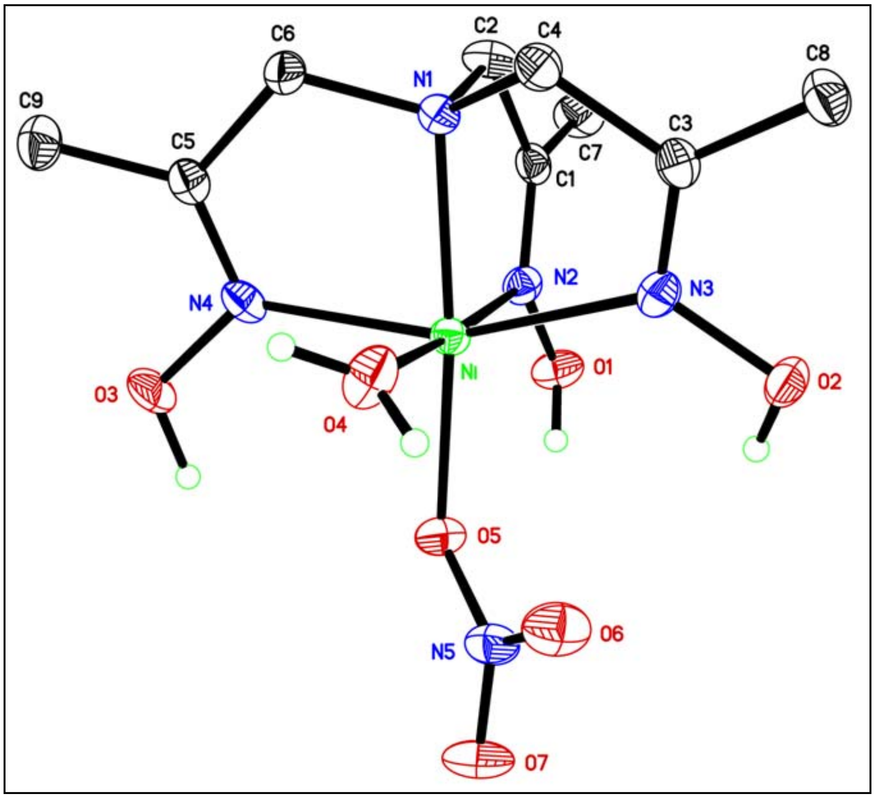

Figure 1.9. X-ray crystal structure of **1**.

This dissertation describes the investigation of the reaction between **3** and molecular oxygen. The reactivity of the complex was studied and it was revealed that the oxygen reaction requires an exogenous source of hydrogen atoms to drive the reaction (see Chapter 2). Several different substrates were observed to undergo oxidation via two-hydrogen atom abstraction, making this the first reported homogeneous Ni(II) catalyst that reacts with dioxygen without undergoing irreversible ligand oxidation.[35] The substrates oxidized include methanol, ethanol, benzyl alcohol, benzylamine and *N*-methylbenzylamine. Triphenylphosphine is also oxidized, although the oxidation is through oxygen atom transfer rather than hydrogen atom abstraction.

A wide variety of spectroscopic techniques were also utilized in this project, including UV/visible absorption spectroscopy, spectroelectrochemistry, electron paramagnetic resonance, resonance Raman, and X-ray absorbance spectroscopies. The information obtained from these experiments, combined with the insights gained from the reactivity studies allowed the formation of a proposed reaction scheme, which is described in Chapter 3.

1.4. Biological implications. Many biological systems contain oxygen active transition metal centers that catalyze various oxidation reactions very efficiently. Although nickel is present in several enzymes such as urease, hydrogenase, and Ni superoxide dismutase, it typically does not promote biological oxidation reactions in conjunction with dioxygen.[36] However, a nickel dioxygenase (Ni-acireductone dioxygenase) has been reported to produce methylthiopropionate, carbon monoxide and formate.[37] The metal center is six-coordinate with oxygen and nitrogen donor ligands.

Studying the factors necessary to allow a normally non-oxygen active transition metal to become oxygen active provides insight into the metal dioxygen reactions observed in nature. For example, galactose oxidase, a copper containing enzyme, catalyzes the oxidation of a primary alcohol to form an aldehyde, ammonia, and hydrogen peroxide, which is observed in our reaction between **3** and O_2 in primary alcohols.[38] Copper amine oxidases promote the oxidation of primary amines to form an aldehyde and hydrogen peroxide.[39] This is a possible reaction pathway for our reaction of **3** and O_2 with a primary amine. Finally, heme and manganese catalase enzymes catalyze the disproportionation of hydrogen peroxide, as does **3**.[40-41] This is discussed in Chapter 3.

1.5. Conclusions. This dissertation describes the spectroscopic and reactivity studies of an unusual Ni(II) polyoximate complex that reacts with dioxygen in the presence of a two-hydrogen atom donating substrate to produce multiple equivalents of oxidized product. The reaction was studied spectrocopically and insight was gained into the processes involved.

References

(1) Shiren, K.; Ogo, S.; Fujinami, S.; Hayashi, H.; Suzuki, M.; Uehara, A.; Watanabe, Y.; Moro-oka, Y. *J. Am. Chem. Soc.* **2000**, *122*, 254.

(2) Drago, R. S.; Beer, R. H. *Inorg. Chim. Acta,* **1992**, *198-200*, 359.

(3) Holland, P. L.; Cramer, C. J.; Wilkinson, E. C.; Mahapatra, S.; Rodgers, K. R.; Itoh, S.; Taki, M.; Fukuzumi, S.; Que., L. Jr.; Tolman, W. B. *J. Am.Chem. Soc.*, **2000**, *122*, 792.

(4) Mandimutsira, B. S.; Yamarik, J. L.; Brunold, T. C.; Gu, W.; Cramer, S. P.; Riordan, C. G. *J. Am, Chem. Soc.*, **2001**, *123*, 9194.

(5) Itoh, S.; Bandoh, H.; Nakagawa, M., Nagatomo, S., Kitagawa, T.; Karlin, K. D.; Fukuzumi, S. *J. Am. Chem. Soc.*, **2001**, *123*, 11168.

(6) Kitajima, N.; Moro-oka, Y. *Chem. Rev.* **1994**, *94*, 737.

(7) Feig, A. L.; Lippard, S. J. *Chem. Rev.* **1994**, *94*, 759.

(8) Pecoraro, V. L.; Baldwin, M. J.; Gelasco, A. *Chem. Rev.* **1994**, *94*, 807.

(9) Soloman, E. I. ; Tuczek, F.; Root, D. E.; Brown, C. A. *Chem. Rev.* **1994**, *94*, 827.

(10) Bossu, F. P.; Paniago, E. B.; Margerum, D. W.; Kirskey, S. T. J.; Kurtz, J. L. *Inorg. Chem.*, **1978**, *17*, 1034.

(11) Bal, W.; Djuran, M. I.; Margerum, D. W.; Gray, E. T. J.; Mazid, M. A.; Tom, R. T.; Nieboer, E.; Sadler, P. J. *J. Chem. Soc., Chem. Commun.*, **1994**, 1889.

(12) Cotelle, N.; Tremolieres, E.; Bernier, J. L.; Catteau, J. P.; Henichart, J. P. J. *Inorg. Biochem.* **1992**, *46*, 7.

(13) Inoue, S.; Kawanishi, S. *Biochem. Biophys. Res. Commun.* **1989**, *159,* 445.

(14) Machida, R.; Kimura, E.; Kushi, Y. *Inorg. Chem.* **1986**, *25*, 3461.

(15) Kimura, E.; Sasada, M.; Shionoya, M.; Koike, T.; Kurosaki, H.; Shiro, M. *J. Bioinorg. Chem.* **1997**, *2*, 74.

(16) Cheng, C.-C.; Gulia, J.; Rokita, S. E.; Burrows, C. J. *N. Mol. Catal. A.,* **1996**, *113*, 379-391.

(17) Chen, D.; Motekaitis, R. J.; Martell, A. E. *Inorg. Chem.*, **1991**, *30*, 1396.

(18) Grapperhaus, C. A.; Darensbourg, M. Y. *Acc. Chem. Res.,***1998**, *31*, 451-459.

(19) Yamada, T.; Takai, T.; Rhode, O.; Mukaiyama, T. *Bull. Chem. Soc. Jpn.* **1991**, *64*, 2109.

(20) Nishida, Y.; Takahashi, S.; Watanabe, I. *Chem. Lett.* **1993**, 17.

(21) Nam, W.; Kim, H. J.; Kim, S. H.; Ho, R. Y. N.; Valentine, J. S. *Inorg. Chem.* **1996**, *35*, 1045.

(22) Dibble, B. R.; Sigman, M. S. *J. Am. Chem. Soc.* **2003,** *125*, 872-873.

(23) Collins, T. J.; Nichols, T. R.; Uffelman, E. S. *J. Am. Chem. Soc.* **1991**, *113*, 4708.

(24) Ray, M.; Hammes, B. S.; Yap, G. P. A.; Rheingold, A. L.; Borovik, A. S. *Inorg. Chem.* **1998**, *37*, 1527.

(25) Patra, A. K.; Mukherjee, R. *Inorg. Chem.* **1999**, *38*, 1388.

(26) Sproul, G.; Stucky, G. D. *Inorg. Chem.* **1973**, *12,* 2898.

(27) Singh, A. N.; Singh, R. P.; Mohanty, J. G.; Chakravorty, A. *Inorg. Chem.* **1997**, *16*, 2597.

(28) Mohanty, J. G.; Singh, R. P.; Chakravorty, A. *Inorg. Chem.* **1975**, *14,* 2178.

(29) Korvenranta, J.; Saarinen, H.; Nasakkala, M. *Inorg. Chem.* **1982**, *21,* 4296.

(30) Martone, D. P.; Osvath, P.; Lappin, A. G. *Inorg. Chem.* **1987**, *26,* 3094.

(31) Singh, A. N.; Chakravorty, A. *Inorg. Chem.* **1980**, *19,* 969.

(32) Cha, M.; Gatlin, C. L.; Critchlow, S. C.; Kovacs, J. A. *Inorg. Chem.* **1993**, *32,* 5868.

(33) Goldcamp, M. J.; Edison, S. E.; Squires, L. N.; Rosa, D. T.; Vowels, N. K.; Krause Bauer, J. A.; Coker, N. L.; Baldwin, M. J. *Inorg. Chem.* **2003**, *42,* 717-728.

(34) Goldcamp, M. J.; Robison, S. E.; Krause Bauer, J. A.; Baldwin, M. J. *Inorg. Chem.* **2002,** *41*, 2307-2309.

(35) Edison, S. E.; Hotz, R. P.; Baldwin, M. J. *Chem. Comm.*, in press.

(36) Hausinger, Robert. P. Biochemistry of Nickel, New York, Plenum Press, **1993**.

(37) Al-Mjeni, F.; Ju, T.; Pochapsky, T. C.; Maroney, M. J. *Biochemistry,* **2002**, *41*, 6761-6769.

(38) Clark, K.; Penner-Hahn, J. E.; Whittaker, M. M.; Whittaker, J. W. *J. Am. Chem. Soc.,* **1990**, *112*, 6433-6434.

(39) Mure, M.; Klinman, J. P. *J. Amer. Chem. Soc.,***1995,***117,* 8698-8706.

(40) Putnam, C. D.; Arvai, A. S.; Bourne, Y.; Trainer, J. A. *J. Mol. Biol.*, **2000**, *296*, 295-309.

(41) Wu, A. J.; Penner-Hahn, J. E.; Pecoraro, V. L. *Chem. Rev.*, **2004**, *104*, 903-938.

Chapter 2. Reactivity Studies of $[Ni(II)(TRISOX)]_2^{2-}$

2.1. Introduction.

The observation that addition of three equivalents of hydroxide to a methanolic solution of **1** in the presence of dioxygen results in a color change from purple to brown that is absent under anaerobic conditions[1] led to a series of experiments designed to investigate the conditions necessary for the reaction to occur. The first parameter scrutinized was the solvent. Performing the deprotonation reaction in acetonitrile in the presence of dioxygen did not produce the expected color change to brown – instead, a darker purple color was observed. Attempts to grow a crystal of this darker purple complex were unsuccessful; however, a crystal of the light purple, singly deprotonated complex was obtained by vapor diffusion of diethyl ether into an acetonitrile solution (see Figure 2.1).

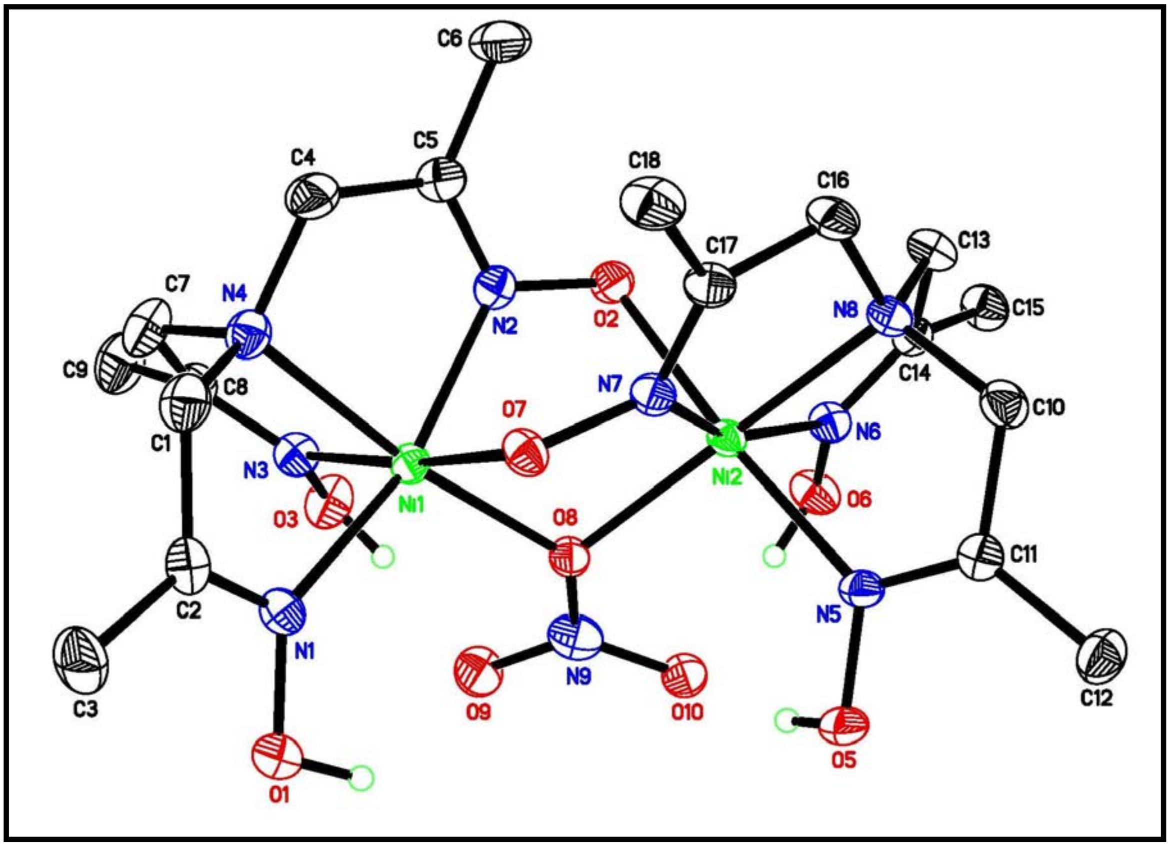

Figure 2.1. X-ray crystal structure of singly deprotonated $[(Ni(TRISOX))_2(NO_3)]^-$

A full report of the X-ray crystallographic data is available in Appendix A.

From the X-ray data, it can be seen that the oximate has formed a bridge to another nickel complex in solution, forming a dimer containing two oximate bridges and a third bridge from a nitrate group. Each nickel is six coordinate pseudo-octahedral. The nitrate bridge in this structure differs from a previously published structure obtained by Dr. Goldcamp, in which the dimeric species is bridged by two oximates and an acetonitrile molecule fills the remaining coordination position on each nickel.[1] In the previously published structure the acetonitrile molecules are trans to each other, suggesting that displacement of the solvent to allow substrate binding in a cis fashion would be difficult in that ligand configuration. Based on the structure in Figure 2.1 it seems reasonable to speculate that the oxygen active species (**3**) is also a dimer and that O_2 or a possible substrate could displace the nitrate bridge and bind in that pocket.

2.2 Oxidation of methanol to form formaldehyde.

Addition of methanol to the acetonitrile solution of **3** caused the purple solution to turn brown. This led to the hypothesis that methanol was acting as an oxidation substrate that is required to drive this reaction, perhaps by losing two hydrogen atoms to form formaldehyde. The presence of formaldehyde was tested by addition of an aliquot of the sample to an equivalent volume of Hantzsch colorimetric reagent.[2] Figure 2.2 shows the reaction of the Hantzsch reagent with formaldehyde to form 3,5-diacetyl-1,4-dihydrolutidine (DDL), a bright yellow complex that has a molar absorptivity of 8000 M^{-1} cm^{-1} at 412 nm. Figure 2.23 shows the UV/vis spectra of standards containing known amounts of formaldehyde, **1**, and methanol and the Hantzsch reagent, as well as the calibration curve that was constructed based on the absorbance at 412 nm.

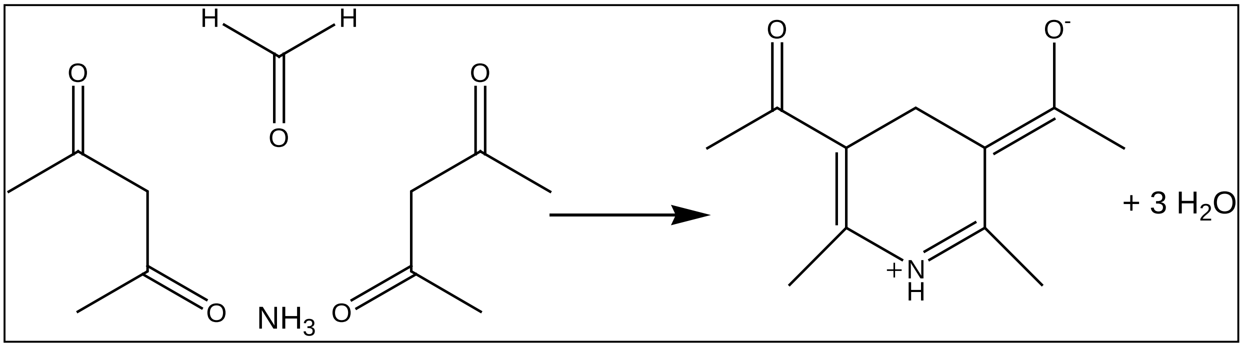

Figure 2.2. Formation of 3,5-diacetyl-1,4-dihydrolutidine (DDL) from reaction of formaldehyde with the Hantzsch reagent

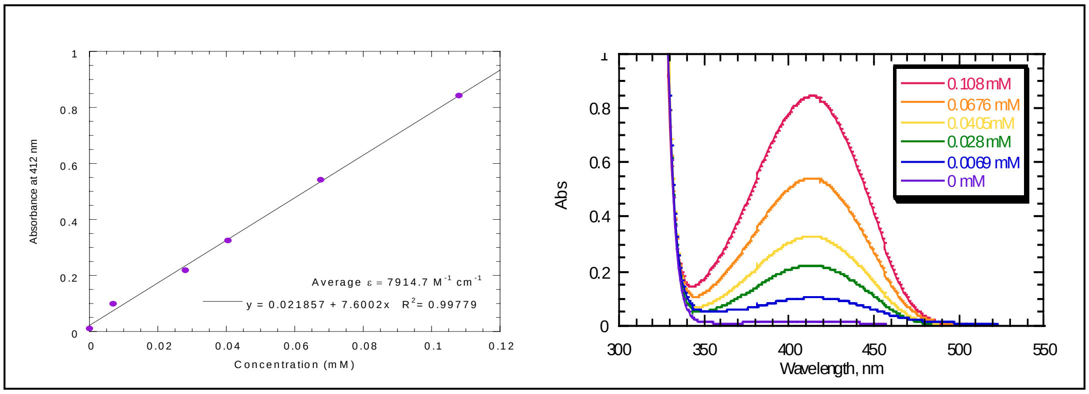

Figure 2.3. Calibration curve and UV/vis spectra of standards containing known amounts of formaldehyde, **1**, methanol, and the Hantzsch reagent. The legend indicates the amount of formaldehyde present.

Experimental. A typical 0.5 mM reaction solution consisted of 6.7 mg (0.0149 mmol) **1** dissolved in 30 mL of methanol that was distilled from calcium hydride. 0.05 mL of 1.0 M tetrabutylammonium hydroxide (in methanol) was added to form **3** and initiate the reaction with dioxygen, which is characterized by a rapid color change from purple to dark brown. The reaction was allowed to proceed for a designated amount of time and then stopped by removing a 1.0 mL aliquot of the sample and adding it to 1.0 mL of the Hantzsch reagent, which consisted of 3.8 g ammonium acetate, 75 µL acetic acid, and 50 µL acetyl acetone dissolved in 25 mL of deionized water. The sample containing the

Hantzch reagent and the nickel complex was diluted to about 90 mL with deionized water in a 100 mL volumetric flask. The reaction was considered quenched as the Hantzsch reagent is acidic (which stops the reaction with O_2) and water also inhibits the reaction. The pH was adjusted to 6.0 using dilute acetic acid and dilute sodium hydroxide and then the solution was diluted to the mark with deionized water. The solution was stored in the dark overnight as a bright yellow color developed (signifying the formation of DDL). The UV/vis spectrum of each sample was collected on a Hewlett-Packard 8453 spectrometer and the absorbance was monitored at 412 nm (the literature value of 8000 M^{-1} cm^{-1} was used for quantitation; experimental values ranging from 7800-8100 M^{-1} cm^{-1} were obtained while constructing the calibration curve that is shown in Figure 2.3. The standards used for the calibration curve were prepared by adding 1.0 mL of known concentrations of formaldehyde to 1.0 mL of the Hantzsch reagent and 1.0 mL of a 0.5 mM methanolic solution of **1**, and then following the above procedure for preparation of DDL.) From this, the concentration of formaldehyde present at different time points of the **3** + O_2 reaction was determined. Figure 2.4 tracks the amount of formaldehyde formed as a solution of **3** reacts with methanol and O_2. Each data point is the average of three identical trials and the error bars are the standard deviation between the three according to the following equation: $\sigma = \{[\Sigma\ (X_i-X_{ave})^2] / [n(n-1)]\}^{1/2}$. Although standard deviations based on only three data points are not as significant as those based on numerous data points, it can still give an idea of the experimental error involved.

Several variables were changed to attempt to optimize the reaction, and they will be described in the following section.

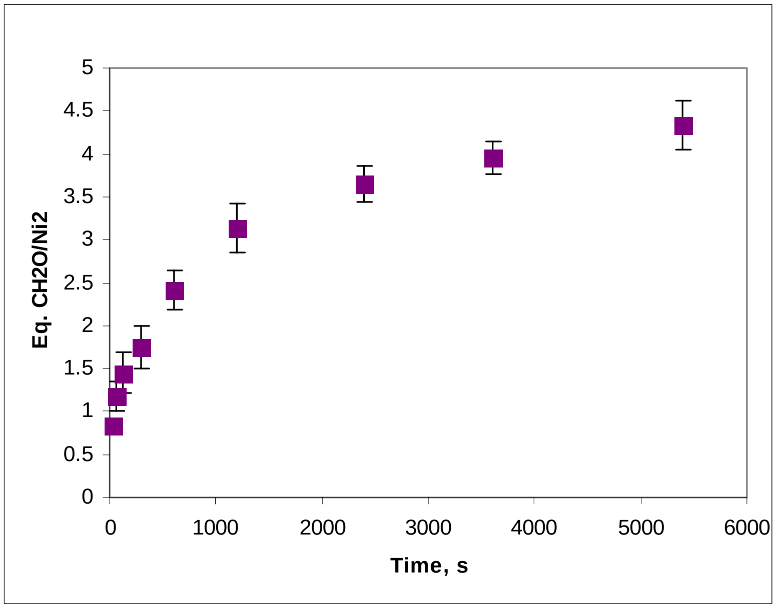

Figure 2.4. Plot of formaldehyde formed from the reaction of 2 mM **1** with KOH, methanol and dioxygen (after 24 hours 10.4 ± 0.45 eq./**3** are formed) versus time (each data point represents the average of three trials and the error bars are the standard deviations between the three trials).

Results and discussion. The methanol oxidation reaction was studied under varying reaction conditions to see if the amount of oxidized product could be increased and to learn more about the reaction by changing different parameters. The first variable studied was the concentration of **1**. Studying the concentration dependence can offer mechanistic insight into the kinetics of the reaction. Also, it was expected that if the "dead-end" product was a result of cluster formation, the amount of oxidized product formed per Ni may increase as the amount of nickel complex decreased. Three solutions (0.1, 0.5, and 2 mM) of **1** in methanol were prepared, deprotonated, and allowed to react with dioxygen. The amount of formaldehyde formed was monitored using the Hantzsch reagent. Figure 2.5 compares the results for the three concentrations.

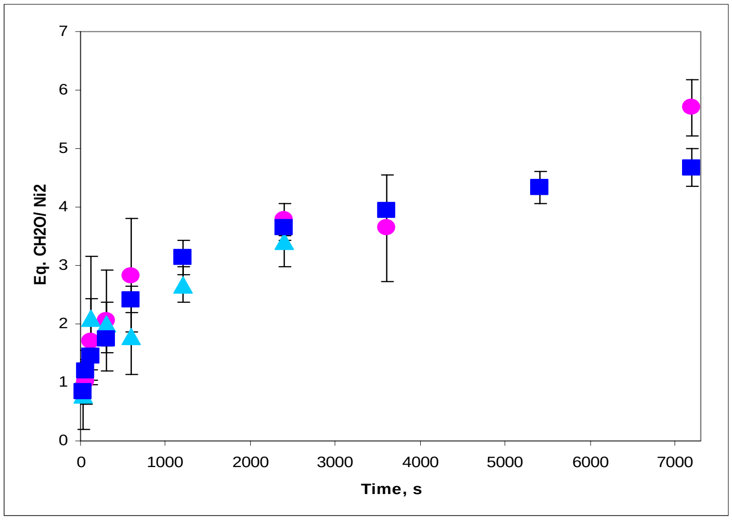

Figure 2.5. Plot of formaldehyde formed by **1**, KOH, O_2, and methanol versus time. Blue squares = 2mM, Blue triangles = 0.5 mM, Pink circles = 0.1 mM (each data point represents the average of three trials and the error bars are the standard deviations between the three trials).

As can be seen from Figure 2.5, changing the concentration of the nickel catalyst does not appear to affect the methanol oxidation reaction, even after twenty-four hours of reaction time when the complex is believed to have reached its dead-end point. After twenty-four hours each concentration investigated produced approximately 10 equivalents of formaldehyde.

The next variable investigated was the amount of dioxygen present in the solution. In one experiment, the oxidation reaction was conducted under atmospheric pressure of air and in another, pure dioxygen was bubbled through the solution. Figure 2.6 displays the results from this reaction. Within experimental error, these two experiments did not show a difference in the amount of formaldehyde formed, probably because the atmospheric sample contained enough dioxygen to saturate the sample. To test this, a 1 mM solution of **3** in methanol was prepared and sparged with argon for one hour. Next, 1 mL of air was syringed into the solution (~2 eq. of O_2/**3**) and allowed to react for one hour. After one hour the sample was worked up using the Hantzsch reagent and 0.61 ± 0.08 equivalents of formaldehyde per **3** were observed, compared to 3.95 ± 0.18 equivalents formed in the atmospheric sample after one hour. Therefore, decreasing the amount of dioxygen in the solution decreases the amount of formaldehyde formed, although diffusion of O_2 through the argon probably affected the reaction as well.

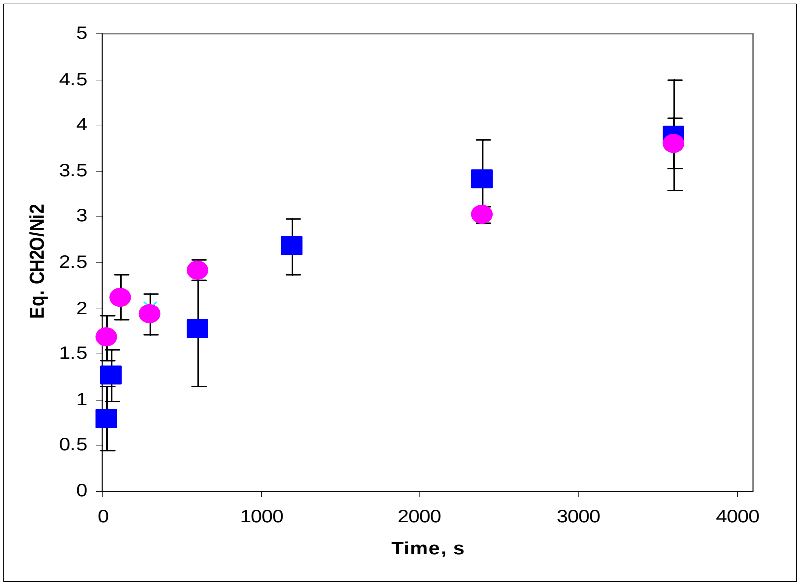

Figure 2.6. Plot of formaldehyde formed by **1**, KOH, O_2, and methanol versus time. Blue squares = atmospheric pressure, Pink circles = pure dioxygen (each data point represents the average of three trials and the error bars are the standard deviations between the three trials).

Another variable altered in this reaction was the amount of methanol present. It was anticipated that diluting the amount of methanol by adding other solvents would inhibit the reaction by either reducing the amount of methanol available and therefore reducing the amount of product formed or by competing for binding sites on the catalyst. To test this, varying amounts of acetonitrile were added to the reaction mixture. Figure 2.7 shows the results of adding 0%, 25%, 50%, and 75% acetonitrile to the solution.

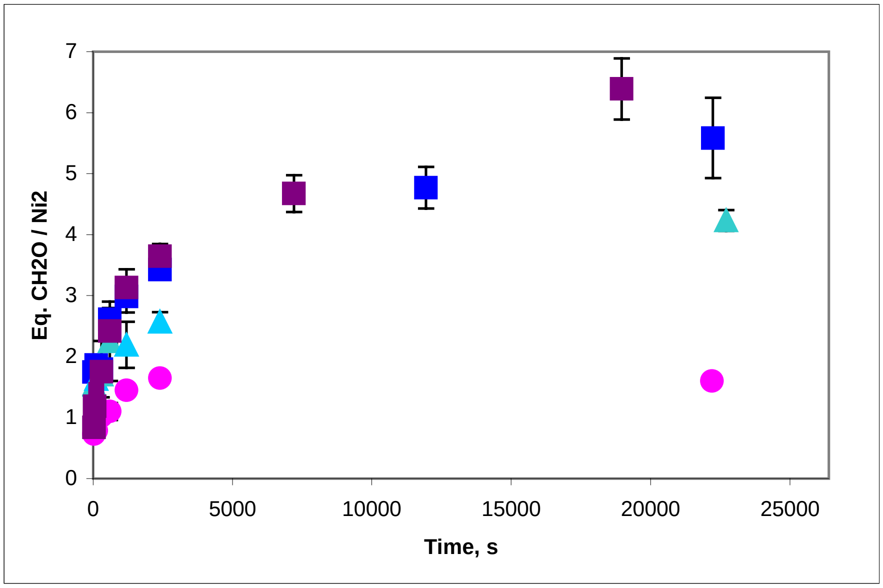

Figure 2.7. Plot of formaldehyde formed by **1**, KOH, O_2, and methanol versus time. Purple squares = 0% MeCN (24 hrs 10.4 ± 0.5) Blue squares = 25% MeCN (24 hrs 6.7 ± 0.2 eq./**3**), Blue triangles = 50% MeCN (24 hrs 5.1 ± 0.3 eq./**3**), Pink circles = 75% MeCN (24 hrs 2.5 ± 0.3 eq./**3**), (each data point represents the average of three trials and the error bars are the standard deviations between the three trials).

The reaction displays a dependence on the concentration of methanol, particularly at later times in the reaction. Decreasing the amount of methanol present decreased the amount of oxidized product formed per dimer in roughly the same amount. For example, solutions containing 25% MeOH produced 25% as much formaldehyde after twenty-four hours (2.5 ± 0.3 eq. compared to 10.4 ± 0.5 eq.in 100% MeOH).

Using water as the additive in place of acetonitrile caused an even more dramatic inhibition. Figure 2.8 shows the effect water has on the methanol oxidation reaction.

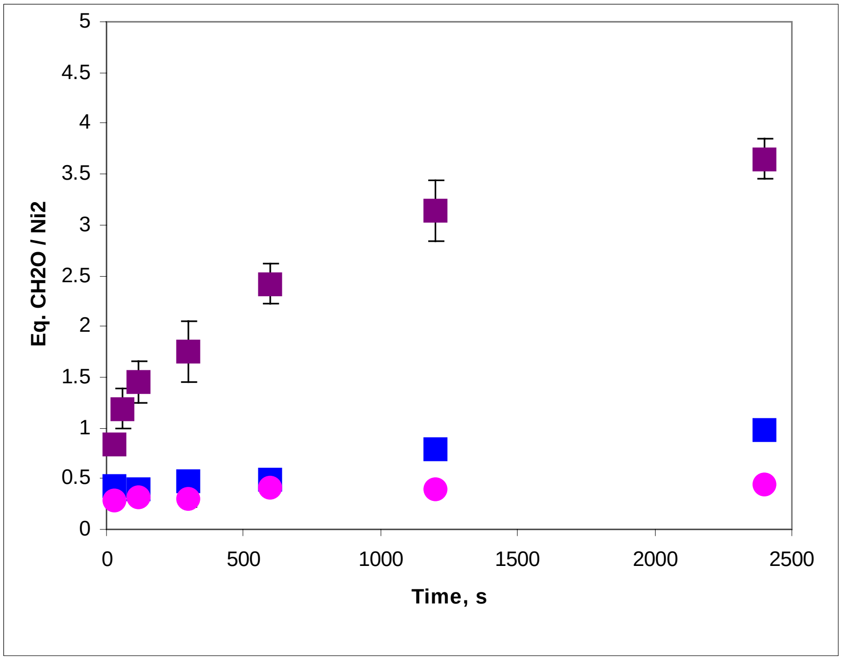

Figure 2.8. Plot of formation of formaldehyde by **1**, KOH, O_2, and methanol versus time. Purple squares = 0% H_2O (24 hrs 10.4 ± 0.5) Blue squares = 25% H_2O (24 hrs 1.6 ± 0.1 eq./**3**), Pink circles = 50% H_2O (24 hrs 0.9 ± 0.01 eq./**3**), (each data point represents the average of three trials and the error bars are the standard deviations between the three trials).

The addition of water significantly inhibited the formation of formaldehyde. In a solution containing 50% water the system ceased to be catalytic, with less than one equivalent of oxidized product being formed. Solutions containing 75% water did not display the expected color change from purple to brown, so they were not tested for formaldehyde.

Addition of one equivalent of methanol to an acetonitrile solution of **3** did not result in the expected color change to brown and it did not produce one equivalent of oxidized product. After eighteen hours of reaction time only 0.16 equivalents per **3** were observed.

Finally, the affect of the counter anion on the formation of formaldehyde was studied. Solutions containing 2 mM (Ni[TRISOX]X_2), where X = nitrate, chloride, perchlorate, or tetrafluoroborate counter anions, were prepared and the methanol oxidation reaction was repeated. It was expected that changing the counter anion would not significantly affect the oxidation because it was postulated that the active species, **3**, is a dimer with no counter anions coordinated to the metal. Figure 2.9 shows the affect that the counter anion has on the reactivity.

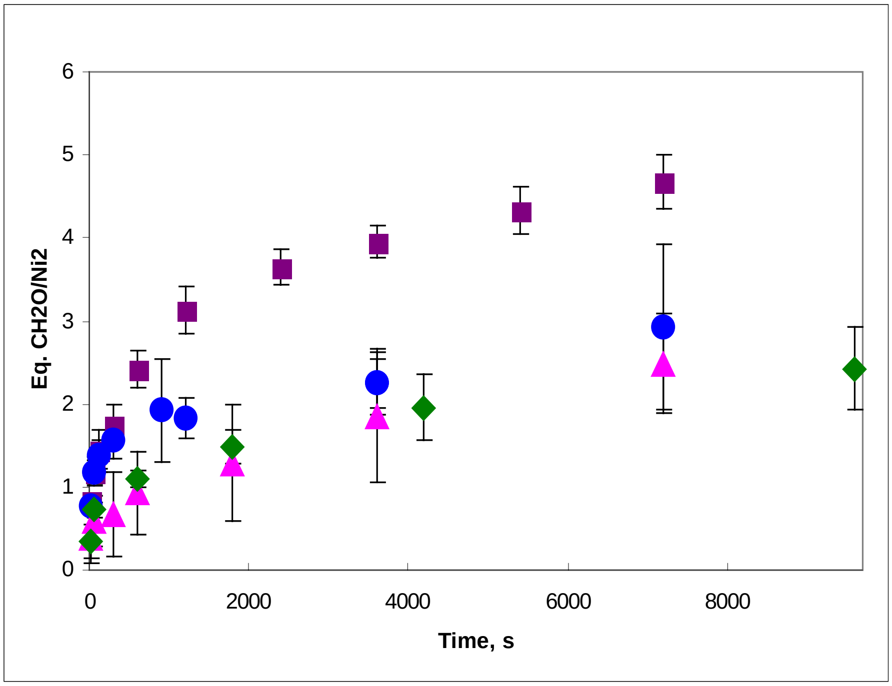

Figure 2.9. Plot of formaldehyde formation by **1** containing different counter anions, KOH, O_2, and methanol versus time. Purple squares = nitrate, Blue circles = chloride, Pink triangles = perchlorate, green diamonds = tetrafluoroborate (each data point represents the average of three trials and the error bars are the standard deviations between the three trials).

Surprisingly, as can be seen in Figure 2.9, the complex from the nitrate containing starting material produced more oxidized product than the other counter anions that performed in a similar fashion, although the chloride containing complex appeared to produce formaldehyde in an amount comparable to the nitrate containing complex during the beginning of the experiment. Interestingly, nitrate, perchlorate, and tetrafluoroborate are all weakly coordinating counterions, and thus would be expected to react in a similar fashion if the counter anion actually did play a role.

The role of the metal was also tested. A 3 mM solution of [Zn(TRISOX)Cl_2] was prepared and evaluated for formaldehyde production using the same procedure as the nickel experiment. Zinc, a d^{10} metal, is a spectroscopically silent and redox inactive metal, making it ideal for control experiments designed to test the role of the metal. The complex containing zinc produced 0.05 equivalents of formaldehyde per dimer after twenty-four hours, which is zero equivalents within experimental error, indicating that a redox active metal is required for the oxidation of methanol to occur. This result was confirmed by an additional control experiment involving a 3 mM solution of free ligand in methanol. This solution also did not produce formaldehyde upon addition of base.

Next, copper(II) was substituted in place of the nickel and a 3 mM [Cu(TRISOX)(NO_3)]•(NO_3) solution was evaluated for formaldehyde formation. After twenty-four hours, 0.62 equivalents of formaldehyde per dimeric species were observed. Copper is a redox active metal, yet it does not promote the oxidation reaction as efficiently as the nickel complex.

Based on the impact of the various parameters studied in this reaction, it was concluded that the oxidation is linearly dependent on the concentration of **3** and sensitive to the amount of dioxygen present (although more experiments are necessary to make conclusive statements). Addition of acetonitrile reduces the amount of formaldehyde formed in a predictable fashion (e.g. a sample containing 50% MeOH produces ~50% as much formaldehyde as a pure methanol sample). Adding water to the reaction mixture greatly inhibits the oxidation reaction, perhaps by competing with methanol for binding positions on **3**. Changing the metal to zinc or copper results in a decrease in formation of formaldehyde, particularly in the case of zinc, where the amount produced is within experimental error of zero equivalents.

2.3. Oxidation of ethanol to form acetaldehyde.

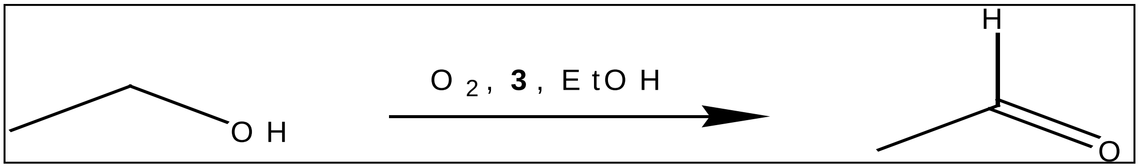

Figure 2.10. Reaction of ethanol with **3** and dioxygen to form acetaldehyde.

Using ethanol as a solvent for the deprotonation of **1** in the presence of air produced the expected color change to brown and resulted in acetaldehyde formation according to the reaction displayed in Figure 2.10.

Experimental. A typical reaction consisted of 27 mg (0.06 mmol) **1** dissolved in 30 mL of ethanol that was distilled from calcium hydride. 0.4 mL of 0.5 M potassium hydroxide (in ethanol) was added to form **3** and initiate the reaction with dioxygen. After one and twenty-four hours a 2.0 mL aliquot of the reaction mixture was diluted to 10.0 mL with dichloromethane, run through a 1-2 cm silica gel column, and analyzed by gas chromatography (GC) on a Shimadzu GC 17A equipped with a flame ionization detector (FID) and a DB5 column (thickness = 0.25 micron, 15 m X 0.250 mm). A control solution of ethanol and acetaldehyde was also run through a silica gel column to ensure that this step did not affect the quantitation. The temperature program employed is as follows: the initial temperature of 26°C was held for 5 minutes, then the temperature was increased at a rate of 10°C per minute until the temperature reached 200°C to clean off the column.

Results and discussion. The concentrations of ethanol and acetaldehyde in the reaction product solutions were calculated by comparison of the analyte peak area : solvent peak area ratio to that of known ethanol and acetaldehyde standards. From the plot of ethanol standards (Figure 2.11),

$$\mathbf{[Ethanol] = (Area_{Ethanol} / Area_{Dichloromethane}) / 0.302}$$

From the plot of acetaldehyde standards (Figure 2.9),

$$\mathbf{[Acetaldehyde] = (Area_{Acetaldehyde} / Area_{Dichloromethane}) / 0.174}$$

A representative chromatogram is shown in Figure 2.12. There are two unassigned peaks present in the reaction mixture. After one hour of reaction time the concentrations of acetaldehyde in three different solutions were 0.420 mM, 0.520 mM, and 0.191 mM. The concentrations of ethanol in the three different solutions were 2.23 M, 2.27 M and 2.13 M. The amount of acetaldehyde produced can be calculated by:

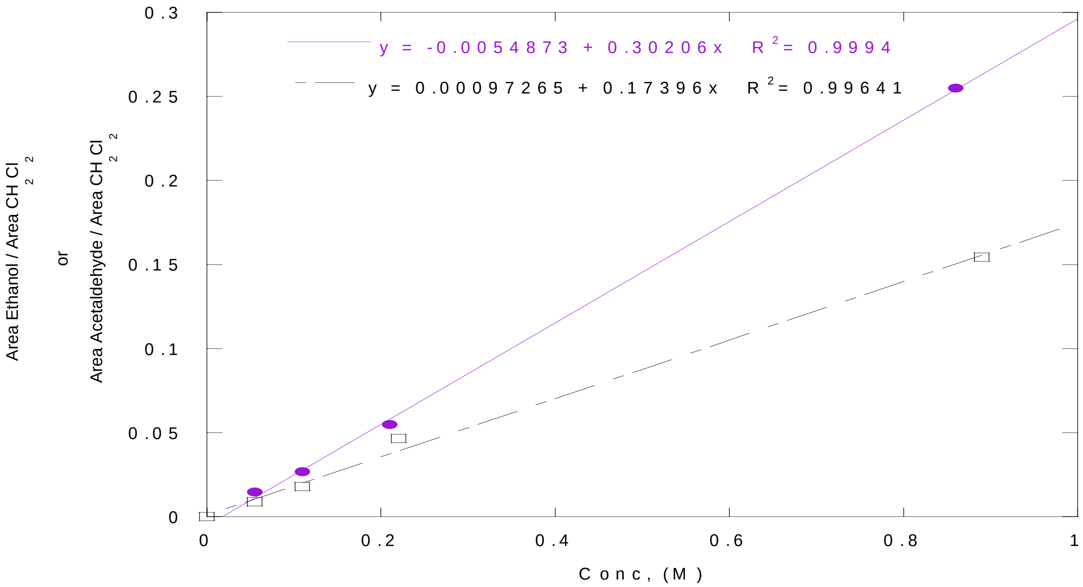

Figure 2.11. Plot of the GC/FID data from ethanol (purple circles, purple line) and acetaldehyde (black squares, black dashed line) standards. The ratio of the area of the standard peak to the area of the CH_2Cl_2 peak (used as an internal standard) is plotted versus the concentration of the standard analyte, ethanol or acetaldehyde.

Mol acetaldehyde = (mol ethanol at start in 2.0 mL aliquot) X [acetaldehyde] / ([acetaldehyde] + [ethanol])

Equivalents of acetaldehyde per 3 = ((mol acetaldehyde) / (mol 1 in 2.0 mL aliquot)) X 2

This calculation was employed instead of finding the concentration of product from the calibration curve because it takes into account the internal standard (dichloromethane) and eliminates errors that arises from rotary evaporation of the solvent and dilution with dichloromethane.

The acetaldehyde peak in the reaction mixture chromatogram shows a peak with a "shoulder". This was also observed in the chromatograms of distilled acetaldehyde, and it increased in size as the concentration of acetaldehyde increased. Therefore, the entire peak (including the shoulder) was used for quantitation. Pure CH_2Cl_2 did not display that "shoulder" in its chromatogram.

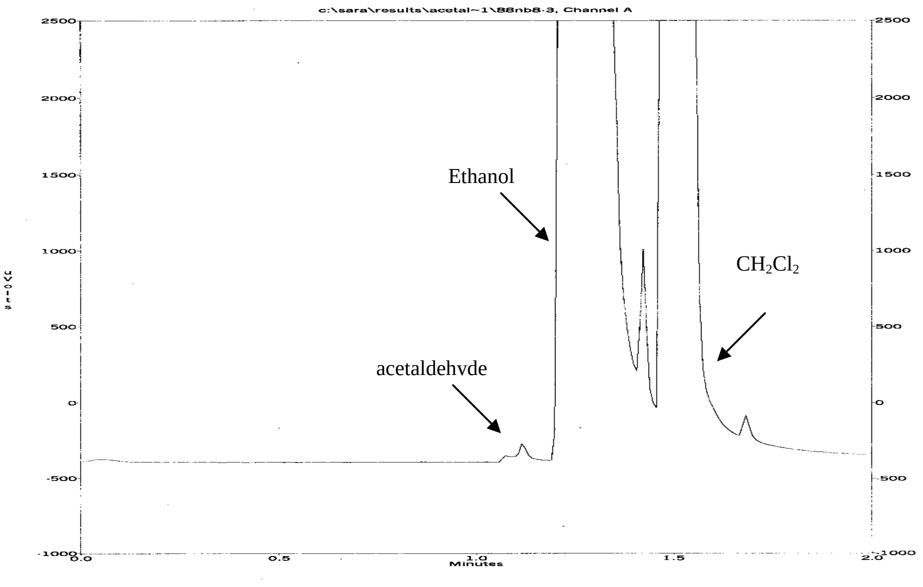

Figure 2.12. Gas chromatogram of the reaction of **3**, O_2, and ethanol (in dichloromethane). (The chromatogram is enlarged to show the product peaks. Quantitation is based on the total peak areas).

After one hour 3.30, 4.01, and 1.57 equivalents of acetaldehyde per **3** were formed (average = 3 ± 1; the error is based on the standard deviation between the three trials). After twenty-four hours of reaction time the workup was repeated and 7.57, 12.34, and 6.24 equivalents of acetaldehyde per **3** were observed (average = 9 ± 3). This is similar to the amount of oxidized product formed during the methanol reaction.

2.4. Oxidation of benzyl alcohol to form benzaldehyde.

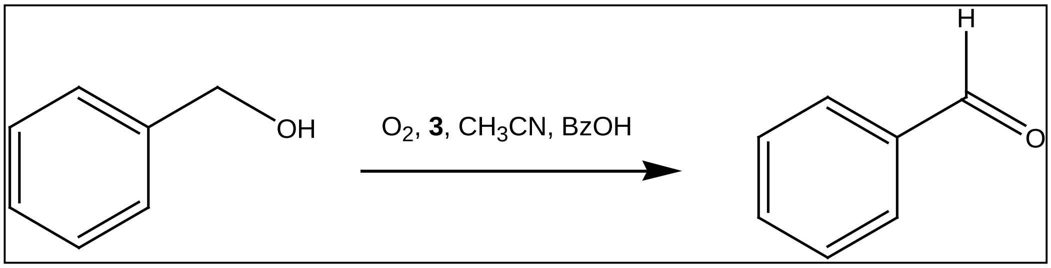

Figure 2.13. Reaction of benzyl alcohol with **3** and dioxygen to form benzaldehyde.

Although benzyl alcohol is a primary alcohol, it differs from the previous two substrates in that it has a bulky phenyl group attached to the alcohol. If benzyl alcohol is oxidized in the same way as methanol and ethanol, benzaldehyde should be formed according to the reaction shown in Figure 2.13.

Experimental. A typical reaction solution consisted of 9 mg (0.02 mmol) of **1** dissolved in 10.0 mL of acetonitrile that was distilled from calcium hydride. 0.41 mL of benzyl alcohol was added to the solution (200 equivalents per **1**, using benzyl alcohol at the solvent did not affect the reaction). Next, 0.12 mL of 0.5 M potassium hydroxide (in benzyl alcohol) was added to deprotonate the oximes and form **3** to initiate the reaction with dioxygen. After one and twenty-four hours, the acetonitrile (b.p. 81.6° C) was removed by rotary evaporation (no benzyl alcohol (b.p. 204.7° C) or benzaldehyde (b.p. 179° C) was removed during this step as confirmed by GC analysis of the solution removed by rotary evaporation). The reaction mixture was then dissolved in 2.0 mL of dichloromethane and run through a 1-2 cm column of silica gel to remove the nickel complex. The sample was analyzed by gas chromatography on a Shimadzu GC 17A equipped with a flame ionization detector (FID) and a DB5 column (thickness = 0.25 micron, 15 m X 0.250 mm). A control solution of benzyl alcohol and benzaldehyde was also run through a silica gel column to ensure that this step did not affect the quantitation. The temperature program employed is as follows: the initial temperature of 35°C is held for 2 minutes, then the temperature is increased at a rate of 20°C per minute until the temperature reaches 200°C and then it is held for 5 minutes. Next, the temperature is increased at a rate of 30°C per minute until the temperature reaches 250°C to clean off the column.

Results and discussion. The concentrations of benzyl alcohol and benzaldehyde in the reaction product were calculated by comparison of the analyte peak area : solvent peak area ratio of known benzyl alcohol and benzaldehyde standards.

From the plot of benzyl alcohol standards (Figure 2.14),

$$\mathbf{[Benzyl\ Alcohol] = (Area_{benzyl\ alcohol} / Area_{Dichloromethane}) / 1.64 \times 10^{-3}}$$

From the plot of benzaldehyde standards (Figure 2.14),

$$\mathbf{[Benzaldehyde] = (Area_{benzaldehyde} / Area_{dichloromethane}) / 1.68 \times 10^{-3}}$$

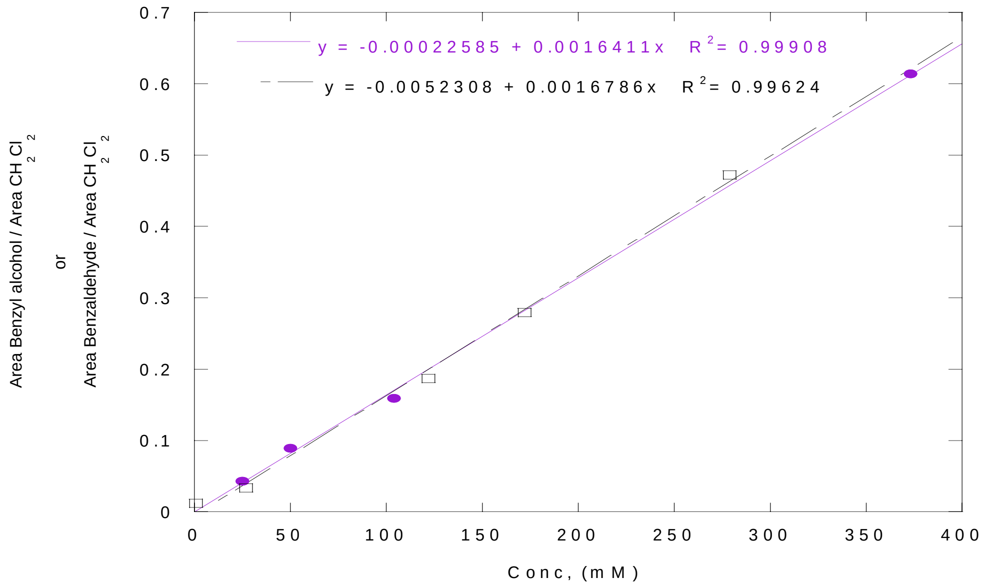

Figure 2.14. Plot of the GC/FID data from benzyl alcohol (purple circles, purple line) and benzaldehyde (black squares, black dashed line) standards. The ratio of the area of the standard peak to the area of the CH_2Cl_2 peak (used as an internal standard) is plotted versus the concentration of the standard analyte, benzyl alcohol or benzaldehyde.

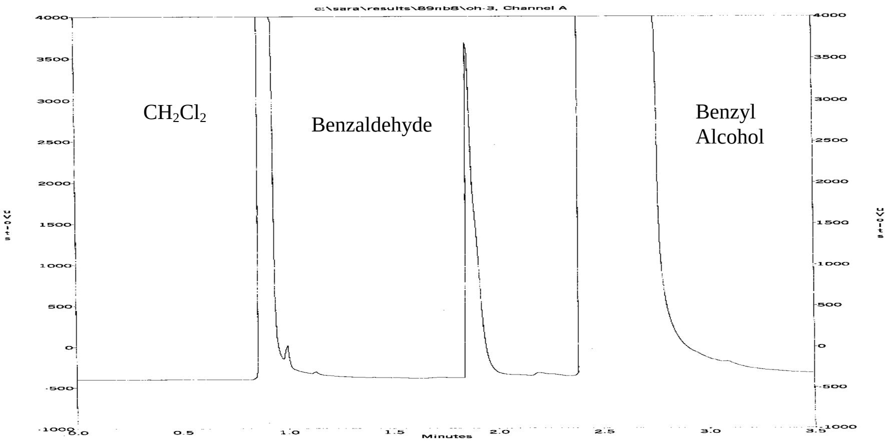

Figure 2.15. Gas chromatogram of the reaction of **3**, O_2, and benzyl alcohol (in dichloromethane). (The chromatogram is enlarged to show the product peaks. Quantitation is based on the total peak areas).

A representative chromatogram can be seen in Figure 2.15. After one hour of reaction time the concentrations of benzaldehyde in three different solutions were 2.91 mM, 3.91 mM and 3.56 mM and the concentration of benzyl alcohol in each of the three samples were 1.34 M, 1.81 M, and 1.91 M. The amount of benzaldehyde produced can be calculated by:

Mol benzaldehyde = (mol benzyl alcohol at start) X [benzyaldehyde] / ([benzaldehyde] + [benzyl alcohol])

Equivalents of benzaldehyde per 3 = ((mol benzaldehyde) / (mol 1)) X 2

After one hour 0.87, 0.86, and 0.74 (average 0.82 ± 0.07; the error is the standard deviation between the three trials) equivalents of benzaldehyde per **3** were detected and after twenty-four hours 3.02 ± 0.57 equivalents per **3** were produced. This is significantly less than the amount of oxidized product observed in the reaction using methanol or ethanol as the solvent, which may be due to steric hindrance from the phenyl ring.

2.5 Oxidation of benzylamine with formation of a Schiff-base adduct.

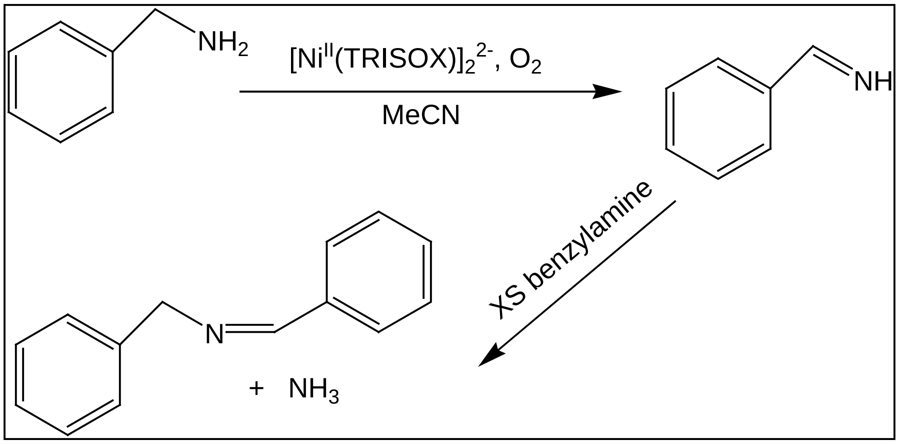

Figure 2.16. Reaction of benzylamine with **3**, and O$_2$ to form *N*-benzylidene benzylamine

After investigating several primary alcohols (methanol, ethanol, and benzyl alcohol), a primary amine was screened to see if it would promote the oxygen reaction.

Addition of this substrate resulted in the color change from purple to brown, indicating that oxidation occurred. This reaction likely proceeds via one of two pathways. One possibility is that the amine reacts in the same way that the alcohols do, losing two hydrogen atoms to form an imine. Another possibility is that the amine undergoes oxidative deamination, where the carbon nitrogen bond is cleaved and benzaldehyde is formed if water is present.[3] Neither of these products is observed, as they can both undergo the favorable Schiff-base reaction with the excess benzylamine to form *N*-benzylidene benzylamine, as shown in Figure 2.16.

Experimental. A typical reaction solution consisted of 9 mg (0.02 mmol) of **1** dissolved in 10.0 mL of acetonitrile that was distilled from calcium hydride. Hydroxide was not added to this reaction as the amine is basic enough to deprotonate the oximes, although a control experiment was performed to see if addition of hydroxide affected the results. Addition of excess solid KOH did not significantly affect the amount of oxidized product observed. Next, 0.44 mL (0.004 mol, ~200 equivalents per nickel) of benzylamine were added to the sample, which was subsequently exposed to the air. The solution turned a dark brown color. After one and twenty-four hour time periods a portion of the reaction mixture was submitted for electrospray ionization mass spectrometry analysis (ESI-MS) on a Micro-mass QTOF-II with electrospray sample induction (Figure 2.17). Then the acetonitrile (b.p. 81.6° C) was removed by rotary evaporation (no benzylamine (b.p. 185°C) or Schiff base product (solid) was removed by rotary evaporation, as confirmed by GC analysis of the solution removed during this step). It was then dissolved in 2.0 mL of dichloromethane, run through a 1-2 cm column of silica gel to remove the nickel complex (neither substrate nor product bound to the silica gel after repeated flushing with dichloromethane, as determined by GC), and analyzed by GC on a Shimadzu GC 17A equipped with a flame ionization detector (FID) and a DB5 column (thickness = 0.25 micron, 15 m X 0.250 mm). A control solution of benzylamine and *N*-benzylidene benzylamine was also run through a silica gel column to ensure that this step did not affect the quantitation. The temperature program employed is as follows: the initial temperature of 50°C is held for 1 minute, then the temperature is increased at a rate of 15°C per minute until the temperature reaches 325°C and it is held for 5 minutes to clean off the column.

In the aqueous experiments, diethyl ether was used to extract the organics from the aqueous layer after twenty-four hours. Rotary evaporation was employed to remove the diethyl ether, and then the sample was diluted to 2.0 mL with dichloromethane, run through a 1-2 cm column of silica gel and analyzed by GC.

Ammonia was detected as one of the products of this reaction using the indophenol colorimetric technique.[4] A 5 mL aliquot of the reaction mixture was separated from the sample and run through a 1-2 cm column of silica gel to remove the nickel complex. A 0.5 mL aliquot of this solution was removed and added to 10 mL acetonitrile, 5 mL of dilute NaOCl (Clorox bleach) and then 5 mL of a 4% solution of phenol was added. This solution was heated for 2 minutes in a boiling water bath, causing a deep blue color to form.

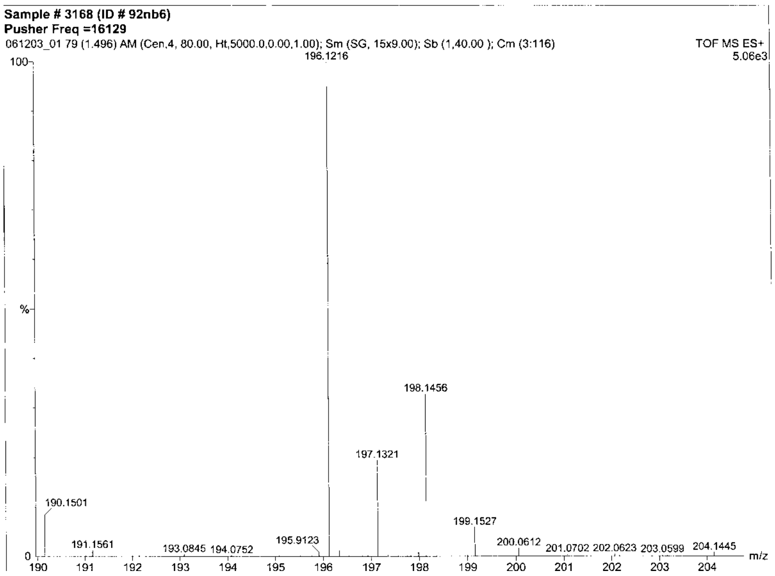

Figure 2.17. ESI-Mass spectrum of reaction product from reaction of **3** with benzylamine in acetonitrile showing the M+1 (196.1216) peak of *N*-benzylidenebenzylamine.

Results and discussion. From the plot of benzylamine standards in dichloromethane (Figure 2.18),

$$\mathbf{[Benzylamine] = (Area_{Benzylamine} / Area_{Dichloromethane}) / 1.32}$$

From the plot of *N*-benzylidene benzylamine standards (Figure 2.18),

$$\mathbf{[\mathit{N}\text{-}Benzylidene\ benzylamine] = (Area_{\mathit{N}\text{-}Benzylidene\ benzylamine} / Area_{Dichloromethane}) / 2.73}$$

A representative chromatogram of the reaction mixture is shown in Figure 2.19.

After one hour of reaction time, the concentrations of *N*-benzylidene benzylamine in three different solutions were 1.09 mM, 0.97 mM, and 0.52 mM. The concentrations of benzylamine in the three different solutions were 0.615 M, 0.950 M and 0.656 M. The amount of *N*-benzylidene benzylamine produced can be calculated by:

Mol *N*-benzylidene benzylamine = (mol benzylamine at start) X [*N*-benzylidene benzylamine] / ([*N*-benzylidene benzylamine] + [benzylamine])

Equivalents of *N*-benzylidene benzylamine per 3 = ((mol *N*-benzylidene benzylamine) / (mol 1)) X 2

After one hour, 0.71, 0.41, and 0.32 equivalents per 3 were formed (average 0.5 ± 0.2, the error is the standard deviation between the three trials). After twenty-four hours, 5.0 ± 1.0 equivalents were formed. It should be noted that this reaction is much more efficient than the oxidation of methanol, as this experiment only contained 4% substrate whereas the methanol experiments were conducted in the presence of 25, 50, or 100% substrate.

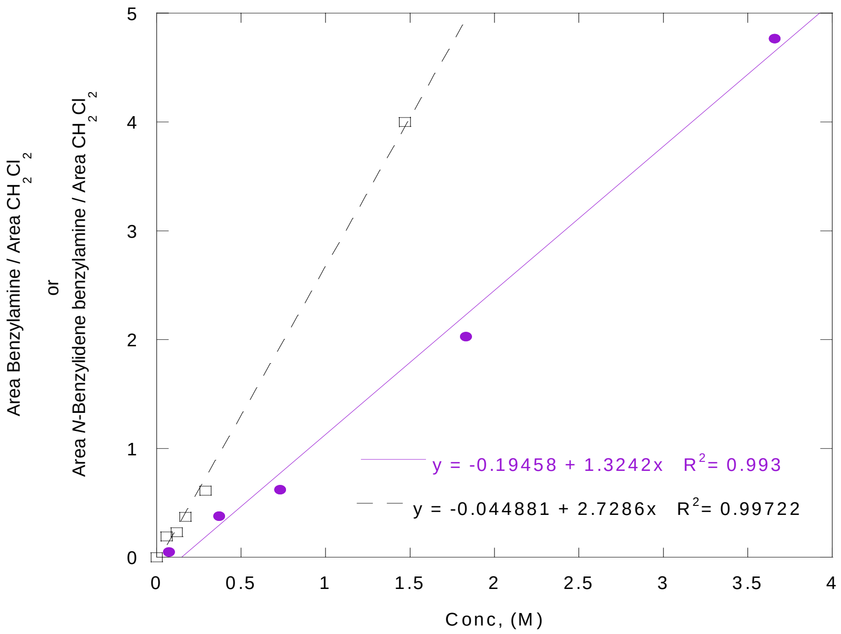

Figure 2.18. Plot of the GC/FID data from benzylamine (purple circles, purple line) and *N*-benzylidene benzylamine (black squares, black dashed line) standards. The ratio of the area of the standard peak to the area of the CH_2Cl_2 peak (used as an internal standard) is plotted versus the concentration of the standard analyte, benzylamine or *N*-benzylidene benzylamine.

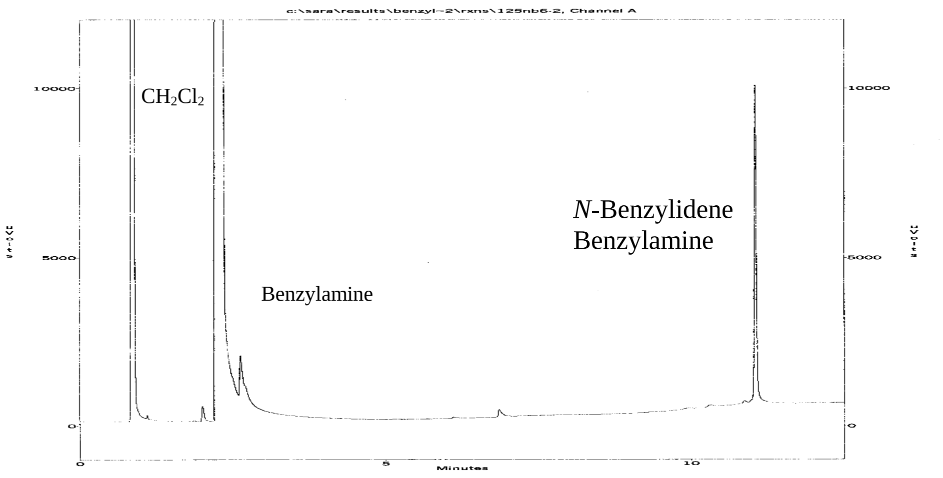

Figure 2.19. Gas chromatogram of the reaction of **3**, O_2, and benzylamine (in dichloromethane). (The chromatogram is enlarged to show the product peaks. Quantitation is based on the total peak areas).

Ammonia was also observed in this reaction using the indophenol colorimetric procedure, where formation of a dark blue color indicates the presence of ammonia.[4] This response was not seen for benzylamine or *N*-benzylidene benzylamine alone. Ammonia is another product in the oxidative deamination reaction that would produce benzaldehyde, or it could be formed when the imine reacts with the excess benzylamine to form the Schiff-base adduct.

This reaction was repeated using H_2O as the solvent. It was determined that the concentration of *N*-benzylidene benzylamine was 19 mM, 24 mM, and 23 mM and the concentration of benzylamine in the three solutions was 1.42 M, 1.50 M, and 1.68 M. This resulted in 5.28, 6.30, and 5.40 equivalents of oxidized product per **3** formed after twenty-four hours (average = 5.67 ± 0.6, the error is the standard deviation between the three trials). As a control, a standard sample of *N*-benzylidene benzylamine was stirred in water for twenty-four hours. It was then extracted with diethyl ether and worked up in the same fashion as the sample containing **3** and benzylamine. The GC only showed a peak at 11.5 minutes, consistent with *N*-benzylidene benzylamine. This confirmed that the Schiff-base product is the fate of all of the oxidized substrate and that no products are formed via hydrolysis.

Another experiment was performed in which one equivalent of benzylamine was added to an acetonitrile solution of **3** in the presence of dioxygen. No color change was observed and after twenty-four hours no oxidized product was detected via GC.

2.6. Oxidation of *N*-methylbenzylamine to form a Schiff-adduct.

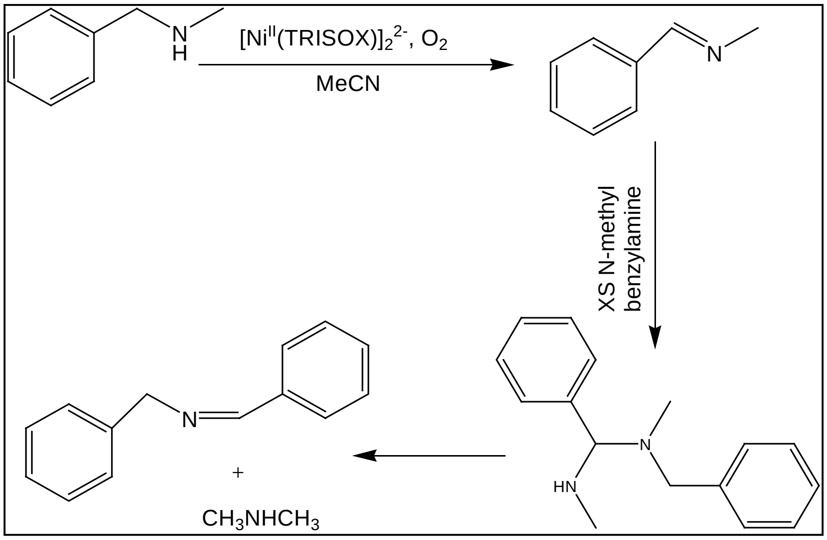

Figure 2.20. Reaction of **3** with O_2 and *N*-methylbenzylamine.

After investigating a primary amine, a secondary amine, *N*-methylbenzylamine, was screened. Figure 2.20 shows this reaction, which resulted in the same Schiff-base adduct, *N*-benzylidene benzylamine that was observed during the reaction with benzylamine as the substrate. It is likely that *N*-methylbenzylamine was oxidized by two hydrogen atom abstraction to produce the imine, which then underwent reversible addition-elimination through an aminal intermediate to produce *N*-benzylidene benzylamine, as previously reported.[5]

Experimental. In a typical experiment 9 mg (0.02 mmol) of **1** was dissolved in 10 mL of acetonitrile. Hydroxide was not added to this reaction as the amine is basic enough to deprotonate the oximes. A 0.52 mL aliquot (0.004 mol, ~200 equivalents per nickel) of *N*-methylbenzylamine was added to the sample and exposed to the air. The solution turned a dark brown color. After one and twenty-four hour time periods, a portion of the reaction mixture was submitted for electrospray ionization mass spectrometry analysis (ESI-MS) on a Micro-mass QTOF-II with electrospray sample induction (Figure 2.21). A 5.0 mL aliquot of the solution was rotovapped to remove acetonitrile, then diluted to 2.0 mL with dichloromethane and run through a 1-2 cm column of silica gel (neither substrate nor product bound to the silica gel after repeated flushing with dichloromethane as determined via GC during a control experiment). This sample was analyzed by GC on a Shimadzu GC 17A equipped with a flame ionization detector (FID) and a DB5 column (thickness = 0.25 micron, 15 m X 0.250 mm). A control solution of *N*-methylbenzylamine and *N*-benzylidene benzylamine was also run through a silica gel column to ensure that this step did not affect the quantitation. The temperature program employed is as follows: the initial temperature of 50°C is held for 1 minute, then the temperature is increased at a rate of 15°C per minute until the temperature reaches 325°C.

.

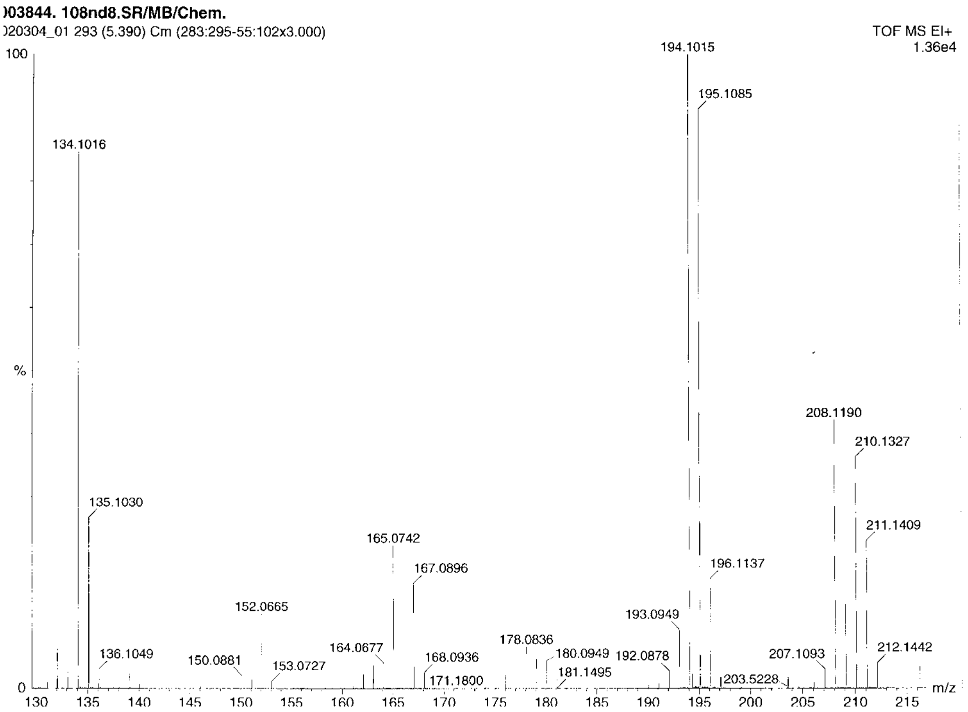

Figure 2.21. Mass spectrum of reaction product from reaction of **3** with *N*-methylbenzylamine in acetonitrile showing the 195.1085 peak of *N*-benzylidenebenzylamine.

Results and discussion. From the plot of benzylamine standards in dichloromethane (Figure 2.22),

[*N*-Methylbenzylamine] = (Area$_{N\text{-Methylbenzylamine}}$ / Area$_{\text{Dichloromethane}}$) / 1.38

From the plot of *N*-benzylidene benzylamine standards (Figure 2.22),

[*N*-Benzylidene benzylamine] = (Area$_{N\text{-Benzylidene benzylamine}}$ / Area$_{\text{Dichloromethane}}$) / 2.73

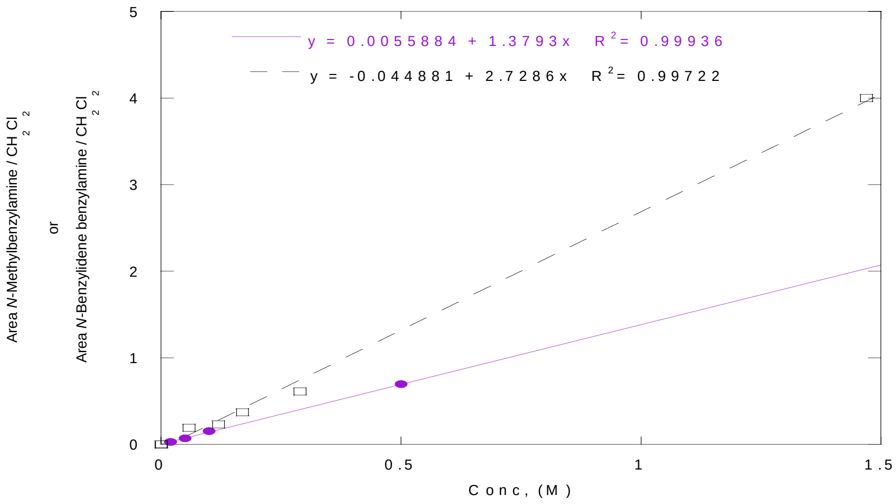

Figure 2.22. Plot of the GC/FID data from *N*-methylbenzylamine (purple circles, purple line) and *N*-benzylidene benzylamine (black squares, black dashed line) standards. The ratio of the area of the standard peak to the area of the CH_2Cl_2 peak (used as an internal standard) is plotted versus the concentration of the standard analyte, *N*-methylbenzylamine or *N*-benzylidene benzylamine.

A representative chromatogram of the reaction solution can be seen in Figure 2.23. After one hour of reaction time the concentrations of *N*-benzylidene benzylamine in three different solutions were 0.009 mM, 0.035 mM, and 0.033 mM. The concentrations of *N*-methylbenzylamine in the three different solutions were 0.139 M, 0.53 M and 0.71 M. The amount of *N*-benzylidene benzylamine produced can be calculated by:

Mol *N*-benzylidene benzylamine = (mol *N*-methylbenzylamine at start) X [*N*-benzylidene benzylamine] / ([*N*-benzylidene benzylamine] + [*N*-methylbenzylamine])

Equivalents of *N*-benzylidene benzylamine per 3 = ((mol *N*-benzylidene benzylamine) / (mol 1)) X 2

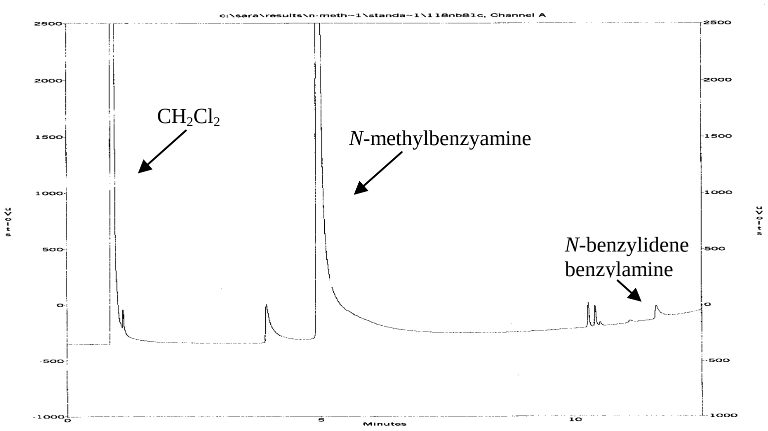

Figure 2.23. Gas chromatogram of the reaction of **3**, O_2, and *N*-methylbenzylamine (in dichloromethane). (The chromatogram is enlarged to show the product peaks. Quantitation is based on the total peak areas).

This substrate was not oxidized catalytically, with 0.24 ± 0.04 equivalents being formed after one hour and 0.6 ± 0.1 equivalents observed after twenty-four hours. Apparently, the secondary nature of this substrate inhibited the oxidation reaction significantly.

2.7. Consumption of oxygen during the reaction.

After screening several alcohols and amines to ascertain what substrates promote the dioxygen reaction with **3**, it was determined that a source of hydrogen atoms must be present for the reaction to take place. The other necessary component for this reaction is, of course, dioxygen. The amount O_2 consumed during the reaction in both methanol and acetonitrile was determined.

Experimental. The manometric apparatus consists of a U-shaped tube partially filled with Hg, open to the atmosphere on one end and connected to a closed system. The system consists of a 250 mL round bottom flask as the oxygen reservoir and a 50 mL Schlenk type flask (with a side arm and stopcock) as the sample vessel, connected via a T-shaped adapter. The total volume of closed system is 0.344 L. In a typical experiment, 30 mg (6.68×10^{-5} mol) of **1** was dissolved in 30 mL of solvent (either methanol or acetonitrile) and placed into the manometer sample flask. In the experiments using methanol as the solvent, 0.2 mL of 1.0 M KOH (in methanol) was added to the solution via syringe through the open stopcock, which was then immediately closed. When acetonitrile was used as the solvent, an excess amount of crushed KOH (generally 35 mg) was added to the purple solution and the system was sealed. Pressure changes were then measured, and the amount of O_2 consumed was calculated using the ideal gas law, taking into account barometric changes.

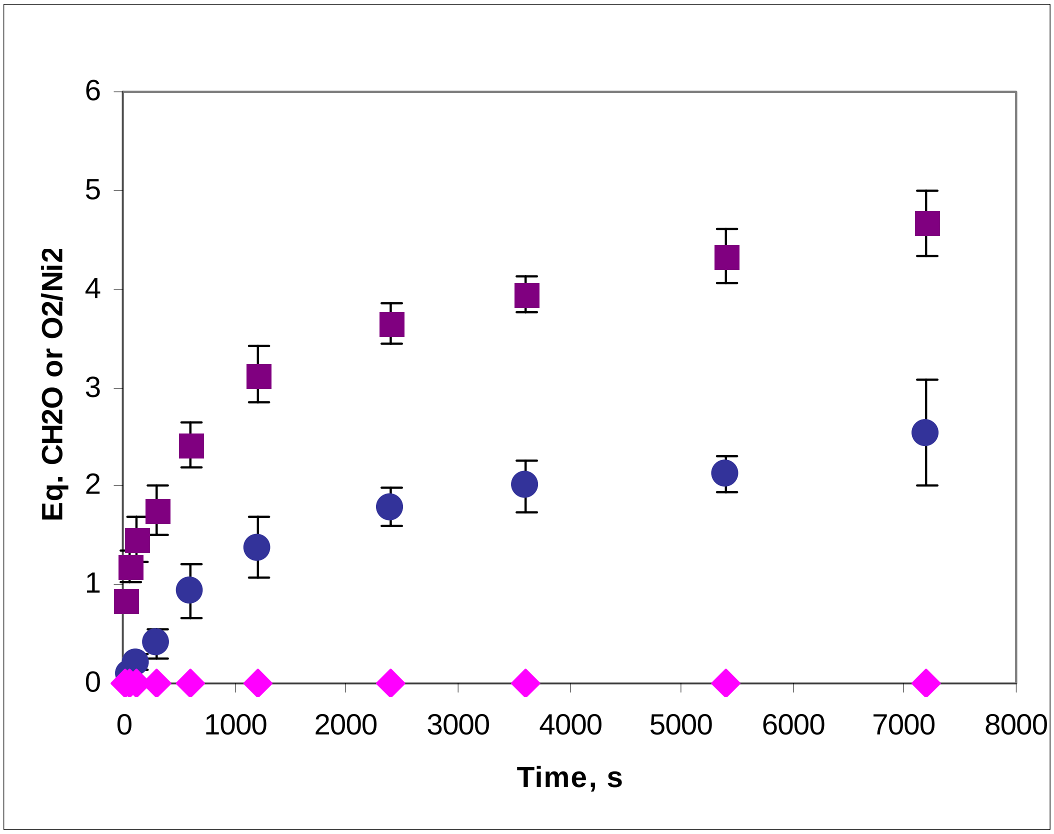

Figure 2.24. Plot of the amount of formaldehyde formed during the reaction of **3** in methanol (purple squares), the amount of dioxygen consumed during the reaction of **3** in methanol (blue circles), and the amount of dioxygen consumed during the reaction of **3** in acetonitrile (pink diamonds) versus time, (each data point represents the average of three trials and the error bars are the standard deviations between the three trials).

Results and discussion. The results are compared to the amount of formaldehyde formed in Figure 2.24. A solution of **3** in acetonitrile not only does not display a color change to brown in the presence of dioxygen, it also does not consume dioxygen, which indicates that no reaction is taking place. However, the color change in the reaction of **3** with dioxygen and methanol is accompanied by both formation of formaldehyde and consumption of dioxygen. The amount of dioxygen consumed is approximately one half the amount of formaldehyde formed. One explanation for this observation is that hydrogen peroxide is also a product, and is disproportionated to O_2 and water. The following section discusses this.

2.8. Catalase-like activity of the oxygen active complex.

It has been observed that **3** can disproportionate hydrogen peroxide to form half an equivalent of O_2 and water according to the following reaction:

$$\mathbf{H_2O_2 \longrightarrow \tfrac{1}{2}\,O_2 + H_2O}$$

The efficiency of this reaction was investigated via manometry and colorimetry.

Experimental. Standard reaction conditions are 11.1 mg (0.025 mmol) of **1** dissolved in 50 mL of a 99 mM H_2O_2 methanolic solution (~200 equivalents of H_2O_2 per nickel) in the manometer described in Chapter 2.7. 0.1 mL of 1.0 M Bu_4NOH in methanol was added to the solution to initiate the reaction. Bubbles were observed as the color changed from purple to brown.

Colorimetry experiments were also performed to test the ability of **3** to disproportionate hydrogen peroxide. A titanium sulfate test reagent was prepared by digesting 1 g of anhydrous titanium dioxide with 100 mL of sulfuric acid for 16 hours on a sand bath at 150° C. The solution was cooled, diluted with 4 parts of distilled water, and filtered through a thin layer of celite prior to use. 1.0 mL of this indicator was added to 10.0 mL of solution containing hydrogen peroxide, causing a yellow color to appear as pertitanic acid forms (ε = 690 M^{-1} cm^{-1} at 407 nm).[6]

Results and discussion. Figure 2.25 shows the disproportion of hydrogen peroxide as determined manometrically. After approximately 15 minutes the bubbling ceased and 100 equivalents of dioxygen were produced. This efficiency is more than adequate to rapidly disproportionate the amount of hydrogen peroxide suspected of being formed during the reaction of **3** with dioxygen and methanol (~10 equivalents over twenty four hours).

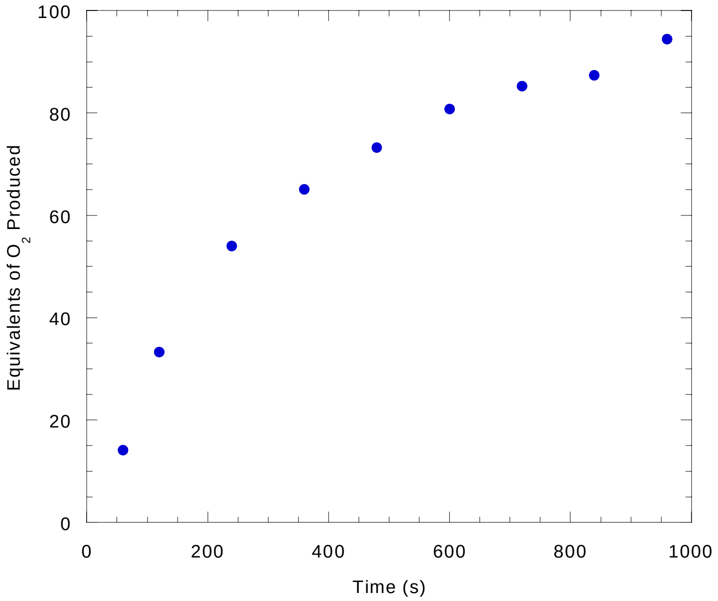

Figure 2.25. Plot of disproportionation of 200 equivalents of hydrogen peroxide by **3** in methanol as observed by manometry versus time (monitoring the production of O_2).

During the colorimetry experiments the solution containing **3** remained colorless upon addition of the indicator, signifying that all of the hydrogen peroxide initially present (~400 equivalents) had been disproportionated (using this technique $[H_2O_2] \geq 18$ ppm, or 0.03 eq./**3,** can be detected). The control experiment using Zn(TRISOX)Cl_2 in place of **1** turned yellow when the indicator was added.

An additional experiment was conducted to see if the catalase-like activity was maintained at later times. A 2 mM methanolic solution of **1** was deprotonated in the presence of dioxygen and allowed to react for twenty-four hours. Then, an aliquot was removed and tested with the $Ti(SO_4)_2$ indicator. No hydrogen peroxide was present. 200 equivalents of hydrogen peroxide were then added to the remaining nickel solution. No bubbling was observed and addition of the indicator after 30 minutes revealed that hydrogen peroxide was still present. From this experiment it can be concluded that the catalase-like activity of the complex is destroyed over time, but no hydrogen peroxide is built up in solution.

2.9. Thermodynamic requirements of the substrate oxidations.

All of the substrates studied were oxidized by the abstraction of two hydrogen atoms according to the following reaction:

$$RH_2 + O_2 \longrightarrow R + H_2O_2$$

Table 2.1 displays bond dissociation energies for the substrates analyzed and compares them to the amount of energy gained by forming hydrogen peroxide from O_2.

Table 2.1. Bond dissociation energies (kcal/mol) for hydrogen atom donors and hydrogen peroxide.[7] Product quantities are the average of three experiments. (NA = not available). (a = used as solvent, b = 200 eq./**3** added to MeCN)

Substrate	**1st H•**	**2nd H•**	**Total**	**Eq. of Product after 1 hour**	**Eq. of Product after 24 hours**
Methanol[a]	93	31	124	4.0 ± 0.2	10.4 ± 0.5
Ethanol[a]	90	26	116	3.0 ± 1.0	9.0 ± 3.0
Benzyl[b] Alcohol	87.5	18	105.5	0.9 ± 0.1	3.0 ± 0.6
N-Methylbenzyl[b] amine	NA	NA	NA	0.24 ± 0.04	0.6 ± 0.1
Benzyamine[b]	100	23	123	0.5 ± 0.2	5.0 ± 1.0
H_2O_2	88.5	46	134.5		

The first hydrogen atom is fairly difficult to remove in the case of each substrate; however, the second hydrogen atom is fairly easy to remove, and the total amount of energy required to remove both hydrogen atoms is less than the amount of energy gained by forming hydrogen peroxide, making this a thermodynamically reasonable explanation for the observed oxidation reactions. The addition of one hydrogen atom to O_2 does not provide much energy ($O_2 + \bullet H \longrightarrow \bullet HO_2$) but addition of a second hydrogen atom ($\bullet HO_2 + \bullet H \longrightarrow H_2O_2$) produces a significant amount, making the overall thermodynamics favorable. It is clear that other factors influence this reaction. Benzyl alcohol requires the least amount of energy to remove both hydrogen atoms, but it forms the least amount of oxidized product (in comparison to the other primary substrates investigated). Furthermore, other potential substrates whose thermodynamics suggest that they should promote the oxidation reaction do not show a color change or produce oxidized products. Table 2.2 shows the potential substrates that did not get oxidized by this reaction.

Table 2.2. Bond dissociation energies (kcal/mol) for hydrogen atom donors and hydrogen peroxide.[7] (NA = not available, NR = no reaction).

Substrate	1st H•	2nd H•	Total	Eq. of Product after 1 hour	Eq. of Product after 24 hours
Isopropanol	91	26	117	NR	NR
D,L-1-phenylethanol	88	14	102	NR	NR
α-Methylbenzylamine	NA	NA	NA	NR	NR
H_2O_2	88.5	46	134.5		

If isopropanol were to be oxidized by this reaction, acetone would be formed. D,L-1-phenylethanol should form acetophenone and α-methylbenzylamine would form another Schiff-base adduct. All of these products are stable and the bond dissociation energies for the removal of two hydrogen atoms are favorable relative to H_2O_2. These complexes all share the common feature that they are branched at the α-carbon position. This indicates that perhaps there is a steric hindrance associated with branching at that position.

2.10. Oxidation of triphenylphosphine to form triphenylphosphine oxide.

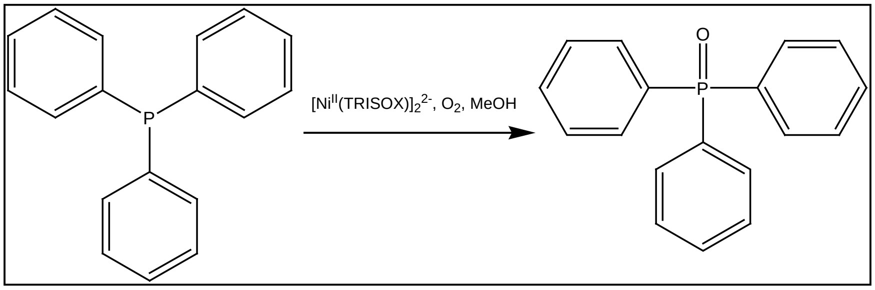

Figure 2.26. Reaction of 3, O_2, and triphenylphosphine in methanol.

All of the substrates mentioned previously were oxidized by the abstraction of two hydrogen atoms. In contrast, triphenylphosphine is relatively easy to oxidize via oxygen atom transfer rather than hydrogen atom abstraction. The reaction is displayed in Figure 2.26. Isotopic labeling using ^{18}O was performed by Dr. Goldcamp to prove that the oxygen atom being transferred came from O_2 rather than from water in the solvent.[1]

Experimental. A typical reaction consisted of 54 mg (0.12 mmol) of **1** and 314 mg (1.2 mmol) of triphenylphosphine dissolved in 60.0 mL of methanol. Next, 0.72 mL of 0.5 M KOH in methanol was added to the reaction in the presence of air and the reaction was allowed to proceed for a designated time. At the end of that time a 20.0 mL aliquot of the sample was pipetted out and quenched with 0.24 mL of 0.5 M HNO_3 in methanol. The methanol was removed by rotary evaporation and the sample was washed with three 10 mL portions of distilled water to remove the nickel complex. The remaining white solid was then placed under vacuum for several hours, dissolved in 2.0 mL of dichloromethane, and analyzed using a BioRad Excaliber Series Fourier Transform Infrared Spectrophotometer (FTIR). The presence of the oxidized species was confirmed by the appearance of strong bands at 1189 cm^{-1} (υ(P=O)) and 1119 cm^{-1} in the FTIR spectum of the reaction product. Figure 2.27 shows the IR spectra of standard samples of triphenylphosphine and triphenylphosphine oxide in dichloromethane. The amount of oxidized product formed was quantitated by measuring the absorbance of the 1189 cm^{-1} peak and comparing it to the absorbance of known Ph_3PO standards in dichloromethane. Figure 2.28 shows the calibration curve constructed for this experiment.

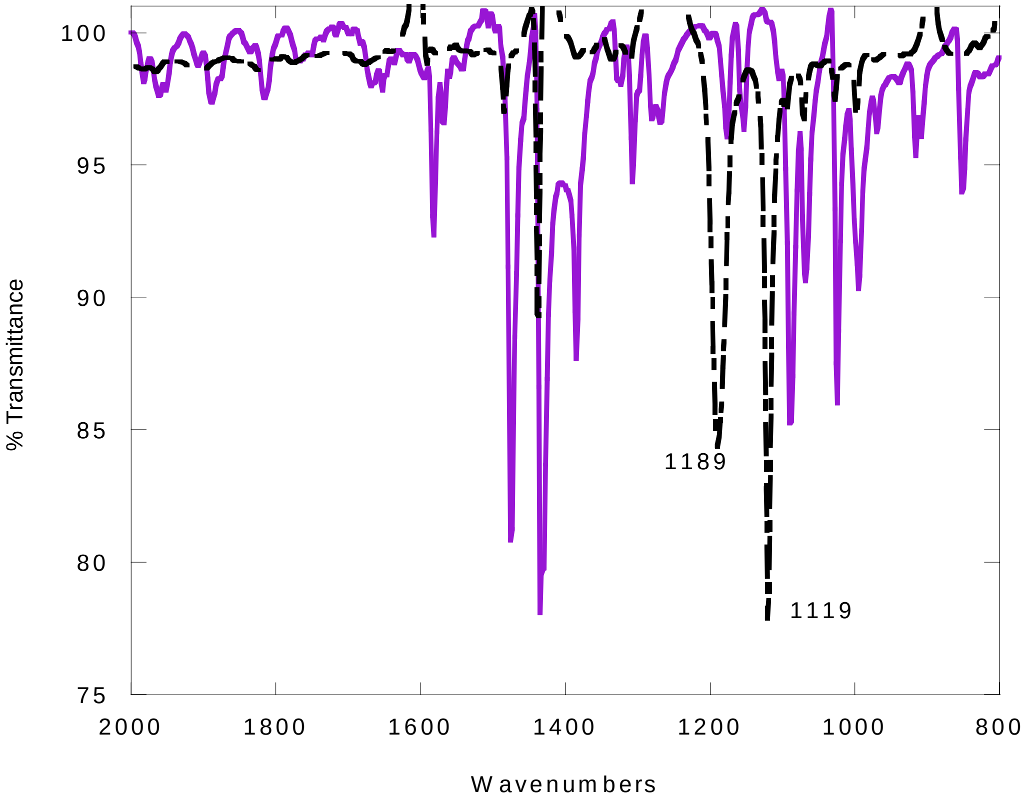

Figure 2.27. FTIR spectra of triphenylphosphine (black dashed line) and triphenylphosphine oxide (purple solid line). The band at 1189 cm^{-1} was used in quantitation.

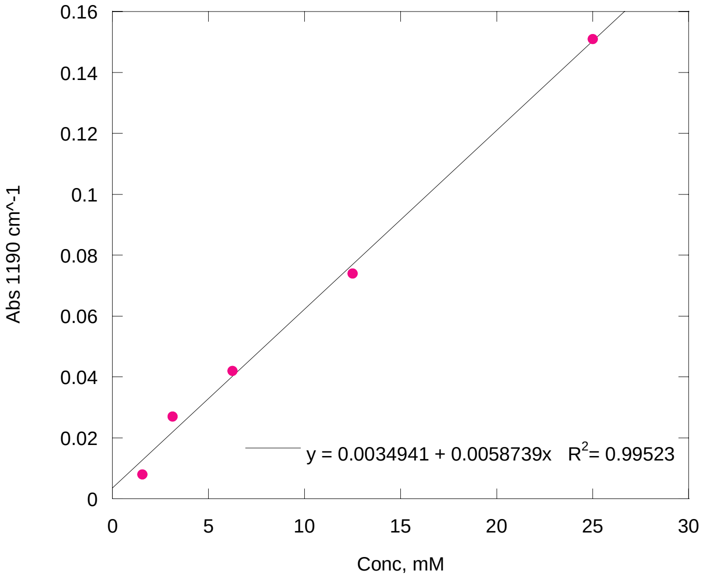

Figure 2.28. Calibration curve of triphenylphospine oxide standards dissolved in dichloromethane.

A representative FTIR spectrum of the reaction mixture can be seen in Figure 2.29. The characteristic bands at 1189 (υ(P=O)) and 1119 cm^{-1} are present.

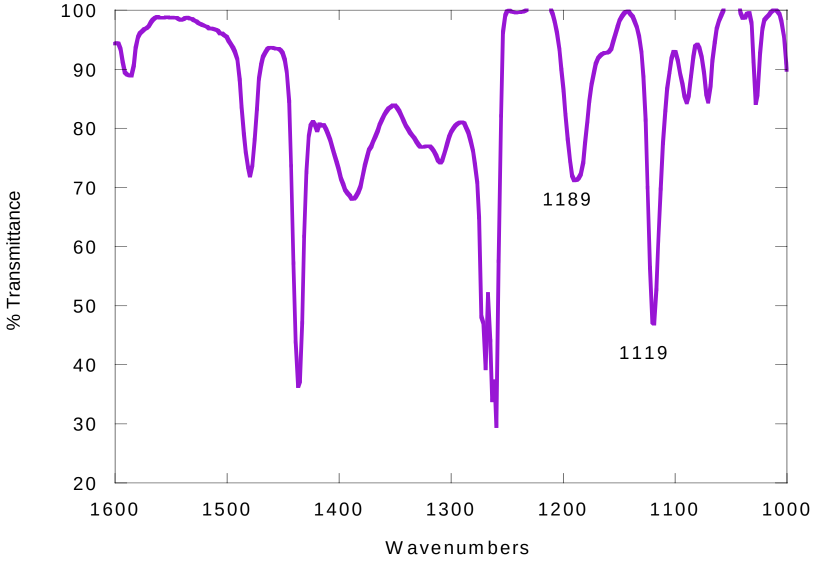

Figure 2.29. FTIR spectrum of triphenylphosphine oxide produced during the reaction with **3** and O_2 in methanol.

Results and discussion. The amount of triphenylphosphine oxide formed was monitored at several time periods and compared to the amount of formaldehyde formed under equivalent conditions. The results can be seen in Figure 2.30.

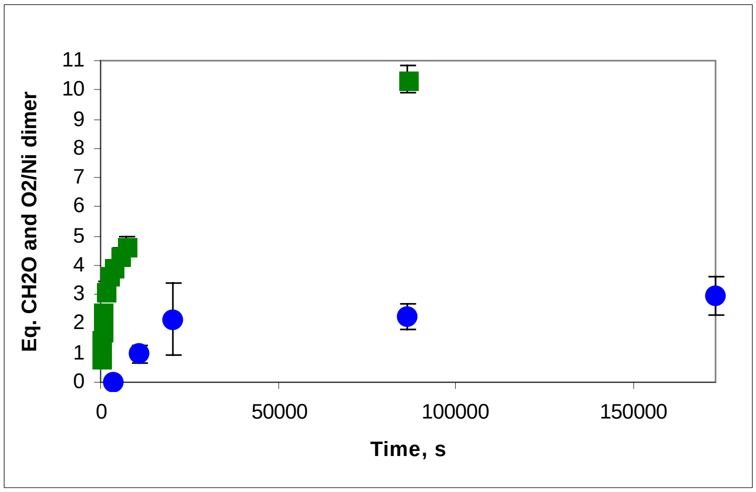

Figure 2.30. Plot of equivalents of formaldehyde formed (green squares) and equivalents of Ph_3PO formed (blue circles) versus time. Each data point is the average of three trials and the error bars are the standard deviations.

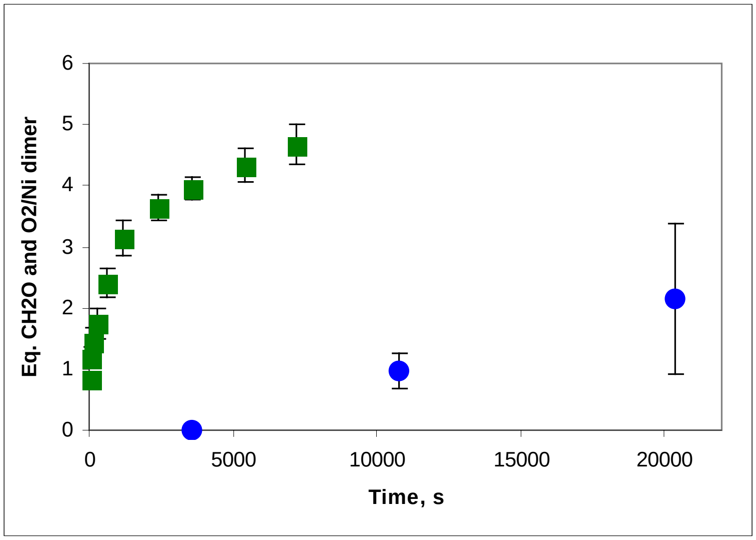

Figure 2.31. Plot of equivalents of formaldehyde formed (green squares) and equivalents of Ph_3PO formed (blue circles) versus time (on a shorter time scale). Each data point is the average of three trials and the error bars are the standard deviations.

Figure 2.31 shows the same experiment on a shorter time scale. The oxidation of triphenylphosphine is slower and less efficient than the oxidation of methanol to form formaldehyde. After one hour no triphenylphosphine oxide is detected, while 3.95 ± 0.29 equivalents of formaldehyde are observed after that same time period (38% of the total oxidized product). The oxidation of triphenylphosphine appears to be slow to begin and then levels off after about 5.5 hours. This oxidation is first observed at approximately the same time the oxidation of methanol begins to level off. One explanation for this observation is that the catalyst changes over time, performing different types of chemistry (first hydrogen atom abstraction, then oxygen atom transfer) before it eventually reaches its dead-end product. Another possibility is that the catalase-like efficiency of the catalyst slows down at later reaction times. Then, the rate of oxidation of triphenylphosphine by hydrogen peroxide may be sufficient to out compete the disproportionation reaction.

2.11. Conclusions.

Complex **3** undergoes multiple turnovers during reaction with O_2 without significant ligand decomposition, making this the first homogeneous Ni(II) + O_2 reaction that is not driven by irreversible ligand oxidation.[8] It has been determined that a two-hydrogen atom donating substrate must be present in order for the reaction to occur and it is postulated that the abstracted hydrogen atoms combine with dioxygen to form hydrogen peroxide, which is not observed as **3** is also very efficient at catalase-like activity.

Several of the substrate oxidations observed are reminiscent of oxidation reactions that occur in biological systems containing a redox active metal center. For example, galactose oxidase, a copper containing enzyme, promotes the oxidation of a primary alcohol to form an aldehyde along with concurrent formation of hydrogen peroxide, which is similar to what is observed in the reaction of **3** with dioxygen and methanol, ethanol, or benzyl alcohol.[9] Copper amine oxidases catalyze the aerobic oxidation of a primary amine to form an aldehyde, ammonia, and hydrogen peroxide, which may be related to the reaction of **3** with benzylamine to form *N*-benzylidene benzylamine and ammonia.[3] Both heme and dinuclear manganese catalase enzymes catalyze the disproportionation of hydrogen peroxide.[10] Studying reactions in the laboratory that are also observed in nature can offer insight into the workings of these biological enzymes.

References

1. Goldcamp, M. J.; Robison, S. E.; Krause Bauer, J. A.; Baldwin, M. J.; *Inorg. Chem.*, **2002**, *41*, 2307-2309.
2. Nash, T. *Biochem. J.* **1953,** *55*, 416-421.
3. Mure, M.; Klinman, J. P. *J. Amer. Chem. Soc.*,**1995,***117*, 8698-8706.
4. Yoe, J. H. Photometric Chemical Analysis (Colorimetry and Nephelometry); Wiley: New York, 1928, Vol. I, 307-308.
5. Murahashi, S.-I.; Yoshimura, N.; Tsumiyama, T.; Kojima, T. *J. Amer. Chem. Soc.*, **1983**, *105*, 5002-5011.
6. Eisenburg, G. M. *Indust. and Eng. Chem.* **1943,** *15*, 327-328.
7. (a) Dean, J. A. "Lange's Handbook of Chemistry," 13th Ed., New York: McGraw-Hill Book Co., 1985. (b) Vedeneyev, V. I.; Gurvich, L. V.; Kondrat'yev, V. N.; Medvedev, V. A.; Frankevich, Ye. L. "Bond Energies, Ionization Potentials, and Electron Affinities," London: Edward Arnold LTD., 1966. (c) Luo, Y.-R.; "Bond Dissociation Energies in Organic Compounds," Boca Raton, CRC Press, 2003.
8. Edison, S. E.; Hotz, R. P.; Baldwin, M. J. *Chem. Comm.*, in press.
9. Clark, K.; Penner-Hahn, J. E.; Whittaker, M. M.; Whittaker, J. W. *J. Am. Chem. Soc.*, **1990**, *112*, 6433-6434.
10. (a) Putnam, C. D.; Arvai, A. S.; Bourne, Y.; Trainer, J. A. *J. Mol. Biol.*, **2000**, *296*, 295-309. (b) Wu, A. J.; Penner-Hahn, J. E.; Pecararo, V. L. *Chem. Rev.*, **2004**, *104*, 903-938.

Chapter 3. Spectroscopic Investigation of the Reaction of [Ni(II)(TRISOX)]$_2^{2-}$ with O$_2$.

3.1. Introduction. A complementary approach to the reactivity studies reported in Chapter 2 uses spectroscopic techniques to probe the reaction between **3** and O_2. The spectroscopic toolbox for this project contained UV/visible absorption (UV/vis), resonance Raman, X-ray absorbance (XAS), and electron paramagnetic resonance (EPR) spectroscopies. The results from the various spectroscopic experiments were combined with the information obtained in the reactivity experiments to produce a proposed reaction scheme that is reported at the end of this chapter.

3.2. Monitoring the reaction via UV/visible absorption spectroscopy. UV/visible absorption spectroscopy is an excellent tool to examine this reaction because it is characterized by a color change from purple to brown.

Experimental. The reaction was monitored using a Spectral Instruments, Inc. 400 Series dip probe CCD-array spectrometer. In a typical reaction 6.7 mg (0.015 mmol) of **1** was dissolved in 30 mL of methanol or ethanol. A spectrum was collected of the neutral purple solution. Next, 0.1 mL of a methanolic 0.5 M KOH solution was added to the air-exposed sample and spectra were collected at regular time intervals. Variables such as the counter anion and the temperature were also investigated and the results will be reported.

Addition of substrates. In a typical reaction 19 mg (0.04 mmol) of **1** are dissolved in 40 mL of acetonitrile and an excess of crushed KOH (typically 50 mg) is added to the solution and allowed to stir for at least one hour, during which time the solution becomes a darker purple color. The excess KOH and the solid potassium nitrate that is formed during the deprotonation reaction are removed by filtration. The acetonitrile is then removed by rotary evaporation. The dark purple solid is washed with hexanes and diethyl ether and the oxygen activity of the solution is confirmed by dissolving a small amount of the solid in methanol. If the color change to brown occurs, the sample is considered oxygen active. This solid is then re-dissolved in acetonitrile and a UV/vis spectrum is collected on the dark purple solution. Next, 200-300 equivalents of substrate (1,4-cyclohexadiene (1,4-chd), benzyl alcohol, benzylamine, or *N*-methylbenzylamine) are added to the solution under aerobic conditions. The color change is monitored via UV/visible absorption spectroscopy.

Triphenylphosphine (3 equivalents) was also added to a 2 mM, methanolic solution of **3** that was prepared as described previously and the spectrum was collected.

Results and discussion. Monitoring the reaction with UV/visible absorption spectroscopy revealed an absorption band at 350 nm with a shoulder at 420 nm that maximized after approximately 60 seconds and then began to decay (Figure 3.1). Repeating the experiment at 0° C produced the expected result of a slower reaction that took longer for the intermediate to appear and decay. The absorption band at 350 nm maximized after thirty minutes and then began to decay (Figure 3.2).

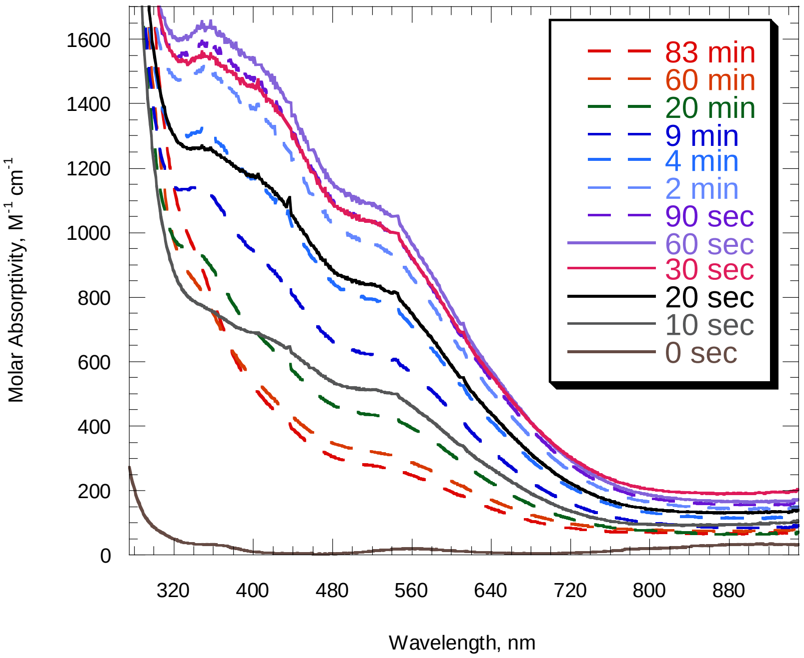

Figure 3.1. UV/visible absorption spectra of the reaction between **3** and O_2 in methanol. The solid lines indicate an increase in intensity while the dashed lines indicate decay in intensity.

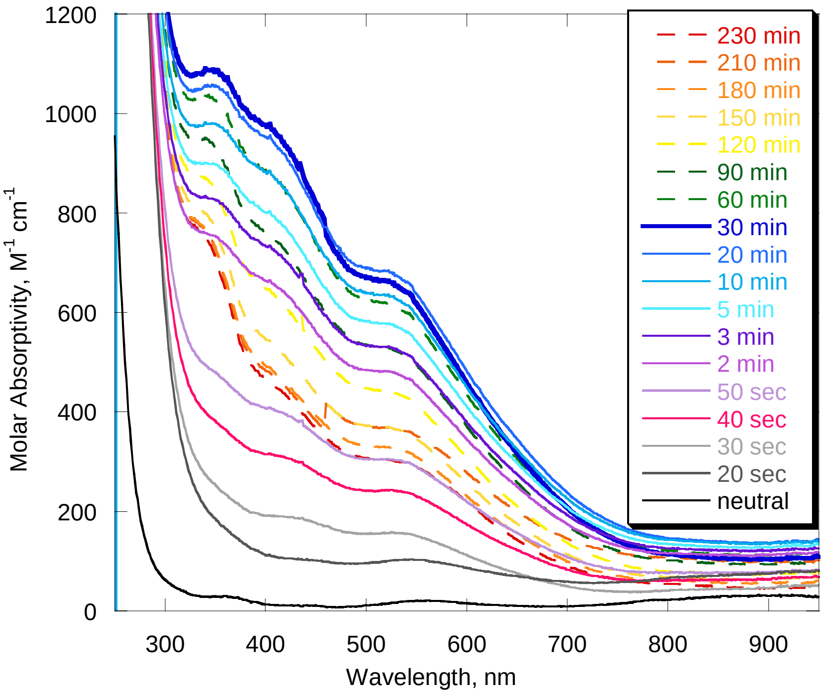

Figure 3.2. UV/visible absorption spectra of the reaction between **3** and O_2 in methanol at 0° C. The solid lines indicate an increase in intensity while the dashed lines indicate decay in intensity.

The intensity of the absorption band at 350 nm appears to be greater during the room temperature experiment; however, later experiments showed that the intensity of that band is highly irreproducible. At –40° C the color change from purple to brown was not observed and the absorption band at 350 nm did not grow in.

The room temperature experiment was repeated in a closed system with pure dioxygen bubbling through the sample. This set of spectra is shown in Figure 3.3.

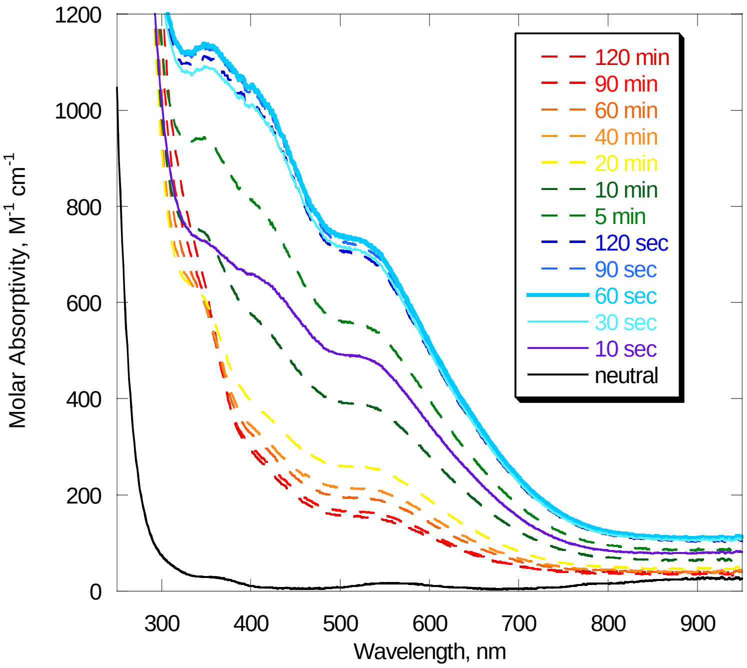

Figure 3.3. UV/visible absorption spectra of the reaction between **3** and O_2 in methanol (bubbling pure O_2 through the solution). The solid lines indicate an increase in intensity while the dashed lines indicate decay in intensity.

Saturating the solution with pure dioxygen does not appear to significantly affect the reaction (at least not spectroscopically), although at the early stages of the reaction the intensity of the band at 350 nm appears to increase more quickly in the sample that was sparged with dioxygen. After ten seconds the ambient air sample reached 47% of the 60 s peak height at 350 nm while the pure dioxygen sample had reached 64% of the intensity.

However, by thirty seconds both samples had reached 96% absorption intensity of the 60 s spectrum. The rate of decay is also similar. After five minutes both bands are 80% as intense as the 60 s spectrum and after sixty minutes the band has disappeared. These results support the idea that there is sufficient oxygen present in the air-exposed solution to saturate the sample, as suggested in Chapter 2.2.

The UV/vis spectrum was monitored during the reaction of O_2 with KOH + **1** containing different counter anions in methanol. For these experiments, 1 mM solutions of the complexes were prepared in methanol and then 3 equivalents of base were added to initiate the reaction under atmospheric conditions. The resulting color change from blue or purple to brown was monitored by UV/vis. Figure 3.4 shows the reaction with the chloride containing complex, Figure 3.5 displays the reaction with the complex with tetrafluoroborate as the counter anion, and Figure 3.6 represents the reaction of the complex containing perchlorate.

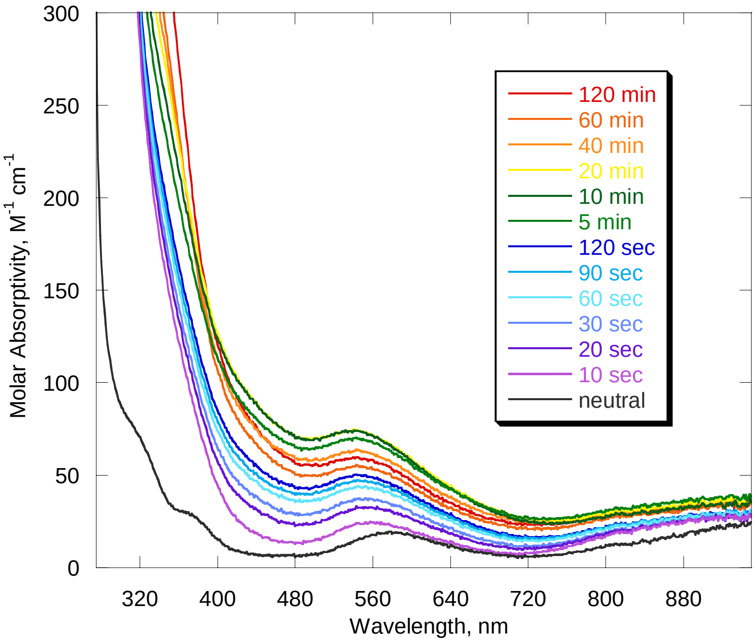

Figure 3.4. UV/visible absorption spectra of the reaction between **1** containing chloride as the counter anion, KOH, and O_2 in methanol.

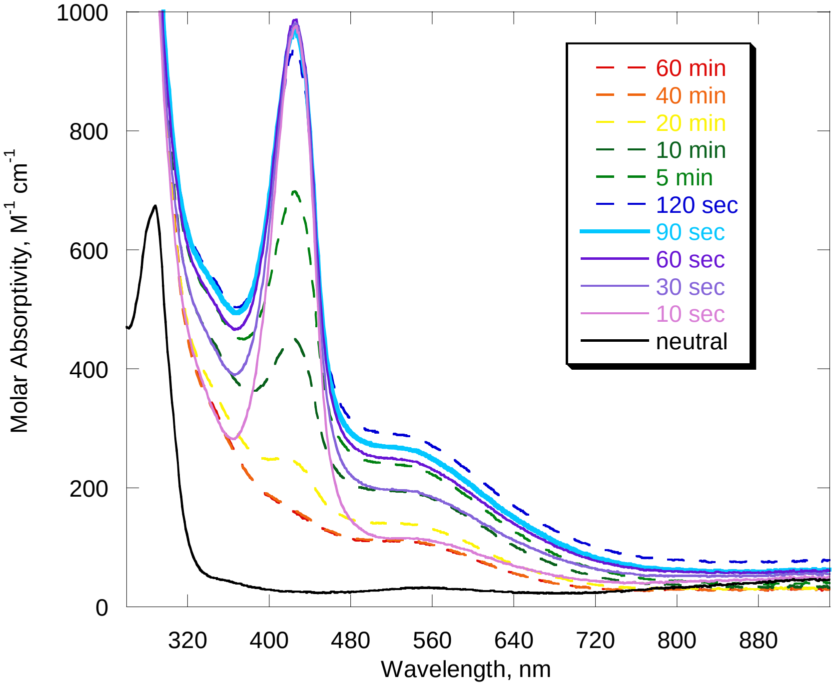

Figure 3.5. UV/visible absorption spectra of the reaction between **1** containing tetrafluoroborate as the counter anion, KOH, and O_2 in methanol. The solid lines indicate an increase in intensity while the dashed lines indicate decay in intensity.

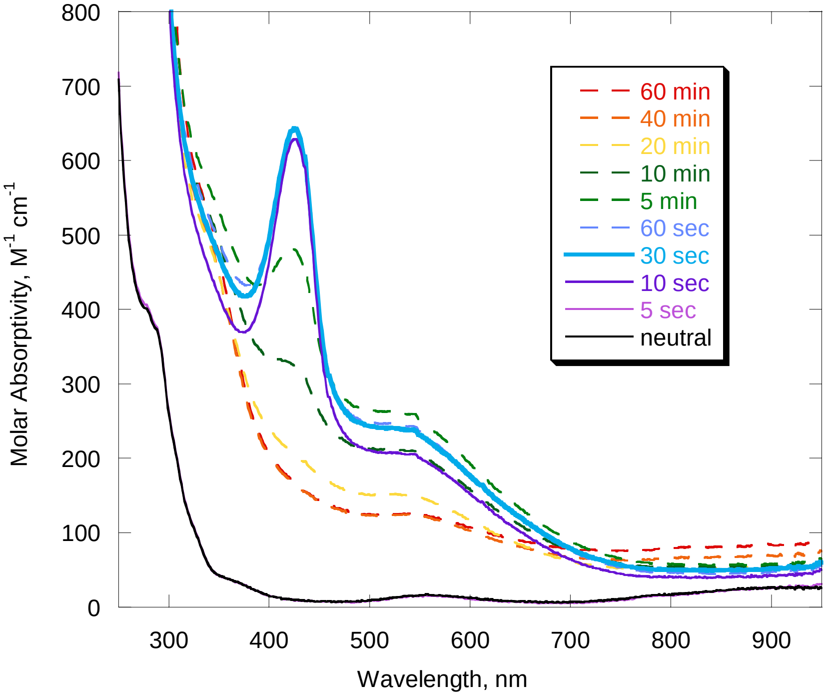

Figure 3.6. UV/visible absorption spectra of the reaction between **1** containing perchlorate as the counter anion, KOH, and O_2 in methanol. The solid lines indicate an increase in intensity while the dashed lines indicate decay in intensity.

The reaction involving the complex containing chloride as the counter anion did not display the intermediate band at 350 nm in the UV/vis spectrum, although the solution did turn brown and it did oxidize methanol to form formaldehyde. Both of the complexes containing the traditionally non-coordinating counter anions (perchlorate and tetrafluoroborate) show an intense, fairly sharp band at 425 nm that maximizes around sixty seconds and then begins to decay. Both of these solutions turned brown and both complexes oxidized methanol. It appears that the presence of a weakly or noncoordinating anion results in the appearance of an intermediate in the UV/vis spectrum, but this does not appear to significantly affect methanol oxidation (Ch. 2.2).

The UV/vis spectrum was also monitored as an acetonitrile solution of **3** was exposed to air in the presence of 1,4-cyclohexadiene (1,4-chd), a known hydrogen atom donor. This potential substrate satisfies the thermodynamic requirements discussed in Chapter 2.9. Addition of 1,4-chd resulted in a color change from purple to brown that was not observed under anaerobic conditions. The spectral changes observed are markedly similar to those seen during the reaction performed with methanol as the solvent (Figure 3.7). 1,4-chd can lose two hydrogen atoms fairly easily to form benzene. However, this oxidation product was not detected in the reaction mixture (benzene is present in 1,4-chd as a stabilizer, but an increase in the amount of benzene was not observed, although it was expected that formation of even a few equivalents of benzene should be detected by GC). Also, oxygen consumption was not observed during this reaction. This suggests that the reaction cycle does not go to completion.

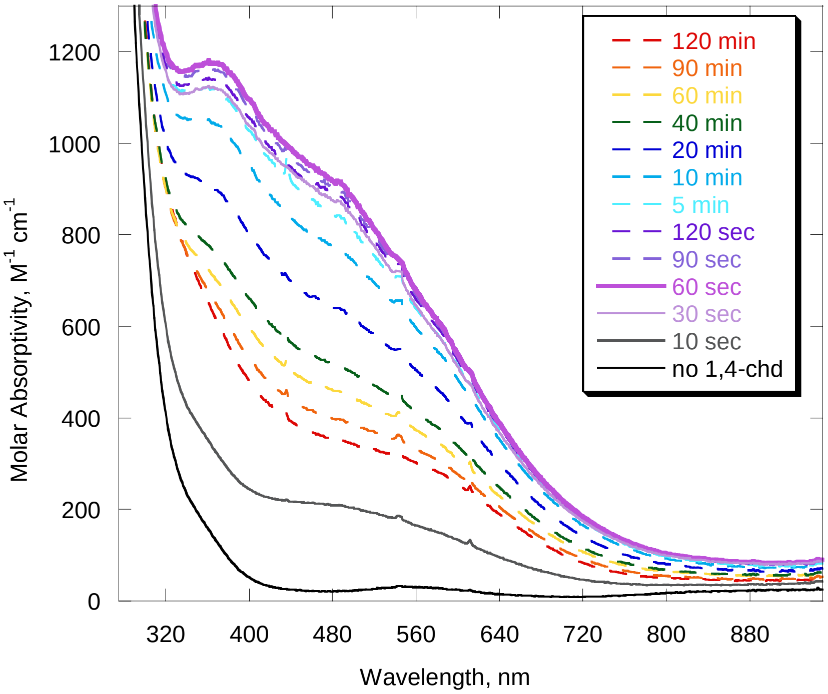

Figure 3.7. UV/visible absorption spectra of the reaction between **3** and O_2 in acetonitrile with 1,4-cyclohexadiene added. The solid lines indicate an increase in intensity while the dashed lines indicate decay in intensity.

The UV/vis spectra of the reaction with other substrates were also monitored. The experiment performed in methanol was repeated using ethanol as the solvent. The color change was observed, as was a similar intermediate spectrum (Figure 3.8); however, this spectrum maximized after 5 seconds and then the band at 350 nm began to decay. This reaction appears to be much more rapid than the reaction conducted in methanol, at least with regards to spectroscopic observables, as might be expected from the relative substrate bond strengths (Table 2.1), although later reaction steps probably also affect the reaction rate. However, as reported in Chapter 2.3, the amount of acetaldehyde formed during the oxidation of ethanol is comparable to the amount of formaldehyde produced from the methanol oxidation reaction, suggesting that the rate of the intermediate's formation and decay are not predictors of the overall yield, which is probably determined by the rate of formation of the "dead-end" product. This hypothesis was further supported when the UV/vis spectrum was monitored during reaction with different substrates.

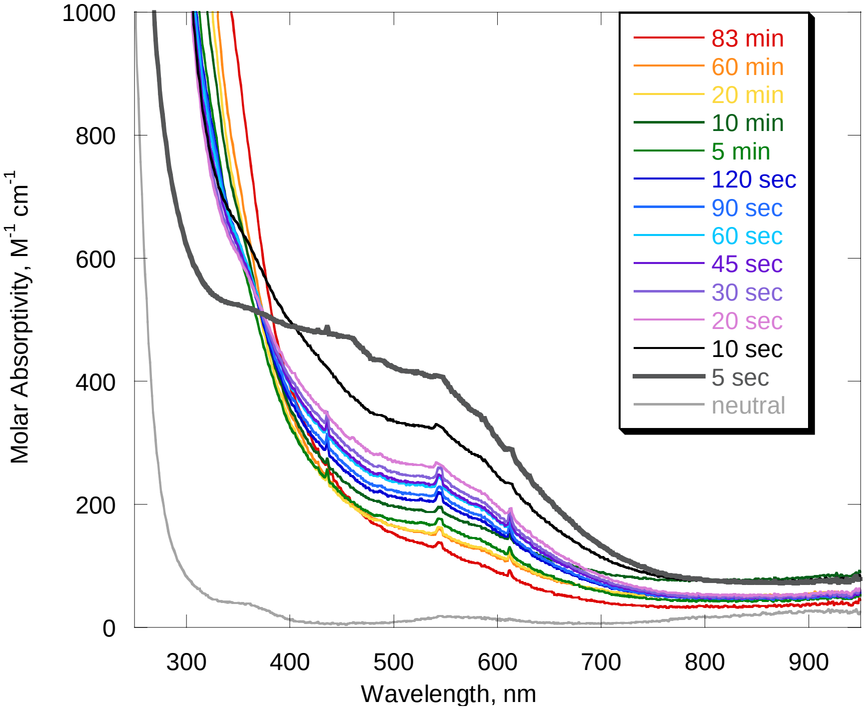

Figure 3.8. UV/visible absorption spectra of the reaction between **3** and O_2 in ethanol.

Addition of 2 mL (318 eq./**3**, 0.019 mol) of benzyl alcohol to a 2 mM acetonitrile solution of **3** produced the expected color change to brown as well as benzaldehyde, the oxidation product (see Chapter 2.4). However, the UV/vis spectrum of this reaction does not closely resemble the reaction spectra observed using methanol, ethanol, or 1,4-chd as the substrate. Figure 3.9 shows the fairly unremarkable set of spectra. Before adding benzyl alcohol the spectrum shows two absorption bands rather than the typical three bands that are observed in the spectrum of the neutral complex. Deprotonation of the oximes causes an increase in intensity of the highest energy absorption band. Addition of benzyl alcohol causes the high baseline in the first spectrum as well as an increase in intensity of the band at 500 nm that gradually decays. It is possible that the spectra were not collected quickly enough to catch the intermediate spectrum. This qualitative initial rate is supported by the relative bond strengths reported in Table 2.1. The spectra collected immediately upon addition of the substrate were very noisy with a high baseline. These spectra were subsequently discarded as no usable information could be extracted.

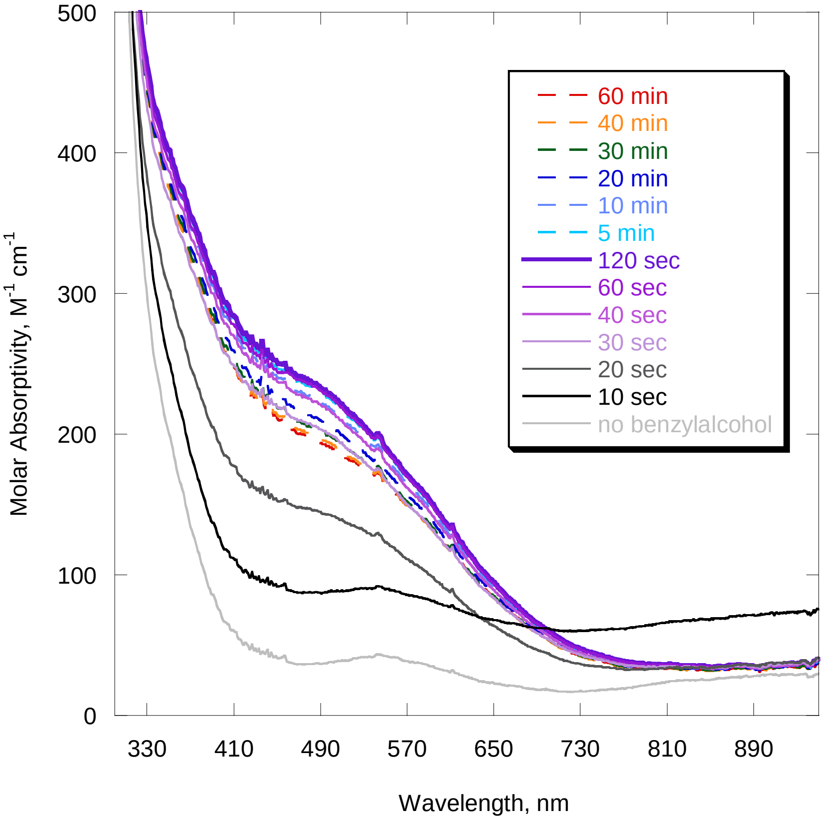

Figure 3.9. UV/visible absorption spectra of the reaction between **3** and O_2 in acetonitrile with benzyl alcohol added. The solid lines indicate an increase in intensity while the dashed lines indicate decay in intensity.

Addition of 2 mL (0.018 mol, 300 eq./**3**) of benzylamine to a 2 mM solution of **3** in acetonitrile resulted in a slow color change (~30-40 minutes) and observation of a product consistent with a Schiff-base reaction of excess benzylamine with an oxidized species (either an imine or benzaldehyde, see Chapter 2.5). Monitoring the UV/vis spectrum as it changed over time showed a band at 350 nm that grows in slowly, maximizes after forty minutes, and then begins to decay (Figure 3.10). This reaction appears to be slower than the ethanol or methanol oxidation; however, those substrates were used as the solvent, so comparisons cannot be readily made, although the qualitative rates observed are consistent with the bond strengths reported in Table 2.1, particularly with the first dissociation which would provide the largest energy barrier to the reaction.

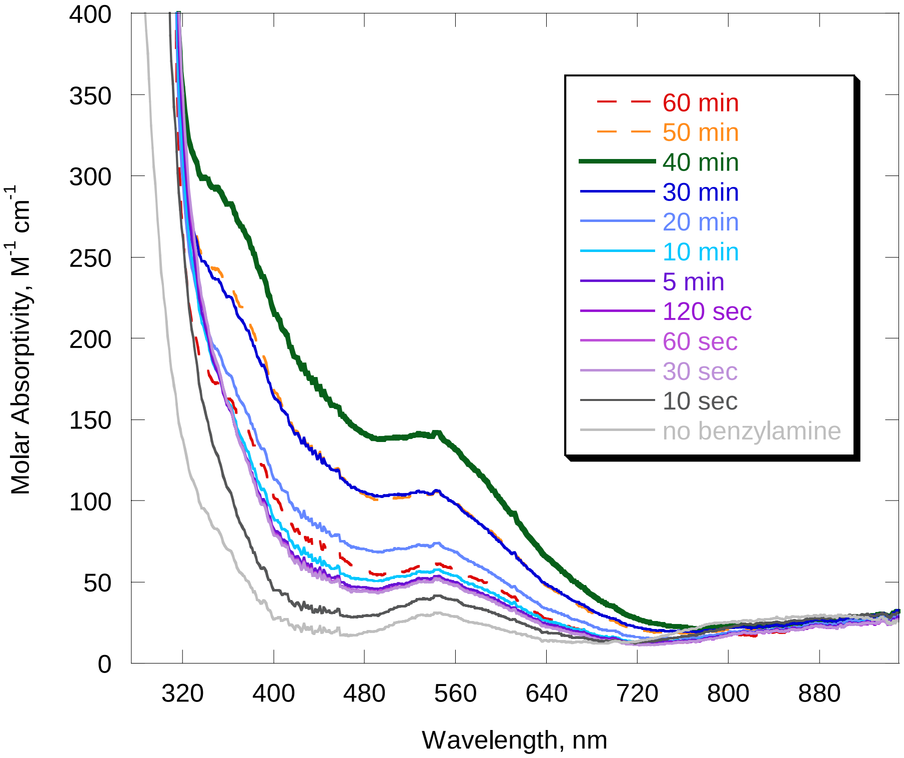

Figure 3.10. UV/visible absorption spectra of the reaction between **3** and O_2 in acetonitrile with benzylamine added. The solid lines indicate an increase in intensity while the dashed lines indicate decay in intensity.

The UV/vis spectrum was also monitored during the reaction of **3** with O_2 using *N*-methylbenzylamine as a substrate. 0.14 mL (100 eq./**3**, 0.0011 mol) of substrate were added to a 0.5 mM solution of **3** in acetonitrile. The color change occurred and the same Schiff-base product that was observed during the reaction with benzylamine was detected (see Chapter 2.6). This reaction was accompanied by the appearance of a band at 440 nm that maximized after two minutes and then began to decay, as can be seen in Figure 3.11.

Comparison of the UV/vis spectra of the reaction of **3** with dioxygen in the presence of several hydrogen atom-donating substrates reveals that the spectroscopic changes that occur are not consistent for each substrate. However, experimental conditions were not identical in each experiment, which may account for the differences in spectral intensities.

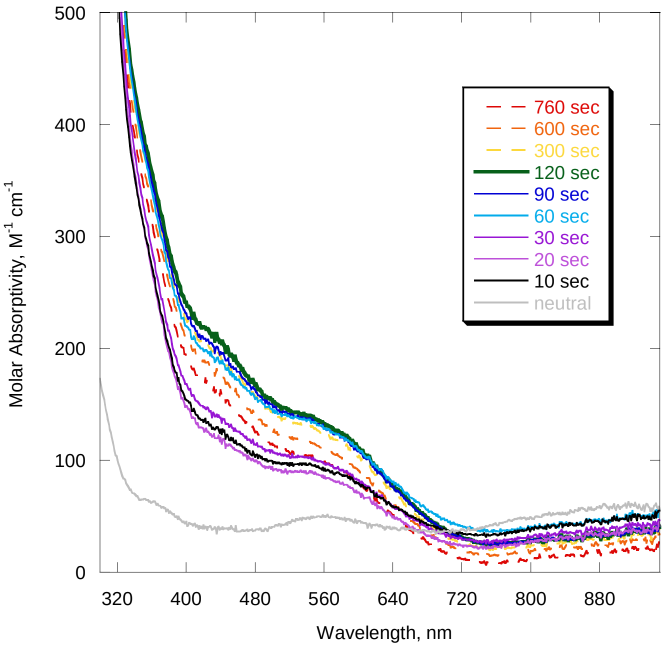

Figure 3.11. UV/visible absorption spectra of the reaction between **3** and O_2 in acetonitrile with *N*-methylbenzylamine added. The solid lines indicate an increase in intensity while the dashed lines indicate decay in intensity.

Finally, the UV/vis absorption spectrum was monitored as **3** reacted with dioxygen in methanol in the presence of triphenylphospine. For this experiment, 15 mg (5.9×10^{-5} mol, 3.3 eq./**3**) of triphenylphosphine was added to a 1.2 mM methanolic solution of **1**. Then, 0.053 mL(3 eq./**1**) of a 1 M solution of KOH in methanol were added to the aerobic solution to initiate the reaction and the UV/Vis spectra were collected (Figure 3.12). As expected, the spectra look very similar to the reaction in methanol with no triphenylphosphine added. The oxidation of triphenylphosphine takes several hours to occur (see Chapter 2.9), so the early reaction should not be affected. The UV/vis spectrum looks identical after two and five hours of reaction time (five hour spectrum not shown), indicating that even at later times the spectroscopic properties are not affected by the presence of this substrate.

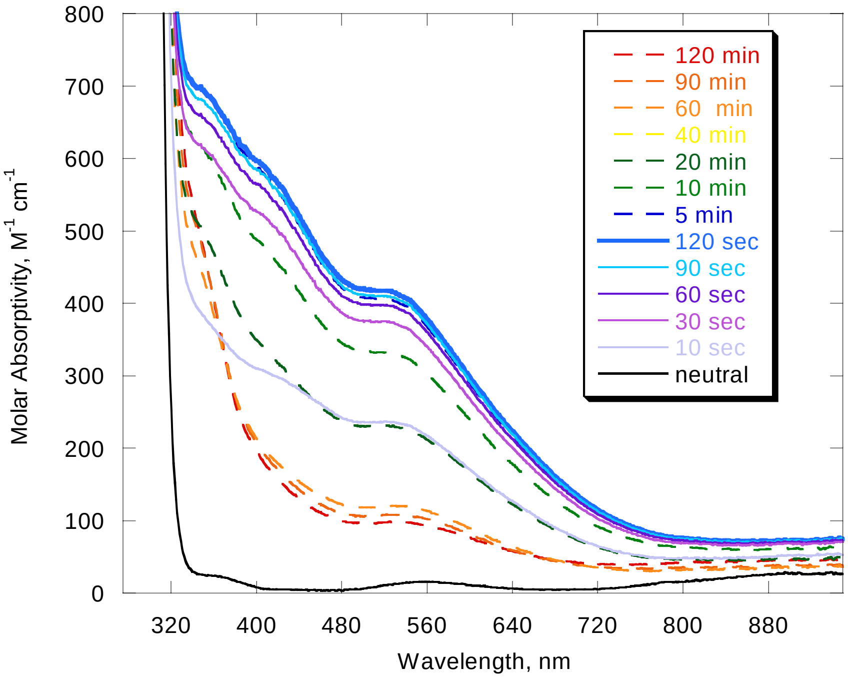

Figure 3.12. UV/visible absorption spectra of the reaction between **3** and O_2 in methanol with triphenylphosphine added. The solid lines indicate an increase in intensity while the dashed lines indicate decay in intensity.

3.3. Spectroelectrochemical analysis of $[Ni(II)(TRISOX)]_2^{2-}$. Solutions of **3** were electrochemically oxidized and their UV/vis spectrum collected and compared to the spectrum of the air exposed sample.

Experimental (Bulk Electrolysis). A solution of **3** was bulk electrolyzed while monitoring the absorption spectrum. In a typical experiment 35 mg (0.078 mmol) of **1** are dissolved in 160 mL of distilled DMF that also contained 6 g (0.015 mol) of tetrabutylammonium hexafluorophosphate (TBA PF_6) as the supporting electrolyte. The sample was purged with argon both before and during the reaction, and 0.23 mL of 1 M KOH in methanol was added to the sample immediately prior to starting the experiment. First, a cyclic voltammagram (CV) was collected on a 10 mL portion of the sample in a dry ice/acetonitrile bath that maintained the temperature at –40° C. A glassy carbon working electrode was used along with a platinum wire auxiliary electrode and a Ag/Ag(NO_3) reference electrode. A scan rate of 250 mV/second was employed. A potential of 0 mV was chosen for the bulk electrolysis experiment. The CV looked fairly featureless at low temperature, so the room temperature CV was also collected.

The sample cell contained the solution, a working electrode composed of reticulated vitreous carbon with a large surface area, a platinum wire auxiliary electrode, and a Ag/Ag(NO_3) reference electrode. The solution was continuously purged with Ar. The cell was placed into an acetonitrile/dry ice bath (-40° C). The electrolysis reaction was started and the dip probe simultaneously began collecting data.

This experiment was repeated using acetonitrile as the solvent. A 1.95 mM sample of **3** (made by deprotonating **1** in acetonitrile and isolating the solid) was prepared in 10 mL of distilled acetonitrile that also contained 0.4 g of TBA PF_6 (1.0×10^{-5} mol).

This sample was used to look at the cyclic voltammagram of the acetonitrile solution at ~ -30° C (temperature was maintained in a nitromethane/liquid nitrogen bath). The same electrodes and scan rate were used in this experiment as in the experiment using DMF as the solvent. A potential of 675 mV was applied during the bulk electrolysis experiment since it is more positive than any of the oxidation features seen in the CV. For this experiment a 150 mL solution of 0.25 mM **3** and 100 mM TBA PF_6 was prepared in distilled acetonitrile. The same electrochemical cell was used as in the experiment using DMF as the solvent, and the cell was immersed in a nitromethane/liquid nitrogen bath to maintain a temperature of approximately -30° C. The UV/vis spectrum was monitored during the electrochemical oxidation.

Results and discussion. The CV of **3** in DMF is shown in Figure 3.13. Three low potential oxidation features are observed. This is different than the CV of **3** in acetonitrile (see Figures 3.16 and 3.19), which has two oxidation features. The CV of **3** in methanol (Figure 3.21) also has three oxidation features. This may mean that in more strongly coordinating solvents, such as DMF and methanol, inhomogeneity occurs where species with different solvations or monomer-dimer equilibria are present, leading to multiple oxidation features. However, it is also possible that the third process is a follow-up reaction that occurs in coordinating solvents.

Before bulk electrolyzing the sample, Faraday’s Law was used to calculate the number of electrons that would be transferred per molecule during the reaction. To determine how much charge must be passed to oxidize each monomeric nickel complex present, the following equation was used:

$$Q = nFN$$

where Q is the total charged passed during the experiment, n is the number of electrons transferred per molecule, F is Faraday's constant (96500 C/mole), and N is the number of moles in the sample (equal to ½ the amount of **1** added, since **3** is presumed to be a dimer). For this experiment 3.56 C must be passed to singly oxidize all of **3**.

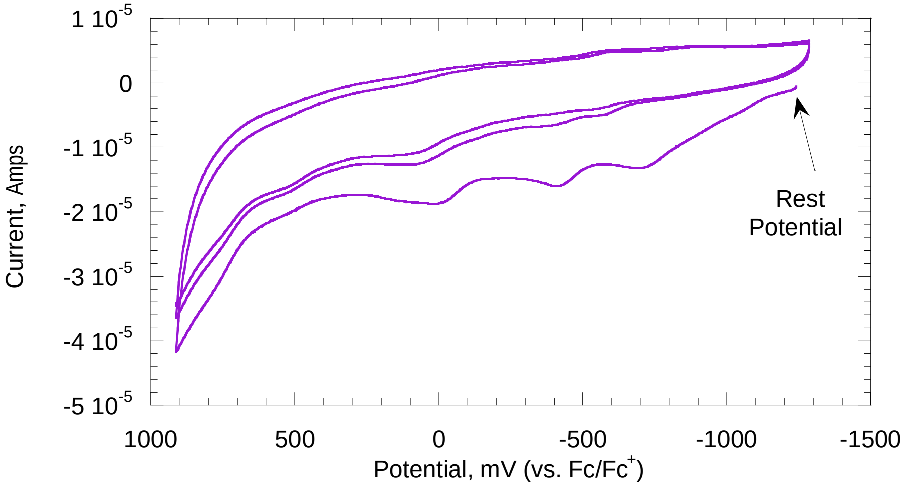

Figure 3.13. Cyclic voltammagram of **3** in DMF with TBA PF_6 as the supporting electrolyte.

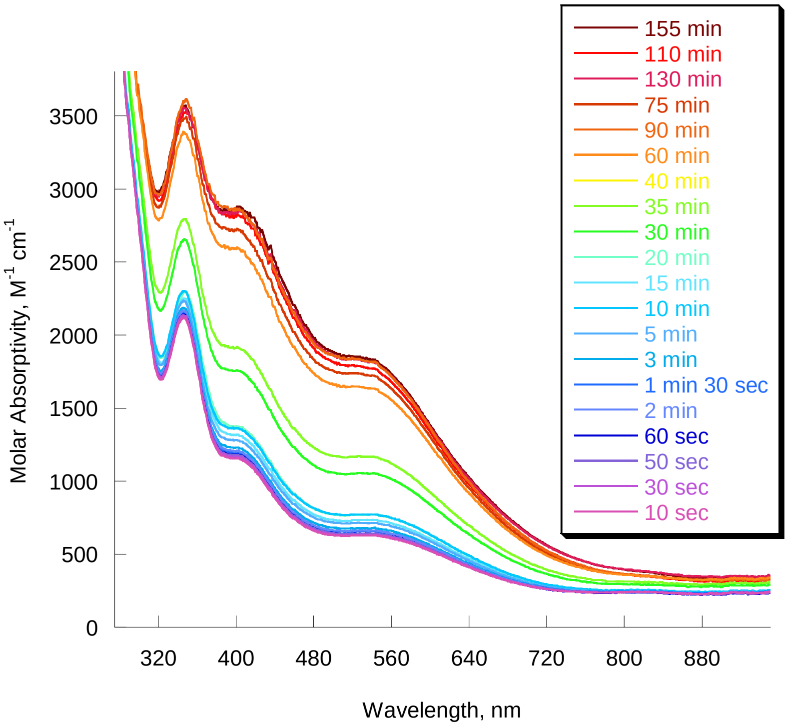

Figure 3.14. UV/visible absorption spectra of the electrochemical oxidation of **3** in DMF.

During this experiment the solution became a very dark brown, much like in the dioxygen reaction. The three bands seen in the absorption spectrum in Figure 3.14 increase as more and more of the sample is oxidized. The most intense band is at 350 nm, which is where the intermediate band appears and then disappears during the air oxidation reaction. This suggests that the electrochemically oxidized species and air oxidized intermediate are similar. That is, the Ni(TRISOX) unit is oxidized in the observed intermediate.

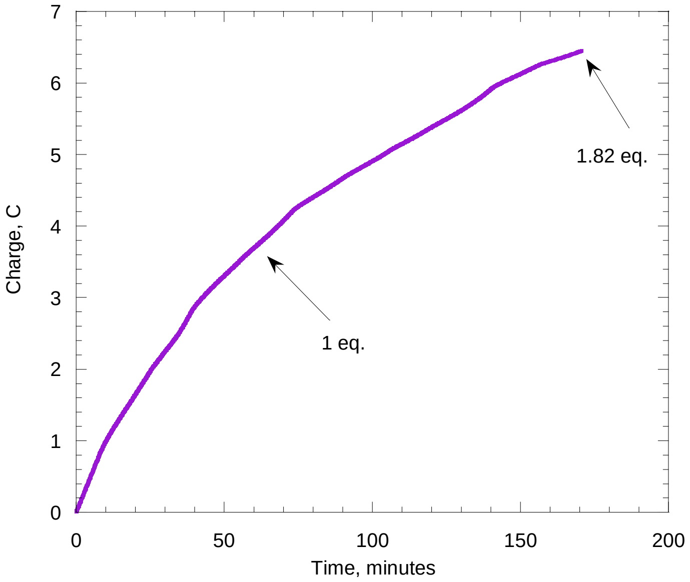

Figure 3.15. Plot of the amount of charged passed through the sample versus time. At the conclusion of the experiment 90% of the sample had been oxidized by two equivalents.

At the end of this experiment, 6.45 C had been passed, meaning that 1.82 oxidizing equivalents per **3** had been passed, or that 91% of **3** was doubly oxidized, or 82% was doubly oxidized and the remainder singly oxidized, or any combination of oxidized species could be present (see Figure 3.15).

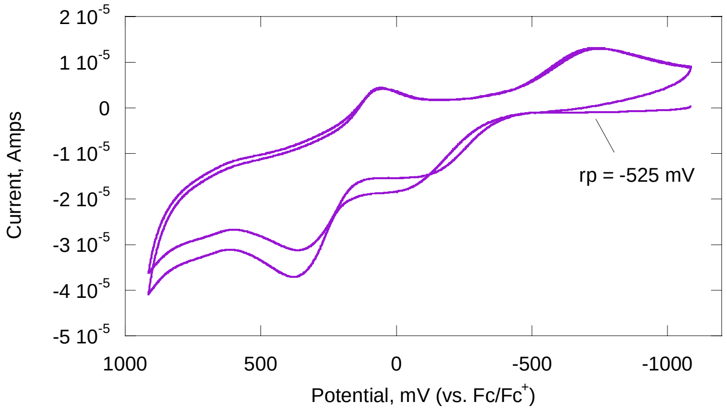

Figure 3.16. Cyclic voltammagram of **3** in acetonitrile at –30°C with TBA PF_6 as the supporting electrolyte.

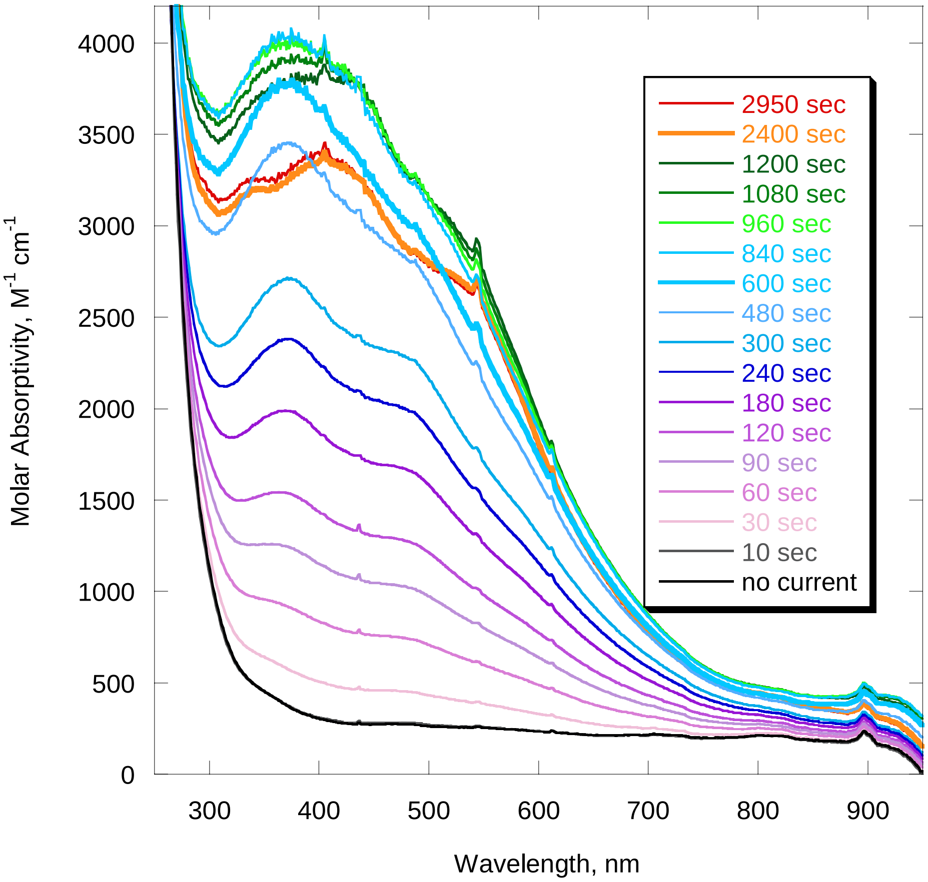

Figure 3.17. UV/visible absorption spectra of the electrochemical oxidation of **3** in acetonitrile. Bold lines indicate the passage of an oxidizing equivalent.

The experiment was repeated in acetonitrile. Figure 3.16 shows the low temperature CV which consists of two oxidation features. Applying a potential of 675 mV resulted in a color change to brown. The UV/vis spectrum was monitored during this experiment and can be seen in Figure 3.17. The absorption bands in this set of spectra are not as well-resolved as those observed during the reaction in DMF, but they do more closely resemble the spectra that resulted from the air oxidation reaction in both methanol and in acetonitrile with 1,4-chd added, which supports the hypothesis that the electrochemically and air oxidized intermediate species are similar. It was calculated that 3.65 C must be passed to singly oxidize each complex of **3**. At the end of this experiment, 7.7 C (more than two oxidizing equivalents) were passed (see Figure 3.18). As the first oxidizing equivalent is being passed, a band at 370 nm grows in. However, after passage of one oxidizing equivalent that band becomes less intense and a band at 405 nm becomes prominent.

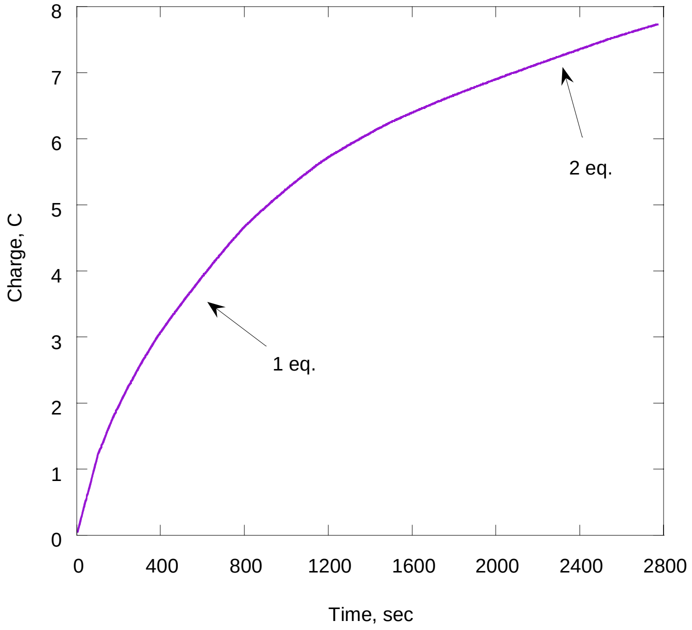

Figure 3.18. Plot of the amount of charged passed through the sample versus time. At the conclusion of the experiment the entire sample had been oxidized by two equivalents.

This experiment was also repeated using methanol as the solvent. However, the solution became cloudy at the low temperatures required to do the bulk electrolysis (bulk electrolysis of **3** at room temperature did not oxidize the entire sample), probably due to a lowering of the solubility of the electrolyte, resulting in noisy spectra with a high baseline. The spectra did qualitatively resemble those collected during the air oxidation reaction of **3** in methanol.

These results offer insight into the nature of the reaction involving **3** and dioxygen by demonstrating that the spectra observed during the electrochemical and air oxidation reactions resemble each other. However, there was some concern that an impurity could be responsible for the spectroscopic observables. Therefore, experiments were conducted with the help of the Seliskar research group using an optically transparent thin layer electrochemical cell (OTTLE)[1] to ensure that the entire sample was being oxidized while the UV/vis absorption spectrum was collected. Photographs of the OTTLE cell can be seen in Figures 3.19 and 3.20.

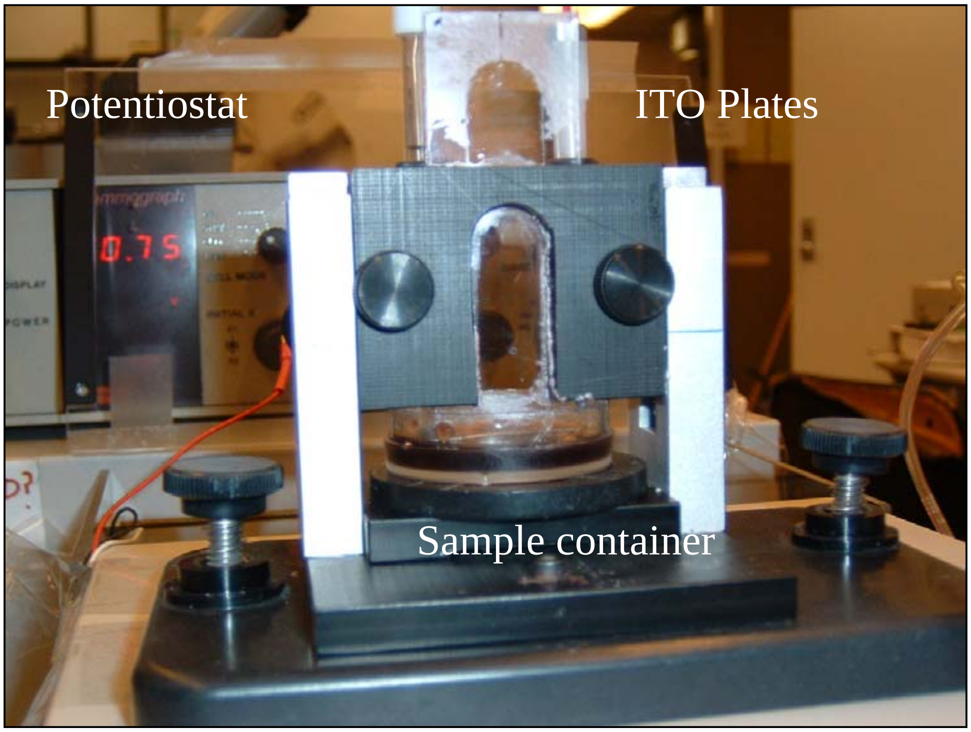

Figure 3.19. Photograph of OTTLE cell (side view).

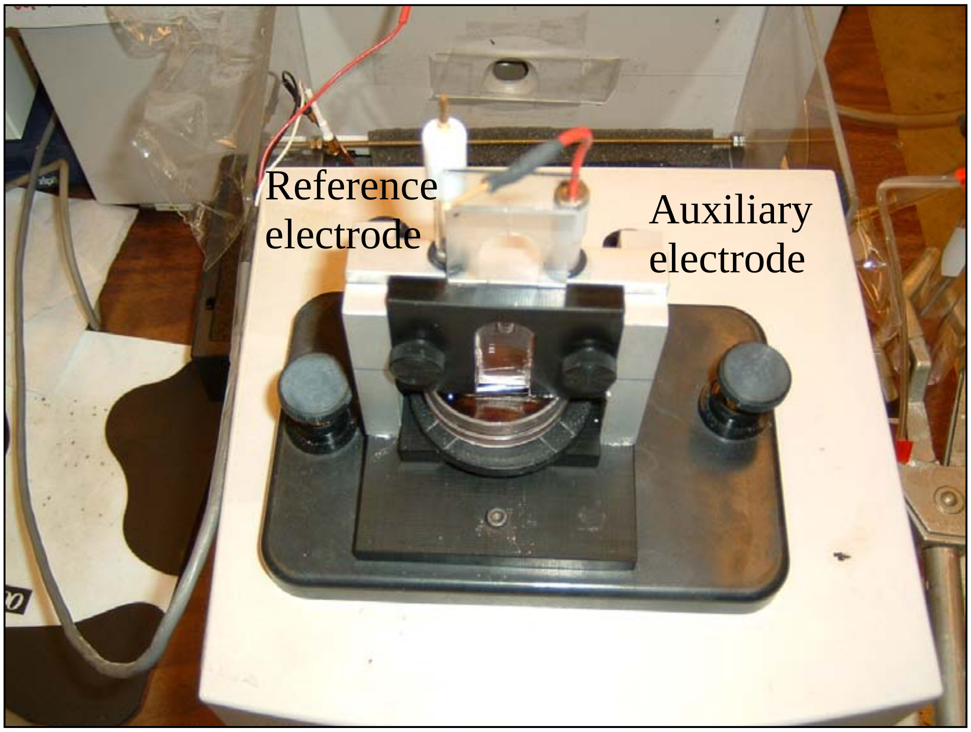

Figure 3.20. Photograph of OTTLE cell. (aerial view).

Experimental (Thin Layer Spectroelectrochemistry). In this experiment a solution of 2 mM **3** and 100 mM TBA PF_6 was prepared in acetonitrile. First, an aliquot was removed, and a CV was collected using the same electrode set up and scan rate used in the previously described experiments. The remaining solution was placed into a shallow glass dish and then the OTTLE cell, which consisted of two indium tin oxide (ITO) plates sandwiched together with a 0.02 cm silicon spacer between them, was also placed into the dish and capillary action drew the sample into the cell. The OTTLE cell functioned as both the working electrode and the UV/vis cell. It was connected to a potentiostat, as were the Ag/AgCl reference electrode and the platinum wire auxiliary electrode. Various potentials were applied to the entire sample and the UV/Vis absorption spectrum was collected.

Anaerobic spectroelectrochemistry was also performed on a solution of **3** in methanol by constructing (with the assistance of the Seliskar group) an acrylic box that fit into the space between the lamp and the detector of the spectrophotometer, over the OTTLE cell. This box was continuously flushed with argon, as was a 2 mM methanolic solution of **3** containing 80 mM $NaClO_4$ as the supporting electrolyte. After this sample and the box were sparged for approximately one hour, the sample was transferred into the glass dish beneath the OTTLE cell via a Tygon tube (positive pressure from the flowing argon facilitated the transfer). Next, various potentials were applied to the sample in the OTTLE cell as described for the acetonitrile experiment, using the CV collected from the same sample as a guide to the potentials applied.

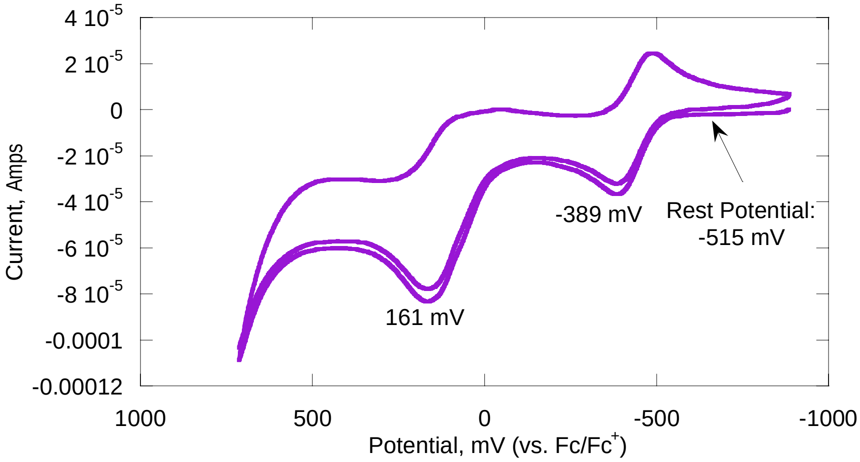

Figure 3.21. Cyclic voltammagram of **3** in acetonitrile at room temperature with TBA PF_6 as the supporting electrolyte.

Results and Discussion. The CV of the acetonitrile solution of **3** showed two fairly low potential oxidation features, one at –389 mV that is reversible and one at 161 mV that is not, (Figure 3.21).

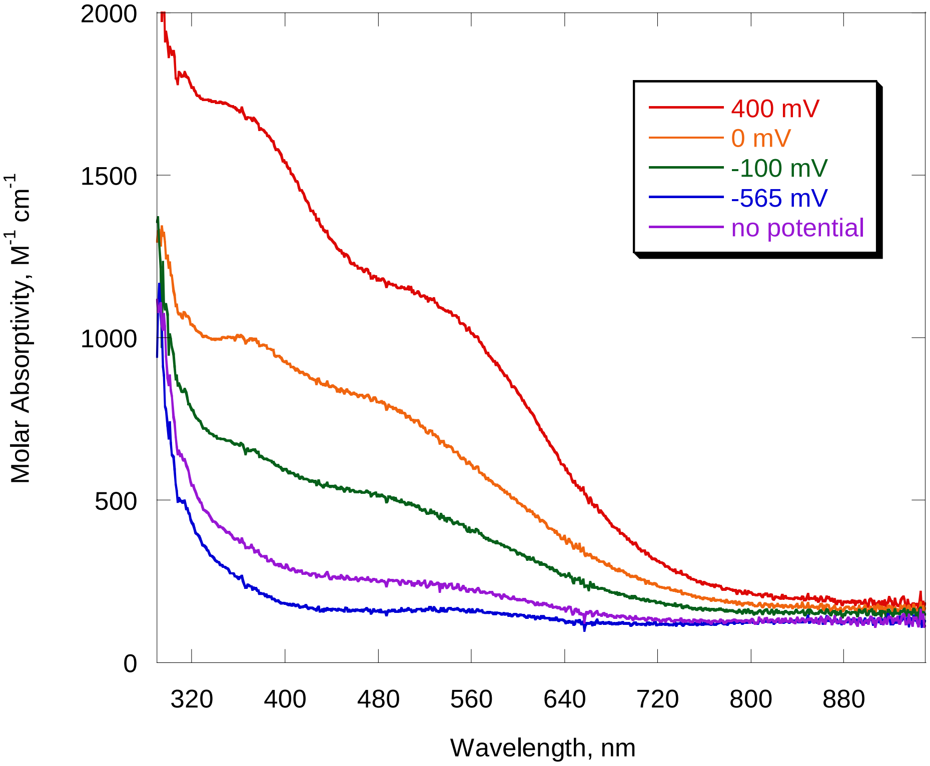

Figure 3.22. UV/vis spectra of **3** in acetonitrile as collected in an OTTLE cell as various potentials are applied. Red = 400 mV, orange = 0 mV, green = -100 mV, blue = -565 mV, purple = no potential is applied.

A potential was applied on either side of the second oxidation feature observed in the CV, at-100 mV, 0 mV, and at 450 mV. In Figure 3.22, the purple spectrum was collected when no potential was applied and the blue spectrum was collected when a potential more negative than the resting potential was applied (-565 mV). Applying a potential of 400 mV, 0 mV, or –100 mV resulted in the red, orange, and green spectra, respectively. In each case a band appears at 350 nm although it becomes more intense as the potential becomes more positive. One explanation could be that both oxidations are fairly similar, thus producing similar spectra. For example, each oxidation could occur on an oximate on the ligand, resulting in a similar spectroscopic response or the oxidations could be due to one Ni(II) being oxidized to Ni(III) and then the second Ni(II) on the dimer being oxidized to Ni(III). Another explanation for these similarities could be that a chemical disproportionation step occurs, where the dimeric active species is oxidized by one equivalent at -100 mV only to disproportionate into the doubly oxidized dimer and the unoxidized dimer.

The electrochemically oxidized, non-oxygen active acetonitrile solution of **3** produced a UV/vis spectrum that was similar to the air exposed methanolic sample. In order to make a direct comparison of the air exposed and electrochemically oxidized sample of **3** in methanol an anaerobic spectroelectrochemical cell was constructed with the help of the Seliskar group at the University of Cincinnati. Figures 3.23 and 3.24 show photographs of the setup.

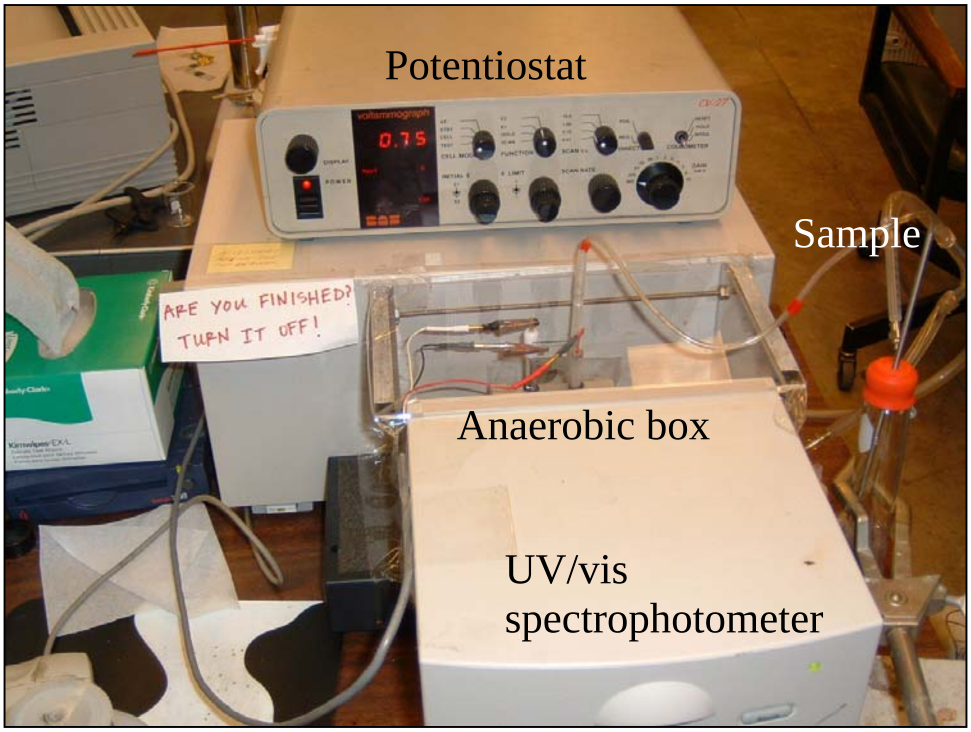

Figure 3.23. Photograph of anaerobic spectroelectrochemistry set up (aerial view).

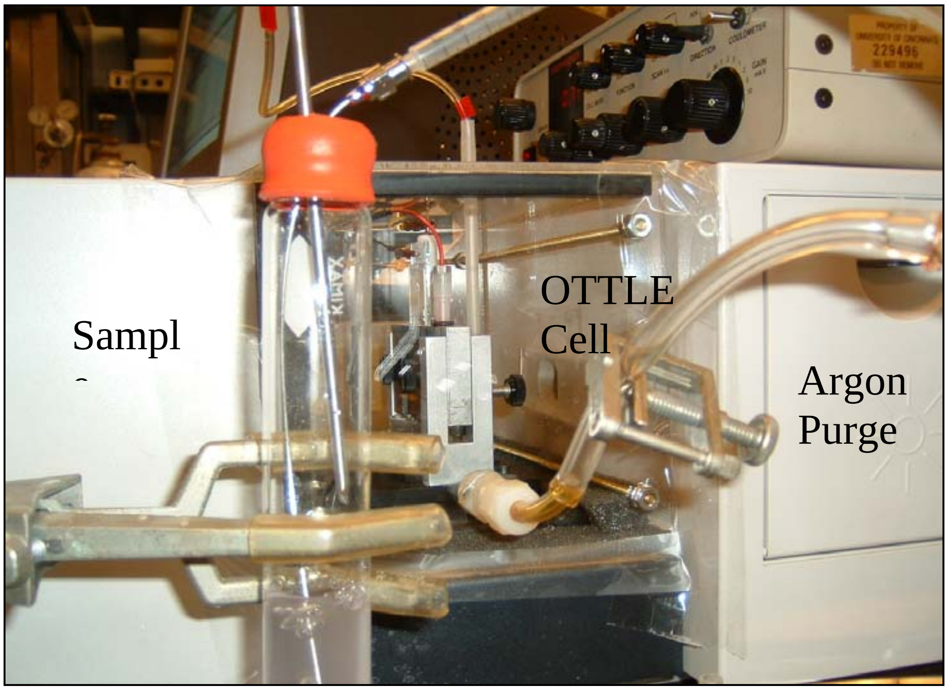

Figure 3.24. Photograph of anaerobic spectroelectrochemistry set up (side view).

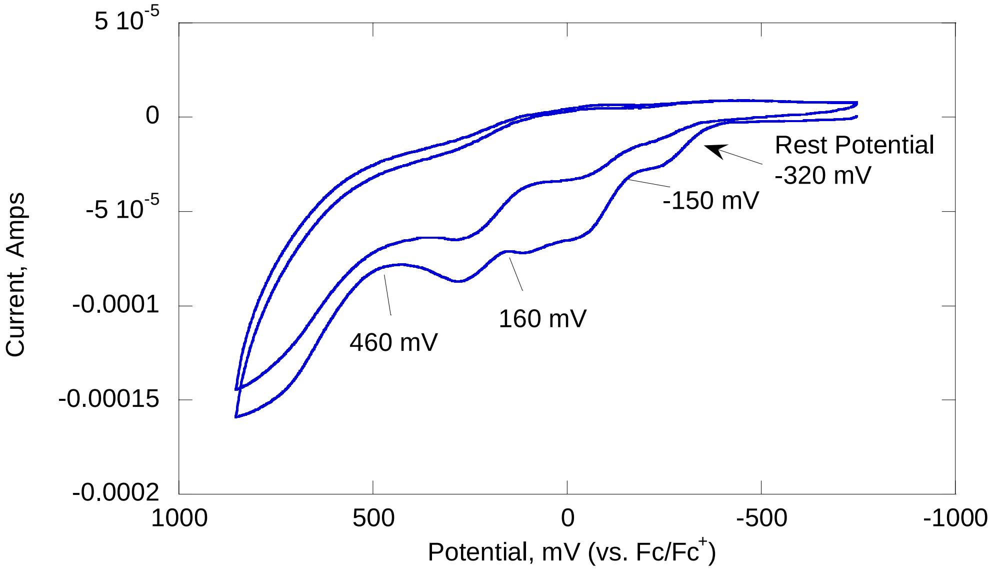

Figure 3.25. Cyclic voltammagram of **3** in methanol at room temperature with $NaClO_4$ as the supporting electrolyte.

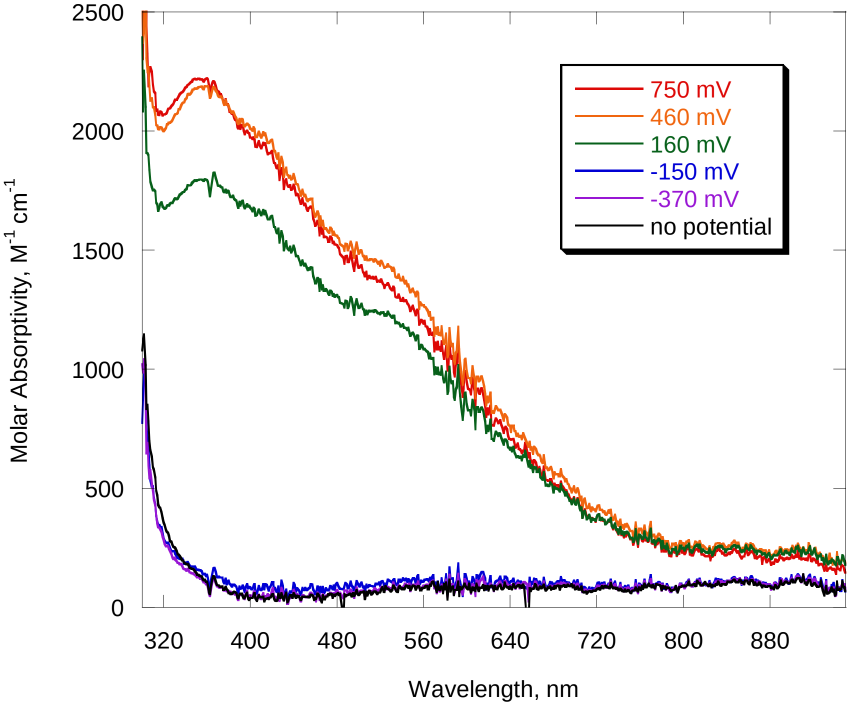

Figure 3.26. UV/vis spectra of **3** in methanol as collected in an OTTLE cell under anaerobic conditions as various potentials are applied. Red = 750 mV, orange = 460 mV, green = 160 mV, blue = -150 mV, purple = -370 mV, black = no potential is applied.

The CV of **3** in methanol (Figure 3.25) has three oxidation features, similar to the CV of **3** in DMF (Figure 3.13). This CV was used to determine what potentials to apply to the sample. When no potential is applied, or when a potential more negative than the resting potential is applied, the UV/vis spectrum is fairly featureless, as can be seen in the black and purple spectra in Figure 3.26. The spectrum remains featureless when a potential of –150 mV is applied, which is to the left of the first oxidation feature (blue spectrum in Figure 3.26). This indicates that this oxidation feature does not form the same type of species observed in the air exposed sample or the electrochemically oxidized sample in acetonitrile, which supports the theory that more coordinating solvents result in inhomogeneity of the sample. Applying potentials of 160 mV (green spectrum), 460 mV (orange spectrum), and 750 mV (red spectrum) results in the appearance of bands at 350, 410, and 550 nm. This is comparable to the spectra observed in the electrochemically oxidized acetonitrile sample as well as the air exposed methanol sample.

Reproducing the spectroelectrochemical results using an OTTLE cell that oxidized the entire sample confirms that the spectroscopic observables are due to the sample and not to an impurity present in solution. The appearance of the band at around 350 and 550 nm in both the electrochemically oxidized sample and the air oxidized sample suggests that the two species are quite similar.

3.4. X-ray absorption spectroscopy of $[Ni(II)(TRISOX)]_2^{2-}$.

X-ray absorption spectroscopy (XAS) is similar to UV/visible absorption spectroscopy, employing X-rays rather than ultra-violet or visible radiation. However, while UV/visible absorption spectroscopy shows electronic transitions of the complex (i.e. MLCT, LMCT, d-d bands), X-ray absorption spectroscopy allows one to determine the oxidation state of the atom of interest, through the X-ray absorption near edge spectroscopy (XANES) experiment, the XAS spectrum of a given sample will exhibit a sharp edge at a photon energy equal to the ionization potential of a bound electron in the constituent atoms of the sample. The core electrons require different energies to dislodge from atoms in different excitation states. XAS can also determine what other atoms are connected at what distance to the atom of interest based on interference patterns from scattered photoelectron waves, using the extended X-ray absorption fine structure (EXAFS) experiment.

A collaboration was formed with the Penner-Hahn group at the University of Michigan to collect XANES spectra, to obtain information about the oxidation state of the Ni, as well as information about the geometry around that atom.

Experimental. XANES data were collected at 10 and 0.5 mM concentrations of **1** dissolved in methanol distilled from CaH_2. First, 1 M KOH (in methanol) was added to each sample to initiate the reaction with O_2, and the samples were then placed into sample cells and quickly frozen in liquid nitrogen at various time intervals, including times near the maximum intensity of the intermediate observed in the UV/vis spectrum. The samples remained in liquid nitrogen until the XANES spectra were collected. X-ray absorption spectra were measured as fluorescence excitation spectra at beamline 7-3 at the Stanford Synchrotron Radiation Laboratory (SSRL) using a thirty-element solid-state energy-dispersive detector and at beamline X9B at the National Synchrotron Light Source (NSLS) using a thirteen element dectector. Incident radiation was monochromatized using either a Si[220] or a Si[111] double crystal monochromator, at SSRL and NSLS respectively. At NSLS, a mirror was used for harmonic rejection and the monochromator was operated fully tuned; at SSRL, harmonic rejection was accomplished by detuning the monochromator by 50%. Incident intensity was measured with a N_2 filled ion chamber, and energies were calibrated to the first rising inflection point in the edge spectrum of a nickel metal foil, which was defined to be 8333 eV. Sample temperature was held at approximately 10 K using an Oxford liquid helium flow cryostat at SSRL and at 13-20 K using a Displex cryostat at NSLS. A minimum of 2, and typically 4 scans were measured for each sample. In every case, the first and last scans were compared; no evidence was found for radiation-induced changes in the samples during the measurements. Each detector channel of every scan was checked for glitches and the good channels (~28 for SSRL and ~10 for NSLS) were averaged for each sample to yield the final spectrum. The XANES data were normalized to tabulated X-ray absorption cross sections using an error function plus a third order polynomial to model the background over both the pre- and post-edge regions simultaneously.

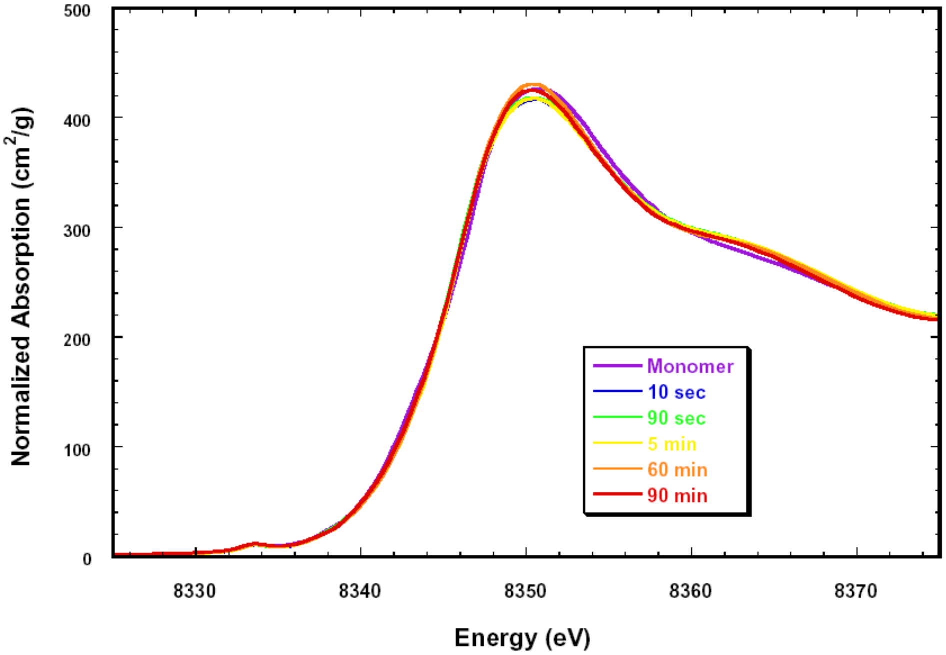

Figure 3.27. XANES spectra of 10 mM **3** as it reacts with dioxygen in methanol.

Results and discussion. If the metal center of interest is oxidized or reduced during the reaction, it will absorb a different amount of energy during the XANES experiment, causing a shift in the edge energy of the spectrum. As can be seen in Figures 3.27 and 3.28, the edge energy did not shift during the XANES experiment for either concentration analyzed, indicating that a significant amount of Ni(III) is not formed during the reaction. One possibility that would explain the apparently conflicting spectroelectrochemistry and XANES results is that the oxidation features observed in the CV are not due to the oxidation of nickel. Instead the oxidizing equivalents may be stored on the ligand during the early stages of the reaction.

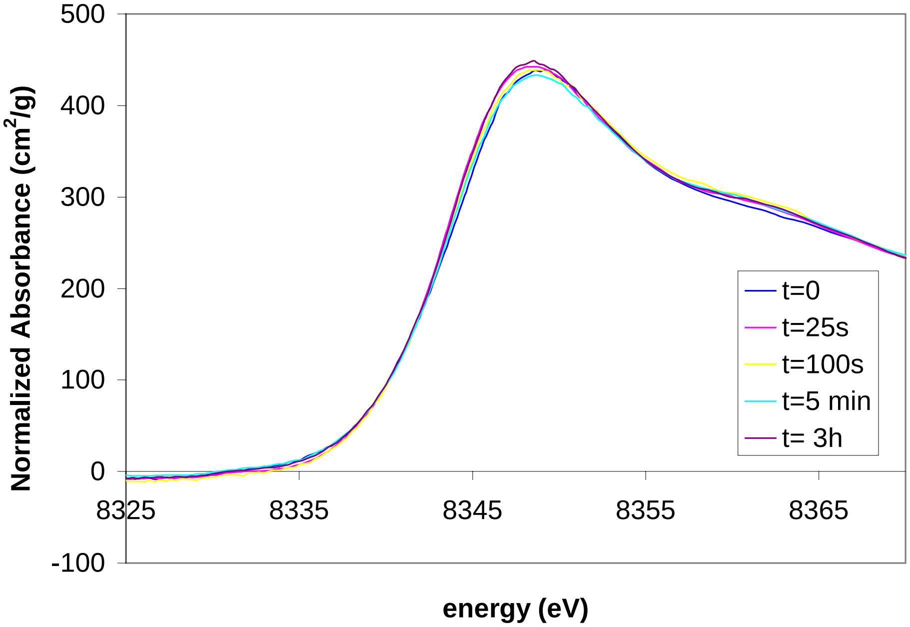

Figure 3.28. XANES spectra of 0.5 mM **3** as it reacts with dioxygen in methanol.

Another piece of information that can be obtained from this experiment involves the coordination geometry around the nickel. If the coordination number changed during the reaction, the pre-edge region of the spectrum should change shape. However, that is not observed indicating that the nickel remains six-coordinate throughout the reaction.

3.5. Raman spectroscopy of [Ni(II)(TRISOX)]$_2^{2-}$.

The spectroelectrochemistry and XANES experiments suggest the hypothesis that oxidation is occurring on the ligand rather than the metal in the intermediate. Another technique that could provide information is resonance Raman. If ligand oxidation is occurring, the vibrational peaks assigned to that portion of the ligand should shift upon oxidation.

Experimental. Raman spectroscopy was performed on a solid sample of **3** using a Coherent Sabre Innova Argon ion laser with tunable wavelengths coupled to a Spex 1404 0.85m double spectrometer monochromator with a CCD camera. The solid was obtained by deprotonating **1** in acetonitrile, filtering the excess KOH and KNO_3 formed in the metathesis reaction, removing the acetonitrile by rotary evaporation, and then recrystallizing the sample using vapor diffusion with an acetonitrile/diethyl ether solvent system. This purified solid was placed in a capillary tube that was inserted into a quartz cooling tube that had cold N_2 blowing through it. The sample was spun using a drill. A wavelength of 514.5 nm was used and a Kaiser notch filter was employed to remove the Raleigh line. A power of 400 mW at the source was employed and the detector collected data for sixty, sixty-second accumulations.

Results and discussion. Representative Raman spectra of solid **3** are shown in Figures 3.29 and 3.30. These data were reproducible and showed peaks in regions where ligand vibrations had been assigned by another group member.[2] In order to determine where on the ligand oxidation is occurring, the Raman spectrum of the air oxidized sample must be collected and compared to the non-oxidized sample. However, this proved to be very difficult for several reasons. One complication arose from the solvent. Methanol (and ethanol) have large vibrations in the area of interest for the sample, making it impossible to see any of the vibrations due to the complex. Another obstacle is that the air oxidized sample appears to be a much better absorber than a Raman scatterer of light, resulting in very poor signal to noise ratios. Finally, since the target of this experiment is an intermediate, the solution contains many different species, which complicates the experiment. The combination of these difficulties prevented the collection of useful spectra on the air oxidized sample. The electrochemically oxidized sample posed a similar problem that was compounded by the low concentrations required for the bulk electrolysis experiments as well as the spectral interference of the supporting electrolyte. Consequently, this technique was abandoned as a useful means of investigating the oxidation reaction.

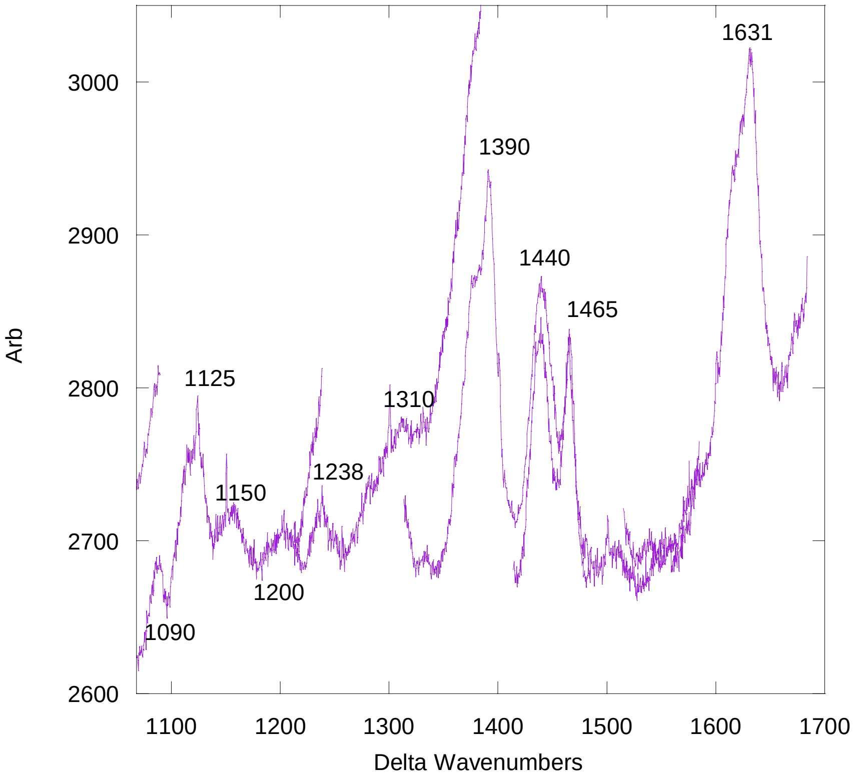

Figure 3.29. Raman spectrum of a solid sample of **3.**

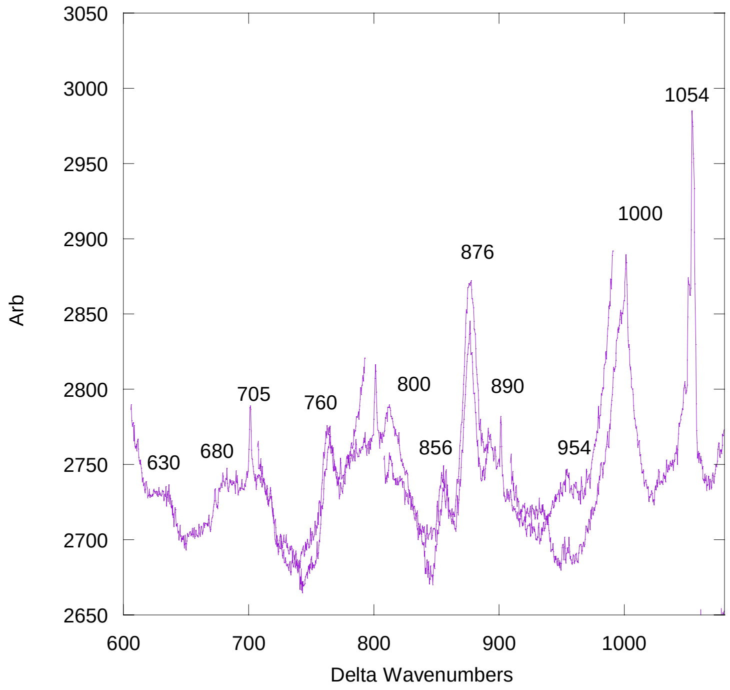

Figure 3.30. Raman spectrum of a solid sample of **3.**

3.6. Electron paramagnetic resonance spectroscopy of $[Ni(II)(TRISOX)]_2^{2-}$.

Electron paramagnetic resonance (EPR) spectroscopy is a technique used to monitor unpaired electrons in a sample. This is useful in examining the oxidation reaction of **3**, since this reaction should result in an unpaired electron somewhere on the complex. A collaboration was formed with the Buchanan group at the University of Louisville and EPR spectra were obtained for the reaction of **3** with O_2 in methanol.

Experimental. The data were recorded on a Varian Associates E-109 spectrometer. The magnetic field was calibrated using a Varian E-500 NMR Gauss meter. An insert dewar was used to keep the samples at liquid nitrogen temperature. Table 3.1 summarizes the experimental parameters.In a typical experiment, 113 mg (0.25 mmol) of **1** were dissolved in 5 mL of distilled methanol. 1.5 mL of 0.5 M KOH in methanol (3 eq.) were added to the sample to initiate the reaction and then aliquots were withdrawn at various time intervals and frozen in EPR tubes in liquid nitrogen. These samples were then analyzed to monitor the reaction.

For the experiment using deuterated methanol as the solvent, a 10 mM sample was prepared by dissolving 15 mg (4.11 X 10^{-5} mol) of **1** in 4 mL of $DOCD_3$ and then 0.25 mL of 0.5 M KOH in methanol was added to initiate the dioxygen reaction. This sample was placed in an EPR tube and frozen in liquid nitrogen after seventy seconds.

For the bulk electrolysis experiment, 137 mg (3.05 X 10^{-4} mol, 5.1 mM) of **1** were dissolved in 60 mL of acetonitrile along with 851 mg (6.94 X 10^{-3} mol, 115 mM) of sodium perchlorate, which acted as the supporting electrolyte. This solution was purged with argon before and during the electrochemical oxidation. The electrochemical cell was identical to that described in Chapter 3.3 and it was immersed in an acetonitrile/dry ice bath which maintained a temperature of ~ -40°C. 0.92 mL of 1 M NaOH in methanol was added to the solution to form **3** (2.55 mM). The sample was oxidized at a potential of 200 mV. An aliquot was then removed and frozen in liquid nitrogen and the EPR spectrum was collected.

Table 3.1. EPR experimental parameters.

Number of Scans	4
Center Field	3200 G
Sweep Width	2000 G
Resolution	512 points
Microwave Frequency	9.487 GHz
Microwave Power	1.001 mW
Receiver Gain	1.00×10^5
Phase	0 degree
Harmonic	1
Modulation Frequency	100.00 kHz
Modulation Amplitude	10.00 G
Signal Channel Conversion	163.840 ms
Signal Channel Time Constant	40.960 ms
Signal Channel Sweep Time	83.886 s

Results and discussion. Figure 3.31 shows a set of spectra collected over three hours. At the beginning of the experiment (within the first 60 seconds) a sharp signal grows in with a g value of 2.00, characteristic of an organic radical. This is on the same timescale that the band at 350 nm grows in and maximizes during the UV/visible absorption experiment (Figure 3.1). This signal decays, and at later time periods a classic Ni(III) signal grows in with a g value of 2.14 and superhyperfine structure from the nitrogens on the ligand. This was very unexpected since the XANES experiment (Chapter

3.4) showed that Ni(III) was not present in the sample, even at later time points. However, spin-quantitation using Cu(II) standards showed that the amount of Ni(III) present was very small (<1%), too small to be observed in the XANES experiment. This experiment was repeated under several different conditions. Lowering the concentration of the complex resulted in a very weak signal. Concentrations below 10 mM produced spectra that were too noisy to be useful. Using a different counter anion (chloride instead of nitrate) did not affect the results.

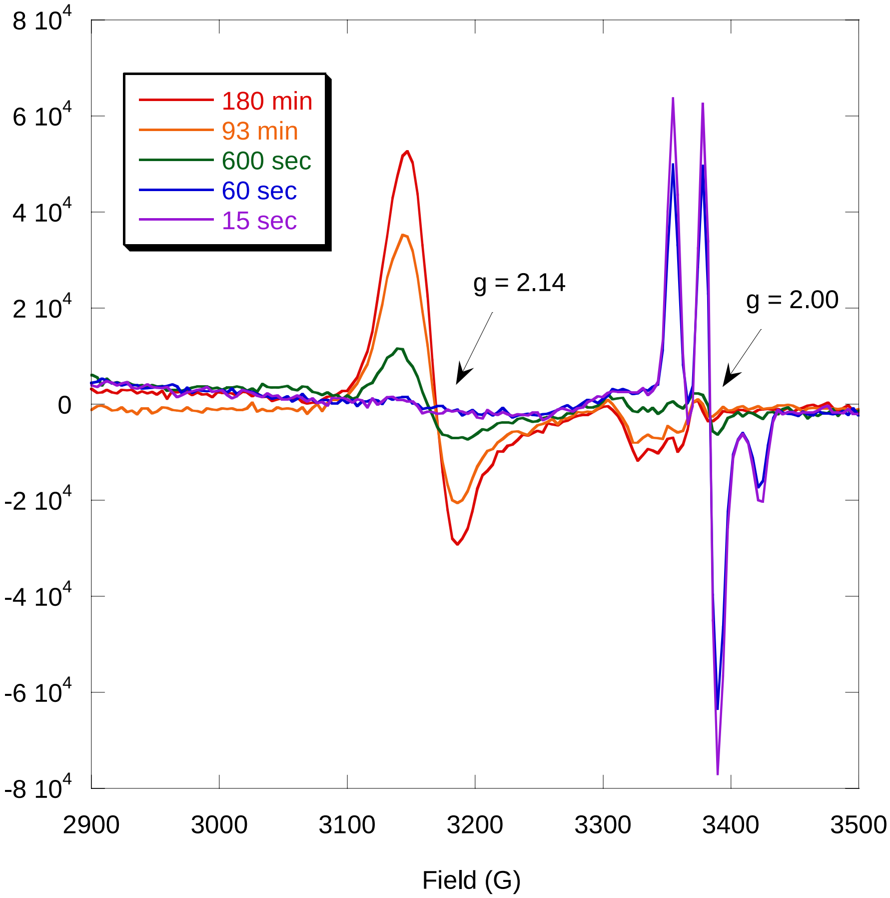

Figure 3.31. EPR spectra of the reaction of 39 mM **3** with O_2 in methanol.

In order to determine if the signal with a g value of 2.00 was due to a methoxy radical formed during the production of formaldehyde, the experiment was repeated using deuterated methanol ($DOCD_3$). The comparison of this spectrum to the one collected in regular methanol under identical conditions can be seen in Figure 3.32.

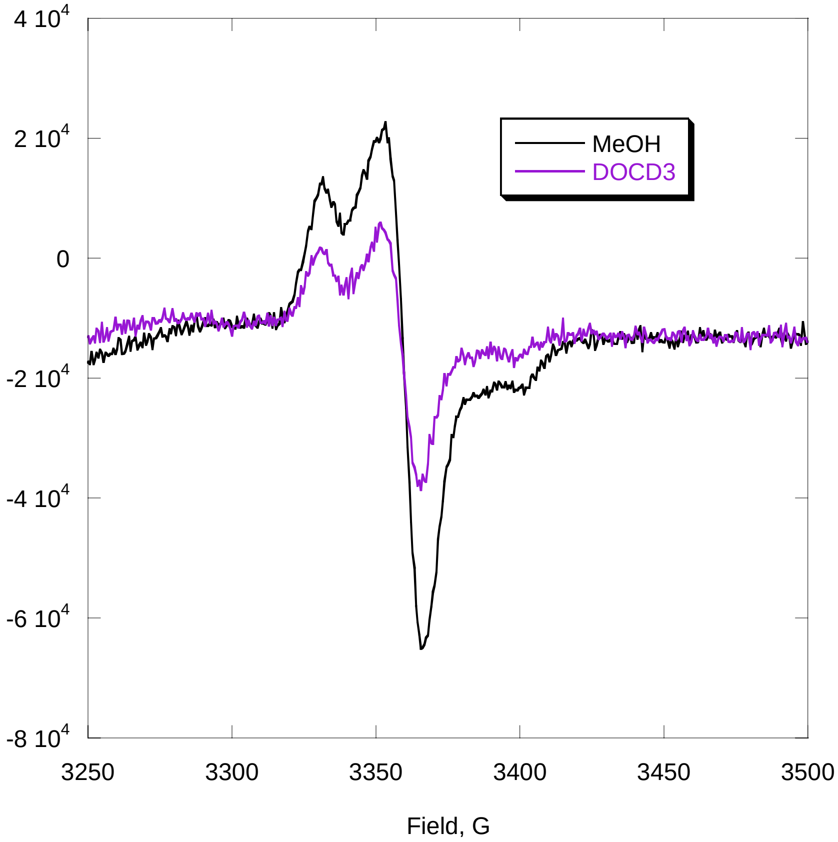

Figure 3.32. EPR spectra of the reaction of 10 mM **3** with O_2 in methanol and $DOCD_3$.

Performing the reaction in deuterated solvent did not significantly affect the EPR spectrum at the beginning of the reaction, as confirmed by comparing the Full Width at Half Maximum (FWHM) for each baseline corrected, integrated spectrum (MeOH FWHM = 27 G, $DOCD_3$ FWHM = 29 G). This confirms that the spectrum is not due to a solvent (substrate) radical observed transiently and is actually related to the nickel complex. Isotopically labeled complexes were synthesized to ascertain where the oxidation was occurring. ^{15}N was substituted in either the amine nitrogen position or the oxime nitrogen position, and the experiment was repeated using 41 mM solutions of these samples. The organic radical signal changed shape in the spectrum of the sample containing the ^{15}N labeled oxime complex, whereas the ^{15}N labeled amine complex closely resembled the sample containing the natural abundance ligand (Figure 3.33).

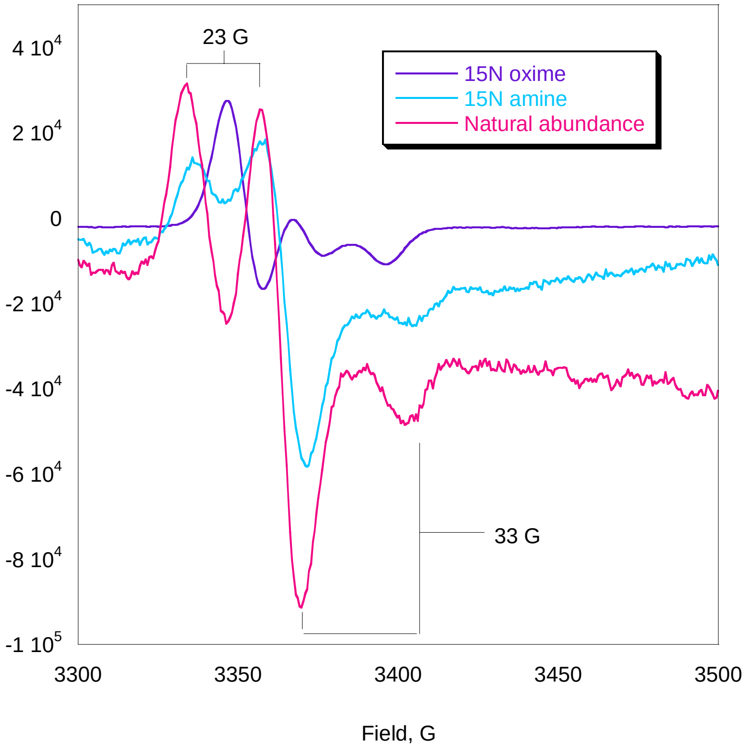

Figure 3.33. EPR spectra of the reaction of isotopically labeled 41 mM **3** with O_2 in methanol. Intensities are normalized for ease of comparison.

The isotopically labeled EPR experiment determined unambiguously that the oxidation equivalents are stored on the oximates during the early stages of the reaction. The oxidation of an oxime to form an iminoxyl radical ($C{=}NO^{\bullet}$) has literature precedent. They were first characterized in 1964 using EPR spectroscopy and it was observed that iminoxyl radicals exhibit characteristically large nitrogen coupling constants (28 – 33 G).[3] The spacing in the intermediate radical signal has a coupling constant of 33 G (Figure 3.24). Additionally, it was reported that the UV/visible absorption spectrum of the iminoxyl radical is characterized by two absorption bands at 330 nm and 580 nm.[4] The intermediate in the UV/vis spectrum of **3** is at 350 nm and a band at 560 nm is observed during the entire reaction. This, along with the large coupling constant observed in the EPR specturm, further supports the assignment that the oxidation equivalents are stored on the oximate in the observed intermediate.

It has been reported that the unpaired electron of iminoxyl radicals is in a π-type orbital derived from a nitrogen sp^2 orbital and an oxygen p orbital. This π-type orbital is believed to lie in the nodal plane of the C=N π bond, which requires it to be orthogonal to the molecular π system. Because of this, iminoxyl radicals have been described as σ radicals.[4]

This type of radical has been observed in biological systems. For example, iminoxyl radicals are formed when nitric oxide interacts with the tyrosine radical of photosystem II and the tyrosyl radical of prostaglandin H synthase-2.[5] Additionally, both O and N centered iminoxyl-type radicals are possible candidates in the nitric oxide synthase (NOS)-catalyzed oxidation of N^{G}-hydroxy-L-arginine to nitric oxide and citrulline.[6] They are also proposed to be putative intermediates in the oxidation of aryl oximes by cytochrome P450 mono-oxygenases[7] and NOS.[8]

In order to further determine whether the electrochemically oxidized species and air oxidized intermediate are similar, a solution of **3** in acetonitrile was bulk electrolyzed so that its EPR spectrum could be compared to the EPR spectrum of the air oxidized sample. The sample was oxidized at a potential of 200 mV. To oxidize each dimer present, 14.72 C must be passed. At the end of this experiment 14.23 C had been passed, oxidizing 97% of the dimeric species present by one equivalent or 48% of the dimeric species by two equivalents. Double oxidation seems more likely for the air oxidation reaction based on the two-electron reactivity. This experiment was repeated using methanol as the solvent under identical conditions except the potential applied was 0 mV. 13.23 C would be expected to oxidize each dimer by one equivalent. At the conclusion of this experiment 10.6 C were passed, oxidizing 80% of the dimer present by one equivalent or 40% of the dimer by two equivalents.

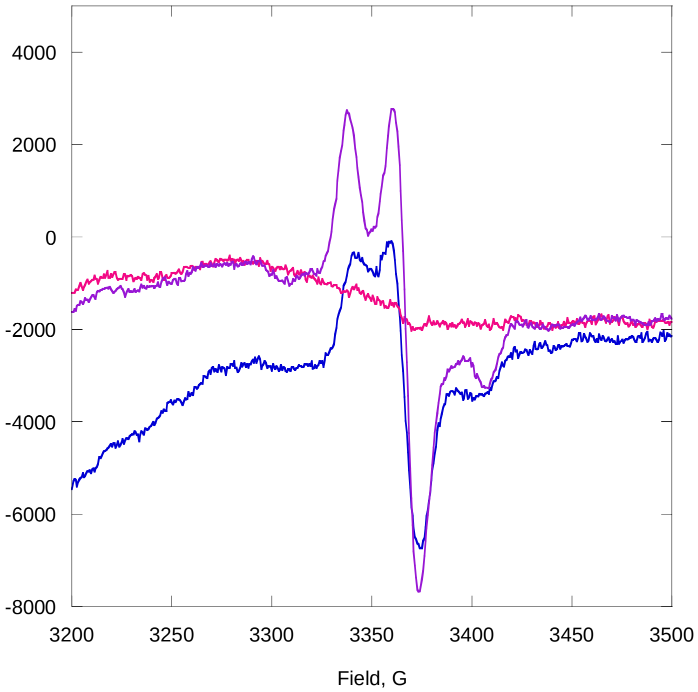

Figure 3.34. EPR spectra of the reaction of electrochemically oxidized 5 mM **3** in methanol (pink spectrum, 80% oxidized) and acetonitrile (blue spectrum, 97% oxidized) and 39 mM **3** as it reacts with O_2 in methanol (purple spectrum).

These spectra were compared to the spectrum collected from the air oxidized sample during the initial stages of the reaction and can be seen in Figure 3.34. The electrochemically oxidized experiment using acetonitrile as the solvent produced a spectrum that resembles the air oxidized intermediate sample in methanol. However, the electrochemically oxidized methanolic sample of 3 is relatively featureless.

In summary, the isotopically labeled EPR experiments proved that the oxidation equivalents are transiently stored on the oximates during the initial stages of the reaction. EPR experiments also support the hypothesis that the electrochemically oxidized and air oxidized intermediate species are similar.

3.7. Conclusions.

From the reactivity studies described in Chapter 2, it was concluded that a substrate that is capable of donating two hydrogen atoms must be present in order for the oxygen reaction to take place. It also was hypothesized that hydrogen peroxide is one of the products formed during this reaction.

The spectroscopic studies also provided clues about the reaction. The UV/visible absorption spectroscopy showed that an intermediate grows in and goes away during the reaction. Electrochemically oxidized samples produced similar absorption spectra, suggesting that the intermediate observed in the UV/vis spectrum is also due to an oxidized species. From the XANES data it can be concluded that it is not the nickel that is being oxidized during this reaction. This was corroborated by comparing the EPR spectra of isotopically labeled **3** and observing that the spectrum of the complex containing isotopically labeled oximates was very different than the spectrum of the isotopically labeled amine or the natural abundance sample. This result showed that the oxidization initially occurs on the oximates.

All of this information was combined to develop a proposed reaction scheme shown in Scheme 3.1. While some of the details of this scheme are purely speculative, such as the indicated valence tautomerism of the initial O_2 adduct, it provides a chemically reasonable pathway that accounts for the chemical and spectroscopic observations.

Scheme 3.1. Proposed reaction scheme for the reaction of **3** with O_2.

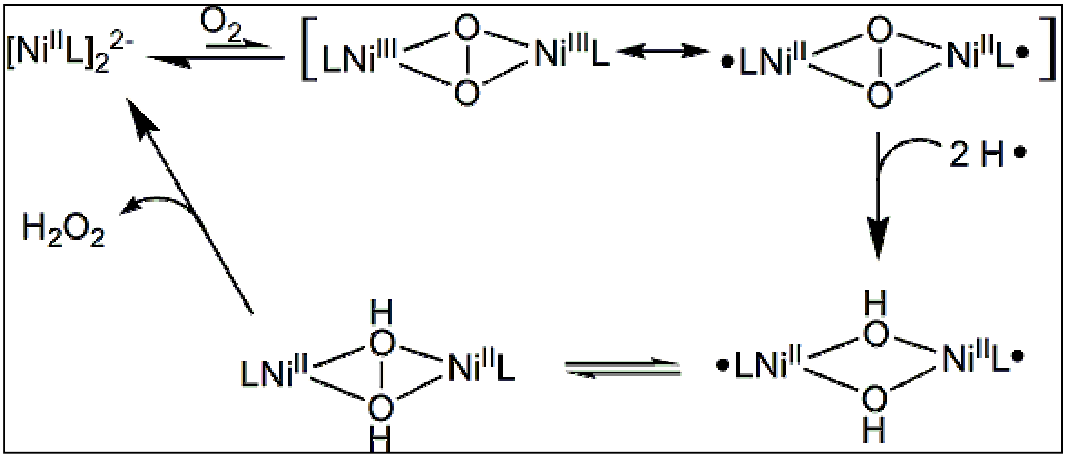

At the beginning of the reaction the active species is in an unfavorable oxygen binding equilibrium. The two valence tautomers, a Ni(III)-Ni(III) peroxo-bridged dimer or a Ni(II)-Ni(II) peroxo-bridged dimer with the oxidizing equivalents stored on the ligand, are examples of possible structures of this oxygen adduct. This species does not build up sufficiently to be observed, since the equilibrium lies far to the left. This is demonstrated by the lack of an observed O_2 reaction in acetonitrile. If there is a two-hydrogen atom source present, the reaction will be rapidly driven forward to form a species that is reduced by two electrons relative to the initial oxygen adduct. Reaction of the hydrogen atoms with the peroxide bridge results in a Ni(II)-Ni(II) hydroxo-bridged species that is oxidized on the oximates. This is proposed to be the observed intermediate. This converts to a Ni(II)-Ni(II) hydroperoxo species by intramolecular electron transfer from the hydroxides to the oxidized oximates. This is analogous to the well-characterized Cu^{II}-O_2^{2-}-Cu^{II} $\longleftrightarrow$ $Cu^{III}(O)_2Cu^{III}$ interconversion.[10] In the final step of this proposed reaction, hydrogen peroxide is released. This brings the catalyst back to its original form. The hydrogen peroxide product is rapidly disproportionated as shown in Chapter 2.8.

References

1. Anderson, C. W.; Cushman, M. R. *Anal. Chem.*, **1982**, *54(12)*, 2122-2123.
2. Jones, R. M.; Baldwin, M. J. *J. Phys. Chem. A.*, **2004**, *108(16)*, 3537-3544.
3. Thomas, J. R. *J. Am. Chem. Soc.*, **1964**, 86, 1446-1447.
4. Everett, S. A.; Naylor, M. A.; Stratford, M. R. L.; Patel, K. B.; Ford, E.; Mortensen, A.; Ferguson, A. C.; Vojnovic, B.; Wardman, P. *J. Chem. Soc., Perkin Trans. 2,* **2001**, 1989-1997.
5. Sanakis, Y.; Goussias, C.; Mason, R. P.; Petrouleas, V. *Biochemistry,* **1997**, *36*, 1411.
6. Tantillo, D. J.; Fukuto, J. M.; Hoffman, B. M.; Silverman, R. B.; Houk, K. N. *J. Am. Chem. Soc.*, **2000**, *122*, 536.
7. Clement, B.; Boucher, J.-L.; Dijols, S.; Mansuy, D. Harsdorf, *Biochem. Pharmacol.*, **1999**, 5*8*, 439.
8. Renedon-Corniere, A.; Boucher, J.-L.; Dijols, S.; Stuehr, D. J.; Mansuy, D. *Biochemistry*, **1999**, *38*, 4663.
9. Que, L. Physical Methods in Bioinorganic Chemistry: Spectroscopy and Magnetism, **2000**, University Science Books, p. 128.
10. Cahoy, J.; Holland, P. L.; Tolman, W. B. *Inorg. Chem.*, **1999**, *38(9)*, 2161.

Chapter 4. Investigation of Other Complexes in the Ni(II)-Polyoxime Library.

4.1.Introduction. The Ni(II)-polyoxime library contains complexes that have the same tripodal amine ligand frame work as **3**.[1] However, while **3** has three oxime groups that can be converted to oximates, the other complexes in the library have two oxime groups as well as a variable third arm that can be altered to change the electronic structure of the nickel complexes, as well as the environment around the metal center (such as steric, hydrophobic or polar properties, hydrogen bonding propensity, etc.), and the solubility properties. Tuning these properties is useful in optimizing potential catalysts.

X-ray crystal structures of the complexes can be seen in Chapter 1, Figure 1.8. All of the complexes in the library exhibit a six-coordinate pseudo-octahedral coordination geometry around the nickel center, with the bis(oxime)amine unit coordinating in a facial mode. Three separate structural types were discovered: (1) tetradentate ligands form six-coordinate monomers with solvent and/or counter ions filling the remaining coordination positions; (2) tridentate ligands form six-coordinate monomers when nitrate is the counter anion, with one monodentate and one bidentate nitrate filling the remaining coordination positions; and (3) tridentate ligands assemble as six-coordinate, bis(μ-Cl) dimers when chloride is the counter anion, with one terminal and two bridging chlorides filling the coordination sphere.

The electronic, electrochemical, and reactivity properties of many of the complexes in the library were investigated for comparison to the TRISOX complexes described in the proceeding chapters and will be reported here. Additionally, the synthesis and characterization of *N*-*n*-Octyl-*N*,*N*-bis(1-propan-2-onyl oxime) amine ($OBOH_2$) and ($Ni[OBOH_2]Cl_2$) will be described, as well as the synthesis of [Ni($TRISOXH_3$)(pyridine-*N*-oxide)(H_2O)].

4.2. Probing the electronic properties of complexes in the Ni(II)-polyoximate library.

It is anticipated that variation of the third arm of the ligand will allow optimization of the O_2 reactivity of the Ni(II) complexes by modulation of the electronic structure of the metal through variation of the donor properties of the ligand and by modifying the interaction of the active metal complex with potential oxidation substrates.

One way to explore the electronic structure of the complexes is to measure the value of 10 Dq, or Δ_o. This is the extent to which the 3d orbitals with e_g and t_{2g} symmetry are separated in an octahedral complex. Figure 4.1 demonstrates the spacing of the d orbitals in an octahedral complex.

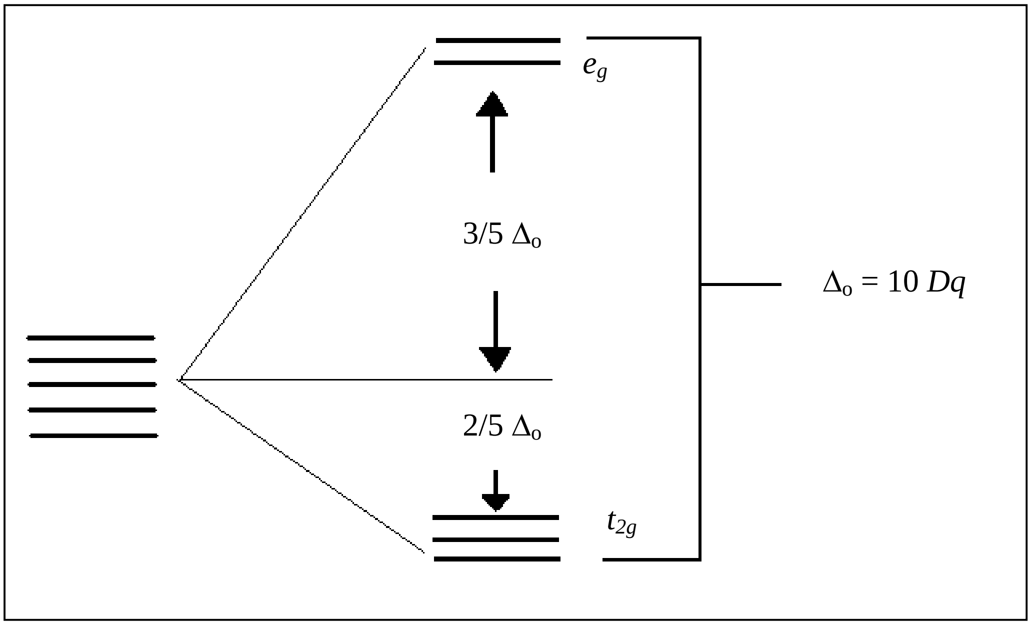

Figure 4.1. Splitting of the five *d* orbitals by an octahedral field. The condition represented by the degenerate levels on the left is a hypothetical spherical field.[2]

Six-coordinate, pseudo-octahedral Ni(II) complexes typically exhibit three absorption bands in the ligand field region (300 – 1200 nm), although occasionally the highest energy band is buried under the tail of intense high energy absorption bands.[3] The lowest energy transition (corresponding to the transition from $^3A_2$ to $^3T_2$) in an octahedral d^8 complex corresponds to 10 *Dq*. The other two absorption bands are due to the transitions from $^3A_2$ to $^3T_1(^3P)$ and $^3A_2$ to $^3T_1(^3F)$. The value of 10 *Dq* was determined for the complexes in the library.

Experimental. Soluitions **(**5 mM) of each complex were prepared in several different solvents (methanol, acetonitrile, water) with both chloride and nitrate counter anions and the UV/visible absorption spectra were collected using a Hewlett-Packard 8453 spectrometer with a 2 cm path length cell. The deprotonated complexes were also analyzed in acetonitrile. The 5 mM solutions were placed into a UV/vis cell that was sealed using a septum. The solution was sparged with argon for ~ten minutes, then three equivalents of a purged solution of 0.5 M potassium hydroxide dissolved in methanol were transferred via canula to the sample cell.

Circular dichroism spectra were collected using a Jasco J-715 spectropolarimeter (interfaced with a PC) using a 2 cm path length cell.

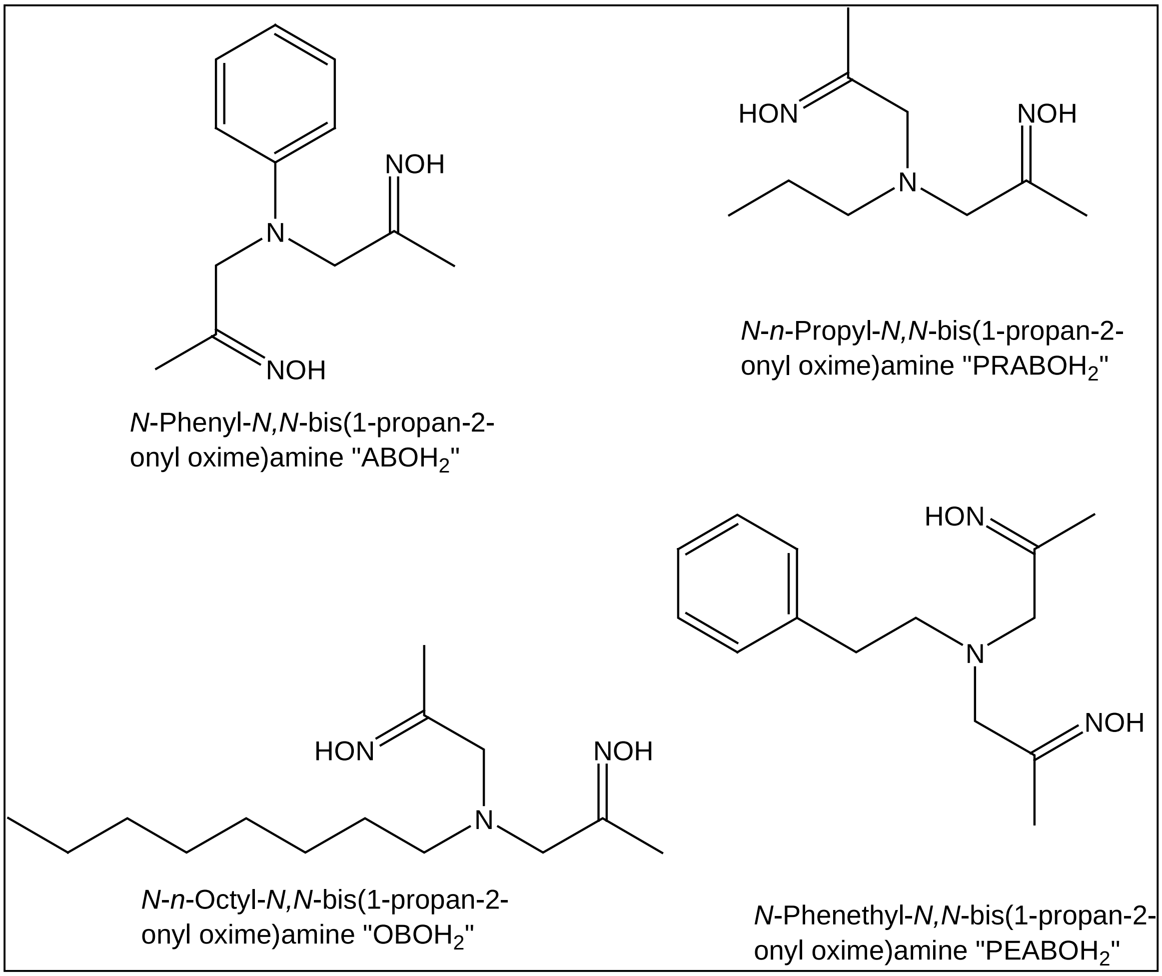

N-Phenyl-*N,N*-bis(1-propan-2-onyl oxime)amine "ABOH$_2$"

N-*n*-Propyl-*N,N*-bis(1-propan-2-onyl oxime)amine "PRABOH$_2$"

N-*n*-Octyl-*N,N*-bis(1-propan-2-onyl oxime)amine "OBOH$_2$"

N-Phenethyl-*N,N*-bis(1-propan-2-onyl oxime)amine "PEABOH$_2$"

Figure 4.2. Tridentate tripodal amine bis-oxime ligands.

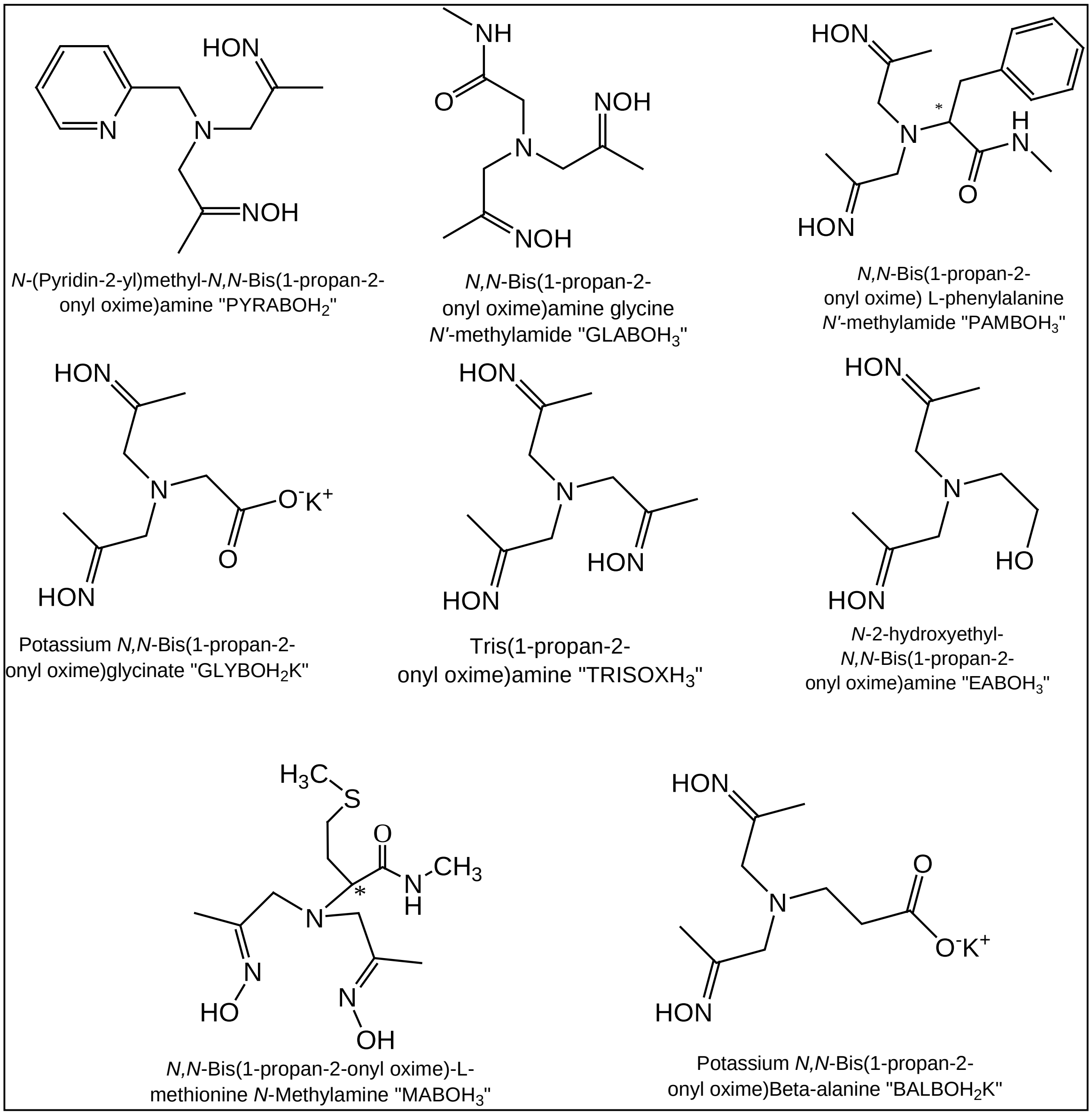

N-(Pyridin-2-yl)methyl-*N,N*-Bis(1-propan-2-onyl oxime)amine "PYRABOH$_2$"

N,N-Bis(1-propan-2-onyl oxime)amine glycine *N′*-methylamide "GLABOH$_3$"

N,N-Bis(1-propan-2-onyl oxime) L-phenylalanine *N′*-methylamide "PAMBOH$_3$"

Potassium *N,N*-Bis(1-propan-2-onyl oxime)glycinate "GLYBOH$_2$K"

Tris(1-propan-2-onyl oxime)amine "TRISOXH$_3$"

N-2-hydroxyethyl-*N,N*-Bis(1-propan-2-onyl oxime)amine "EABOH$_3$"

N,N-Bis(1-propan-2-onyl oxime)-L-methionine *N*-Methylamine "MABOH$_3$"

Potassium *N,N*-Bis(1-propan-2-onyl oxime)Beta-alanine "BALBOH$_2$K"

Figure 4.3. Tetradentate tripodal amine bis-oxime ligands.

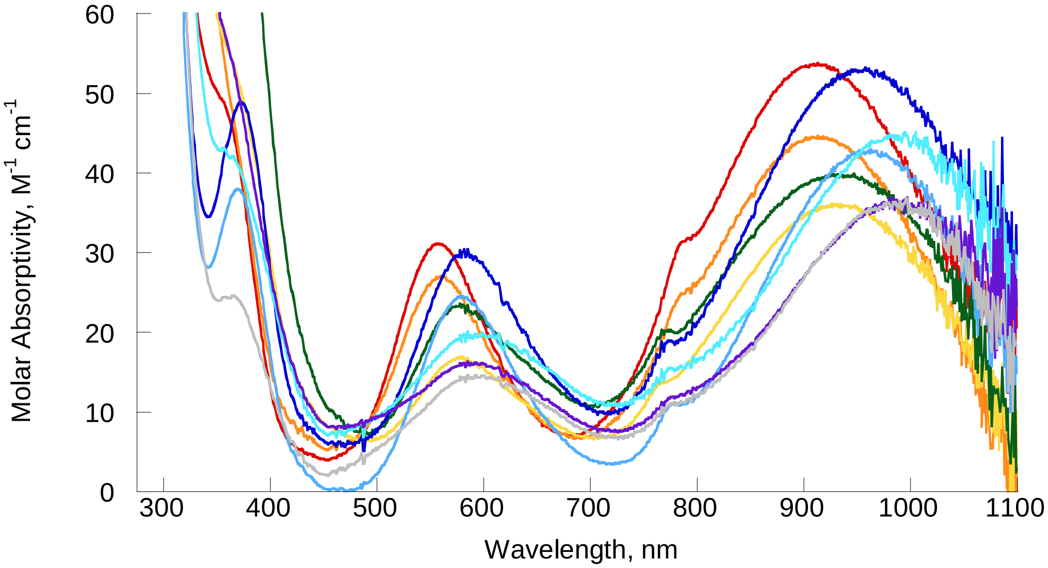

Figure 4.4. UV/visible absorption spectra of 5 mM solutions in methanol. Red = Ni(TRISOXH$_3$)(NO$_3$)$_2$, orange = Ni(PYRABOH$_2$)(NO$_3$)$_2$, yellow = Ni(EABOH$_3$)(NO$_3$)$_2$, green = Ni(GLYBOH$_2$)(NO$_3$)$_2$, dark blue = Ni(GLABOH$_3$)(NO$_3$)$_2$, cornflower blue = Ni(PAMBOH$_3$)(NO$_3$)$_2$, sky blue = Ni(OBOH$_2$)(NO$_3$)$_2$, purple = Ni(PRABOH$_2$)(NO$_3$)$_2$, grey = Ni(PEABOH$_2$)(NO$_3$)$_2$

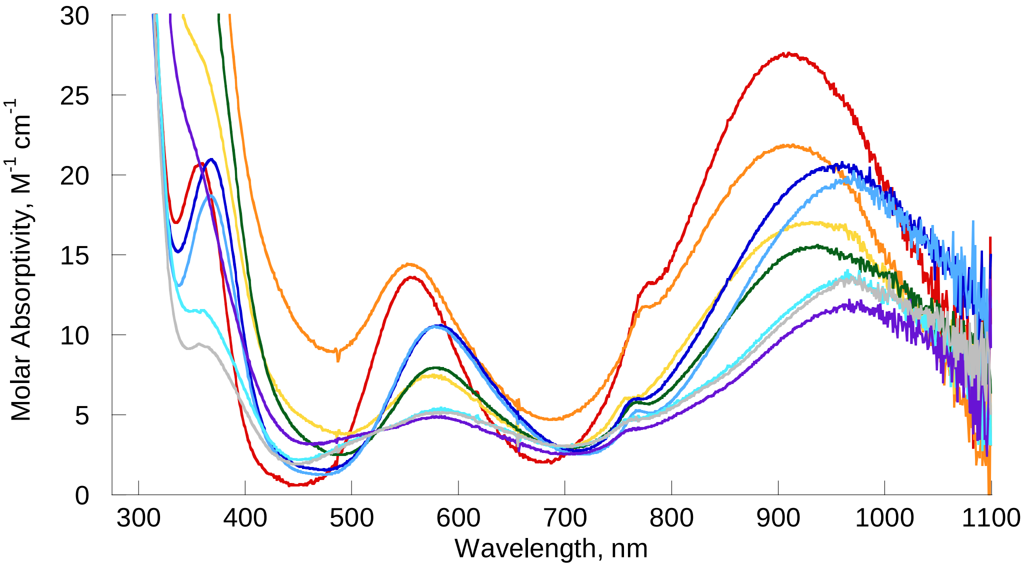

Figure 4.5. UV/visible absorption spectra of 5 mM solutions in water. Red = Ni(TRISOXH$_3$)(NO$_3$)$_2$, orange = Ni(PYRABOH$_2$)(NO$_3$)$_2$, yellow = Ni(EABOH$_3$)(NO$_3$)$_2$, green = Ni(GLYBOH$_2$)(NO$_3$)$_2$, dark blue = Ni(GLABOH$_3$)(NO$_3$)$_2$, cornflower blue = Ni(PAMBOH$_3$)(NO$_3$)$_2$, sky blue = Ni(OBOH$_2$)(NO$_3$)$_2$, purple = Ni(PRABOH$_2$)(NO$_3$)$_2$, grey = Ni(PEABOH$_2$)(NO$_3$)$_2$

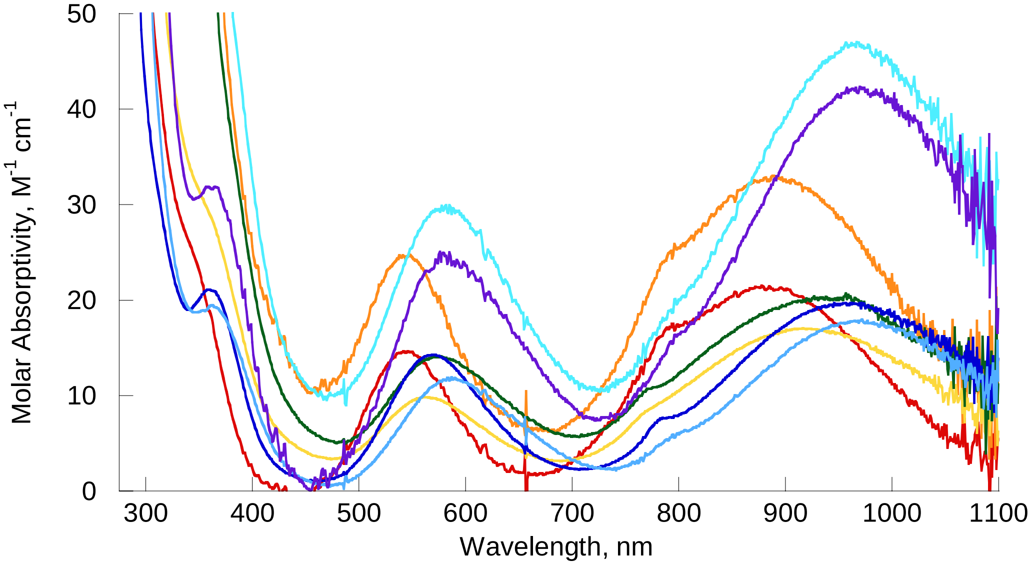

Figure 4.6. UV/visible absorption spectra of 5 mM solutions in acetonitrile. Red = Ni(TRISOXH$_3$)(NO$_3$)$_2$, orange = Ni(PYRABOH$_2$)(NO$_3$)$_2$, yellow = Ni(EABOH$_3$)(NO$_3$)$_2$, green = Ni(GLYBOH$_2$)(NO$_3$)$_2$, dark blue = Ni(GLABOH$_3$)(NO$_3$)$_2$, cornflower blue = Ni(PAMBOH$_3$)(NO$_3$)$_2$, sky blue = Ni(OBOH$_2$)(NO$_3$)$_2$, purple = Ni(PRABOH$_2$)(NO$_3$)$_2$, grey = Ni(PEABOH$_2$)(NO$_3$)$_2$

Figure 4.2 shows stick figures of each of the tridentate ligands investigated and Figure 4.3 shows the tetradentate ligands.

The UV/visible absorption spectra for the complexes containing nitrate as the counter anion were collected in methanol (Figure 4.4), water (Figure 4.5), and acetonitrile (Figure 4.6). The chloride containing complexes were analyzed as aqueous (Figure 4.7) and methanolic solutions (Figure 4.8). The maximum of the lowest energy transition was measured for each complex to determine the value of 10 *Dq*. These values are tabulated in Table 4.1.[3]

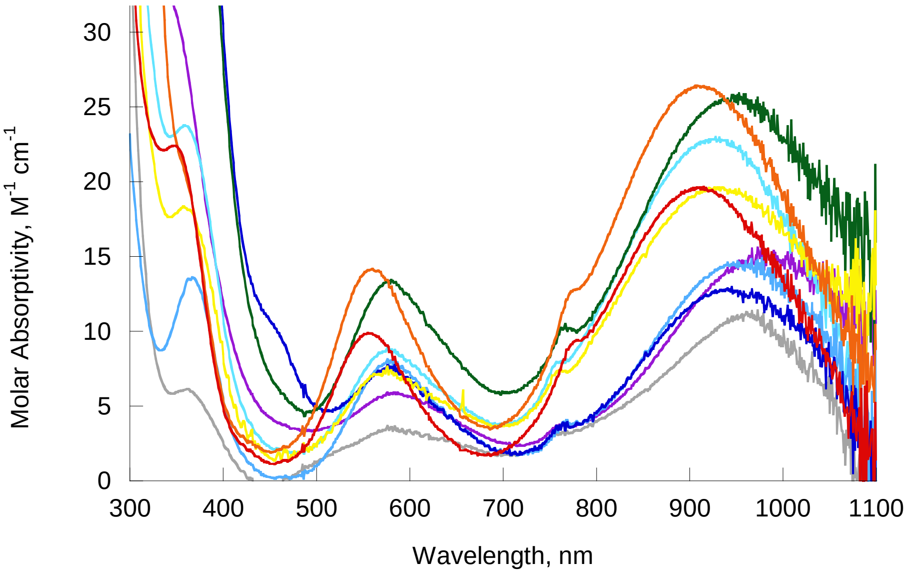

Figure 4.7. UV/visible absorption spectra of 5 mM solutions in water. Red = Ni(TRISOXH$_3$)Cl$_2$, orange = Ni(PYRABOH$_2$)Cl$_2$, yellow = Ni(EABOH$_3$)Cl$_2$, green = Ni(GLYBOH$_2$)Cl$_2$, dark blue = Ni(GLABOH$_3$)Cl$_2$, cornflower blue = Ni(PAMBOH$_3$)Cl$_2$, sky blue = Ni(OBOH$_2$)Cl$_2$, purple = Ni(PRABOH$_2$)Cl$_2$, grey = Ni(PEABOH$_2$)Cl$_2$

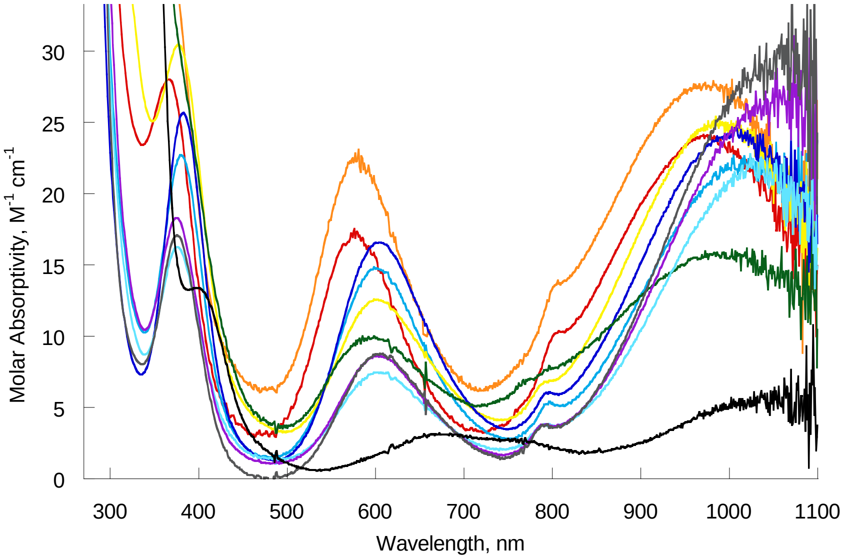

Figure 4.8. UV/visible absorption spectra of 5 mM solutions in methanol. Red = Ni(TRISOXH$_3$)Cl$_2$, orange = Ni(PYRABOH$_2$)Cl$_2$, yellow = Ni(EABOH$_3$)Cl$_2$, green = Ni(GLYBOH$_2$)Cl$_2$, dark blue = Ni(GLABOH$_3$)Cl$_2$, cornflower blue = Ni(PAMBOH$_3$)Cl$_2$, sky blue = Ni(OBOH$_2$)Cl$_2$, purple = Ni(PRABOH$_2$)Cl$_2$, grey = Ni(PEABOH$_2$)Cl$_2$, black = Ni(ABOH$_2$)Cl$_2$

Table 4.1. Values of 10 *Dq* (cm^{-1}) for the Ni(II) complexes in different solvents.[1]

Complex	CH_3OH ($X = Cl^-$)	CH_3OH ($X=NO_3^-$)	H_2O ($X=Cl^-$)	H_2O ($X=NO_3^-$)	CH_3CN ($X=NO_3^-$)
$Ni(TRISOXH_3)X_2$	10260	10990	10990	10990	11360
$Ni(PYRABOH_2)X_2$	10200	10930	10990	10930	11240
$Ni(EABOH_3)X_2$	10100	10750	10750	10640	10870
$Ni(GLYBOH_2)X_2$	10000	10640	10530	10580	10640
$Ni(GLABOH_3)X_2$	9900	10420	10530	10470	10530
$Ni(PAMBOH_3)X_2$	9800	10420	10420	10310	10420
$Ni(PRABOH_2)X_2$	9430	10100	10100	10310	10310
$Ni(OBOH_2)X_2$	9760	10100	10750	10310	10200
$Ni(PEABOH_2)X_2$	9430	10100	10420	10310	10310
$Ni(ABOH_2)X_2$	<9600	N/A	N/A	N/A	9710

Results and discussion. As can be seen in Table 4.1, the value of 10 *Dq* varies according to the nature of the third arm of the ligand, producing a reasonable spectrochemical series for the Ni(II) ligand field transitions. In acetonitrile, a relatively weakly coordinating solvent, the trend based on the third arm follows the order alkyl/aryl < amide < carboxylate < alcohol < pyridyl < oxime, which is consistent with expectations based on the σ-donor strength and π-acceptor ability of the third arm. Changing the counter anion does not affect the ordering of the spectrochemical series in methanol, as both the chloride and nitrate containing complexes follow the series observed in acetonitrile. The series is slightly disordered in water, as weakly coordinating third arms (such as an amide oxygen) can be displaced by the more strongly coordinating solvent. The value of 10 *Dq* is lower for $Ni(ABOH_2)X_2$ than for the complexes of the other tridentate ligands due to the weaker donor strength of the coordinated central amine nitrogen, which is directly bound to the phenyl ring, unlike the other aliphatic amines ($PRABOH_2$, $PEABOH_2$, $OBOH_2$).

The experiment was then altered for the nitrate containing complexes in acetonitrile by deprotonating the complexes under anaerobic conditions. Deprotonation of the complexes of the tetradentate ligands resulted in a color change from purple or blue to a darker purple. The tridentate ligand containing complexes underwent a color change from purple or blue to yellow upon deprotonation. The UV/vis absorption spectra were collected (Figure 4.9) and used to determine the values of 10 *Dq* for the deprotonated complexes. These values can be seen in Table 4.2.

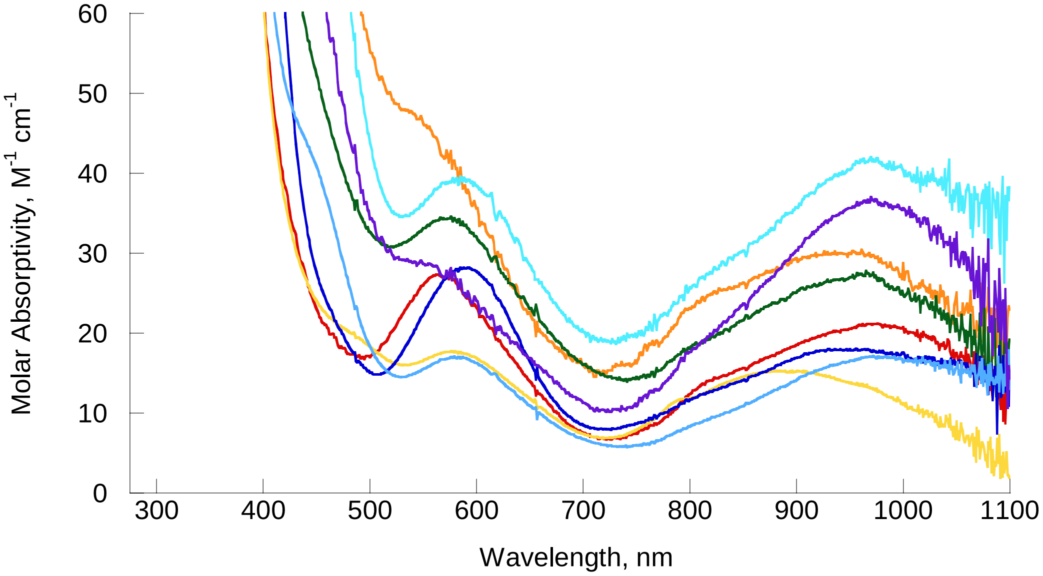

Figure 4.9. UV/visible absorption spectra of 5 mM solutions in acetonitrile, deprotonated anaerobically with KOH in methanol. Red = Ni(TRISOXH$_3$)(NO$_3$)$_2$, orange = Ni(PYRABOH$_2$)(NO$_3$)$_2$, yellow = Ni(EABOH$_3$)(NO$_3$)$_2$, green = Ni(GLYBOH$_2$)(NO$_3$)$_2$, blue = Ni(PAMBOH$_3$)(NO$_3$)$_2$, sky blue = Ni(OBOH$_2$)(NO$_3$)$_2$, cornflower blue = Ni(PRABOH$_2$)(NO$_3$)$_2$, purple = Ni(PEABOH$_2$)(NO$_3$)$_2$

Table 4.2. Values of 10 *Dq* (cm^{-1}) for the Ni(II) complexes in acetonitrile in the protonated and deprotonated forms.

Complex	Protonated	Deprotonated
$Ni(TRISOXH_3)(NO_3)_2$	11360	10250
$Ni(PYRABOH_2)(NO_3)_2$	11240	10490
$Ni(EABOH_3)(NO_3)_2$	10870	11340
$Ni(GLYBOH_2)(NO_3)_2$	10640	10360
$Ni(PAMBOH_3)(NO_3)_2$	10420	10460
$Ni(PRABOH_2)(NO_3)_2$	10310	10100
$Ni(OBOH_2)(NO_3)_2$	10200	10250
$Ni(PEABOH_2)(NO_3)_2$	10310	10270

Deprotonation of the complexes resulted in a shift in the order of the spectrochemical series from alkyl/aryl < amide < carboxylate < alcohol < pyridyl < oxime in the protonated form to alkyl < oximate < carboxylate < amide < pyridyl < alcohol. This was somewhat unexpected since the oximate functional group was expected to be the strongest donor and thus have the largest value of 10 *Dq*, as was seen in the protonated complexes; however, deprotonation makes the ligand a poorer π-acceptor. The shift suggests that ligand-dependent structural changes occur upon deprotonation that affect the electronic structure of the complex, resulting in a shift in the order of the spectrochemical series.

Two of the complexes in this library contain a chiral center (complexes of $PAMBOH_3$ and $MABOH_3$). This allows circular dichroism (CD) to be used as another spectroscopic tool to monitor the reaction and learn more about the electronic structure of the complex. Figure 4.10 shows the CD and UV/vis spectra of a 5 mM solution of $Ni(PAMBOH_3)(NO_3)_2$ in methanol after it has been deprotonated and allowed to react with dioxygen for three hours.

CD spectra contain both positive and negative absorption bands, which can elucidate overlapping bands in the UV/vis spectrum. Also, the selection rules differ, allowing ligand field bands that are covered by more intense charge transfer (CT) bands in the UV/vis spectrum to be observed in the CD spectrum. Although the transitions in Figure 4.10 have not yet been assigned, the comparison of the two spectra demonstrates the significant improvement of resolution in the CD spectrum versus the UV/vis spectrum, since the ligand field bands are not dominated by CT bands in the CD spectrum.

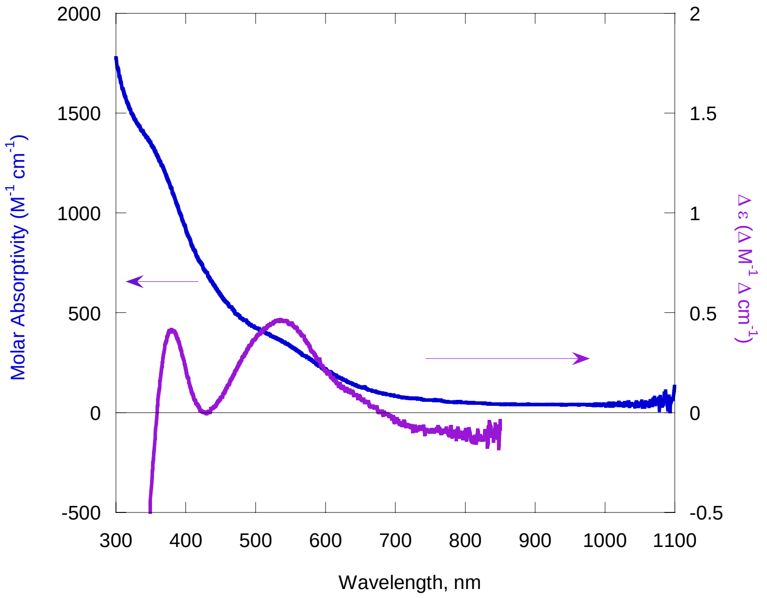

Figure 4.10. CD spectrum (purple) and UV/vis spectrum (blue) of 5 mM Ni(PAMBOH$_3$)(NO$_3$)$_2$ after deprotonation and reaction with O_2 for three hours.

4.3. Electrochemical studies of the complexes in the library.

One reason that the tripodal amine bis(oxime) ligand framework was originally selected was to allow access to higher oxidation states of nickel in order to facilitate oxygen activity. The experiments described in Chapters 2 and 3 indicate that oxidation equivalents are stored on the ligand – however, a redox active metal must also be present, as seen in the control experiments using the free ligand or a complex with zinc in place of nickel. Cyclic voltammatry (CV) was utilized to determine the oxidation potentials for many of the complexes in the Ni(II)-polyoxime library.

Experimental. In a typical experiment, a 5 mM solution of the complex of choice was prepared in either methanol or acetonitrile that also contained 100 mM of a supporting electrolyte (either tetrabutyl ammonium hexafluorophosphate (TBA PF_6) or sodium perchlorate ($NaClO_4$)). This solution was sparged with argon before each scan. A scan rate of 250 mV/s was employed. A $Ag/Ag(NO_3)_2$ reference electrode was used along with a platinum wire auxiliary electrode and a glassy carbon working electrode. Two equivalents of 0.5 M KOH in methanol (three for Ni(TRISOX)) were added to the solution as it sparged.

Results and discussion. The CVs of the fully protonated samples were featureless. Addition of base resulted in the appearance of oxidation features, confirming that oximates rather than oximes are necessary for redox-type chemistry to occur. Figure 4.11 shows the CVs of several complexes with strongly coordinating third arms, Figure 4.12 presents the CVs of several complexes with weakly coordinating third arms, and Figure 4.13 displays the CVs of several complexes with non-coordinating third arms with concentrations of 5 mM in methanol and acetonitrile. Table 4.3 lists the lowest oxidation potential for each complex in acetonitrile and methanol.

Table 4.3. Lowest oxidation potentials for each complex in acetonitrile and methanol vs. Fc/Fc$^+$. (N/A = data is unavailable due to low solubility).

Ligand	Potential of Lowest Oxidation (MeOH) (mV vs. Fc/Fc$^+$)	Potential of Lowest Oxidation (CH_3CN) (mV vs. Fc/Fc$^+$)
TRISOX	-260	-389
PYRABO	170	-60
EABOH	275	-280
GLYBO	N/A	-300
BALBO	N/A	-75
MABOH	-194	-190
PAMBOH	-165	-685
GLABOH	260	-270
OBO	-260	-160
PRABO	255	-520
PEABO	-250	-550
ABO	-275	-650

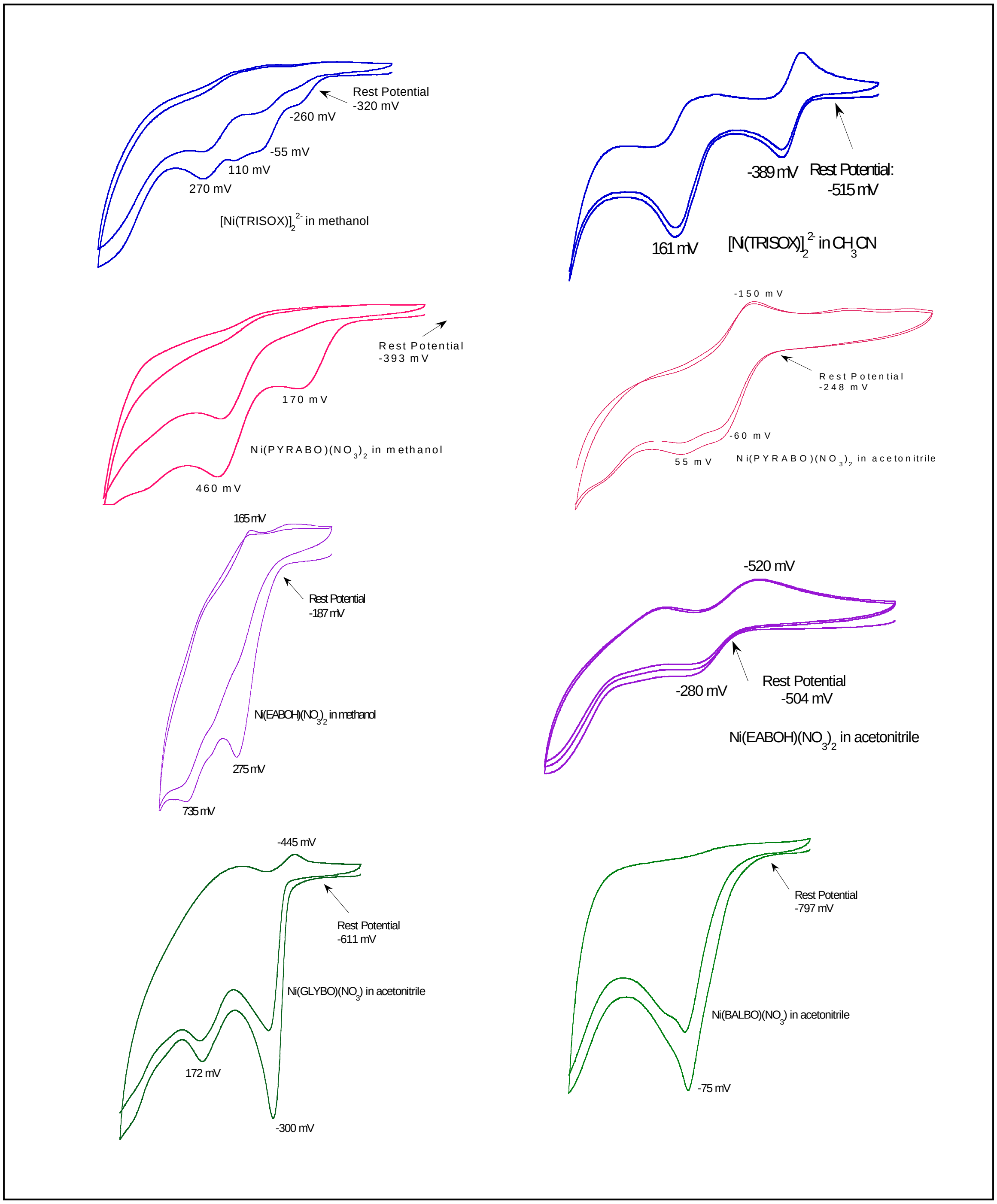

Figure 4.11. CV's of complexes containing strongly coordinating third arms in acetonitrile and methanol. Oxidation potentials are referenced to the ferrocene/ferrocenium couple.

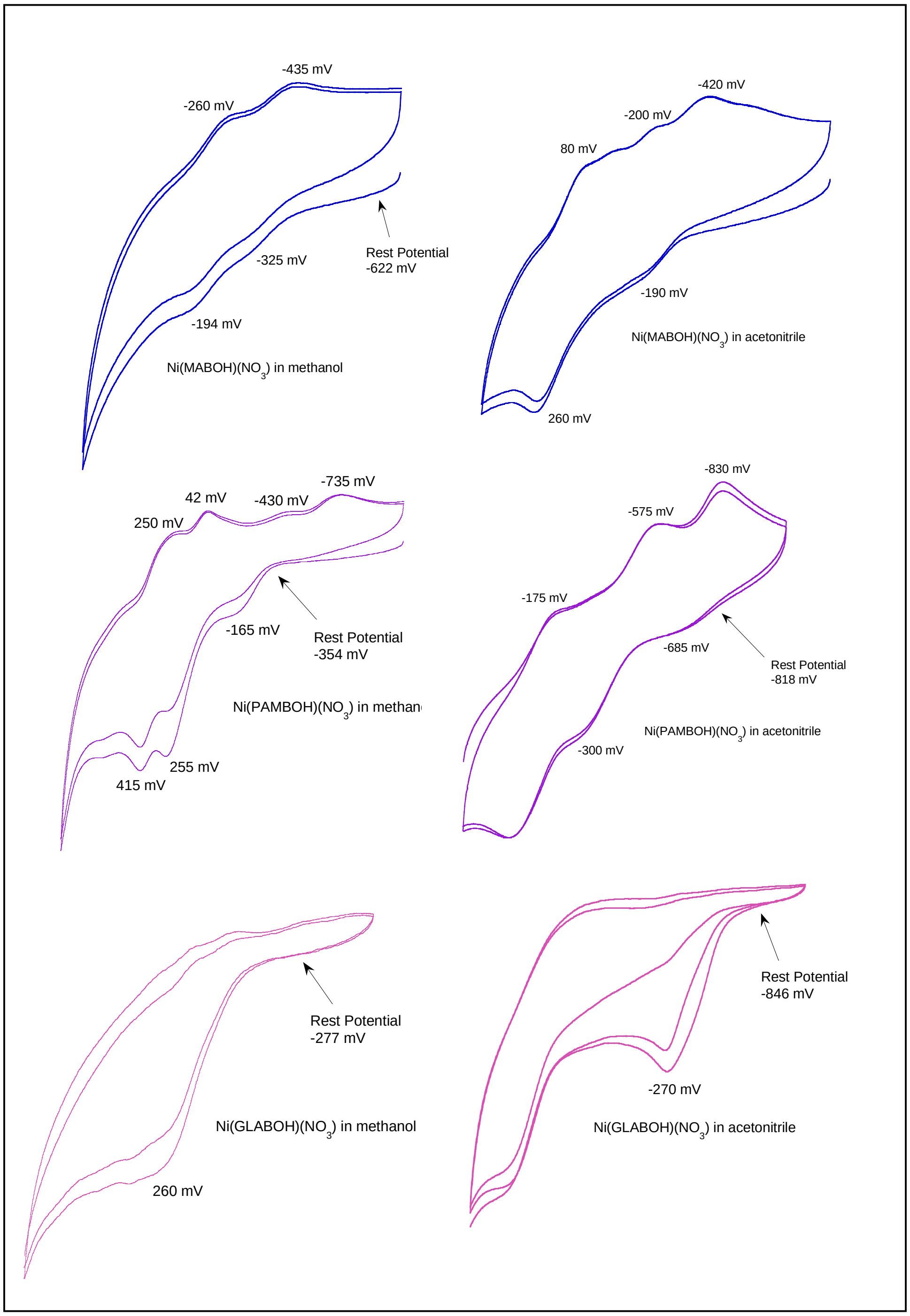

Figure 4.12. CV's of complexes containing weakly coordinating third arms in acetonitrile and methanol. Oxidation potentials are referenced to the ferrocene/ferrocenium couple.

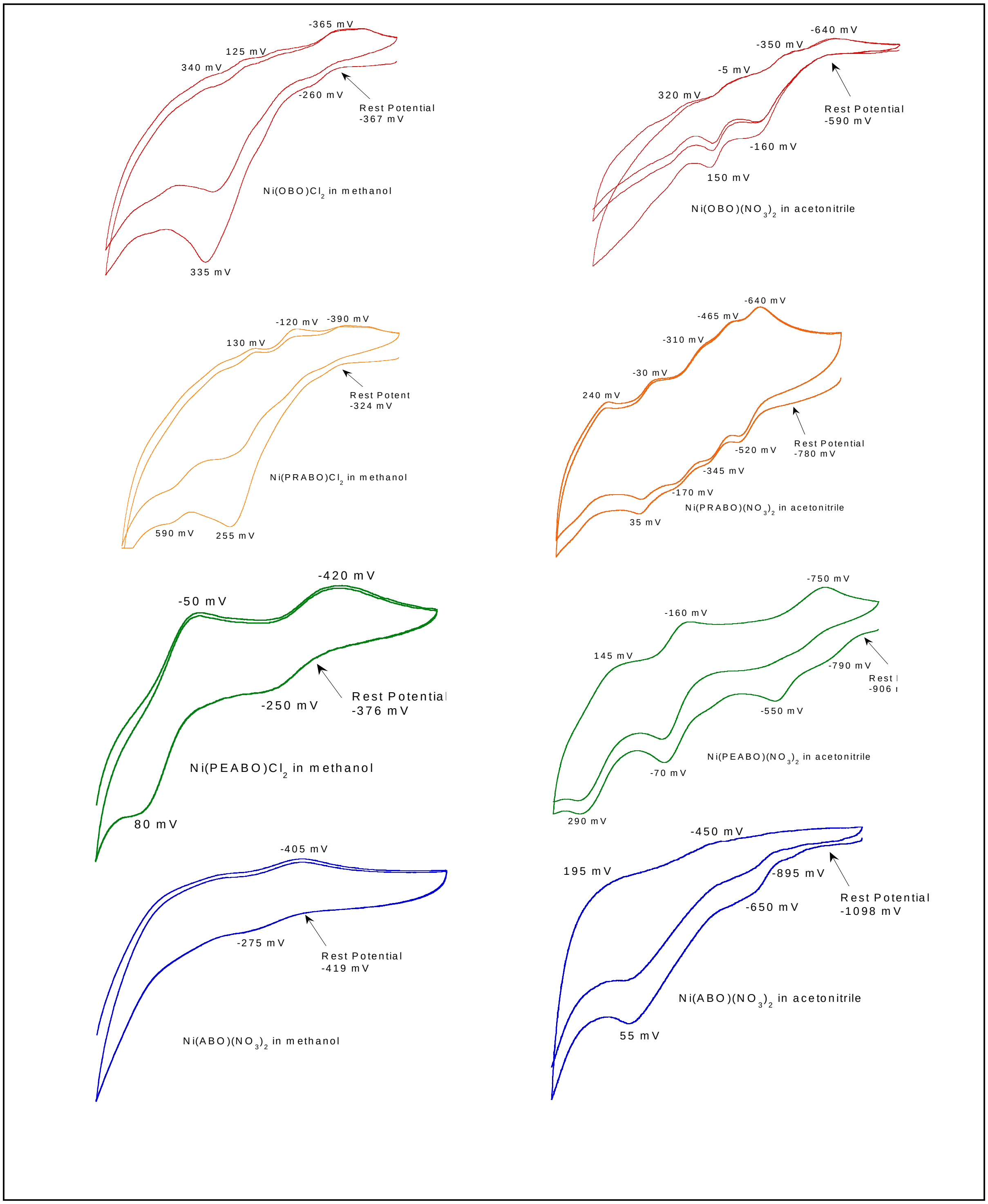

Figure 4.13. CV's of complexes containing non-coordinating third arms in acetonitrile and methanol. Oxidation potentials are referenced to the ferrocene/ferrocenium couple.

Comparison of the cyclic voltammagrams of the complexes containing strongly, weakly, and non-coordinating third arms in acetonitrile and methanol reveal several trends. The complexes containing tetradentate ligands do not display more than two oxidation features in either solvent investigated (with the exception of Ni(PAMBOH)(NO_3)$_2$, which had three), while the complexes containing tridentate ligands had multiple oxidation features in their CVs'. This may indicate that structural changes specific to the denticity of the ligand take place upon deprotonation, for example higher order oligomers may form where each unit may be oxidized. This hypothesis involving structural changes is also supported by the disordering of the spectrochemical series that is observed after deprotonation of the complexes.

Changing solvents from the more coordinating and polar methanol to acetonitrile results in the lowering of the first oxidation potential, except in the case of Ni(MABO)(NO_3)$_2$ (-194 mV in methanol vs. –190 mV in acetonitrile) and the nickel complex of OBO (-260 mV in methanol vs. –160 mV in acetonitrile). In some cases, the drop in oxidation potential is quite drastic, for example Ni(PAMBOH)(NO_3)$_2$ has an oxidation feature at –165 mV in methanol and at –685 mV in acetonitrile. The nickel complex of PRABO has an oxidation at 255 mV in methanol and –520 mV in acetonitrile. However, the reduction potential of O_2 is also lower in acetonitrile than in methanol, (575 mV in methanol, -1040 mV in acetonitrile, vs. Fc/Fc$^+$), which offsets the difference in oxidation potential for the complexes in the different solvents.

The strength of the donor ability of the third arm did not appear to influence the oxidation potentials. The ordering of the oxidation potentials in acetonitrile, from lowest to highest, is as follows: PAMBO (amide) < ABO (aryl) < PEABO < (aryl) < PRABO (alkyl) < TRISOX (oximate) < GLYBO (amide) < EABO (ethyl alcohol) < GLABO (amine) < MABO (amide) < OBO (alkyl) < BALBO (carboxylate) < PYRABO (pyridyl), which again suggests that structural changes occur as a result of deptrotonation and affect the electronic structure of the complex as well as the electrochemical properties, since it was expected that complexes containing strongly donating ligands would have lower oxidation potentials.

The CV's of many of the complexes were collected after the complex had reacted with O_2 for several hours. All of the CV's were featureless, which implies that the redox active (and thus oxygen active) species decays over time as the "dead-end" product builds up.

4.4. Methanol oxidation by complexes in the library.

The library was constructed to provide information about the factors that influence the oxygen activation reaction. Various members of the library were tested for their ability to oxidize methanol to formaldehyde. Their UV/visible absorption spectra were also monitored during this reaction.

Experimental. The first tridentate ligand investigated was $OBOH_2$. For the UV/vis experiment, a 1 mM solution was prepared by dissolving 12 mg (0.03 mmol) of $Ni(OBOH_2)(NO_3)_2$ in 30 mL of methanol. A UV/vis spectrum of this methanolic solution was collected using a Spectral Instruments, Inc. 400 Series dip probe CCD-array spectrometer. Next, 0.12 mL (2 equivalents) of 0.5 M KOH in methanol was added to the solution under atmospheric conditions and the UV/vis spectrum was collected at assigned time intervals. Addition of ≥ 3 equivalents of base did not affect the experiment.

Next, the nickel complex containing $PEABOH_2$ was analyzed. For the UV/vis experiment a 1 mM sample was prepared by dissolving 12 mg (0.03 mmol) of $Ni(PEABOH_2)(NO_3)_2$ in 30 mL of methanol. A UV/vis spectrum of this blue solution was collected and then 0.12 mL (2 eq.) of 0.5 M KOH in methanol was added to the aerobic solution. The UV/vis spectrum was monitored as the solution turned yellow.

A complex containing a ligand with a weakly coordinating third arm, $PAMBOH_3$, was also investigated. 13 mg (0.03 mmol) of $Ni(PAMBOH_3)(NO_3)_2$ were dissolved in 30 mL of methanol and the UV/vis spectrum of this blue solution was collected. Then, 0.12 mL (2 eq.) of a 0.5 M KOH in methanol solution was added to the solution in the presence of O_2 and the UV/vis spectrum monitored as the solution changed from blue to yellow to brown in the span of ~ninety minutes.

Another complex with a ligand that contained a weakly coordinating third arm, $MABOH_3$, was analyzed. The solution consisted of 12 mg (0.03 mmol) of $Ni(MABOH_3)(NO_3)_2$ dissolved in 30 mL of methanol, with 0.12 mL (2 eq.) of 0.5 M KOH in methanol added. The UV/vis spectrum was collected as the solution turned from blue to yellow to brown after about 15 minutes.

Next, complexes containing ligands with strongly coordinating third arms were examined. The first complex was $Ni(EABOH_3)Cl_2$. 10 mg (0.03 mmol) of complex were dissolved in 30 mL of methanol and then the UV/vis spectrum of the light green solution was collected. Next, 0.18 mL (3 eq.) of 0.5 M KOH in methanol was added and the spectrum was collected at various time intervals.

$Ni(PYRABOH_2)(NO_3)_2$ was the next complex studied. A 1 mM solution of this complex consisted of 13 mg (0.03 mmol) of $Ni(PYRABOH_2)(NO_3)_2$ dissolved in 30 mL of methanol. This solution was light purple. Addition of 0.12 mL (2eq.) of 0.5 M KOH in methanol resulted in a color change to darker purple. The UV/vis spectrum was monitored during this reaction.

Finally, the UV/vis spectrum was monitored for [Ni(BALBOH$_2$K)(ClO$_4$)]$_2$. A 1 mM solution of the complex was constructed by dissolving 17 mg (0.02 mmol) of complex in 20 mL of methanol. The complex is fairly insoluble in methanol; however, addition of 0.16 mL (4 eq.) of 0.5 M KOH in methanol makes the complex more soluble, producing a purple solution. The UV/vis spectra of this reaction were collected.

Formaldehyde production by all of these complexes was monitored according to the procedure described in Chapter 2.2.

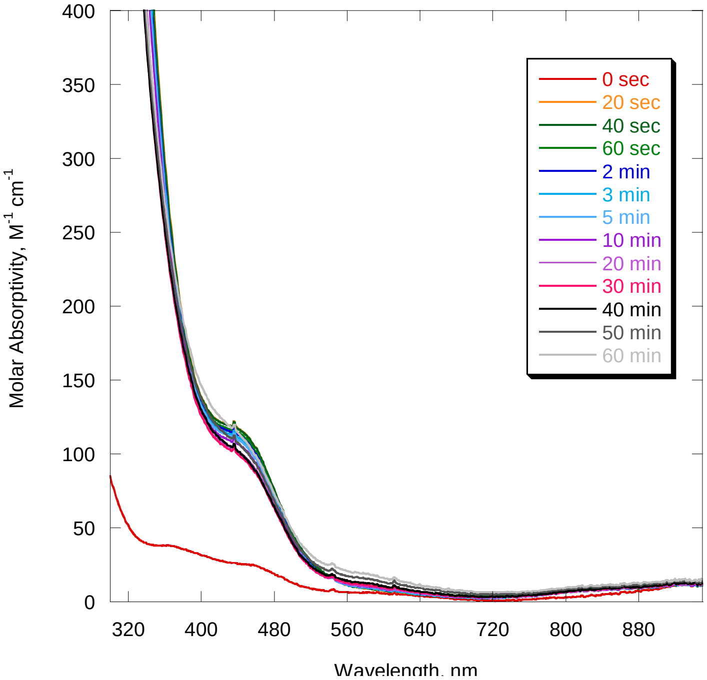

Figure 4.14. UV/vis spectra of the reaction of 1 mM Ni (OBOH$_2$)(NO$_3$)$_2$ + 2KOH + O$_2$ in methanol.

Results and discussion. First, some complexes containing representative tridentate ligands were examined. It was anticipated that complexes with a non-coordinating third arm would not be as efficient as **3** during the oxidation reaction because the ligand would not be able to stabilize an oxidized species as well as a complex with three strongly donating arms.

Addition of two equivalents of base to a 2 mM solution of Ni(OBOH$_2$)(NO$_3$)$_2$ resulted in a color change from light blue to yellow. Adding excess base did not affect the reaction. The spectrum was monitored for one hour, during which time the solution remained yellow (Figure 4.14). After approximately five hours the solution was light brown, and after about twelve hours the solution was dark brown.

A 2 mM solution of Ni(OBOH$_2$)(NO$_3$)$_2$ in methanol was analyzed to see if methanol oxidation took place. Based on the UV/vis experiment, it was expected that this reaction would occur much more slowly than the oxidation of methanol by **3**. Figure 4.15 shows the results.

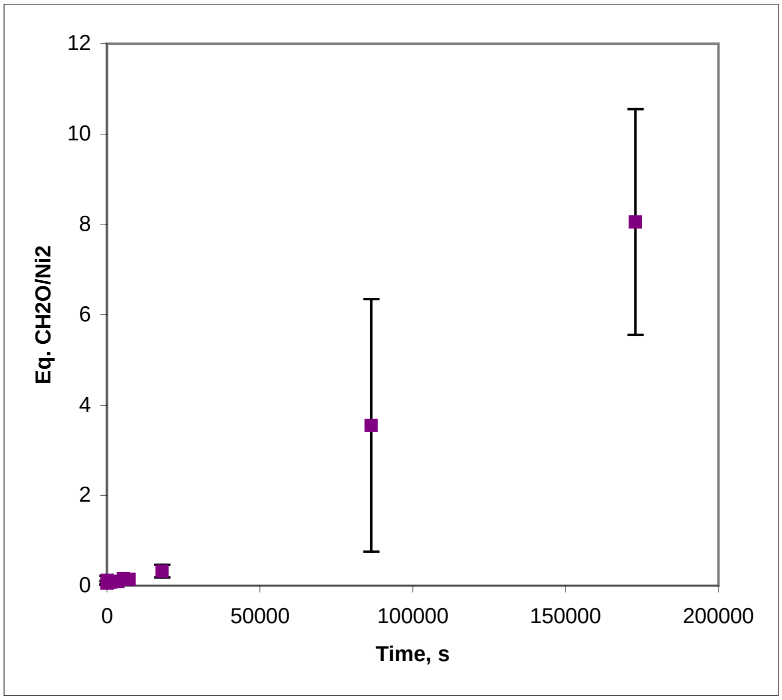

Figure 4.15. Plot of formaldehyde production by the reaction of Ni(OBOH$_2$)(NO$_3$)$_2$ + 2KOH + O$_2$ in methanol versus time. Each data point is the average of three trials and the error bars are the standard deviation between the three.

This reaction proved to be slower than that of **3**, forming only 0.12 ± 0.02 eq. of CH_2O/dimer after one hour as compared to 3.95 ± 0.19 eq./**3**. However, after 48 hours the reaction of Ni(OBOH$_2$)(NO$_3$)$_2$ + 2KOH + O_2 in methanol produced 8.06 ± 2.85 eq./dimer. It should be noted that at later reaction times the quantitation becomes less reproducible. This may indicate that several degradation pathways are available to the complex and that various factors influence the rate at which each occurs.

Another complex containing a tridentate ligand, PEABOH$_2$, was examined. This solution turned brown more rapidly than the solution of Ni(OBOH$_2$)(NO$_3$)$_2$ upon addition of base, but not as fast as the solution of **3**, changing color after about twenty minutes. Figure 4.16 shows the UV/vis spectra for this reaction.

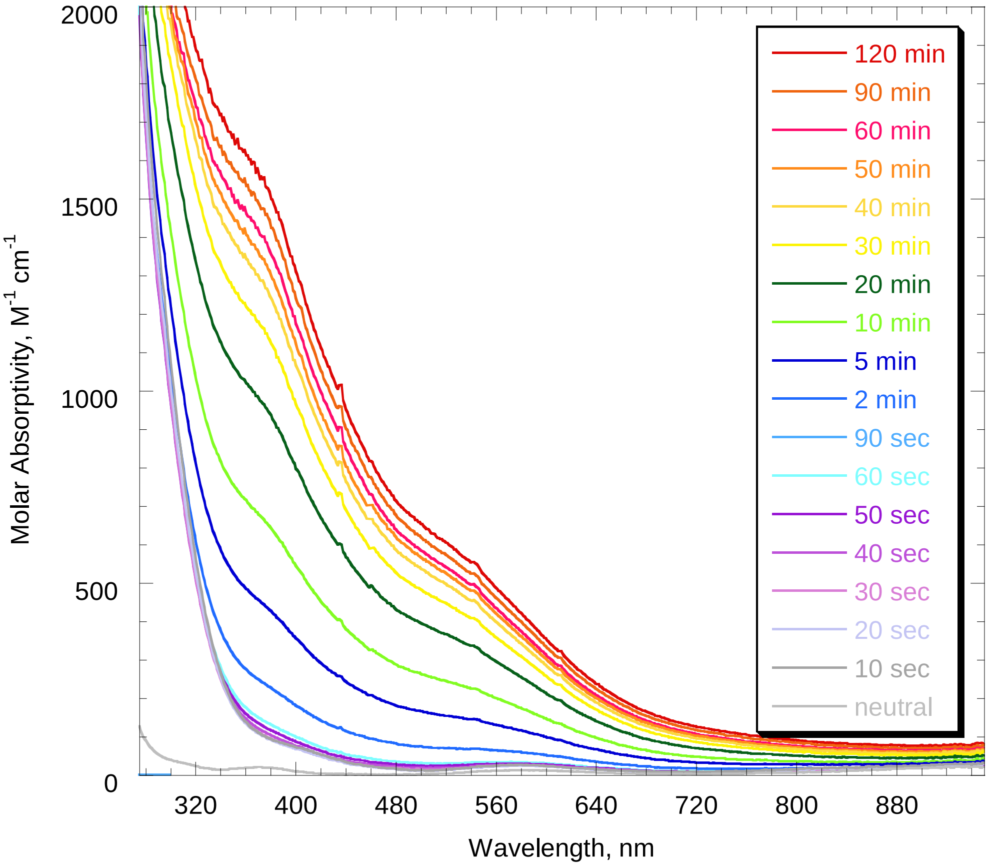

Figure 4.16. UV/vis spectra of the reaction of 1 mM Ni (PEABOH$_2$)(NO$_3$)$_2$ + 2KOH + O_2 in methanol.

The moderate pace of the color change to brown (compared to $Ni(OBOH_2)(NO_3)_2$ and **3**), as well as the appearance of a band at ~360 nm in the UV/vis spectrum led to the expectation that this complex would produce formaldehyde more rapidly than $Ni(OBOH_2)(NO_3)_2$, but not as quickly as **3**. To test this, a 2 mM sample of $Ni(PEABOH_2)(NO_3)_2$ was made in methanol and analyzed for formaldehyde. Figure 4.17 presents the results.

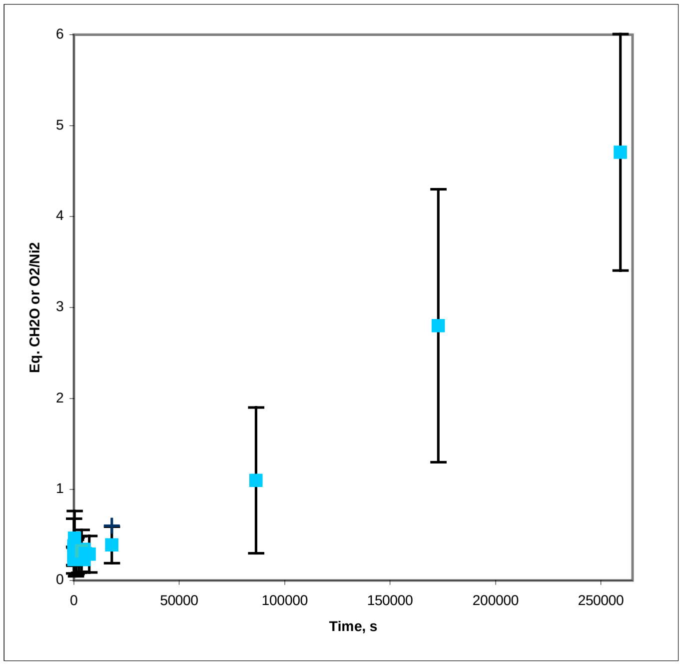

Figure 4.17. Plot of formaldehyde production by the reaction of $Ni(PEABOH_2)(NO_3)_2 + 2KOH + O_2$ in methanol versus time. Each data point is the average of three trials and the error bars are the standard deviation between the three.

This reaction did not proceed more quickly than $Ni(OBOH_2)(NO_3)_2$ and after 72 hours only 4.71 ± 1.38 eq./dimer were formed, less than half the amount formed by **3** after 24 hours. This reaction also displays a decrease in reproducibility at later time points.

Next, complexes containing weakly coordinating third arms were monitored for methanol oxidation. First, the UV/vis experiment was repeated for a 1 mM methanolic solution of Ni(PAMBOH$_3$)(NO$_3$)$_2$ (Figure 4.18).

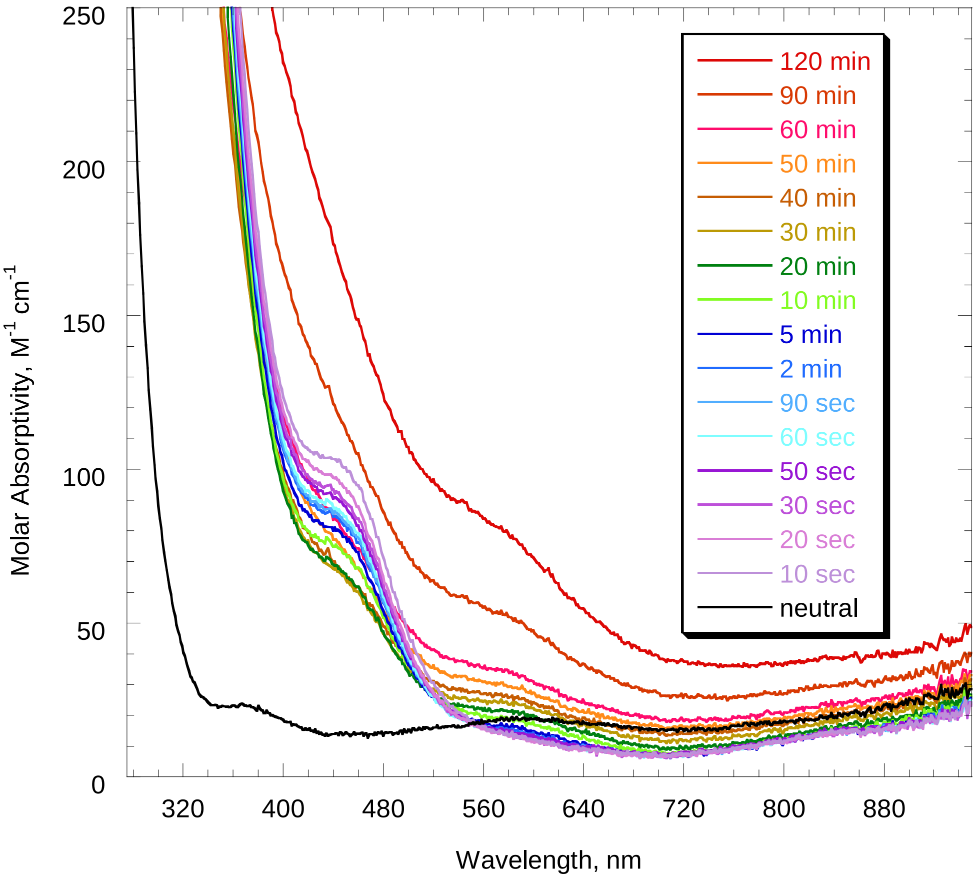

Figure 4.18. UV/vis spectra of the reaction of 1 mM Ni (PAMBOH$_2$)(NO$_3$)$_2$ + 2KOH + O$_2$ in methanol.

The initial band that appears around 450 nm is due to the deprotonation reaction, as it was also observed under anaerobic conditions. The final two spectra resemble the final spectrum of **3**.

Formaldehyde production by a 2 mM solution of Ni(PAMBOH$_3$)(NO$_3$)$_2$ was monitored and the results are displayed in Figure 4.19.

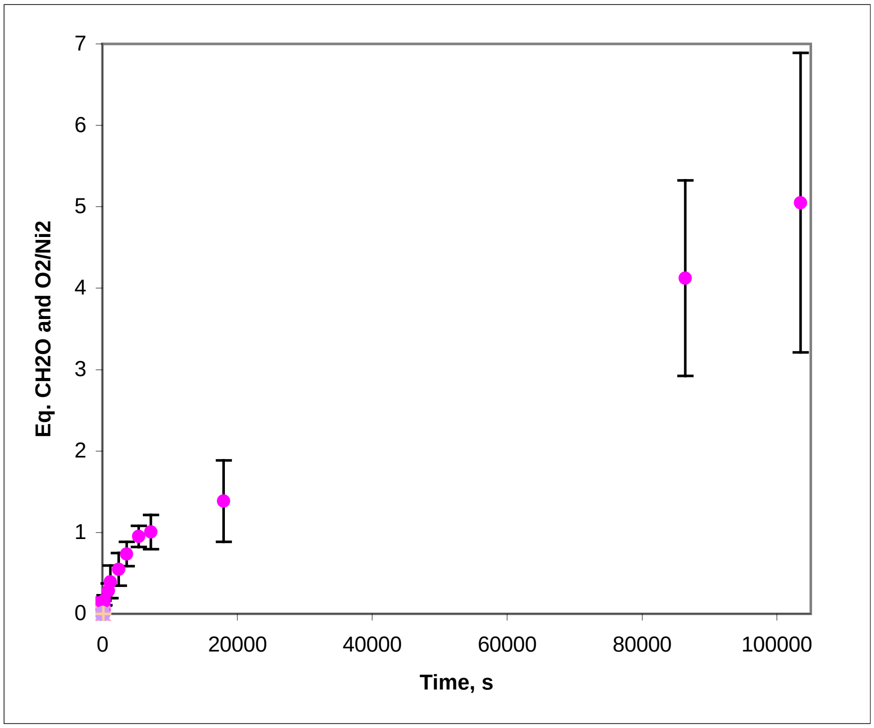

Figure 4.19. Plot of formaldehyde production by the reaction of Ni(PAMBOH$_3$)(NO$_3$)$_2$ + 2KOH + O$_2$ in methanol versus time. Each data point is the average of three trials and the error bars are the standard deviation between the three.

This reaction is slower and less efficient than the reaction with **3**, forming 5.05 ± 1.84 eq. after 28 hours.

Ni(MABOH$_3$)(NO$_3$)$_2$, another complex with a weakly coordinating third arm, was also investigated. The UV/vis spectrum of the reaction between 1 mM Ni(MABOH$_3$)(NO$_3$)$_2$, KOH, and O$_2$ in methanol was monitored. This solution turned brown after approximately fifteen minutes and displayed an absorbance spectrum similar to that of **3** (Figure 4.20).

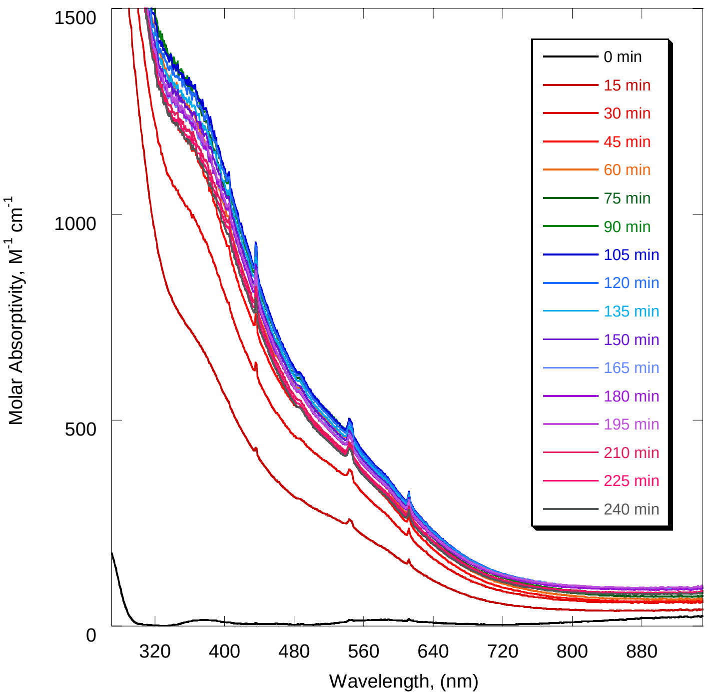

Figure 4.20. UV/vis spectra of the reaction of 1 mM Ni (MABOH$_3$)(NO$_3$)$_2$ + 2KOH + O$_2$ in methanol.

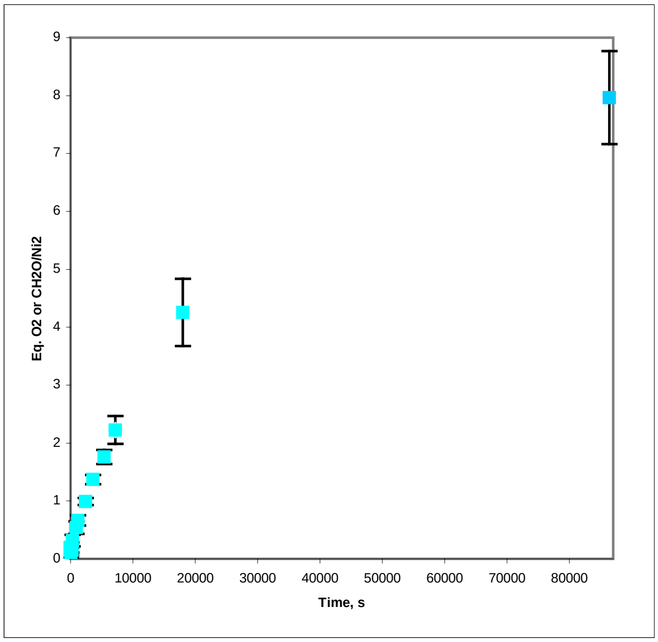

Figure 4.21. Plot of formaldehyde production by the reaction of Ni(MABOH$_3$)(NO$_3$)$_2$ + 2KOH + O$_2$ in methanol versus time. Each data point is the average of three trials and the error bars are the standard deviation between the three.

The formaldehyde production of this complex is displayed in Figure 4.21. The reaction profile of this complex matches that of **3** more closely than the other complexes investigated, forming 7.97 ± 0.83 equivalents per dimer after 24 hours. The error bars at later time points of the reaction are also smaller than many of the other complexes studied, resembling the error observed towards the end of the reaction with **3.**

Next, complexes containing strongly coordinating third arms were investigated. It was anticipated that these complexes would perform as well or better than **3**. The first complex studied was $Ni(EABOH_3)Cl_2$, which displayed the highest value of 10 *Dq* upon deprotonation during the experiment to determine the spectrochemical series of the library. The UV/visible absorption spectrum was monitored as a methanolic solution of 1 mM $Ni(EABOH_3)Cl_2$ was reacted with 3 equivalents of base under atmospheric conditions. Deprotonation caused a color change from light green to yellow, which lasted for several hours. The spectrum did not resemble that of **3** after one hour (Figure 4.22).

For the quantitation of formaldehyde formation a 2 mM solution of $Ni(EABOH_3)Cl_2$ was prepared in methanol. The methanol oxidation reaction was tracked and can be seen in Figure 4.23. This reaction was much less efficient than any of the other complexes studied, only forming 1.36 ± 0.35 eq. of CH_2O/Ni_2 after 72 hours.

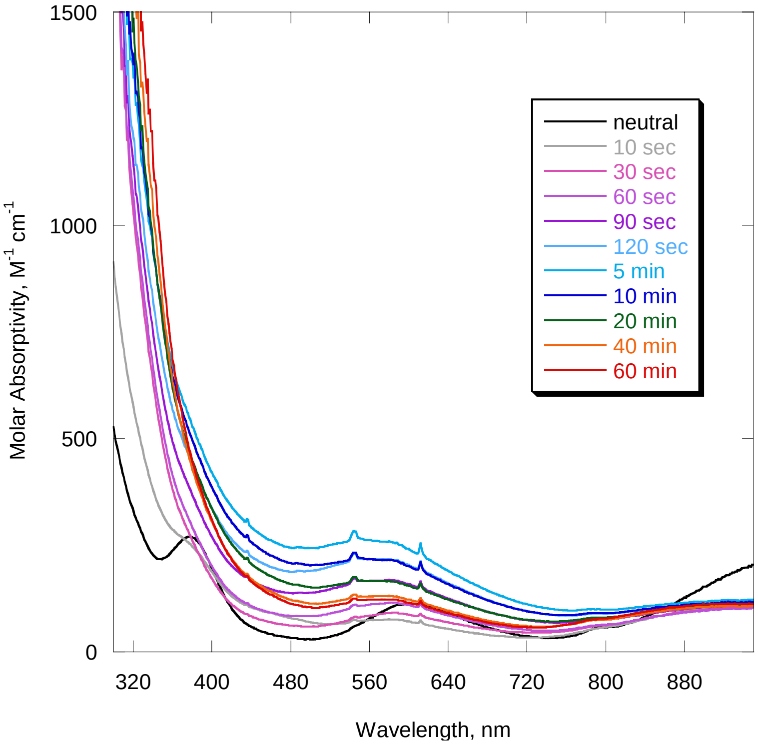

Figure 4.22. UV/vis spectra of the reaction of 1 mM Ni (EABOH$_3$)(NO$_3$)$_2$ + 2KOH + O$_2$ in methanol.

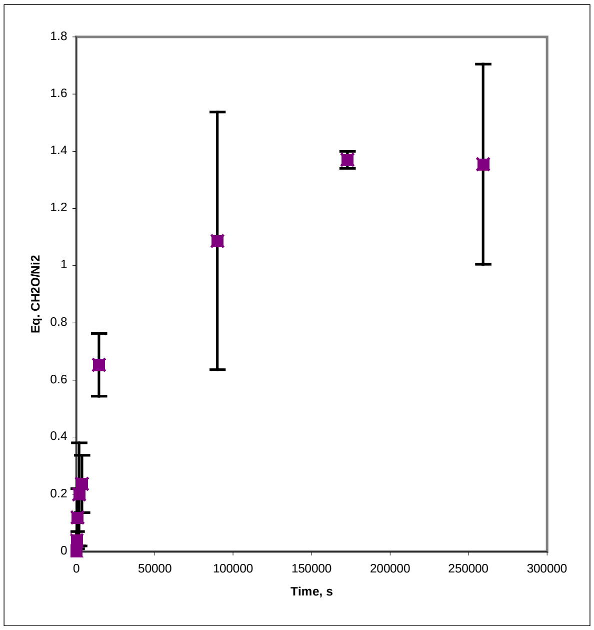

Figure 4.23. Plot of formaldehyde production by the reaction of Ni(EABOH$_3$)(NO$_3$)$_2$ + 2KOH + O$_2$ in methanol versus time. Each data point is the average of three trials and the error bars are the standard deviation between the three.

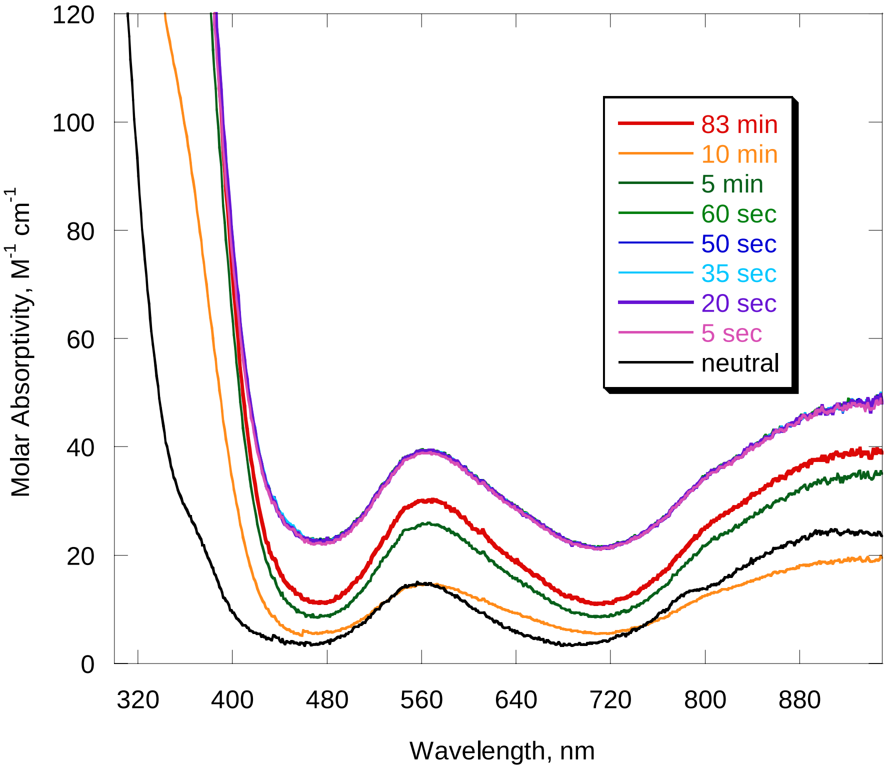

Figure 4.24. UV/vis spectra of the reaction of 1 mM Ni (PYRABOH$_2$)(NO$_3$)$_2$ + 2KOH + O$_2$ in methanol.

The next complex studied was Ni(PYRABOH$_2$)(NO$_3$)$_2$, which has a pyridyl group as its third arm. Addition of two equivalents of base to the light purple solution caused it to become darker purple and slightly cloudy, resulting in the high baseline observed in some of the spectra. The dark purple color never changed, even after 72 hours. Also, formaldehyde was not detected in the solution after 72 hours, indicating that this complex does not activate oxygen like the other complexes in the library. This may be due to steric hindrance caused by the bulky pyridyl ring that is linked to the amine nitrogen via a methylene group. This large group may prevent oximate bridge formation from occurring, in which case the putative dimeric active species would not be formed.

The final complex studied during this experiment was [Ni(BALBOH$_2$K)(ClO$_4$)]$_2$, which contains a carboxylate group for its third arm and is a bis(carboxylate)bridged dimer in its oxime protonated form. Addition of four equivalents of base caused a color change from light purple to dark purple. This color remained for 72 hours and the UV/vis spectra can be seen in Figure 4.25.

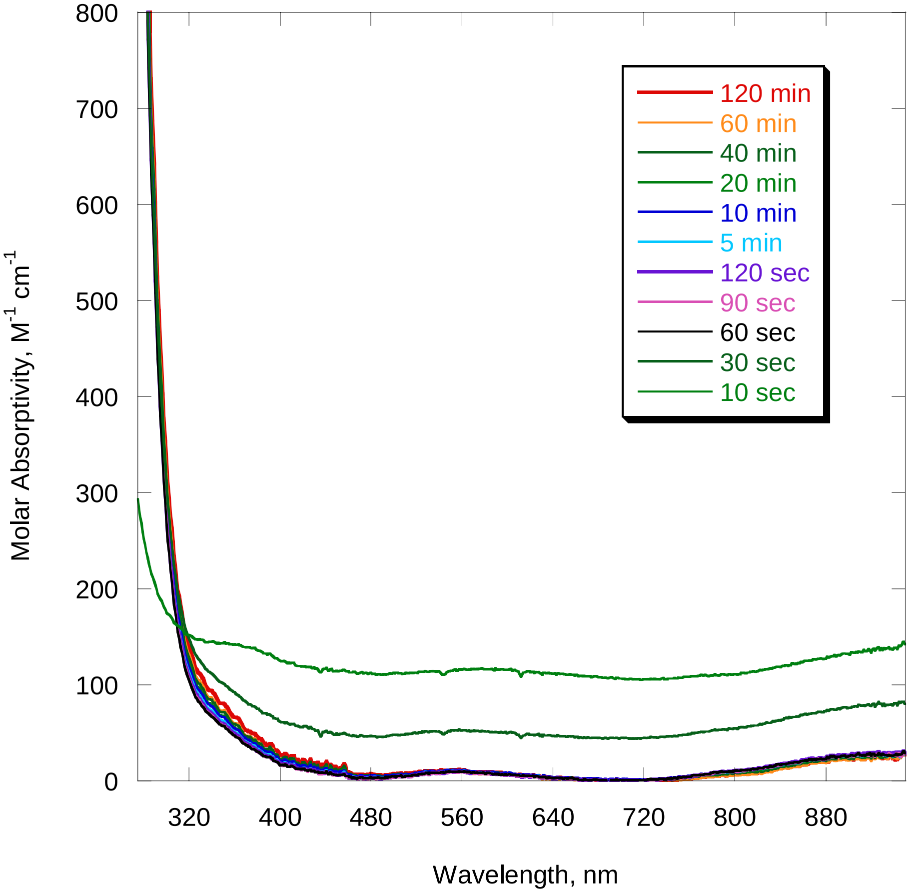

Figure 4.25. UV/vis spectra of the reaction of 1 mM [Ni (BALBOH$_2$)(ClO$_4$)]$_2$ + 4KOH + O$_2$ in methanol.

Formaldehyde production by this complex was also monitored. Due to the lack of color change, formaldehyde production was not expected, even though the complex contained a strongly coordinating third arm. Figure 4.26 shows the results.

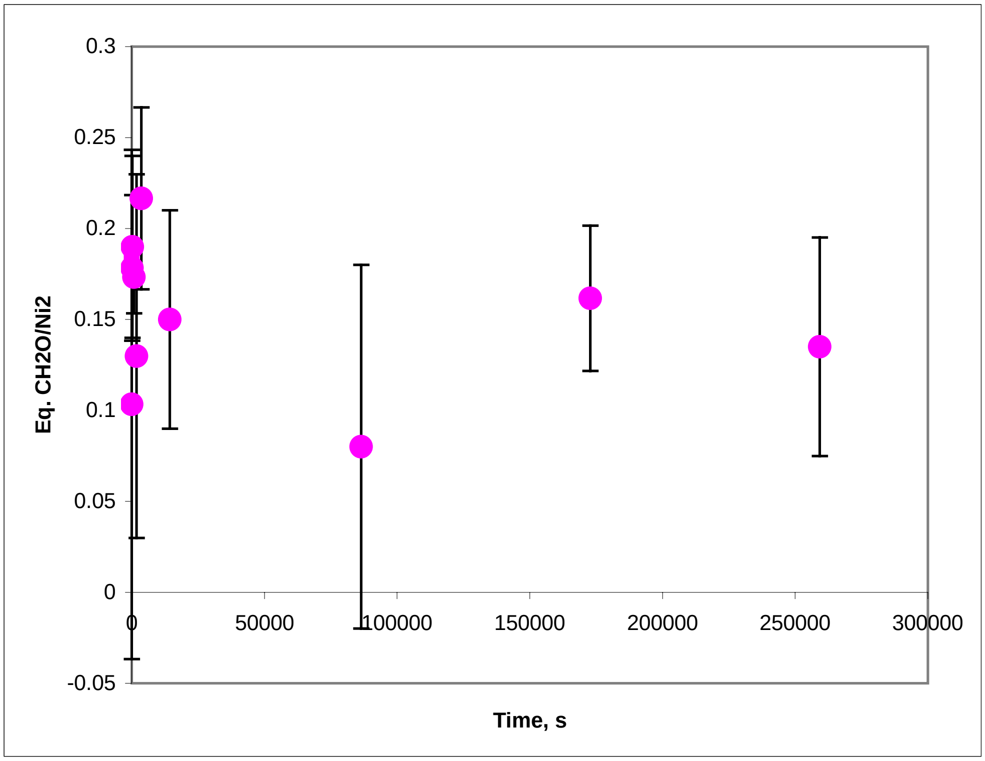

Figure 4.26. Plot of formaldehyde production by the reaction of [Ni(BALBOH$_2$)(ClO4)]$_2$ + 4KOH + O$_2$ in methanol versus time. Each data point is the average of three trials and the error bars are the standard deviation between the three.

The data are very erratic, and do not indicate a smooth increase in formaldehyde formation that is normally observed for these complexes. Also, it was not as efficient as most of the other reactions, forming 0.14 ± 0.06 eq. CH_2O per dimer after 72 hours. This may indicate that oximate bridges are necessary for the reaction to take place and that carboxylate bridges are not acceptable substitutes.

The reaction profiles of all of the complexes studied are plotted together in Figures 4.27 and 4.28.

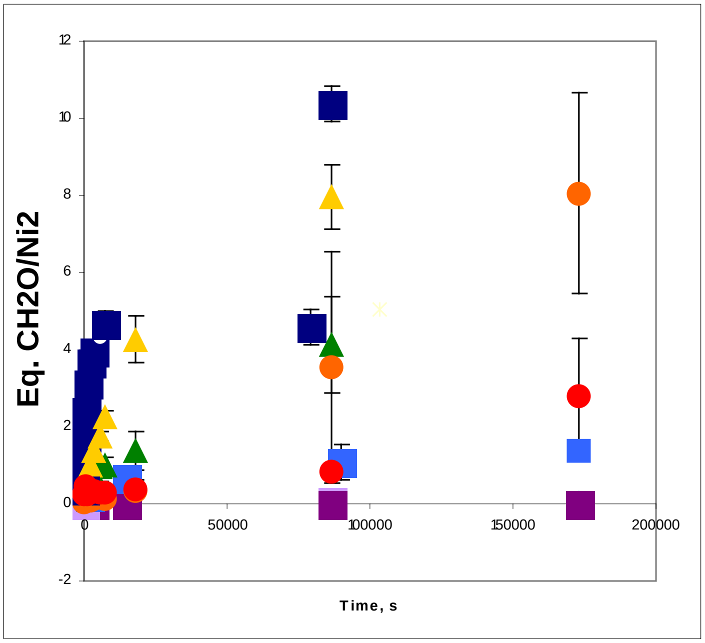

Figure 4.27. Plot of formaldehyde production by the reaction of the complexes + KOH + O_2 in methanol versus time. Dark blue squares = TRISOX, Light blue squares = EABOH, Light purple squares = BALBO, dark purple squares = PYRABO, Green triangles = PAMBOH, Yellow triangles = MABOH, Orange circles = OBO, Red circles = PEABO. Each data point is the average of three trials and the error bars are the standard deviation between the three.

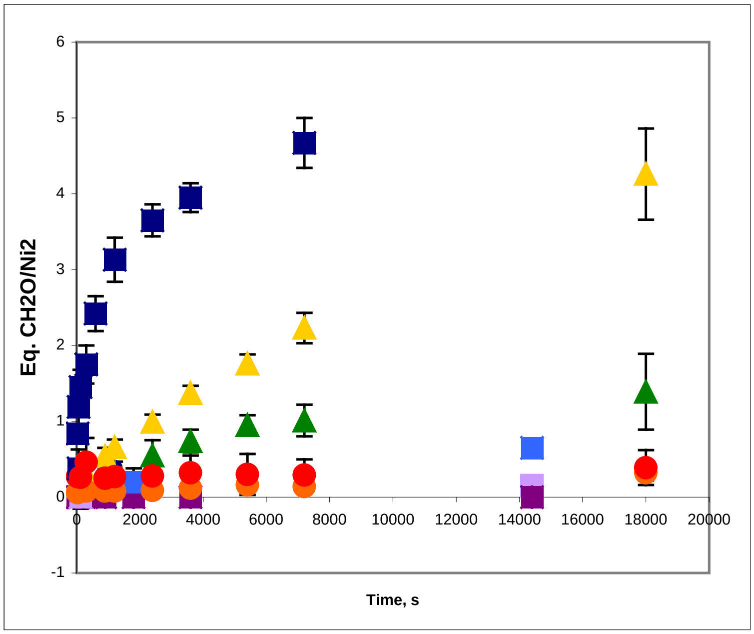

Figure 4.28. Plot of formaldehyde production by the reaction of the complexes + KOH + O_2 in methanol versus time. Dark blue squares = TRISOX, Light blue squares = EABOH, Light purple squares = BALBO, dark purple squares = PYRABO, Green triangles = PAMBOH, Yellow triangles = MABOH, Orange circles = OBO, Red circles = PEABO. Each data point is the average of three trials and the error bars are the standard deviation between the three.

Table 4.4. Equivalents of formaldehyde per dimer formed by the different complexes in the library after 1 and 24 hours. S = strongly donating, W = weakly donating, N = non-coordinating third arm.

Ligand	Eq. CH_2O/Ni_2 after 1 hour	Eq. CH_2O/Ni_2 after 24 hours
TRISOX (s)	3.95 ± 0.19	10.37 ± 0.45
PYRABO (s)	ND	ND
EABOH (s)	0.24 ± 0.10	1.09 ± 0.45
BALBO (s)	0.22 ± 0.05	0.08 ± 0.10
MABOH (w)	1.37 ± 0.08	7.97 ± 0.83
PAMBOH (w)	0.74 ± 0.15	4.12 ± 1.24
OBO (n)	0.12 ± 0.02	3.55 ± 2.98
PEABO (n)	0.32 ± 0.23	0.84 ± 0.13

Table 4.4 lists the amount of formaldehyde per presumptive dimeric species for each of the complexes studied. Comparison of the reaction profiles of the different complexes reveals several trends. TRISOX starts off with the most rapid formaldehyde production and then begins to level off; however, after 24 hours it has produced more oxidized product than any of the other complexes. The complexes containing weakly coordinating third arms begin more slowly, but they do not taper off like TRISOX. Instead they oxidize methanol in a linear fashion, eventually producing an amount that is greater than the amount produced by the other complexes (except TRISOX). The most unexpected trend revealed is that the complexes containing strongly coordinating third arms perform the most poorly, with the notable exception of TRISOX. PYRABO never accomplished the oxidation reaction and BALBO produced a very small, substoichiometric amount. Even EABOH, the complex with the highest value of 10 *Dq* after deprotonation, only produced 1.36 ± 0.35 equivalents after 72 hours. The complexes containing non-coordinating third arms actually produced more formaldehyde than the complexes containing strongly coordinating third arms, for example OBO produced 8.06 ± 2.55 equivalents after 48 hours. This leads to the conclusion that three strong donor

groups are not a requirement for oxygen activation to occur, since complexes containing non-coordinating third arms produced more oxidized product than those containing strongly coordinating third arms. Another observed trend is that at later times during the reaction the error becomes greater. This implies that there may be several degradation pathways occurring at varying rates that are influenced by unknown factors. Also, the lack of correlation between the changes observed in the UV/vis spectra of the complexes and the production of formaldehyde may indicate that the kinetics of the reaction (especially in terms of the observed intermediate) are different for each complex. Another possibility is that the intermediate observed in the UV/vis experiment is not the catalyst. The catalyst may be a minor species with a high turnover whose concentration varies slightly in each experiment, resulting in the variability in yield.

4.5. Synthesis and characterization of *N*-*n*-Octyl-*N*,*N*-bis(1-propan-2-onyl oxime)amine ($OBOH_2$) and $[Ni(OBOH_2)Cl]_2$.

Experimental. The original ligand synthesis of $OBOH_2$ was performed during the course of this project.[3] For this synthesis, 10 g (0.048 mol) of the triethylamine adduct of chloroacetone oxime (TACO, the synthesis of which has been previously reported)[4] was combined with 3.1 g (0.024 mol) of *n*-octylamine in approximately 125 mL of isopropanol. This mixture was heated to reflux for about 30 minutes, during which time almost all of the TACO dissolved and the solution turned a golden yellow. The solution was refluxed for an additional 30 minutes and then the small amount of unreacted TACO was removed by filtration. Next, the solvent was removed by rotary evaporation to give a crude orange solid. This was extracted with 200 mL of diethyl ether and then the ether was removed by rotary evaporation to leave a gold colored oil. This was washed with three 10 mL portions of water and then the oil was placed under vacuum (32% yield). NMR spectra were obtained using a Bruker AC250 spectrometer as $CDCl_3$ solutions and referenced to TMS. FTIR spectra were collected using a Bio-Rad Excalibur spectrometer as KBr pellets. Mass spectra were collected by the University of Cincinnati Mass Spectrometry Facility using a Micro-mass QTOF-II or an IonSpec FT-ICR mass spectrometer with electrospray sample induction. Samples were prepared by dissolution in methanol, with NaCl added to the neutral ligand to induce charge.

^{1}H NMR (Figure 4.29) ($CDCl_3$): 0.08 (3H, t), 1.18 (m, br, 10H), 1.35 (m, br, 2H), 1.83 (s, 6H), 2.30 (t, 2H), 2.96 (s, 4H), 9.53 (s, br, 2H) ppm. ^{13}C NMR (Figure 4.30) ($CDCl_3$): 12.08, 13.75, 18.61, 22.32, 26.50, 26.96, 29.15, 31.52, 53.72, 57.72, 156.91 ppm. FTIR (Figure 4.31) (KBr): 3238 (s, br), 2930 (s), 2855 (m), 1665 (m), 1460 (s), 1367 (s), 1265 (m), 1135 (m), 1032 (s), 967 (s), 670 (m) cm^{-1}. MS (Figure 4.32): $(M + Na)^+$ at *m/z* = 294.2 (90%), $(M + H)^+$ at *m/z* =272.2 (100%).

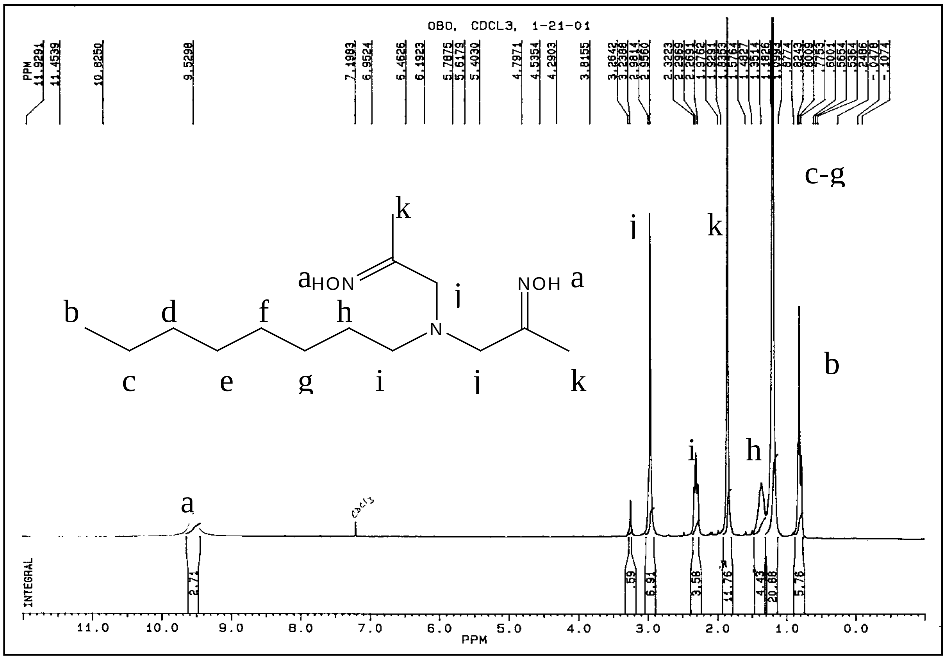

Figure 4.29. ^{1}H NMR spectrum of $OBOH_2$ in chloroform.

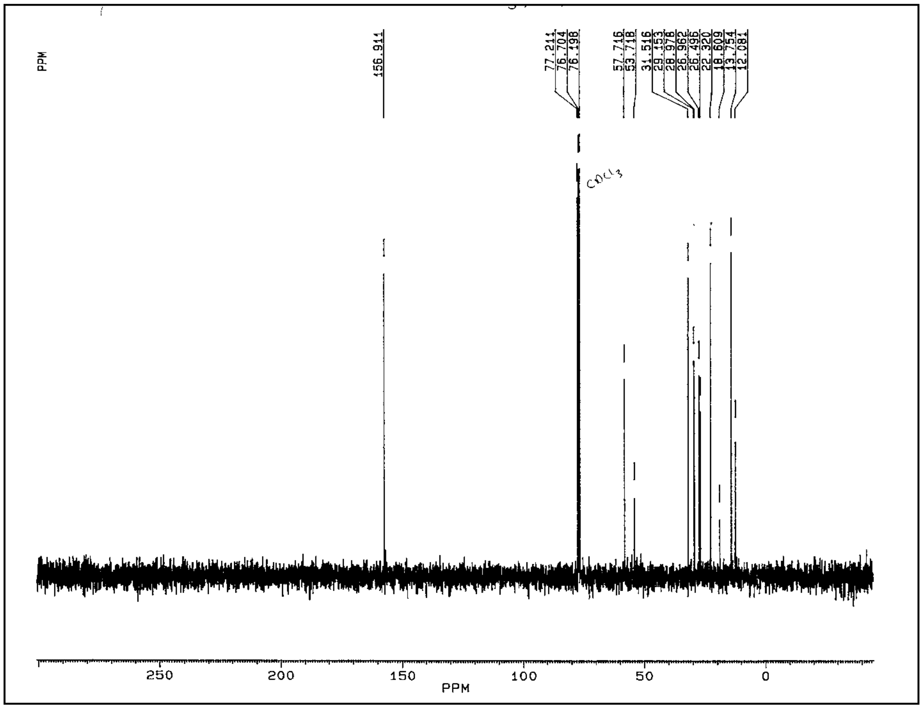

Figure 4.30. ^{13}C NMR spectrum of $OBOH_2$ in chloroform.

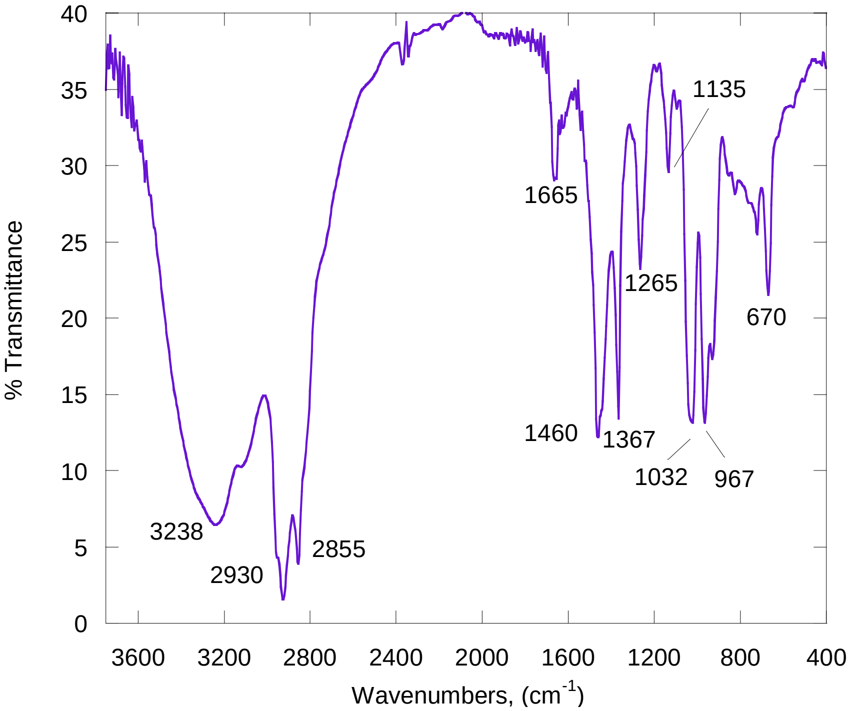

Figure 4.31. FTIR spectrum of $OBOH_2$ (KBr pellet).

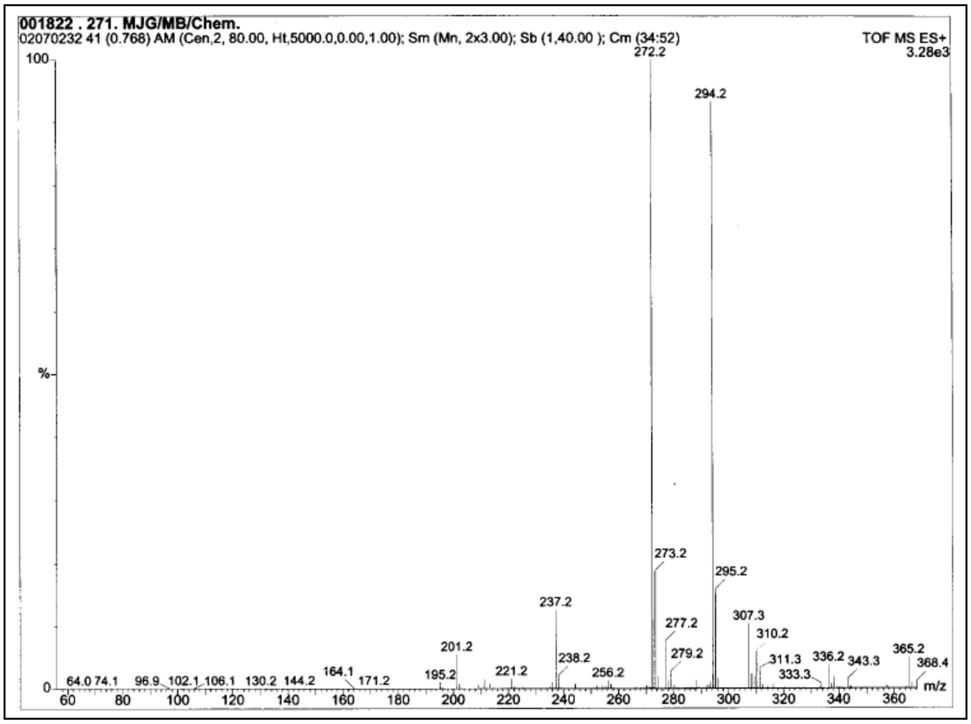

Figure 4.32. Mass spectrum of $OBOH_2$ $(M + Na)^+$ *m/z* = 294.2 (90%), $(M + H)^+$ *m/z* = 272.2 (100%).

$[Ni(OBOH_2)Cl]_2(\mu\text{-}Cl)_2$ was prepared by combining 244 mg (0.9 mmol) of $OBOH_2$ with 215 mg (0.9 mmol) of nickel(II) chloride hexahydrate in about 15 mL of acetonitrile and stirring to give a green solution. A green solid was isolated in 55% yield. Green crystals suitable for X-ray crystallography were obtained by slow evaporation of an acetone/diethyl either solution of $[Ni(OBOH_2)Cl]_2(\mu\text{-}Cl)_2$ in a test tube. Elemental analysis (CHN) was performed by Quantitative Technologies, Inc. (Whitehouse, NJ). The sample was a crystalline solid that was ground to powder and dried under vacuum before submission for CHN analysis.

FTIR (KBr) (Figure 4.33): 3247 (s), 2931 (s), 2856 (m), 1460 (s), 1377 (m), 1228 (m), 1079 (s), 930 (m), 856 (m), 688 (m), 586 (m) cm^{-1}. MS (Figure 4.34): $[Ni(OBOH_2)]Cl_3^+$ at *m/z* = 763 (30%), $Ni(OBOH_2)Cl^+$ at *m/z* = 364 (100%). Anal. Calcd for $Ni(C_{14}H_{29}N_3O_2)Cl_2$ (401.00): C, 41.93; H, 7.29; N, 10.48; Found: C, 42.06; H, 7.17; N, 10.38.

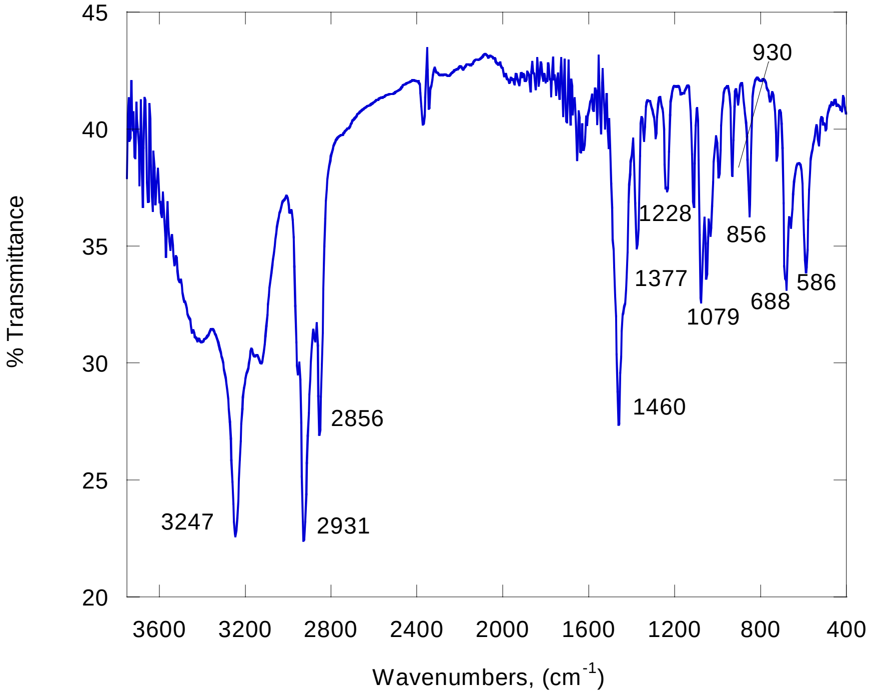

Figure 4.33. FTIR spectrum of $[Ni(OBOH_2)Cl]_2(\mu\text{-}Cl)_2$ (KBr pellet).

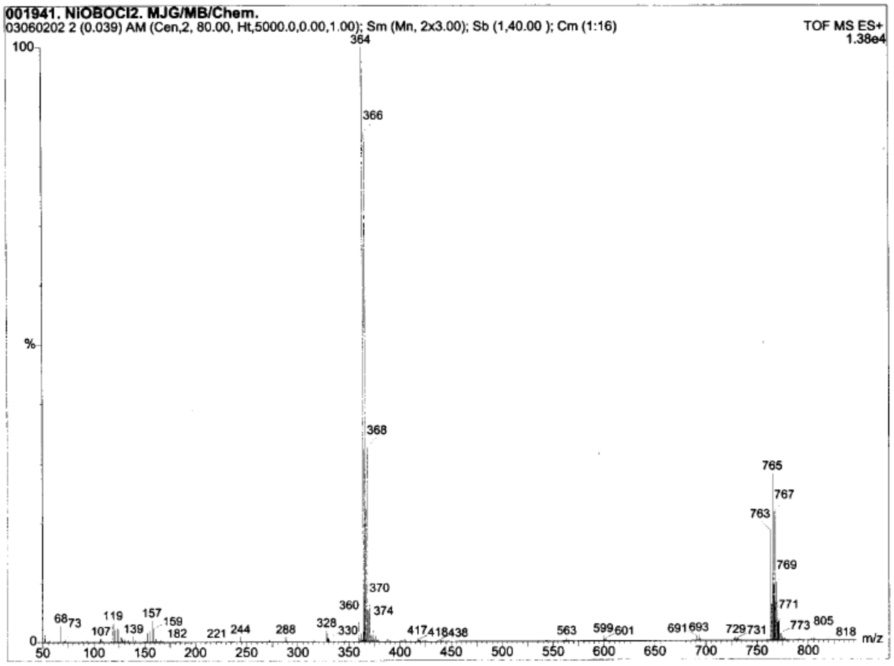

Figure 4.34. Mass spectrum of $[Ni(OBOH_2)Cl]_2(\mu\text{-}Cl)_2[Ni(OBOH_2)]Cl_3^+$ at m/z = 763 (30%), $Ni(OBOH_2)Cl^+$ at m/z = 364 (100%).

Intensity data for $[Ni(OBOH_2)Cl]_2(\mu\text{-}Cl)_2$ were collected at 295 K using a standard Siemens SMART 6000 CCD diffractometer with graphite-monochromated Mo Kα radiation, $\lambda = 0.71073$ Å. The detector was set at a distance of 6.120 cm from the crystal. A series of 20-second data frames measured at 0.3° increments of ω were collected to calculate a unit cell. For data collection, frames were measured for a duration of 20 seconds at 0.3° increments of ω, with a maximum θ value of 28.28°. The octyl group shows disorder. The anisotropic displacement parameter for C14 was held equivalent for C13. The X-ray crystal structure can be viewed in Figure 4.35. A full set of crystallographic data can be viewed in Appendix A.

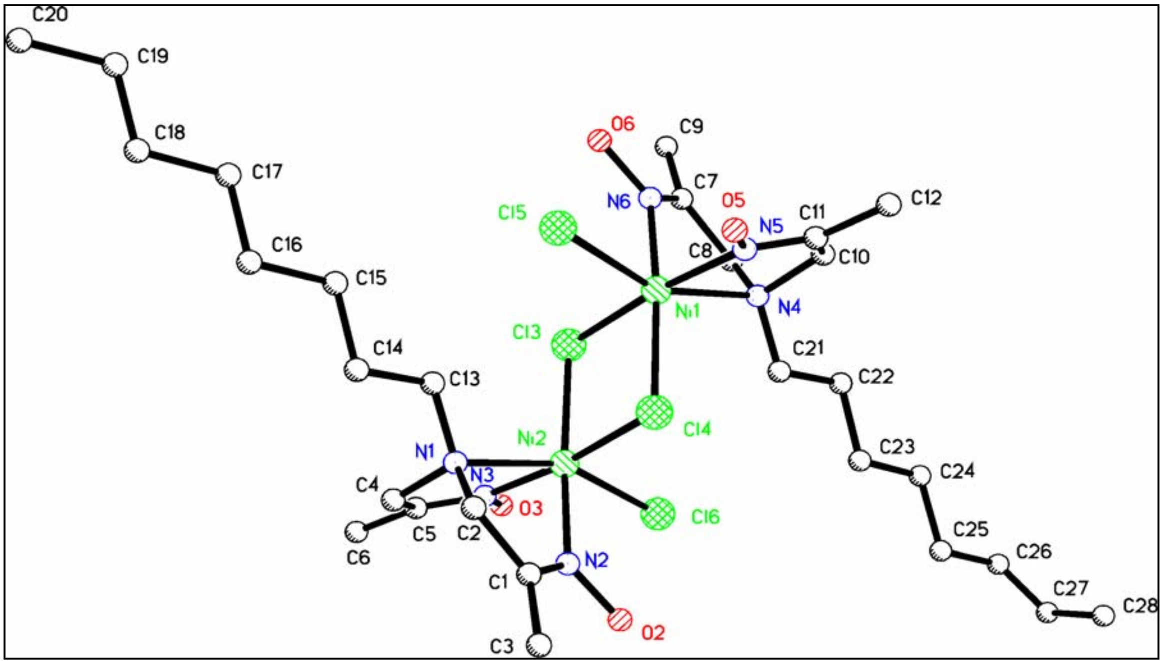

Figure 4.35. X-ray crystal structure of $[Ni(OBOH_2)Cl]_2(\mu\text{-}Cl)_2$.

4.6. Synthesis of $[Ni(TRISOXH_3)(pyridine\text{-}N\text{-}oxide)H_2O]$.

One possible substrate for oxygen activation that was screened during the course of this project was pyridine. Performing the O_2 reaction with **3** using pyridine as the solvent did produce the expected color change from purple to brown; however, products consistent with pyridine oxidation were never observed. It was speculated that perhaps oxygen atom transfer was occurring (similar to that observed with triphenylphosphine), forming pyridine-*N*-oxide, which could then bind to the nickel complex.

Experimental. A solution was concocted containing **1** and pyridine-*N*-oxide in acetonitrile. Vapor diffusion of diethyl ether into an acetonitrile solution resulted in purple blocks suitable for X-ray crystallography.

Intensity data for [Ni(TRISOXH$_3$)(pyridine-*N*-oxide)H$_2$O] were collected at 295 K using a standard Siemens SMART 1K CCD diffractometer with graphite-monochromated Mo Kα radiation, λ = 0.71073 Å. The detector was set at a distance of 5.083 cm from the crystal. A series of 5-second data frames measured at 0.3° increments of ω were collected to calculate a unit cell. For data collection, frames were measured for a duration of 5 seconds at 0.3° increments of ω, with a maximum θ value of 29.40°. The data frames were processed using the program SAINT. The X-ray crystal structure can be viewed in Figure 4.36. A full set of crystallographic data can be viewed in Appendix A.

Although this structure was never confirmed as a product in the reaction involving pyridine, O$_2$, and **3**, it seems like a reasonable possibility.

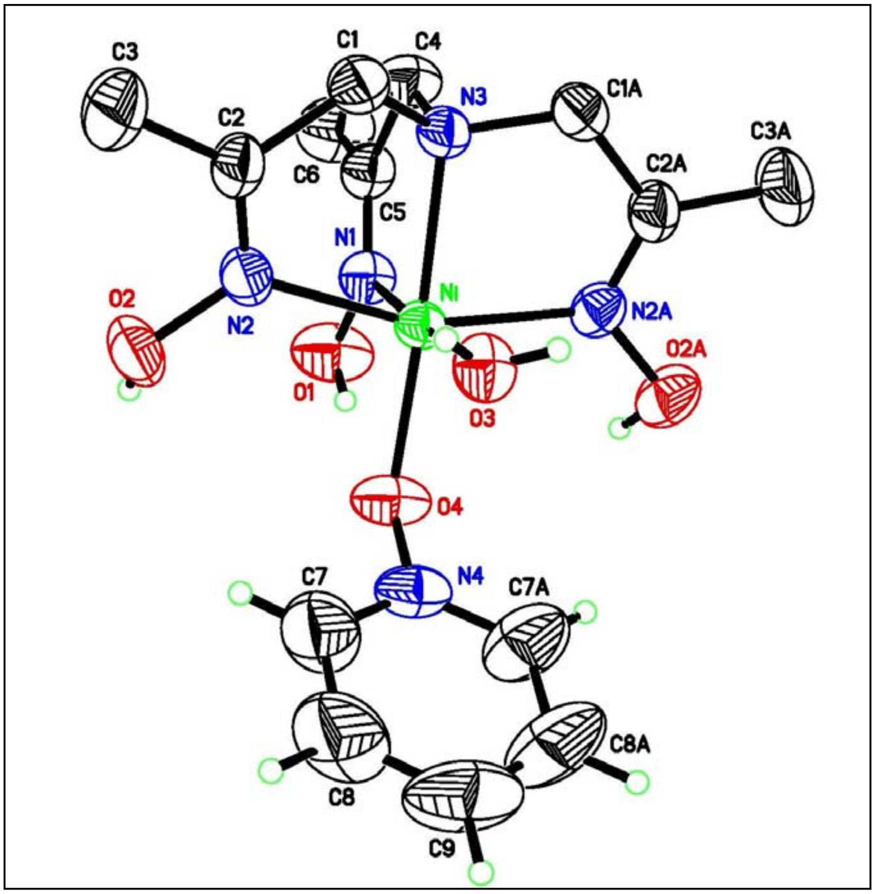

Figure 4.36. X-ray crystal structure of [Ni(TRISOXH$_3$)(pyridine-*N*-oxide)H$_2$O].

4.7. Conclusions.

A library of nickel(II) polyoximate complexes were developed by the Baldwin group. Their electronic structures were probed during the course of this project, as well as their electrochemical properties and their ability to oxidize methanol. The original ligand and complex syntheses of one of the members of the library was also described, as well as an “accidental” complex that may be an oxidation product in the reaction of **3** with pyridine and O$_2$.

References

1. Goldcamp, M. J.; Edison, S. E.; Squires, L. N.; Rosa, D. T.; Vowels, N. K.; Coker, N. L.; Krause Bauer, J. A.; Baldwin, M. J. *Inorg. Chem*, **2003**, *42*, 717-728.
2. Huheey, J. E.; Keiter, E. A.; Keiter, R. L. Inorganic Chemistry: Principles of Structure and Reactivity, 4th Edition, **1993**, HarperCollins College Publishers, p. 398.
3. Lever, A. B. P. Inorganic Electronic Spectroscopy; Elsevier: Amsterdam, 1984.
4. Goldcamp, M. J.; Rosa, D. T.; Landers, N. A.; Mandel, S. M.; Krause Bauer, J. A.; Baldwin, M. J. *Synthesis,* **2000**, *14*, 2033-2038.

Chapter 5. Summary and Future Work

The preceding chapters described the investigation of the reaction between some nickel(II)-polyoximate complexes and molecular oxygen. This chapter will summarize the highlights of those experiments and discuss future directions for this project.

The oxygen inert complex, $[Ni(TRISOXH_3)(NO_3)(H_2O)](NO_3)\bullet(H_2O)$, was deprotonated to form the oxygen active species, **3**. This complex will react with O_2, as characterized by a color change from purple to brown, if a two-hydrogen-atom donating substrate is present. Methanol was the substrate that was studied the most thoroughly. It was determined that after twenty-four hours about 10.4 equivalents of oxidized product (formaldehyde) were formed per **3** (Chapter 2.2).

Several variables were studied for this reaction. It was determined that the oxidation is linearly dependent on the concentration of **3** and that the amount of oxygen present also influences the reaction. More experiments involving the effect of $[O_2]$ should be undertaken, because those described in Chapter 2.2 were inconclusive.

It was also found that the amount of oxidized product formed was linearly dependent on the amount of methanol present when acetonitrile was used as the diluter. Adding water to the methanolic solution results in inhibition of the oxidation reaction. 50% aqueous solutions produce less than one equivalent of formaldehyde per **3** after twenty-four hours. This is consistent with water competing with methanol for binding positions on the catalyst.

Removing the metal, or replacing the nickel with zinc or copper, also decreases the amount of formaldehyde formed. Experiments involving the free ligand or the complex containing zinc did not produce formaldehyde, and the experiment using copper in place of nickel produced a substoichiometric amount of oxidized product. This indicates that a redox active metal is required for this reaction to take place (Chapter 2.2). It would be useful to test the performance of other transition metal complexes of TRISOX to see how nickel compares to other metals that are oxygen active.

Changing the counter anion affects the reaction, which was unexpected because it was hypothesized that the oxygen active species, **3**, is a dimer with no counter anions bound to the metal. However, it was discovered that the complex with the starting material that contained nitrate as the anion produced more oxidized product than the complexes with starting material containing chloride, perchlorate, or tetrafluoroborate. Those complexes all produced approximately the same amount of formaldehyde (Chapter 2.2).

Another useful control experiment that future researchers may wish to consider is the addition of formaldehyde to the solution at the beginning of the reaction to see if the product inhibits the oxidation reaction.

Other primary substrates, such as ethanol (Chapter 2.3), benzyl alcohol (Chapter 2.4), and benzylamine (Chapter 2.5), also promote the reaction with O_2. Ethanol produced acetaldehyde in approximately the same yield as the methanol oxidation reaction, whereas benzyl alcohol produced a relatively small amount of oxidized product (benzaldehyde). This suggests that steric hindrance due to the large phenyl ring prevents the reaction from being as efficient as the other alcohols investigated. Benzylamine produces a Schiff-base adduct, *N*-benzylidene benzylamine, in about the same amount as the reaction involving benzyl alcohol. However, this reaction was conducted under different conditions than the experiments involving methanol, as this experiment only contained 4% substrate whereas the methanol experiments were conducted in the presence of 25, 50, or 100% substrate.

A secondary amine, *N*-methylbenzylamine, was also found to promote the oxidation reaction and form the same Schiff-base adduct, *N*-benzylidene benzylamine; however, this reaction was not catalytic (Chapter 2.6). These substrates are all oxidized by two-hydrogen-atom abstraction. The reaction of **3** with O_2 using methanol as the solvent consumes roughly half as much O_2 as formaldehyde is produced (Chapter 2.7). This observation led to the hypothesis that hydrogen peroxide is another reaction product that is not observed because **3** is very efficient at catalase-like activity (Chapter 2.8). That is, it can disproportionate one equivalent of hydrogen peroxide to form half an equivalent of O_2 and one equivalent of water, which would explain the 2:1 ratio of formaldehyde production to O_2 consumption. Thermodynamically this seems to be a reasonable hypothesis because the amount of energy required to remove both hydrogen atoms from each substrate is less than the amount of energy gained by forming hydrogen peroxide (Chapter 2.9). However, several potential substrates that would form stable products and whose thermodynamic values indicate that the reaction should proceed, do not promote the oxidation reaction. These potential substrates are all branched at the α-carbon position, which indicates that steric hindrance may play a role in this reaction. A future direction could involve screening other potential substrates to learn more about what types of compounds work. One example could be to look at substituted benzyl alcohol derivatives that have electron donating and withdrawing groups on the ring.

Triphenylphosphine also acts as a substrate, becoming oxidized via oxygen atom transfer to form triphenylphosphine oxide (Chapter 2.10). This differs from the previously mentioned substrates that were oxidized by hydrogen atom abstraction. The rate of this reaction is also different from the hydrogen atom abstraction reaction. Oxygen atom transfer begins around the time that hydrogen atom abstraction ends. This indicates that the catalyst is changing over time to perform different types of chemistry before it eventually reaches its “dead-end” product. One explanation could be that the catalase-like activity slows down at later reaction times, allowing the oxidation of triphenylphosphine to out compete the disproportionation reaction. It would be interesting to add another complex that can disproportionate hydrogen peroxide to the reaction mixture to see how it affects the oxidation of triphenylphosphine. Calcium hydroxide has been reported to disproportionate H_2O_2 to generate singlet molecular oxygen through diperoxohydrate peroxide.[1] Manganese(III) complexes that mimic Mn catalase enzymes also disproportionate hydrogen peroxide, going through a Mn(IV)-hydroxo intermediate.[2,3] Mn(III)(salpn) complexes were investigated during this work as a means of detecting hydrogen peroxide; however, the results were inconclusive since the nickel catalyst can disproportionate hydrogen peroxide. The Mn(III) complex was never tested during the triphenylphosphine oxidation experiments. If addition of $Ca(OH)_2$ or a Mn(III) complex inhibited triphenylphosphine oxidation it would clarify the role of the nickel catalyst in this oxidation reaction.

A variety of spectroscopic techniques were employed during this project. The UV/vis spectrum of **3** as it reacts with O_2 in methanol displays an intermediate band (Chapter 3.2). A similar spectroscopic response was seen upon addition of some of the other substrates, most notably 1,4-cyclohexadiene. Addition of some substrates (ethanol, benzylamine) produced spectra that were qualitatively similar to that observed in methanol, but with different reaction rates. Addition of benzyl alcohol and *N*-methylbenzylamine did not produce similar spectra, although the intermediate may have appeared too quickly to be observed. It should be noted that the reaction conditions were not identical for all of these experiments (some substrates were used as solvents, some were added to acetonitrile solutions), so direct comparisons cannot be easily made.

Changing the counter anion affects the UV/vis spectrum during the reaction. The complex containing chloride in the starting material does not display the intermediate while the non-coordinating anions (perchlorate and tetrafluoroborate) display sharp, fairly intense intermediate bands. It may be useful in the future to investigate other counter anions to see if spectroscopic trends are observed. Titrating in different anions to see if displacement occurs would also be interesting.

Bulk electrolysis of **3** in DMF, acetonitrile, and methanol produced UV/vis spectra that were similar to the spectra of the air exposed sample in methanol (Chapter 3.3). These results suggest that the air exposed sample undergoes an oxidation reaction similar to the electrochemical oxidation. There was some concern that the spectroscopic observables were due to some impurity, so the electrochemical oxidation experiments were repeated using an optically transparent thin layer electrochemical cell (OTTLE) to ensure that the entire sample was being oxidized while the UV/vis absorption spectrum was collected. This experiment was conducted aerobically in acetonitrile and anaerobically in methanol. Both experiments produce similar spectra, confirming that the spectrum is due to the sample and not an impurity. It also supports the hypothesis that the air exposed species and electrochemically oxidized species are similar.

X-ray absorbance near edge spectroscopy (XANES) was also performed on samples of **3** that were exposed to air in methanol (Chapter 3.4). If the nickel were undergoing any kind of oxidation or reduction, the XANES experiment should reveal a shift in the edge energy. However, at various time from 0 seconds to 90 minutes there was no observable shift, indicating that the nickel remains in the +2 oxidation state for the duration of this experiment. This apparently contradicts the results from the UV/vis experiments on the electrochemically oxidized samples. This led to the hypothesis that reversible oxidation was occurring on the ligand rather than the metal. Future group members may want to repeat the XANES experiment at later time points (> 24 hours) to see if Ni(III) builds up as the catalytic activity dies. Also, stopped-flow XANES experiments with simultaneous UV/vis monitoring would be useful to ensure that the samples undergoing X-ray absorption analysis bear the spectroscopic signature observed during the other air exposed and electrochemically oxidized experiments.

Resonance Raman spectroscopy was conducted on a deprotonated solid sample of **3** and bands were observed in the regions where ligand vibrations would be expected (Chapter 3.5). However, a myriad of complications arose when the experiment was repeated on the air exposed sample, and no useful spectra were collected.

After abandoning resonance Raman as a useful technique to investigate ligand oxidation, electron paramagnetic resonance (EPR) spectroscopy was conducted on air exposed samples of **3** in methanol (Chapter 3.6). It was found on the same timescale that the intermediate maximizes in the UV/vis experiment a radical signal with a g value of 1.99 appears in the EPR spectrum. This signal subsequently disappears and at later time points a classic nickel(III) signal grows in. Spin quantitation using Cu(II) standards determined that this signal accounts for a very small amount of the nickel present in solution. Isotopic labeling using ^{15}N in either the amine or oximate nitrogen position proved that the oxidation occurs on the oximates, since the radical signal changed shape in the sample containing the labeled oximate whereas the signal for the labeled amine sample strongly resembled the spectrum of the natural abundance sample. This suggests that iminoxyl radicals are formed during the oxidation reaction. This hypothesis is further supported by the large nitrogen hyperfine splitting (33 G), which is characteristic of an iminoxyl radical.[4] The EPR spectrum of a bulk electrolyzed acetonitrile solution of **3** looked very similar to the spectra of the initial air exposed samples in methanol. This further suggests that the air exposed and electrochemically oxidized species are similar.

It may be useful to investigate the effects of addition of hydrogen peroxide to **3** in methanol at later times during the reaction with O_2 to see how it influences the Ni(III) EPR signal. It may be possible that a slowing of the catalase-like activity could allow oxidation of the nickel by hydrogen peroxide to occur.

Various members of the Baldwin group synthesized a series of ligands based on the same tripodal amine framework seen in TRISOX. These ligands differ from TRISOX in that they have two oxime arms and a variable third arm that can be altered to tune the physical and electronic properties to hopefully optimize the reactivity. The library contains ligands with non-coordinating third arms (alkyl and aryl groups), weakly coordinating third arms (amides), and strongly coordinating third arms (carboxylate, alcohol, pyridyl, and oximate groups). The value of 10 Dq was determined for the nickel(II) complexes of the various ligands, and it was found that a reasonable spectrochemical series could be constructed for the neutral complexes, where strongly donating ligands had larger values of 10 *Dq* and weakly and non-coordinating ligands had smaller values (Chapter 4.2). However, anaerobic deprotonation of the complexes resulted in a shift in the spectrochemical series, suggesting that structural changes may occur upon deprotonation. Future researchers might consider testing this hypothesis by growing anaerobic crystals of the deprotonated complexes.

Cyclic voltammagrams were collected on the various nickel complexes (Chapter 4.3) and no trends were observed based on variation of the third arm. All of the complexes displayed fairly low potential oxidation features upon deprotonation of the oximes.

The oxygen activity of the members of the library was investigated (Chapter 4.4). Formaldehyde production was monitored and compared to the results obtained for the identical reaction using TRISOX. It was speculated that complexes containing strongly coordinating third arms should perform as well or better than TRISOX and that complexes containing weakly or non-coordinating third arms would not produce as much oxidized product. However, TRISOX produced the most oxidized product after twenty-four hours, followed by MABOH and PAMBOH (ligands contain weakly coordinating third arms), and then OBO (ligand contains a non-coordinating third arm). The complexes containing ligands with strongly coordinating third arms did not oxidize methanol very efficiently. The complex containing the PYRABO ligand, which has a pyridyl group linked to the amine nitrogen via a methylene group, did not produce any formaldehyde. It also did not turn brown upon addition of base. This may indicate that a dimer with oximate bridges is necessary, because the bulky pyridyl ring may prevent a dimer from forming. BALBO, which has strongly coordinating carboxylate groups that form bridges in the neutral complex, also does not form much formaldehyde. This suggests that oximate bridges are required for the oxygen reaction to proceed, and that carboxylate bridges are not acceptable substitutes. Future work may include testing the other complexes in the library for formaldehyde production and also screening other substrates to see if oxidation occurs. Also, the experiments presented here studied the oxidation reactions over the life-time of the catalyst to determine the overall yield. It would be useful to do another study focusing on the early reaction times (0 – 10 minutes) to correlate the oxidation reaction to the spectroscopic observables and to learn more about the rate of the reaction.

These reactions displayed irreproducibility in yield from experiment to experiment. One possibility that could explain this variability is that the intermediate observed in the UV/vis experiment is not the catalyst. The catalyst may be a minor species with a high turnover whose concentration varies slightly in each experiment. This is always a possibility in catalytic systems and it is very difficult to test.

It would be useful to investigate the kinetics of the reaction. Stopped-flow UV/vis spectroscopy and XANES would provide a means of probing this.

Finally, it would be useful to prove that the oxygen active species, **3**, is really a dimer. Vapor pressure osmometry experiments would clarify this, as would a careful analysis to see if the complex obeys Beer’s law, since a dimer/monomer equilibrium should result in non-Beer’s law behavior. The molar absorptivity of the intermediate band was not reproducible, suggesting that Beer’s law is not obeyed and that the complex is a dimer. However, a more thorough study should be conducted.

In summary, this dissertation discusses the first homogeneous Ni(II) catalyst that reacts with molecular oxygen to do substrate oxidations without undergoing irreversible ligand oxidation, provided a two-hydrogen-atom donating substrate is present. It was determined that the oxidation equivalents are stored on the oximates. A proposed reaction scheme is presented in Chapter 3.7. This is significant because nickel is cheaper than many other transition metals that are used as catalysts in oxidation reactions, and O_2 is a clean and cheap oxidant. This project has revealed many details involving the reaction between this catalyst with O_2.

References

1. Nardello, V.; Briviba, K.; Sies, H.; Aubry, J.-M. *Chem. Commun.*, **1998**, 599-600.
2. Minori, U.; Yuriko, A. *J. Inorg. Biochem.*, **1997**, *67*, 203.
3. Zhang, J.-J.; Luo, Q.-H.; Duan, C.-H.; Wang, Z.-L.; Mei, Y.-H. *J. Inorg. Biochem.*, **2001**, *86*, 573-579.
4. Everett, S. A.; Naylor, M. A.; Stratford, M. R. L.; Patel, K. B.; Ford, E.; Mortensen, A.; Ferguson, A. C.; Vojnovic, B.; Wardman, P. *J. Chem. Soc., Perkin Trans. 2,* **2001**, 1989-1997.

Appendix A. X-ray Crystallographic Data.

Appendix A: Crystallographic Information

Section 1. $[(Ni(TRISOX))_2(NO_3)]^-$ or $(C_{18}H_{34}N_9O_9Ni_2.CH_3CN.5H_2O)$

Description

Molecule crystallizes as a dimer with 2 bridging oximes and 1 NO_3 group.
The lattice contains 1 molecule of acetonitrile and 5 waters.

Experimental:

Single crystals were obtained as purple plates from CH_3CN. For x-ray examination and data collection, a suitable crystal measuring approximate 0.31 x 0.20 x 0.08 mm, was mounted in a Cryo-loop with paratone-N and transferred immediately to the goniostat bathed in a cold stream.

Intensity data were collected at 150K on a SMART6000 CCD diffractometer using graphite-monochromated Mo Kα radiation, λ=0.71073Å. The detector was set at a distance of 5.15 cm from the crystal. A series of 30-s data frames measured at 0.3^o increments of ω were collected to calculate a unit cell. For data collection frames were measured for a duration of 25-s at 0.3^o intervals of ω, which combined measured nearly a sphere of intensity out to ~28^o in θ. The data frames were processed using the program SAINT. The data were corrected for decay, Lorentz and polarization effects as well as absorption and beam corrections based on the multi-scan technique used in SADABS.

The structure was solved by a combination of the Patterson method in SHELXTL v6.12 and the difference Fourier technique and refined by full-matrix least squares on F^2. Non-hydrogen atoms were refined with anisotropic displacement parameters. Weights were assigned as $w^{-1}=[\sigma^2(F_o^2)+ (0.0415P)^2+1.1083P]$ where $P=0.33333F_o^2+0.66667F_c^2$. The oxime hydrogen atoms were located directly and the positions refined. The water hydrogens were located directly and the positions held fixed where located. The remaining hydrogen atoms were either located directly or calculated based on geometric criteria. A riding model was applied in subsequent refinements for all hydrogen atoms with the exception of the oximes. One of the water molecules, O34, is disordered, occupancies set at 0.65 and 0.35 for the two components. The isotropic temperature factors of the H-atoms were defined as $a*U_{eq}$ of the adjacent atom where a=1.5 for –OH and CH_3 and 1.2 for all others. The refinement converged with crystallographic agreement factors of R1=3.17%, wR2=8.43% for 7042 reflections with $I>2\sigma(I)$ (R1=3.75%, wR2=8.82% for all data) and 436 variable parameters.

Table 1. Crystal data and structure refinement for $C_{18}H_{34}N_9O_9Ni_2.CH_3CN.5H_2O$

Empirical formula	$C_{18}H_{34}N_9O_9Ni_2.CH_3CN.5H_2O$	
Formula weight	769.10	
Temperature	150(2) K	
Wavelength	0.71073 Å	
Crystal system	Triclinic	
Space group	P-1	
Unit cell dimensions:	a = 9.6150(10) Å	α = 98.597(2)°
	b = 10.5920(11) Å	β = 100.828(2)°
	c = 17.0107(18) Å	γ = 103.751(2)°
Volume, Z	1618.2(3) $Å^3$, 2	
Density (calculated)	1.578 Mg/m^3	
Absorption coefficient	1.242 mm^{-1}	
F(000)	810	
Crystal size	0.31 x 0.20 x 0.08 mm	
θ range for data collection	2.02 to 28.32°	
Limiting indices	$-12 < h < 12$, $-14 < k < 14$, $-22 < l < 22$	
Reflections collected	22135	
Independent reflections	8017 (R_{int} = 0.0304)	
Completeness to θ = 28.32°	99.7 %	
Absorption correction	Multi-scan	
Max. and min. transmission	0.9072 and 0.6994	
Refinement method	Full-matrix least-squares on F^2	
Data / restraints / parameters	8017 / 0 / 436	
Goodness-of-fit on F^2	1.049	
Final R indices [$I>2\sigma(I)$]	R1 = 0.0317, wR2 = 0.0843	
R indices (all data)	R1 = 0.0375, wR2 = 0.0882	
Largest diff. peak and hole	0.552 and -0.791 $eÅ^{-3}$	

Table 2. Atomic coordinates [x10^4] and equivalent isotropic displacement parameters [$Å^2$x10^3] for $C_{18}H_{34}N_9O_9Ni_2.CH_3CN.5H_2O$. U(eq) is defined as one third of the trace of the orthogonalized U_{ij} tensor.

	x	y	z	U(eq)
Ni(1)	5450(1)	4525(1)	2775(1)	16(1)
Ni(2)	3489(1)	6563(1)	2574(1)	15(1)
O(1)	8387(2)	5378(1)	4181(1)	25(1)
O(2)	2951(1)	4914(1)	1604(1)	21(1)
O(3)	7326(2)	4966(2)	1489(1)	28(1)
O(5)	5224(2)	9148(1)	3836(1)	24(1)
O(6)	4197(2)	8551(1)	1432(1)	25(1)
O(7)	4111(1)	4689(1)	3658(1)	19(1)
O(8)	5630(1)	6476(1)	2747(1)	18(1)
O(9)	7810(2)	7158(2)	2442(1)	31(1)
O(10)	6465(1)	8568(1)	2627(1)	24(1)
N(1)	7086(2)	4429(2)	3732(1)	20(1)
N(2)	3532(2)	3994(2)	1927(1)	18(1)
N(3)	6624(2)	4088(2)	1911(1)	21(1)
N(4)	5000(2)	2439(2)	2659(1)	22(1)
N(5)	3856(2)	8254(2)	3453(1)	18(1)
N(6)	3138(2)	7725(2)	1727(1)	19(1)
N(7)	3049(2)	5229(2)	3292(1)	18(1)
N(8)	1287(2)	6549(2)	2569(1)	18(1)
N(9)	6662(2)	7401(2)	2602(1)	29(1)
C(1)	5479(2)	2252(2)	3504(1)	25(1)
C(2)	6851(2)	3327(2)	3975(1)	23(1)
C(3)	7747(2)	3047(2)	4712(1)	32(1)
C(4)	3396(2)	1899(2)	2308(1)	28(1)
C(5)	2757(2)	2784(2)	1808(1)	23(1)
C(6)	1213(2)	2244(2)	1306(1)	31(1)
C(7)	5859(3)	1903(2)	2118(1)	30(1)
C(8)	6589(2)	2878(2)	1669(1)	24(1)
C(9)	7239(3)	2370(2)	995(1)	36(1)
C(10)	1262(2)	7627(2)	3235(1)	23(1)
C(11)	2746(2)	8569(2)	3647(1)	20(1)
C(12)	2788(2)	9778(2)	4236(1)	27(1)
C(13)	657(2)	6767(2)	1750(1)	21(1)
C(14)	1798(2)	7675(2)	1429(1)	19(1)
C(15)	1265(2)	8371(2)	785(1)	26(1)
C(16)	591(2)	5228(2)	2720(1)	22(1)
C(17)	1686(2)	4700(2)	3250(1)	19(1)
C(18)	1076(2)	3531(2)	3604(1)	26(1)
N(20)	7556(4)	9069(3)	525(2)	77(1)

C(21)	6800(4)	8026(3)	385(2)	59(1)
C(22)	5839(5)	6672(3)	209(2)	71(1)
O(30)	9246(2)	10481(2)	4099(1)	42(1)
O(31)	1452(2)	4833(2)	58(1)	46(1)
O(32)	4132(2)	3357(1)	5033(1)	28(1)
O(33)	1610(2)	2023(2)	5444(1)	32(1)
O(34A)	9444(7)	9831(6)	2368(4)	49(1)
O(34B)	8830(4)	10325(3)	2389(2)	46(1)

Table 3. Bond lengths [Å] and angles [°] for $C_{18}H_{34}N_9O_9Ni_2.CH_3CN.5H_2O$

Ni(1)-N(2)	2.0161(15)	Ni(1)-O(8)	2.0407(12)
Ni(1)-N(1)	2.0724(15)	Ni(1)-N(3)	2.0782(16)
Ni(1)-N(4)	2.1197(16)	Ni(1)-O(7)	2.1675(13)
Ni(2)-N(7)	2.0239(14)	Ni(2)-O(8)	2.0513(12)
Ni(2)-N(6)	2.0612(14)	Ni(2)-N(5)	2.0660(15)
Ni(2)-O(2)	2.1044(13)	Ni(2)-N(8)	2.1119(15)
O(1)-N(1)	1.404(2)	O(2)-N(2)	1.3666(18)
O(3)-N(3)	1.3851(19)	O(5)-N(5)	1.3973(19)
O(6)-N(6)	1.3969(19)	O(7)-N(7)	1.3792(18)
O(8)-N(9)	1.307(2)	O(9)-N(9)	1.260(2)
O(10)-N(9)	1.290(2)	N(1)-C(2)	1.281(2)
N(2)-C(5)	1.285(2)	N(3)-C(8)	1.276(3)
N(4)-C(4)	1.482(3)	N(4)-C(1)	1.482(2)
N(4)-C(7)	1.484(3)	N(5)-C(11)	1.276(2)
N(6)-C(14)	1.278(2)	N(7)-C(17)	1.281(2)
N(8)-C(16)	1.483(2)	N(8)-C(13)	1.485(2)
N(8)-C(10)	1.490(2)	C(1)-C(2)	1.515(3)
C(2)-C(3)	1.492(3)	C(4)-C(5)	1.516(3)
C(5)-C(6)	1.495(3)	C(7)-C(8)	1.497(3)
C(8)-C(9)	1.495(3)	C(10)-C(11)	1.504(3)
C(11)-C(12)	1.491(3)	C(13)-C(14)	1.519(2)
C(14)-C(15)	1.490(2)	C(16)-C(17)	1.520(2)
C(17)-C(18)	1.499(2)	N(20)-C(21)	1.131(4)
C(21)-C(22)	1.462(5)		

N(2)-Ni(1)-O(8)	90.15(5)	N(2)-Ni(1)-N(1)	159.79(6)
O(8)-Ni(1)-N(1)	108.27(6)	N(2)-Ni(1)-N(3)	92.44(6)
O(8)-Ni(1)-N(3)	99.71(6)	N(1)-Ni(1)-N(3)	92.53(6)
N(2)-Ni(1)-N(4)	81.66(6)	O(8)-Ni(1)-N(4)	171.74(6)
N(1)-Ni(1)-N(4)	79.99(6)	N(3)-Ni(1)-N(4)	79.62(6)
N(2)-Ni(1)-O(7)	85.40(5)	O(8)-Ni(1)-O(7)	87.87(5)
N(1)-Ni(1)-O(7)	87.02(5)	N(3)-Ni(1)-O(7)	172.13(6)
N(4)-Ni(1)-O(7)	92.57(5)	N(7)-Ni(2)-O(8)	90.93(5)
N(7)-Ni(2)-N(6)	159.75(6)	O(8)-Ni(2)-N(6)	108.47(5)

N(7)-Ni(2)-N(5)	97.23(6)	O(8)-Ni(2)-N(5)	97.07(5)
N(6)-Ni(2)-N(5)	86.36(6)	N(7)-Ni(2)-O(2)	86.24(6)
O(8)-Ni(2)-O(2)	87.68(5)	N(6)-Ni(2)-O(2)	88.73(6)
N(5)-Ni(2)-O(2)	174.05(5)	N(7)-Ni(2)-N(8)	80.85(6)
O(8)-Ni(2)-N(8)	171.03(5)	N(6)-Ni(2)-N(8)	80.10(6)
N(5)-Ni(2)-N(8)	80.55(6)	O(2)-Ni(2)-N(8)	95.30(5)
N(2)-O(2)-Ni(2)	105.07(9)	N(7)-O(7)-Ni(1)	103.98(9)
N(9)-O(8)-Ni(1)	131.94(11)	N(9)-O(8)-Ni(2)	121.86(11)
Ni(1)-O(8)-Ni(2)	102.96(5)	C(2)-N(1)-O(1)	114.02(15)
C(2)-N(1)-Ni(1)	114.60(13)	O(1)-N(1)-Ni(1)	131.34(11)
C(5)-N(2)-O(2)	120.54(15)	C(5)-N(2)-Ni(1)	116.64(12)
O(2)-N(2)-Ni(1)	121.77(11)	C(8)-N(3)-O(3)	114.67(16)
C(8)-N(3)-Ni(1)	118.60(13)	O(3)-N(3)-Ni(1)	126.31(12)
C(4)-N(4)-C(1)	113.97(15)	C(4)-N(4)-C(7)	111.28(16)
C(1)-N(4)-C(7)	110.71(15)	C(4)-N(4)-Ni(1)	105.89(11)
C(1)-N(4)-Ni(1)	104.36(11)	C(7)-N(4)-Ni(1)	110.25(12)
C(11)-N(5)-O(5)	115.47(15)	C(11)-N(5)-Ni(2)	118.44(13)
O(5)-N(5)-Ni(2)	126.00(11)	C(14)-N(6)-O(6)	116.13(14)
C(14)-N(6)-Ni(2)	116.37(12)	O(6)-N(6)-Ni(2)	127.49(11)
C(17)-N(7)-O(7)	120.27(14)	C(17)-N(7)-Ni(2)	116.21(12)
O(7)-N(7)-Ni(2)	121.89(11)	C(16)-N(8)-C(13)	113.69(14)
C(16)-N(8)-C(10)	110.69(14)	C(13)-N(8)-C(10)	111.56(14)
C(16)-N(8)-Ni(2)	105.34(10)	C(13)-N(8)-Ni(2)	105.64(10)
C(10)-N(8)-Ni(2)	109.54(11)	O(9)-N(9)-O(10)	121.22(16)
O(9)-N((9)-O(8)	120.90(17)	O(10)-N(9)-O(8)	117.88(16)
N(4)-C(1)-C(2)	111.55(15)	N(1)-C(2)-C(3)	125.77(19)
N(1)-C(2)-C(1)	116.57(16)	C(3)-C(2)-C(1)	117.52(17)
N(4)-C(4)-C(5)	112.96(15)	N(2)-C(5)-C(6)	125.05(17)
N(2)-C(5)-C(4)	116.49(16)	C(6)-C(5)-C(4)	117.93(16)
N(4)-C(7)-C(8)	114.10(16)	N(3)-C(8)-C(9)	125.79(19)
N(3)-C(8)-C(7)	116.19(17)	C(9)-C(8)-C(7)	118.01(17)
N(8)-C(10)-C(11)	114.50(15)	N(5)-C(11)-C(12)	126.18(17)
N(5)-C(11)-C(10)	116.27(16)	C(12)-C(11)-C(10)	117.55(16)
N(8)-C(13)-C(14)	111.87(14)	N(6)-C(14)-C(15)	126.31(17)
N(6)-C(14)-C(13)	115.64(15)	C(15)-C(14)-C(13)	118.00(16)
N(8)-C(16)-C(17)	112.00(14)	N(7)-C(17)-C(18)	126.14(16)
N(7)-C(17)-C(16)	116.15(15)	C(18)-C(17)-C(16)	117.40(15)
N(20)-C(21)-C(22)	179.2(4)		

Table 4. Anisotropic displacement parameters [$Å^2 x 10^3$] for $C_{18}H_{34}N_9O_9Ni_2.CH_3CN.5H_2O$. The anisotropic displacement factor exponent takes the form: $-2\pi^2[(ha^*)^2U_{11} + ... + 2hka^*b^*U_{12}]$

	U11	U22	U33	U23	U13	U12
Ni(1)	16(1)	15(1)	18(1)	5(1)	5(1)	4(1)
Ni(2)	13(1)	15(1)	17(1)	4(1)	4(1)	2(1)
O(1)	21(1)	24(1)	26(1)	3(1)	1(1)	5(1)
O(2)	22(1)	19(1)	19(1)	4(1)	0(1)	6(1)
O(3)	32(1)	24(1)	33(1)	10(1)	19(1)	7(1)
O(5)	18(1)	20(1)	28(1)	-2(1)	2(1)	0(1)
O(6)	19(1)	27(1)	31(1)	15(1)	7(1)	1(1)
O(7)	17(1)	21(1)	20(1)	8(1)	4(1)	6(1)
O(8)	14(1)	16(1)	25(1)	5(1)	6(1)	3(1)
O(9)	18(1)	29(1)	46(1)	5(1)	15(1)	4(1)
O(10)	20(1)	18(1)	32(1)	8(1)	7(1)	2(1)
N(1)	17(1)	23(1)	22(1)	5(1)	5(1)	6(1)
N(2)	21(1)	18(1)	17(1)	4(1)	5(1)	6(1)
N(3)	20(1)	22(1)	22(1)	8(1)	7(1)	4(1)
N(4)	23(1)	19(1)	24(1)	6(1)	8(1)	6(1)
N(5)	16(1)	16(1)	19(1)	3(1)	2(1)	1(1)
N(6)	18(1)	18(1)	21(1)	7(1)	7(1)	3(1)
N(7)	17(1)	19(1)	16(1)	4(1)	3(1)	4(1)
N(8)	15(1)	20(1)	17(1)	5(1)	4(1)	3(1)
N(9)	24(1)	32(1)	30(1)	6(1)	5(1)	3(1)
C(1)	30(1)	21(1)	27(1)	12(1)	9(1)	8(1)
C(2)	25(1)	25(1)	23(1)	8(1)	8(1)	12(1)
C(3)	35(1)	35(1)	29(1)	14(1)	3(1)	16(1)
C(4)	26(1)	19(1)	35(1)	8(1)	2(1)	1(1)
C(5)	22(1)	21(1)	22(1)	4(1)	4(1)	3(1)
C(6)	27(1)	25(1)	33(1)	4(1)	-3(1)	-3(1)
C(7)	39(1)	20(1)	36(1)	5(1)	17(1)	10(1)
C(8)	25(1)	25(1)	24(1)	4(1)	7(1)	9(1)
C(9)	45(1)	34(1)	37(1)	5(1)	21(1)	17(1)
C(10)	18(1)	29(1)	23(1)	3(1)	6(1)	7(1)
C(11)	21(1)	20(1)	18(1)	6(1)	5(1)	6(1)
C(12)	30(1)	24(1)	27(1)	1(1)	11(1)	8(1)
C(13)	16(1)	27(1)	19(1)	7(1)	2(1)	3(1)
C(14)	21(1)	19(1)	16(1)	3(1)	4(1)	5(1)
C(15)	26(1)	29(1)	24(1)	10(1)	2(1)	8(1)
C(16)	15(1)	23(1)	25(1)	8(1)	4(1)	1(1)
C(17)	18(1)	20(1)	19(1)	5(1)	5(1)	2(1)
C(18)	23(1)	26(1)	30(1)	12(1)	8(1)	0(1)
N(20)	102(3)	51(2)	86(2)	12(2)	40(2)	24(2)

C(21)	97(3)	48(2)	45(2)	14(1)	26(2)	33(2)
C(22)	129(3)	40(2)	40(2)	8(1)	14(2)	18(2)
O(30)	48(1)	40(1)	37(1)	6(1)	7(1)	9(1)
O(31)	41(1)	71(1)	24(1)	7(1)	1(1)	18(1)
O(32)	30(1)	26(1)	24(1)	6(1)	4(1)	1(1)
O(33)	33(1)	26(1)	38(1)	6(1)	14(1)	5(1)
O(34A)	43(3)	39(3)	62(4)	15(3)	19(3)	-1(3)
O(34B)	40(2)	37(2)	49(2)	16(1)	8(1)	-15(1)

Table 5. Hydrogen coordinates ($x10^4$) and isotropic displacement parameters ($Å^2x10^3$) for $C_{18}H_{34}N_9O_9Ni_2.CH_3CN.5H_2O$.

	x	y	z	U(eq)
H(1)	8250(30)	6160(30)	4133(16)	37
H(3)	7450(30)	5720(30)	1802(18)	42
H(5)	5740(30)	9020(30)	3497(17)	36
H(6)	5010(30)	8640(30)	1801(17)	38
H(1A)	5679	1374	3484	30
H(1B)	4677	2264	3792	30
H(3A)	7158	2919	5120	48
H(3B)	8624	3796	4943	48
H(3C)	8046	2241	4556	48
H(4A)	2888	1782	2758	34
H(4B)	3207	1013	1957	34
H(6A)	1182	1560	841	47
H(6B)	871	2963	1104	47
H(6C)	573	1855	1643	47
H(7A)	5192	1121	1715	36
H(7B)	6623	1596	2453	36
H(9A)	7974	3105	893	54
H(9B)	6459	1980	497	54
H(9C)	7710	1692	1155	54
H(10A)	833	7217	3652	28
H(10B)	608	8140	3004	28
H(12A)	2093	9539	4579	40
H(12B)	2513	10435	3935	40
H(12C)	3784	10155	4583	40
H(13A)	-169	7163	1785	25
H(13B)	261	5901	1362	25
H(15A)	2098	8822	581	39
H(15B)	806	9027	1015	39
H(15C)	541	7724	333	39
H(16A)	163	4595	2190	26
H(16B)	-221	5295	2991	26

H(18A)	1845	3089	3756	40
H(18B)	245	2906	3196	40
H(18C)	741	3834	4090	40
H(22A)	4906	6686	358	107
H(22B)	6319	6130	527	107
H(22C)	5649	6293	-375	107
H(30A)	9345	10492	3594	64
H(30B)	9835	10848	4443	64
H(31A)	1984	4919	570	69
H(31B)	531	4976	77	69
H(32A)	4029	3814	4637	42
H(32B)	4726	3946	5484	42
H(33A)	2414	2204	5296	48
H(33B)	1539	1272	5627	48
H(34A)	8846	10085	1880	68
H(34B)	8214	9677	2378	68

Table 6. Hydrogen bonds for $C_{18}H_{34}N_9O_9Ni_2.CH_3CN.5H_2O$ [Å and º].

D-H...A	d(D-H)	d(H...A)	d(D...A)	<(DHA)	symm. op.
O1-H1..O33	0.88(3)	1.92(3)	2.730(2)	153(3)	-x+1, -y+1, -z+1
O(3)-H(3)..O9	0.86(3)	1.65(3)	2.512(2)	175(3)	x, y, z
O(5)-H(5)..O10	0.84(3)	1.80(3)	2.631(2)	168(3)	x, y, z
O(6)-H(6)..O10	0.88(3)	1.81(3)	2.681(2)	169(3)	x, y, z
O30-H30A..O34B	0.88	1.99	2.835(4)	161	x, y, z
O30-H30A..O34A	0.88	2.13	2.975(7)	161	x, y, z
O30-H30B..O33	0.72	2.15	2.869(2)	177	x+1, y+1, z
O31-H31A..O2	0.90	1.83	2.730(2)	174	x, y, z
O31-H31B..O31	0.94	1.94	2.871(4)	171	-x, -y+1, -z
O32-H32A..O7	0.89	2.03	2.906(2)	168	x, y, z
O32-H32B..O6	0.91	1.86	2.765(2)	173	-x+1, -y+1, -z+1
O33-H33A..O32	0.85	1.98	2.770(2)	156	x, y, z
O33-H33B..O30	0.89	1.99	2.853(2)	163	-x+1, -y+1, -z+1
O34B-H34A..N20	0.87	2.36	3.134(5)	149	x, y, z
O34B-H34B..O10	0.79	1.97	2.713(3)	158	x, y, z

Acknowledgements, References and Notes:

(1) Funding for the Smart6000 diffractometer was through NSF-MRI grant CHE-0215950.

(2) SMART v5.628 and SAINT v6.36A programs were used for data collection and data processing, respectively. Bruker Analytical X-ray Solutions, Inc., Madison, WI. SADABS v2.10 was used for the application of semi-empirical absorption and beam corrections. G. M. Sheldrick, University of Göttingen, Germany. SHELXTL v6.12 was used for the structure solution and generation of figures and tables. G. M. Sheldrick, University of Göttingen, Germany and Bruker Analytical X-ray Solutions, Inc., Madison, WI. Neutral-atom scattering factors were used as stored in this package.

Section 2. [Ni(OBOH$_2$)Cl]$_2$(μ-Cl)$_2$.or $C_{28}H_{58}N_6O_4Cl_4Ni_2$

Description:

The molecule crystallizes as a chloro-bridged dimer (no solvent of crystallization present). A terminal Cl and the OBO ligand complete the coordination about the Ni atom. Intramolecular O-H..Cl hydrogen bonding is observed to the terminal chloride atoms.

Experimental:

Single crystals were obtained as emerald green plates from acetone-Et$_2$O. For x-ray examination and data collection, a suitable crystal, approximate dimensions 0.36 x 0.26 x 0.15 mm, was mounted on the tip of a glass fiber with epoxy resin.

Intensity data were collected at room temperature on a standard Siemens SMART 6000 CCD diffractometer using graphite-monochromated Mo Kα radiation, λ=0.71073Å. The detector was set at a distance of 6.120 cm from the crystal. A series of 20-s data frames measured at 0.3^o increments of ω were collected to calculate a unit cell. For data collection frames were measured for a duration of 20-s at 0.3^o intervals of ω, which combined measured nearly a sphere of intensity data with a maximum θ value of 28.28^o. The data frames were processed using the program SAINT. The data were corrected for decay, Lorentz and polarization effects as well as absorption and beam corrections based on the multi-scan technique.

The structure was solved by a combination of direct methods SHELXTL v6.1 and the difference Fourier technique and refined by full-matrix least squares on F^2. Non-hydrogen atoms were refined with anisotropic displacement parameters. Weights were assigned as $w^{-1}=[\sigma^2(F_o^2)+ (0.0391P)^2 +6.8945P]$ where $P=0.33333F_o^2+0.66667F_c^2$. The -OH hydrogen atoms were located directly and held fixed at that location. The remaining hydrogens were calculated based on geometric criteria and treated with a riding model. The isotropic temperature factors for the hydrogen atoms were set as a*Ueq of the adjacent atom where a=1.5 for –CH$_3$ and –OH, 1.2 for all others. The octyl group shows disorder, the anisotropic displacement parameter for C14 was held equivalent to C13. The refinement converged with crystallographic agreement factors of R1=5.95%, wR2=12.05% for 4012 reflections with I>2σ(I) (R1=7.76%, wR2=12.78% for all data) and 193 variable parameters.

Table 1. Crystal data and structure refinement.

Empirical formula	$C_{28}H_{58}Cl_4N_6Ni_2O_4$	
Formula weight	802.02	
Temperature	295(2) K	
Wavelength	0.71073 Å	
Crystal system	Monoclinic	
Space group	C2/c	
Unit cell dimensions	a = 23.8527(1) Å	$\alpha = 90^o$
	b = 14.0684(6) Å	$\beta = 90.715(1)^o$
	c = 11.7874(5) Å	$\delta = 90^o$
Volume, Z	3955.2(3) $Å^3$, 4	
Density (calculated)	1.347 Mg/m^3	
Absorption coefficient	1.260 mm^{-1}	
F(000)	1696	
Crystal size	0.36 x 0.26 x 0.15 mm	
θ range for data collection	2.40 to 28.28°	
Limiting indices	$-31 < h < 31$, $-18 < k < 18$, $-15 < l < 15$	
Reflections collected	25260	
Independent reflections	4913 (R_{int} = 0.0375)	
Completeness to θ = 28.28°	99.9 %	
Absorption correction	Multi-scan	
Max. and min. transmission	0.8335 and 0.6598	
Refinement method	Full-matrix least-squares on F^2	
Data / restraints / parameters	4913 / 0 / 193	
Goodness-of-fit on F^2	1.169	
Final R indices [I>2σ(I)]	R1 = 0.0595, wR2 = 0.1205	
R indices (all data)	R1 = 0.0776, wR2 = 0.1278	
Largest diff. peak and hole	0.534 and -0.331 $eÅ^{-3}$	

Table 2. Atomic coordinates [x 10^4] and equivalent isotropic displacement parameters [$Å^2$ x 10^3]. U(eq) is defined as one third of the trace of the orthogonalized U_{ij} tensor.

	x	y	z	U(eq)
Ni(1)	2513(1)	2269(1)	8504(1)	43(1)
Cl(1)	3361(1)	1263(1)	8372(1)	71(1)
N(1)	2101(2)	1248(2)	7585(2)	56(1)
C(1)	1324(2)	2230(2)	7812(3)	60(1)
O(1)	2347(2)	386(2)	7284(2)	79(1)
Cl(2)	2098(1)	1597(1)	10201(1)	46(1)
N(2)	2804(1)	2963(2)	7111(2)	52(1)
O(2)	3369(1)	2983(2)	6817(2)	79(1)
C(2)	1586(2)	1302(2)	7439(3)	63(1)
N(3)	1750(1)	2990(2)	7880(2)	44(1)
C(3)	1220(3)	511(4)	6991(5)	111(2)
C(4)	1873(2)	3372(2)	6730(3)	54(1)
C(5)	2473(2)	3408(2)	6440(3)	52(1)
C(6)	2638(2)	3922(3)	5390(3)	75(1)
C(7)	1582(1)	3769(2)	8659(3)	47(1)
C(8)	1037(2)	4287(3)	8392(3)	56(1)
C(9)	964(2)	5121(3)	9203(3)	61(1)
C(10)	472(2)	5763(3)	8933(4)	68(1)
C(11)	438(2)	6603(3)	9709(4)	82(1)
C(12)	-19(2)	7310(4)	9388(6)	106(2)
C(13)	-38(3)	8173(5)	10039(9)	167(3)
C(14)	-459(3)	8873(5)	9631(8)	167(3)

Table 3. Bond lengths [Å] and angles [^{o}].

Ni(1)-N(2)	2.040(3)	Ni(1)-N(1)	2.044(3)
Ni(1)-N(3)	2.201(3)	Ni(1)-Cl(2)#1	2.3882(8)
Ni(1)-Cl(2)	2.4346(8)	Ni(1)-Cl(1)	2.4763(10)
N(1)-C(2)	1.241(5)	N(1)-O(1)	1.395(4)
C(1)-N(3)	1.476(4)	C(1)-C(2)	1.514(5)
N(2)-C(5)	1.276(4)	N(2)-O(2)	1.394(4)
C(2)-C(3)	1.505(6)	N(3)-C(7)	1.488(4)
N(3)-C(4)	1.491(4)	C(4)-C(5)	1.476(5)
C(5)-C(6)	1.490(5)	C(7)-C(8)	1.520(5)
C(8)-C(9)	1.525(5)	C(9)-C(10)	1.512(5)
C(10)-C(11)	1.498(6)	C(11)-C(12)	1.519(6)
C(12)-C(13)	1.437(9)	C(13)-C(14)	1.483(9)
N(2)-Ni(1)-N(1)	94.38(11)	N(2)-Ni(1)-N(3)	78.44(11)
N(1)-Ni(1)-N(3)	75.95(11)	N(2)-Ni(1)-Cl(2)#1	93.49(9)
N(1)-Ni(1)-Cl(2)#1	171.55(9)	N(3)-Ni(1)-Cl(2)#1	102.66(7)
N(2)-Ni(1)-Cl(2)	173.53(8)	N(1)-Ni(1)-Cl(2)	87.98(8)
N(3)-Ni(1)-Cl(2)	96.35(7)	Cl(2)#1-Ni(1)-Cl(2)	83.87(3)
N(2)-Ni(1)-Cl(1)	86.29(9)	N(1)-Ni(1)-Cl(1)	87.29(10)
N(3)-Ni(1)-Cl(1)	156.22(7)	Cl(2)#1-Ni(1)-Cl(1)	96.31(4)
Cl(2)-Ni(1)-Cl(1)	99.85(3)	C(2)-N(1)-O(1)	115.9(3)
C(2)-N(1)-Ni(1)	119.9(2)	O(1)-N(1)-Ni(1)	123.0(3)
N(3)-C(1)-C(2)	110.8(3)	Ni(1)#1-Cl(2)-Ni(1)	96.13(3)
C(5)-N(2)-O(2)	115.4(3)	C(5)-N(2)-Ni(1)	121.3(3)
O(2)-N(2)-Ni(1)	123.4(2)	N(1)-C(2)-C(3)	124.8(4)
N(1)-C(2)-C(1)	115.0(3)	C(3)-C(2)-C(1)	120.1(4)
C(1)-N(3)-C(7)	112.1(3)	C(1)-N(3)-C(4)	110.8(3)
C(7)-N(3)-C(4)	110.6(2)	C(1)-N(3)-Ni(1)	104.5(2)
C(7)-N(3)-Ni(1)	111.23(19)	C(4)-N(3)-Ni(1)	107.4(2)
C(5)-C(4)-N(3)	115.2(3)	N(2)-C(5)-C(4)	115.7(3)
N(2)-C(5)-C(6)	125.8(4)	C(4)-C(5)-C(6)	118.4(3)
N(3)-C(7)-C(8)	117.6(3)	C(7)-C(8)-C(9)	110.0(3)
C(10)-C(9)-C(8)	114.9(3)	C(11)-C(10)-C(9)	113.0(4)
C(10)-C(11)-C(12)	114.1(4)	C(13)-C(12)-C(11)	116.5(5)
C(12)-C(13)-C(14)	114.4(7)		

Symmetry transformations used to generate equivalent atoms:
#1 = -x+1/2, -y+1/2, -z+2

Table 4. Anisotropic displacement parameters [Å^2 x 10^3].
The anisotropic displacement factor exponent takes the form:
$-2\pi^2$ [$(ha^*)^2 U_{11}$ + ... + $2hka^*b^*U_{12}$]

	U11	U22	U33	U23	U13	U12
Ni(1)	66(1)	35(1)	27(1)	0(1)	2(1)	7(1)
Cl(1)	98(1)	70(1)	45(1)	0(1)	8(1)	36(1)
N(1)	103(3)	35(1)	30(1)	-1(1)	-5(1)	2(2)
C(1)	72(2)	52(2)	56(2)	3(2)	-11(2)	-12(2)
O(1)	149(3)	37(1)	50(2)	-11(1)	-2(2)	15(2)
Cl(2)	67(1)	39(1)	33(1)	1(1)	2(1)	-2(1)
N(2)	71(2)	48(2)	38(1)	4(1)	11(1)	6(1)
O(2)	77(2)	94(2)	67(2)	21(2)	24(2)	14(2)
C(2)	100(3)	43(2)	43(2)	-2(1)	-10(2)	-15(2)
N(3)	63(2)	36(1)	33(1)	2(1)	-1(1)	0(1)
C(3)	151(5)	67(3)	114(4)	-16(3)	-37(4)	-36(3)
C(4)	82(3)	46(2)	33(2)	4(1)	-5(2)	7(2)
C(5)	89(3)	38(2)	30(1)	-2(1)	7(2)	3(2)
C(6)	120(4)	63(2)	42(2)	16(2)	17(2)	11(2)
C(7)	60(2)	42(2)	38(2)	0(1)	1(1)	5(1)
C(8)	59(2)	57(2)	54(2)	3(2)	-1(2)	4(2)
C(9)	68(2)	60(2)	54(2)	6(2)	3(2)	18(2)
C(10)	70(3)	66(2)	70(3)	8(2)	3(2)	19(2)
C(11)	77(3)	76(3)	93(3)	-1(2)	3(2)	21(2)
C(12)	98(4)	82(3)	137(5)	1(3)	-6(3)	29(3)
C(13)	144(5)	95(3)	261(8)	10(4)	-18(5)	40(3)
C(14)	144(5)	95(3)	261(8)	10(4)	-18(5)	40(3)

Table 5. Hydrogen coordinates (x 10^4) and isotropic displacement parameters ($Å^2$ x 10^3).

	x	y	z	U(eq)
H(1A)	1032	2412	7275	72
H(1B)	1154	2147	8548	72
H(1)	2691	517	7545	118
H(2)	3518	2552	7246	118
H(3A)	1450	-22	6791	166
H(3B)	1018	728	6331	166
H(3C)	960	323	7563	166
H(4A)	1679	2983	6171	65
H(4B)	1720	4010	6675	65
H(6A)	3038	3889	5307	113
H(6B)	2525	4576	5443	113
H(6C)	2458	3634	4744	113
H(7A)	1881	4236	8677	56
H(7B)	1555	3505	9416	56
H(8A)	724	3852	8465	68
H(8B)	1041	4518	7616	68
H(9A)	921	4872	9965	73
H(9B)	1304	5499	9199	73
H(10A)	502	5986	8158	82
H(10B)	128	5398	8987	82
H(11A)	796	6930	9712	98
H(11B)	373	6379	10474	98
H(12A)	26	7478	8596	127
H(12B)	-378	6993	9455	127
H(13A)	330	8468	10027	200
H(13B)	-118	8013	10821	200
H(14A)	-455	9417	10121	250
H(14B)	-825	8588	9634	250
H(14C)	-370	9066	8873	250

Table 6. Torsion angles [^{o}].

N(2)-Ni(1)-N(1)-C(2)	-101.2(3)	N(3)-Ni(1)-N(1)-C(2)	-24.3(3)
Cl(2)#1-Ni(1)-N(1)-C(2)	57.2(7)	Cl(2)-Ni(1)-N(1)-C(2)	72.7(3)
Cl(1)-Ni(1)-N(1)-C(2)	172.7(3)	N(2)-Ni(1)-N(1)-O(1)	91.4(2)
N(3)-Ni(1)-N(1)-O(1)	168.3(3)	Cl(2)#1-Ni(1)-N(1)-O(1)	-110.2(7)
Cl(2)-Ni(1)-N(1)-O(1)	-94.6(2)	Cl(1)-Ni(1)-N(1)-O(1)	5.3(2)
N(2)-Ni(1)-Cl(2)-Ni(1)#1	-66.2(8)	N(1)-Ni(1)-Cl(2)-Ni(1)#1	-177.73(10)
N(3)-Ni(1)-Cl(2)-Ni(1)#1	-102.11(7)	Cl(1)-Ni(1)-Cl(2)-Ni(1)#1	95.37(4)
N(1)-Ni(1)-N(2)-C(5)	68.5(3)	N(3)-Ni(1)-N(2)-C(5)	-6.2(3)
Cl(2)#1-Ni(1)-N(2)-C(5)	-108.4(3)	Cl(2)-Ni(1)-N(2)-C(5)	-42.7(10)
Cl(1)-Ni(1)-N(2)-C(5)	155.5(3)	N(1)-Ni(1)-N(2)-O(2)	-111.1(3)
N(3)-Ni(1)-N(2)-O(2)	174.2(3)	Cl(2)#1-Ni(1)-N(2)-O(2)	72.0(3)
Cl(2)-Ni(1)-N(2)-O(2)	137.6(7)	Cl(1)-Ni(1)-N(2)-O(2)	-24.1(3)
O(1)-N(1)-C(2)-C(3)	1.1(6)	Ni(1)-N(1)-C(2)-C(3)	-167.1(4)
O(1)-N(1)-C(2)-C(1)	177.9(3)	Ni(1)-N(1)-C(2)-C(1)	9.6(4)
N(3)-C(1)-C(2)-N(1)	20.6(4)	N(3)-C(1)-C(2)-C(3)	-162.5(4)
C(2)-C(1)-N(3)-C(7)	-156.7(3)	C(2)-C(1)-N(3)-C(4)	79.2(3)
C(2)-C(1)-N(3)-Ni(1)	-36.2(3)	N(2)-Ni(1)-N(3)-C(1)	128.8(2)
N(1)-Ni(1)-N(3)-C(1)	31.2(2)	Cl(2)#1-Ni(1)-N(3)-C(1)	-140.22(19)
Cl(2)-Ni(1)-N(3)-C(1)	-55.1(2)	Cl(1)-Ni(1)-N(3)-C(1)	77.7(3)
N(2)-Ni(1)-N(3)-C(7)	-110.1(2)	N(1)-Ni(1)-N(3)-C(7)	152.3(2)
Cl(2)#1-Ni(1)-N(3)-C(7)	-19.1(2)	Cl(2)-Ni(1)-N(3)-C(7)	66.02(19)
Cl(1)-Ni(1)-N(3)-C(7)	-161.20(17)	N(2)-Ni(1)-N(3)-C(4)	11.1(2)
N(1)-Ni(1)-N(3)-C(4)	-86.5(2)	Cl(2)#1-Ni(1)-N(3)-C(4)	102.08(18)
Cl(2)-Ni(1)-N(3)-C(4)	-172.80(18)	Cl(1)-Ni(1)-N(3)-C(4)	-40.0(3)
C(1)-N(3)-C(4)-C(5)	-128.8(3)	C(7)-N(3)-C(4)-C(5)	106.3(3)
Ni(1)-N(3)-C(4)-C(5)	-15.2(3)	O(2)-N(2)-C(5)-C(4)	178.7(3)
Ni(1)-N(2)-C(5)-C(4)	-0.9(4)	O(2)-N(2)-C(5)-C(6)	0.8(5)
Ni(1)-N(2)-C(5)-C(6)	-178.8(3)	N(3)-C(4)-C(5)-N(2)	11.7(4)
N(3)-C(4)-C(5)-C(6)	-170.3(3)	C(1)-N(3)-C(7)-C(8)	-58.9(4)
C(4)-N(3)-C(7)-C(8)	65.3(4)	Ni(1)-N(3)-C(7)-C(8)	-175.4(2)
N(3)-C(7)-C(8)-C(9)	-174.2(3)	C(7)-C(8)-C(9)-C(10)	173.0(3)
C(8)-C(9)-C(10)-C(11)	-176.5(4)	C(9)-C(10)-C(11)-C(12)	174.5(4)
C(10)-C(11)-C(12)-C(13)	-174.4(6)	C(11)-C(12)-C(13)-C(14)	175.0(7)

Symmetry transformations used to generate equivalent atoms:
#1 = -x+1/2,-y+1/2,-z+2

Table 7. Hydrogen bonds [Å and °].

D-H...A	d(H...A)	<(DHA)	d(D...A)	SYMM
O1-H1..Cl1	2.14	160	2.991(4)	X, Y, Z
O2-H2..Cl	2.28	146	3.036(3)	X, Y, Z

Acknowledgements, References and Notes:

(1) JAKB thanks Dr. Alan Pinkerton (Department of Chemistry, University of Toledo) for the use of the SMART 6000 diffractometer.

(2) SMART v6.625 and SAINT v6.26A programs were used for data collection and data processing, respectively. Siemens Analytical X-ray Instruments, Inc., Madison, WI.

(3) SADABS was used for the application of semi-empirical absorption and beam corrections. G. M. Sheldrick, University of Goettingen, Germany.

(4) SHELXTL v6.1 was used for the structure solution and generation of figures and tables. G. M. Sheldrick, University of Goettingen, Germany and Siemens Analytical X-ray Instruments, Inc., Madison, WI. Neutral-atom scattering factors were used as stored in the SHELXTL v6.1 structure determination package.

Section 3. [Ni(TRISOXH$_3$)(pyridine-*N*-oxide)H$_2$O] or [$C_{14}H_{25}N_5O_5Ni$](NO_3)$_2$

Description:

The molecule shows metrical details consistent with previously solved structures of this type. The molecular and crystallographic mirror symmetry coincide with atoms Ni, O1, O3, O4, N1, N3, N4, C4, C5, C6, C9, H1 and H9 lying on special positions.

Experimental:

Single crystals were obtained as purple blocks from Et_2O. For x-ray examination and data collection, a suitable crystal, approximate dimensions 0.54 x 0.45 x 0.30 mm, was mounted on the tip of a glass fiber with epoxy resin.

Intensity data were collected at room temperature on a standard Siemens SMART 1K CCD diffractometer using graphite-monochromated Mo Kα radiation, λ=0.71073Å. The detector was set at a distance of 5.083 cm from the crystal. A series of 5-s data frames measured at 0.3° increments of ω were collected to calculate a unit cell. For data collection frames were measured for a duration of 5-s at 0.3° intervals of ω, which combined measured nearly a hemisphere of intensity data with a maximum θ value of 29.40°. The data frames were processed using the program SAINT. The data were corrected for decay, Lorentz and polarization effects as well as absorption and beam corrections based on the multi-scan technique.

The structure was solved by a combination of direct methods SHELXTL v5.1 and the difference Fourier technique and refined by full-matrix least squares on F^2. Non-hydrogen atoms were refined with anisotropic displacement parameters. Weights were assigned as $w^{-1}=[\sigma^2(F_o^2)+(0.0306P)^2+1.2296P]$ where $P=0.33333F_o^2+0.66667F_c^2$. The molecular and crystallographic mirror symmetry coincide with atoms Ni, O1, O3, O4, N1, N3, N4, C4, C5, C6, C9, H1 and H9 lying on special positions. Some disorder is present as indicated by the enlarged anisotropic displacement parameters of the phenyl group and the nitrate anion. Reasonable alternate positions were observed for O5 and O5B of the nitrate anion (occupancies set at 0.5). The –OH hydrogens were located directly and held fixed at that position. All remaining hydrogen atoms were either located directly or calculated based on geometric criteria and treated with a riding model. The isotropic temperature factors for the hydrogen atoms were set as a*Ueq of the adjacent atom where a=1.5 for –OH and $-CH_3$ and 1.2 for all others. The refinement converged with crystallographic agreement factors of R1=2.98%, wR2=6.87% for 2427 reflections with $I \geq 2\sigma(I)$ (R1=3.21%, wR2=6.96% for all data) and 177 variable parameters.

Table 1. Crystal data and structure refinement

Empirical formula	$[C_{14}H_{25}N_5O_5Ni](NO_3)_2$	
Formula weight	526.12	
Temperature	294(2) K	
Wavelength	0.71073 Å	
Crystal system	Orthorhombic	
Space group	$Cmc2_1$	
Unit cell dimensions:	a = 11.0671(10) Å	α = 90°
	b = 14.0481(10) Å	β = 90°
	c = 14.8625(12) Å	γ = 90°
Volume, Z	2310.7(3) Å^3, 4	
Density (calculated)	1.512 Mg/m^3	
Absorption coefficient	0.907 mm^{-1}	
F(000)	1096	
Crystal size	0.54 x 0.45 x 0.30 mm	
θ range for data collection	2.71 to 29.40°	
Limiting indices	$-14 < h < 15, -17 < k < 19, -20 < l < 14$	
Reflections collected	7484	
Independent reflections	2547 (R_{int} = 0.0312)	
Absorption correction	Multi-scan	
Max. and min. transmission	0.7725 and 0.6400	
Refinement method	Full-matrix least-squares on F^2	
Data / restraints / parameters	2547 / 1 / 177	

Goodness-of-fit on F^2	1.092
Final R indices [$I>2\sigma(I)$]	R1 = 0.0298, wR2 = 0.0687
R indices (all data)	R1 = 0.0321, wR2 = 0.0696
Absolute structure parameter	0.066(16)
Largest diff. peak and hole	0.271 and -0.485 eÅ^{-3}

Table 2. Atomic coordinates [$\times 10^4$] and equivalent isotropic displacement parameters [$\text{Å}^2 \times 10^3$]. U(eq) is defined as one third of the trace of the orthogonalized U_{ij} tensor.

	x	y	z	U(eq)
Ni	10000	3556(1)	-2492(1)	30(1)
O(1)	10000	4925(2)	-4088(2)	63(1)
O(2)	7222(2)	3368(1)	-2825(1)	54(1)
O(3)	10000	2301(2)	-1728(2)	43(1)
O(4)	10000	2840(2)	-3656(2)	51(1)
N(1)	10000	4815(2)	-3154(2)	38(1)
N(2)	8174(2)	3670(1)	-2274(1)	38(1)
N(3)	10000	4471(2)	-1382(2)	35(1)
N(4)	10000	1893(2)	-3639(2)	48(1)
C(1)	8876(2)	4239(2)	-875(2)	45(1)
C(2)	7870(2)	3960(2)	-1497(2)	43(1)
C(3)	6601(3)	4008(3)	-1164(3)	75(1)
C(4)	10000	5470(3)	-1703(3)	50(1)
C(5)	10000	5582(2)	-2701(2)	40(1)
C(6)	10000	6567(3)	-3079(4)	69(1)
C(7)	8958(4)	1431(2)	-3627(3)	78(1)
C(8)	8946(5)	449(2)	-3616(4)	97(1)
C(9)	10000	-45(3)	-3614(5)	99(2)
N(5)	7180(2)	3329(2)	-5118(2)	57(1)
O(5A)	6842(9)	2614(10)	-4752(11)	88(3)
O(5B)	6330(9)	2856(11)	-4774(10)	106(4)
O(6)	7124(3)	3444(2)	-5939(2)	85(1)
O(7)	7827(3)	3820(2)	-4643(2)	86(1)

Table 3. Bond lengths [Å] and angles [°].

Ni-O(4)	2.002(3)	Ni-N(1)	2.024(3)
Ni-N(2)	2.0523(19)	Ni-N(3)	2.090(3)
Ni-O(3)	2.097(3)	O(1)-N(1)	1.396(4)
O(1)-H(1)	0.8452	O(2)-N(2)	1.401(2)
O(2)-H(2)	0.9908	O(3)-H(3)	0.7917
O(4)-N(4)	1.331(4)	N(1)-C(5)	1.271(4)
N(2)-C(2)	1.270(3)	N(3)-C(4)	1.483(5)
N(3)-C(1)	1.490(3)	N(4)-C(7)	1.323(4)
C(1)-C(2)	1.500(4)	C(2)-C(3)	1.491(4)
C(4)-C(5)	1.491(6)	C(5)-C(6)	1.493(5)
C(7)-C(8)	1.379(4)	C(8)-C(9)	1.358(5)
N(5)-O(5A)	1.202(14)	N(5)-O(7)	1.219(3)
N(5)-O(6)	1.233(3)	N(5)-O(5B)	1.260(13)

O(4)-Ni-N(1)	91.06(11)	O(4)-Ni-N(2)	100.10(6)
N(1)-Ni-N(2)	90.50(5)	N(2)#1-Ni-N(2)	159.76(11)
O(4)-Ni-N(3)	172.24(11)	N(1)-Ni-N(3)	81.18(13)
N(2)-Ni-N(3)	80.09(5)	O(4)-Ni-O(3)	92.58(11)
N(1)-Ni-O(3)	176.37(13)	N(2)-Ni-O(3)	88.86(5)
N(3)-Ni-O(3)	95.18(11)	N(1)-O(1)-H(1)	79.7
N(2)-O(2)-H(2)	107.6	Ni-O(3)-H(3)	119.6
N(4)-O(4)-Ni	119.1(2)	C(5)-N(1)-O(1)	115.6(3)
C(5)-N(1)-Ni	118.9(3)	O(1)-N(1)-Ni	125.5(2)
C(2)-N(2)-O(2)	115.4(2)	C(2)-N(2)-Ni	115.43(16)
O(2)-N(2)-Ni	128.69(15)	C(4)-N(3)-C(1)	111.70(18)
C(1)#1-N(3)-C(1)	113.1(3)	C(4)-N(3)-Ni	109.2(2)
C(1)-N(3)-Ni	105.37(16)	C(7)-N(4)-C(7)#1	121.3(4)
C(7)-N(4)-O(4)	119.36(19)	N(3)-C(1)-C(2)	111.4(2)
N(2)-C(2)-C(3)	124.5(3)	N(2)-C(2)-C(1)	116.6(2)
C(3)-C(2)-C(1)	118.9(3)	N(3)-C(4)-C(5)	114.8(3)
N(1)-C(5)-C(4)	116.0(3)	N(1)-C(5)-C(6)	125.9(4)
C(4)-C(5)-C(6)	118.2(3)	N(4)-C(7)-C(8)	119.9(4)
C(9)-C(8)-C(7)	120.2(4)	C(8)#1-C(9)-C(8)	118.5(4)
O(5A)-N(5)-O(7)	113.1(8)	O(5A)-N(5)-O(6)	122.9(8)
O(7)-N(5)-O(6)	121.9(3)	O(7)-N(5)-O(5B)	120.1(8)
O(6)-N(5)-O(5B)	115.6(7)		

Symmetry transformations used to generate equivalent atoms:
#1 -x+2,y,z

Table 4. Anisotropic displacement parameters [$Å^2x10^3$]. The anisotropic displacement factor exponent takes the form: $-2\pi^2[(ha^*)^2U_{11} + ... + 2hka^*b^*U_{12}]$

	U11	U22	U33	U23	U13	U12
Ni	33(1)	29(1)	27(1)	0(1)	0	0
O(1)	107(3)	49(2)	34(2)	9(1)	0	0
O(2)	43(1)	63(1)	56(1)	-5(1)	-18(1)	-5(1)
O(3)	45(1)	49(1)	34(1)	10(1)	0	0
O(4)	88(2)	32(1)	32(1)	0(1)	0	0
N(1)	45(2)	36(1)	34(2)	3(1)	0	0
N(2)	34(1)	39(1)	41(1)	-1(1)	-6(1)	-1(1)
N(3)	34(1)	40(1)	31(2)	-2(1)	0	0
N(4)	75(2)	34(2)	33(2)	-1(1)	0	0
C(1)	39(1)	59(2)	37(1)	-7(1)	4(1)	-1(1)
C(2)	29(1)	53(1)	47(2)	-1(1)	1(1)	1(1)
C(3)	36(1)	113(3)	74(2)	-17(2)	13(2)	-1(2)
C(4)	62(2)	38(2)	50(2)	-9(2)	0	0
C(5)	41(2)	33(1)	46(3)	4(1)	0	0
C(6)	97(4)	33(2)	77(3)	7(2)	0	0
C(7)	79(2)	50(2)	106(3)	1(2)	-21(2)	-6(2)
C(8)	109(3)	48(2)	133(4)	6(2)	-29(3)	-23(2)
C(9)	168(7)	34(2)	94(4)	-2(2)	0	0
N(5)	64(2)	48(1)	58(2)	-6(1)	-11(1)	-8(1)
O(5A)	97(7)	73(5)	93(6)	15(4)	-20(7)	-29(5)
O(5B)	107(8)	128(11)	82(6)	-17(7)	17(7)	-69(7)
O(6)	101(2)	102(2)	52(2)	-2(1)	-14(2)	-29(2)
O(7)	86(2)	100(2)	71(2)	-2(1)	-30(2)	-32(2)

Table 5. Hydrogen coordinates (x10^4) and isotropic displacement parameters (Å^{2}x10^3).

	x	y	z	U(eq)
H(1)	10000	4325	-4049	95
H(2)	7379	3611	-3440	81
H(3)	9454	2194	-1399	64
H(1A)	8631	4789	-525	54
H(1B)	9038	3721	-461	54
H(3A)	6520	3622	-635	112
H(3B)	6063	3778	-1623	112
H(3C)	6401	4656	-1022	112
H(3D)	6122	4387	-1567	112
H(3E)	6579	4298	-580	112
H(3F)	6261	3334	-1130	112
H(4A)	10701	5792	-1453	60
H(6A)	9525	6975	-2702	103
H(6B)	9662	6557	-3674	103
H(6C)	10814	6801	-3106	103
H(7)	8235	1768	-3626	94
H(8)	8213	125	-3611	116
H(9)	10000	-707	-3611	119

Table 6. Intra- and Intermolecular Interactions (Å,°).

	d(D-H)	d(H..A)	d(D..A)	<DHA	Symm. Op.
O1-H1..O4	0.85	2.17	2.999(4)	168	x, y, z
O2-H2..O7	0.99	1.88	2.855(4)	168	x, y, z
O2-H2..O5A	0.99	2.47	3.08(2)	119	x, y, z
O2-H2..O5B	0.99	2.53	3.14(2)	120	x, y, z
O3-H3..O6	0.79	2.08	2.827(3)	158	-x+3/2, -y+1/2, z+1/2
O3-H3..O5B	0.79	2.57	3.26(1)	148	-x+3/2, -y+1/2, z+1/2
O2-H2..N5	0.99	2.53	3.408(4)	147	x, y, z

Acknowledgements, References and Notes:

(1) Data was collected through the Ohio Crystallographic Consortium, funded by the Ohio Board of Regents 1995 Investment Fund (CAP-075) located at the University of Toledo, Instrumentation Center in A&S, Toledo, OH 43606.

(2) SMART v5.622 and SAINT v6.02A programs were used for data collection and data processing, respectively. Siemens Analytical X-ray Instruments, Inc., Madison, WI.

(3) SADABS was used for the application of semi-empirical absorption and beam corrections. G. M. Sheldrick, University of Goettingen, Germany.

(4) SHELXTL v5.1 was used for the structure solution and generation of figures and tables.
G. M. Sheldrick, University of Goettingen, Germany and Siemens Analytical X-ray Instruments, Inc., Madison, WI.

(5) Neutral-atom scattering factors were used as stored in the SHELXTL v5.1 structure determination package.